

Cleavable Peptide-Triterpene Conjugates for Improved Gene Delivery

Inaugural-Dissertation to obtain the academic degree Doctor rerum naturalium (Dr. rer. nat.)
Submitted to the Department of Biology, Chemistry, Pharmacy of Freie Universität Berlin
By Meike Karen Kolster
Date of submission: 17.04.2024

Work on this thesis was carried out from 01.04.2019 to 17.04.2024 under the supervision of PD Dr. Alexander Weng at the Institute of Pharmacy of Freie Universität Berlin.

1st reviewer: PD Dr. rer. nat. Alexander Weng

2nd reviewer: Prof. Dr. rer. nat. Timo Niedermeyer

Date of defense: 26.06.2024

Please cite this thesis as <http://dx.doi.org/10.17169/refubium-43752>

For Melchi



Declaration of authorship

I hereby declare that I alone am responsible for the content of my doctoral dissertation and that I have only used the sources or references cited in the dissertation.

Berlin, 17.04.2024

M. K. Kolster

Zusammenfassung

Gentherapien stellen vielversprechende neue Therapieoptionen für eine Vielzahl von Indikationen dar. Trotz mehrerer zugelassener Medikamente, die auf viralen Gentransfer-Vektoren basieren, bleibt das volle Potenzial gentherapeutischer Ansätze bislang ungenutzt. Dies liegt zum einen an der hohen Immunogenität und aufwändigen Herstellung viraler Vektoren, zum anderen an der geringen Effizienz nicht-viraler Gentransfersysteme, die vor allem auf den Einschluss der verwendeten Nanopartikel in Endosomen und den damit verbundenen Abbau zurückzuführen ist.

SO1861, ein aus *Saponaria officinalis* L. isoliertes Triterpensaponin, kann die Freisetzung aus den Endosomen fördern und wird daher als Transfektionsverstärker eingesetzt. Die Saponin-unterstützte Transfektion wird als Sapofektion bezeichnet und beinhaltet die parallele Verabreichung des Saponins und der Nanopartikel. *In vitro* funktioniert dies problemlos, *in vivo* erweist sich die Synchronisation der beiden Komponenten jedoch als schwierig. Ziel der vorliegenden Arbeit war daher die Entwicklung und Optimierung eines nicht-viralen Gentransfersystems, das die zu transfizierende DNA und das transfektionsverstärkende Saponin in einem Partikel enthält und intravenös verabreicht werden kann. Durch die Integration eines zielgerichteten Liganden in den zu entwickelnden Nanopartikel sollte zusätzlich die zielgerichtete Wirkung des Gentransfersystems sichergestellt werden.

Um dieses Forschungsziel zu erreichen, wurde SO1861 mit Hilfe eines pH-sensitiven Hydrazon-Linkers kovalent an ein Poly-L-Lysin-basiertes Peptidgerüst konjugiert. Die hergestellten SO1861-funktionalisierten Peptide wurden zur Komplexierung von DNA durch elektrostatische Wechselwirkung verwendet. Die resultierenden Nanoplexe wurden *in vitro* auf ihre Transfektionseffizienz und Verträglichkeit hin untersucht. In allen untersuchten Zelllinien transfizierten die Nanoplexe mit konjugiertem SO1861 deutlich effektiver als nicht-funktionalisierte Nanoplexe unter Zugabe von freiem SO1861 zum Transfektionsmedium. Die Transfektion mit den SO1861 enthaltenden Nanoplexen beeinflusste die Zellviabilität nicht.

Zielgerichtete, konjugiertes SO1861 enthaltende Nanoplexe wurden durch Integration eines zielgerichteten Peptids hergestellt und *in vivo* in einem Allograft-Tumormodell in Mäusen getestet. Unter Verwendung eines Selbstmordgen-Vektors, der für das zytotoxische Protein Saporin kodiert, wurde bei der Behandlung mit zielgerichteten, SO1861 enthaltenden Nanoplexen im Vergleich zur Vehikelkontrolle ein verlangsamtes Tumorwachstum und eine verbesserte Überlebensrate beobachtet. Die intravenöse Injektion der SO1861 enthaltenden Nanoplexe war dabei gut verträglich.

Abstract

Gene therapies represent promising new therapeutic options for a variety of indications. Despite several approved drugs based on viral gene delivery vectors, the full potential of gene therapy approaches remains unexploited. This is due to the high immunogenicity and complex production of viral vectors as well as the low efficacy of non-viral gene delivery vehicles that is in particular attributable to endosomal entrapment and degradation of the nanoparticles used.

SO1861, a naturally occurring triterpenoid saponin isolated from *Saponaria officinalis* L., promotes endosomal escape and is therefore used as a transfection enhancer. The saponin-enhanced transfection was termed sapofection and involves the parallel administration of the endosomal-escape enhancing saponin and the DNA-containing nanoparticles. Parallel administration is not a problem *in vitro*, but the synchronization of the two components is a challenge *in vivo*. The aim of the present work was therefore to develop and optimize a non-viral gene delivery vehicle that contains the DNA to be transfected and the transfection-enhancing saponin SO1861 in one particle that can be administered intravenously. The integration of a targeting ligand into the gene delivery vehicle to be developed shall ensure the targeted delivery of the nanoparticles.

To achieve this research goal, SO1861 was covalently conjugated to a poly-L-lysine-based peptide scaffold using a pH-sensitive hydrazone linker. The prepared SO1861-functionalized peptides were used to complex DNA by electrostatic interaction. The resulting nanoplexes were evaluated for *in vitro* transfection efficiency and tolerability. In a variety of cell lines, the nanoplexes with conjugated SO1861 transfected significantly more effectively than non-functionalized nanoplexes with supplementation of free SO1861 in the transfection medium. The transfection with SO1861-nanoplexes was well tolerated.

Targeted nanoplexes containing covalently conjugated SO1861 were prepared by incorporation of a targeting peptide and tested *in vivo* in an allograft tumor model in mice. Using a suicide gene vector encoding the cytotoxic protein saporin, treatment with targeted SO1861-containing nanoplexes was observed to slow tumor growth and improve survival compared to vehicle control. Intravenous injection of nanoplexes containing SO1861 was well tolerated.

Contents

Acronyms	xix
1 Introduction	1
1.1 Vectors: Gene Delivery Vehicles	1
1.1.1 Viral Gene Delivery Vehicles	2
1.1.2 Non-Viral Gene Delivery Vehicles	3
1.1.2.1 Plasmid DNA Vectors	5
1.1.2.2 Molecular Carriers	8
1.2 Sapofection - Overcoming Endosomal Entrapment for Efficient Gene Delivery	10
1.3 Targeted Gene Delivery	13
1.4 Chemical Strategy	15
2 Materials	19
2.1 Chemicals	19
2.1.1 Molecular Biology	19
2.1.2 Polyacrylamide Gel Electrophoresis	20
2.1.3 Cell Culture	20
2.1.4 Peptides	20
2.1.5 Nucleid Acids	20
2.1.6 Miscellaneous	22
2.2 Biomaterials	22
2.3 Kits	23
2.4 Consumables	23
2.4.1 Cell Culture	23
2.4.2 Dialysis	23
2.4.3 Analytics	24
2.4.4 Miscellaneous	24
2.5 Devices	24
2.5.1 Molecular Biology	24
2.5.2 Polyacrylamide Gel Electrophoresis	25
2.5.3 Cell Culture	25
2.5.4 Centrifuges and Scales	25
2.5.5 Miscellaneous	25

3	Methods	27
3.1	Molecular Biology	27
3.1.1	Agarose Gel Electrophoresis	27
3.1.2	Spectrophotometric Analysis of DNA	27
3.1.3	Molecular Cloning of Recombinant Plasmid DNA Vectors	28
3.1.3.1	Polymerase Chain Reaction	29
3.1.3.2	Restriction Digest	30
3.1.3.3	Ligation	32
3.1.3.4	Transformation, Recovery, and Selection	32
3.1.3.5	Amplification and Preparation of Plasmid DNA	33
3.1.4	Preparation of Minicircle DNA	33
3.2	Preparation of Peptide-Triterpene Conjugates	33
3.2.1	Conjugation of SO1861-EMCH and Peptide Scaffolds	34
3.2.2	Purification of Peptide Conjugates using Solid Phase Extraction	34
3.3	Nanoplex Formulation	34
3.3.1	Preparation of Targeted Nanoplexes	36
3.4	Analytical Methods	36
3.4.1	Nuclear Magnetic Resonance Spectroscopy	36
3.4.2	Matrix-Assisted Laser Desorption/Ionization Time-of-Flight Mass Spectrometry	37
3.4.3	Liquid Chromatography Mass Spectrometry	38
3.4.4	Polyacrylamide Gel Electrophoresis	38
3.4.5	Fluorescence Spectroscopy	39
3.4.6	Dynamic and Electrophoretic Light Scattering	40
3.4.7	Electron Microscopy	41
3.4.8	Flow Cytometry	42
3.5	<i>In Vitro</i> Investigations	44
3.5.1	Culture Conditions	44
3.5.2	Transfection	44
3.5.3	Transfection Efficiency	45
3.5.4	Cellular Impedance	46
3.5.5	Internalization of Epidermal Growth Factor	47
3.6	<i>In Vivo</i> Investigations	48
3.6.1	Tolerability Studies	48
3.6.2	Anti-Tumor Efficacy	49
3.7	Statistical Analysis	49
4	Results and Discussion	51
4.1	Stability of SO1861-EMCH	51
4.2	Peptide Scaffolds	53
4.2.1	Initial Peptide Design	53



4.2.2	Initial Functionalization Conditions	54
4.2.3	Optimization of Peptide Sequence and Functionalization Conditions	56
4.2.4	Purification of Equipped Peptide Scaffolds	58
4.2.5	Release of SO1861	60
4.2.6	Batch-to-Batch Reproducibility	61
4.3	Nanoplex Characterization	63
4.3.1	DNA Complexation Efficiency	63
4.3.2	Size, Size Distribution and ζ -Potential	63
4.4	<i>In Vitro</i> Investigations of Nanoplexes	68
4.4.1	Preliminary Investigations with SO1861-EMCH	68
4.4.2	Transfection Efficiency of Equipped Peptide Scaffolds	70
4.4.3	Tolerability of Equipped Peptide Scaffolds	76
4.4.4	Kinetics of Endosomal Release	76
4.5	Targeted Nanoplexes	80
4.5.1	Epidermal Growth Factor as Targeting Ligand	81
4.5.1.1	Characterization of Cellular Internalization	81
4.5.1.2	Transfection Efficiency of Epidermal Growth Factor Receptor-Targeted Nanoplexes	86
4.5.2	Targeting with Peptide Y	89
4.5.2.1	Transfection Efficiency <i>In Vitro</i>	90
4.5.2.2	Characterization of PepY-Nanoplexes	93
4.5.2.3	Tolerability <i>In Vivo</i>	96
4.5.2.4	Efficacy <i>In Vivo</i>	96
4.6	Molecular Biology	100
4.6.1	Molecular Cloning of Minicircle DNA Vectors	100
4.6.2	Preparation of Minicircle DNA	101
4.6.3	Optimization of DNA Vector	103
5	Conclusion and Outlook	107
6	Bibliography	111
7	Appendix	133
7.1	Organ Weights of Mice	133
7.2	MALDI-Spectra of Peptide Batches	133
7.3	Kinetics of Transfection with PepY-SO1861-Nanoplex	141

List of Figures

1.1	Schematic illustration of gene expression through pDNA transfection using non-viral gene delivery vehicles.	5
1.2	Structural formulas of polymeric molecular carriers.	9
1.3	Structural formula of SO1861 with highlighted endosomal-enhancing structural characteristics.	12
1.4	Suggested chemical strategy for the preparation of targeted, SO1861-equipped peptide scaffolds.	17
3.1	Schematic illustration of molecular cloning workflow.	29
3.2	Evaluation of flow cytometry experiments.	43
4.1	Hydrazone groups with adjacent substituents of SO1861-EMCH and Aldoxorubicin.	52
4.2	Schematic illustration of initial peptide scaffold design.	53
4.3	MALDI-TOF MS spectra of peptide scaffold functionalization with SO1861-EMCH using different incubation times.	54
4.4	MALDI-TOF MS spectra of peptide scaffold functionalization with SO1861-EMCH using different molar ratios.	55
4.5	Schematic illustration of optimized peptide scaffold design.	56
4.6	Elution of peptide scaffold in SPE.	59
4.7	Removal of unreacted SO1861-EMCH by SPE indicated by LC-MS analysis.	59
4.8	Release of SO1861 from the equipped peptide scaffolds depending on pH value.	60
4.9	Transfection efficiency <i>in vitro</i> indicating reproducibility of the peptide functionalization reaction.	62
4.10	DNA complexation efficiency of peptide scaffolds.	64
4.11	Size distribution by intensity of nanoplexes formulated with set of (equipped) peptide scaffolds.	67
4.12	Comparison of transfection-enhancing capability of SO1861 and SO1861-EMCH.	68
4.13	Tolerability of SO1861-EMCH <i>in vitro</i> in Huh-7 cell line.	69
4.14	<i>In vitro</i> transfection efficiency of pEGFP-N3/peptide scaffold nanoplexes in various cell lines.	73



4.15 Fluorescence micrographs of cell lines HEK293-FT, A2058, and HCT 116 48 h after transfection with pEGFP-N3-nanoplexes illustrating the transfection-enhancing performance of covalently conjugated and externally supplemented SO1861-EMCH. 75

4.16 Cell viability during transfection with SO1861-EMCH-equipped and non-equipped nanoplexes. 77

4.17 Kinetics of endosomal release of nanoplexes as a function of mode of SO1861-EMCH supplementation. 79

4.18 Cy5-EGF-internalization in target- and non-target cell lines. 83

4.19 Time dependency and competitive inhibition of Cy5-EGF-internalization. 84

4.20 Cy5-EGF-internalization in A-431 cell line. 85

4.21 Transfection efficiency of EGF-functionalized nanoplexes in non-target and target cell lines. 87

4.22 Fluorescence micrographs of transfections with EGF-functionalized nanoplexes in MDA-MB-468 cell line. 89

4.23 *In vitro* transfection efficiency of PepMix-nanoplexes in Neuro-2a cell line. 91

4.24 Kinetic profile of eGFP expression in Neuro-2a cell line during transfection with pepY-SO1861-nanoplexes. 92

4.25 Dose-response curves of PepMix-nanoplexes in Neuro-2a cell line. 93

4.26 Size distribution by intensity of pepY-nanoplexes and pepY-SO1861-nanoplexes. 94

4.27 Scanning electron micrographs of pepY-nanoplexes and pepY-SO1861-nanoplexes. 95

4.28 Cryogenic transmission electron micrographs of pepY-nanoplexes and pepY-SO1861-nanoplexes. 95

4.29 Body weight of three mice during tolerability study. 96

4.30 Anti-tumor efficacy of and survival rates during treatment with pepY-SO1861-nanoplexes and pepY-nanoplexes *in vivo*. 97

4.31 Quality control of constructs eGFP/MN501A1 and CMV/eGFP/MN501A1. 101

4.32 Quality control of constructs HLP/hFIX/MN501A1 and HLP/eGFP/MN501A1. 102

4.33 Quality control of produced mcDNA MC-eGFP and MC-HLP/eGFP. 102

4.34 *In vitro* transfection efficiency of nanoplexes formulated with different GFP-encoding pDNA vectors in cell lines A2058 and Huh-7. 104

4.35 Kinetic profile of eGFP expression after transfection with pEGFP-N3 and NP-eGFP in cell lines A2058 and Huh-7. 105

List of Tables

2.1	Peptide acronyms, sequences and molecular weights.	21
2.2	Plasmid DNA vectors, their acronyms and sources.	21
2.3	Cell lines, their origin and sources.	22
3.1	PCR primers and settings for molecular cloning of eGFP/MN501A1, CMV/eGFP/MN501A1, HLP/hFIX/MN501A1, and HLP/eGFP/MN501A1.	31
3.2	Cell culture media and seeding densities of cell lines.	44
4.1	Hydrolysis rates of hydrazone and maleimide group in SO1861-EMCH. . .	52
4.2	Hydrodynamic diameter, polydispersity index, and ζ -potential of nanoplexes formulated with pEGFP-N3 and (equipped) peptide scaffolds produced in 20 mM citrate, pH 6.0.	65
4.3	Hydrodynamic diameter, polydispersity index, and ζ -potential of nanoplexes formulated with pEGFP-N3 and (equipped) peptide scaffolds produced in DPBS, pH 6.5.	65
4.4	Hydrodynamic diameter, polydispersity index, and ζ -potential of pepY-nanoplexes and pepY-SO1861-nanoplexes.	94
4.5	GFP-encoding pDNA vectors tested <i>in vitro</i>	103
7.1	Organ weights of mice included in the <i>in vivo</i> efficacy study.	133

Acronyms

E. coli *Escherichia coli*.

¹H NMR ¹H nuclear magnetic resonance.

AAV adeno-associated virus.

ACN acetonitrile.

ADP adenosine diphosphate.

APC allophycocyanin.

ApoAI Apolipoprotein AI.

APS ammonium persulfate.

ATP adenosine triphosphate.

AUC area under the curve.

bp base pairs.

CMV enhancer + promoter Cytomegalovirus immediate-early enhancer + Cytomegalovirus immediate-early promoter.

CMV promoter Cytomegalovirus immediate-early promoter.

copGFP green fluorescent protein 2 from the copepod *Pontellina plumata*.

Cy5 cyanine5.

D_h hydrodynamic diameter.

DBCO dibenzocyclooctene.

DLS dynamic light scattering.

DMEM Dulbecco's modified Eagle's medium.

DMSO dimethylsulfoxide.

DNA deoxyribonucleic acid.

DPBS Dulbecco's phosphate-buffered saline, without Ca^{2+} or Mg^{2+} .

dsDNA double-stranded DNA.

EDTA ethylenediaminetetraacetic acid.

EEE endosomal escape enhancer.

eee endosomal escape-enhancing.

EGF epidermal growth factor.

eGFP enhanced green fluorescent protein.

EGFR epidermal growth factor receptor.

EMA European Medicines Agency.

EMCH *N*- ϵ -maleimidocaproic acid hydrazide.

EPR enhanced permeability and retention.

ESI electrospray ionization.

FA formic acid.

FBS fetal bovine serum.

FDA U.S. Food & Drug Administration.

FITC fluorescein isothiocyanate.

FITC-K₁₆ FITC-K₁₆.

GalNAc *N*-Acetylgalactosamine.

GFP green fluorescent protein.

HBM HEPES-buffered mannitol.

HCCA α -cyano-4-hydroxycinnamic acid.

HEPES *N*-2-Hydroxyethylpiperazine-*N'*-2-ethane sulfonic acid.

hFIX human coagulation factor IX.

HILIC hydrophilic interaction liquid chromatography.

HL promoter hybrid liver promoter.

HPLC high pressure liquid chromatography.

HTLV-I R human T-lymphotropic virus type I region.

i.v. intravenous.

K(N₃) azidolysine.

K₁₆ K₁₆.

K₁₆C K₁₆G₄CG₂YK(N₃).

K₁₆C₃ K₁₆CGCGCGK(N₃).

K₁₆C₃PEG K₁₆CGCGCG-PEG₈-K(N₃).

K₁₆Ceq0.25 S-SO1861_{0.25}-(K₁₆G₄CG₂YK(N₃)).

K₁₆Ceq0.5 S-SO1861_{0.5}-(K₁₆G₄CG₂YK(N₃)).

K₁₆CPEG K₁₆G₄CG₂Y-PEG₈-K(N₃).

K₁₆CPEGeq0.25 S-SO1861_{0.25}-(K₁₆G₄CG₂Y-(PEG₈)-K(N₃)).

K₁₆CPEGeq0.5 S-SO1861_{0.5}-(K₁₆G₄CG₂Y-(PEG₈)-K(N₃)).

kb kilobases.

LB lysogeny broth.

LC liquid chromatography.

LNP lipid nanoparticle.

m/z mass-to-charge ratio.

MALDI matrix-assisted laser desorption/ionization.

mcDNA minicircle DNA.

MeOH methanol.

MES MES.

MPS mononuclear phagocyte system.

mRNA messenger ribonucleic acid.

MS mass spectrometry.

MTS 3-(4,5-dimethylthiazol-2-yl)-5-(3-carboxymethoxyphenyl)-2-(4-sulfophenyl)-2H-tetrazolium, inner salt.

MTT 3-(4,5-dimethylthiazol-2-yl)-2,5-diphenyl tetrazolium bromide.

MWCO molecular weight cut-off.

NMR nuclear magnetic resonance.

NP Nanoplasmid™.

NP-eGFP NTC9385R-EGFP-BGH pA.

NP-Luc NTC9385R-Luc-BGH pA.

NP-Sap NTC9385R-Sap-BGH pA.

nTPM normalized transcripts per million.

ORI origin of replication.

PAGE polyacrylamide gel electrophoresis.

PAMAM poly(amidoamine).

PAMP pathogen-associated molecular pattern.

PB phosphate buffer.

PBS phosphate-buffered saline.

PCR polymerase chain reaction.

Pdi polydispersity index.

pDNA plasmid DNA.

PEG polyethylene glycol.

PEG₈ PEG₈.

PEI polyethylenimine.

pepY K₁₆GACYGLPHKFCG.

pepY-nanoplex NP-Sap complexed with 70 % pepY and 30 % K₁₆CPEG.

pepY-SO1861-nanoplex NP-Sap complexed with 70 % pepY and 30 % K₁₆CPEGeq0.5.

PES phenazine ethosulfate.

PLL poly-L-lysine.

PP polypropylen.

PS polystyrene.

pUC plasmid University of California.

RIP ribosome-inactivating protein.

RNA ribonucleic acid.

RP Reverse Phase.

s.c. subcutaneous.

SA sinapinic acid.

SDS sodium dodecyl sulfate.

SEC size exclusion chromatography.

SEM scanning electron microscopy.

SPAAC strain-promoted azide-alkyne-cycloaddition.

SPE solid phase extraction.


TAE tris-acetate-EDTA.

TAPS *N*-tris[hydroxymethyl]methyl-3-aminopropane-sulfonic-acid.

TCEP Tris(2-carboxyethyl)phosphine.

TEM transmission electron microscopy.

TEMED tetramethylethylenediamine.



TOF time-of-flight.

Tris tris(hydroxymethyl)aminomethane.

TV tumor volume.

UV ultraviolet.

1 Introduction

Gene therapy medicinal products, defined as biological drugs whose active ingredient consists of or contains a nucleic acid, are used to regulate, repair, replace, supplement, or remove a nucleic acid sequence (PEI 2024). With 3900 gene therapy clinical trials completed, underway, or approved by March 2023, gene therapy strategies have emerged as promising and widely explored approaches for a variety of therapeutic indications, mainly cancer and monogenic diseases (The Journal of Gene Medicine 2023).

Particularly in the case of cancer, a leading cause of global mortality with almost 10 million deaths in 2020 (Sung et al. 2021), the development of efficient and safe gene therapeutics is expected to have a major impact on medical progress. Promising approaches for cancer gene therapy include, amongst others, corrective gene therapy of mutations, boosting the immune response against tumor cells, (e.g., by infusing autologous immune cells genetically modified *ex vivo*), RNA interference, and suicide gene based cancer treatment (Duarte et al. 2012; Navarro et al. 2016; Vassaux and Martin-Duque 2004).

Despite the diversity of research approaches, a closer look at the registered gene therapy trials, 94 % of which are in phase I or II (The Journal of Gene Medicine 2023), and the approval of only 22 gene therapy drugs by the U.S. Food & Drug Administration (FDA) and/or the European Medicines Agency (EMA) (FDA 2024; PEI 2024) to date, indicates difficulties in translating preclinical research into clinical application. These are briefly discussed below.

1.1 Vectors: Gene Delivery Vehicles

Unprotected, naked DNA is rapidly eliminated by phagocytes and nucleases. For the therapeutic application of nucleic acids, their protection by so-called vectors, also referred to as gene delivery vehicles, is therefore essential. In addition to protecting and stabilizing DNA, these delivery vehicles are critical for the efficient delivery of therapeutic nucleic acids into target tissues or cells. Gene therapy vectors are broadly classified as either non-viral or viral, with the latter further subdivided into integrating and non-integrating viral vectors (Hardee et al. 2017; Mali 2013; Singh et al. 2021).

1.1.1 Viral Gene Delivery Vehicles

Viral vectors, due to their natural ability to infect cells, typically exhibit significantly higher gene delivery efficacy than non-viral vectors. However, several obstacles prevent their widespread clinical application.

Recombinant viral vectors are generated by integrating the transgene to be introduced into the viral genome while eliminating all genes encoding viral proteins. Although the viruses are rendered harmless by their lack of replication ability, the immune system of the recipient reacts to the pathogen-associated molecular patterns of the replication-incompetent virus. In addition to severe acute immune reactions as a safety risk (Raper et al. 2003), the inactivation of the virus by neutralizing antibodies upon repeated administration is an obstacle to the use of viral vectors for gene therapy applications requiring multiple administrations. In addition, the manufacturing process of viral vectors is both costly and complicated (Jooss and Chirmule 2003; Singh et al. 2021).

Integrating viral vectors such as retroviruses or lentiviruses are capable of permanently integrating the transgene into the host genome. Successful transduction with these viral vectors results in stable and long-lasting expression of the transgene. Several gene therapy products using integrating viral vectors are currently approved for *ex vivo* transduction of autologous cells, for example in the context of chimeric antigen receptor T-cell therapy (Bulcha et al. 2021; Kulkarni et al. 2021). In addition to the safety concerns mentioned above, the risk of insertional mutagenesis with consequent oncogenesis (Check 2002; Vargas et al. 2016) is another reason why integrating viral vectors are currently used exclusively *ex vivo*.

Adenoviral vectors are non-integrating viral vectors, which minimizes the risk of insertional mutagenesis, but only allows transient expression of the transgene. Their application as viral vectors is characterized by high transduction efficiency of both dividing and quiescent cells, as well as robust and rapid transgene expression. High titer production is also possible (Kay et al. 2001). The main obstacle to the use of adenoviral vectors is widespread humoral and cellular immunity to common adenovirus serotypes, estimated to exceed 80% (Garnett et al. 2002). Non-human adenoviral vectors, which circumvent preexisting immunity to human adenoviruses, have been explored as an alternative, but the strong innate response to the viral vectors and inactivation by neutralizing antibodies, which prevent re-administration have led to widespread abandonment of adenoviral vectors for gene therapy (Ahi et al. 2011; Lopez-Gordo et al. 2014; Shirley et al. 2020). Despite these limitations, nadofaragene firadenovec was recently approved as the first adenoviral vector-based gene therapy (FDA 2023) for a specific type of bladder cancer. Its dosing regimen includes intravesical administration every three months. The phase IV trial will show whether local application in combination with a low dose and the optimized adenoviral vector sufficiently reduces immunogenicity, given that only 157 patients were enrolled in the pivotal phase III trial, of whom only 64 received four doses (Boorjian et al. 2021).

Adeno-associated virus (AAV) is a naturally non-pathogenic virus that requires parallel

infection with a helper virus such as an adenovirus for replication. None of the wild-type AAV serotypes have been described to cause disease in humans. Compared to other viral vectors, the administration of recombinant AAVs induces only a mild inflammatory response. Although AAVs are not highly immunogenic, neutralizing antibodies are still generated, preventing repeated administration of the same AAV-vector. In addition, neutralizing antibodies against multiple AAV serotypes are typically developed in childhood. Seroprevalence varies geographically and between serotypes, ranging from 5 % to 60 % (Jeune et al. 2013). This fact is taken into account by screening for neutralizing antibodies before attempting therapy. AAV-based viral vectors are capable of transducing a wide variety of cells, regardless of their stage in the cell cycle. Episomal transgene expression and random chromosomal integration are described mechanisms for transgene expression after infection with AAV-based vectors. Insertional mutagenesis by AAV vectors leading to oncogenesis has been reported in mice, raising safety concerns for the clinical use of AAV vectors (Donsante et al. 2007). When transduced with AAV-based vectors, the onset of transgene expression takes longer than with adenoviral vectors, typically reaching a plateau four weeks after administration. In addition, significantly longer lasting transgene expression is observed when using AAV vectors. Recombinant AAVs have a limited packing capacity of ≈ 5.0 kilobases (kb), limiting their use to transgenes that do not exceed this limit (Jooss and Chirmule 2003; Kay et al. 2001; Shirley et al. 2020; Singh et al. 2021). Despite the limitations described above, several drugs using recombinant AAV-vectors have been approved by the EMA and/or FDA as one-time therapy for monogenic diseases (Burdett and Nuseibeh 2022).

In summary, the constraints described above, as well as the severe side effects and enormous costs for the widespread use of viral vectors, make the further development and improvement of alternative, non-viral vectors for gene therapy approaches highly relevant.

1.1.2 Non-Viral Gene Delivery Vehicles

While viral vectors act as both carrier and protector of the transgene, these two functions are typically separated in non-viral gene delivery vehicles.

The transgene is usually part of a plasmid, which are small, circular, double-stranded DNA molecules, hereafter referred to as plasmid DNA (pDNA) vectors. To protect against nuclease degradation, enhance cellular uptake, and minimize immunogenicity, molecular carriers are used to incorporate the pDNA vector, resulting in nanoparticles used as non-viral gene delivery vehicles.

In contrast to viruses, whose evolution has optimized gene transfer, successful gene delivery using non-viral approaches presents several obstacles. Successful gene expression *in vitro* upon transfection, defined as the introduction of nucleic acids into eukaryotic cells, is shown schematically in Figure 1.1 and requires:

- *Cellular internalization* of the gene delivery vehicle: Particle size is a critical factor in

determining the route and efficiency of cellular uptake and subsequent intracellular trafficking. Nanoparticles have been shown to be internalized via clathrin- or caveolae-mediated endocytosis (Foroozandeh and Aziz 2018; Rehman et al. 2011). 200 nm is generally being considered the upper size limit for clathrin-mediated endocytosis (Ehrlich et al. 2004; Rejman et al. 2004). The most efficient internalization with high uptake rates was demonstrated for 50 nm nanoparticles by S.-H. Wang et al. (2010). Uptake was shown to decrease for both smaller and larger particles.

- *Escape from the endo-lysosomal pathway:* Endosome maturation involves gradual acidification and eventual fusion of late endosomes with lysosomes, where cargo is degraded by lysosomal enzymes at pH 4.5 to pH 5 (Ohkuma and B. Poole 1978; Pei and Buyanova 2018). Endosomal escape has been described as very inefficient for most non-viral gene delivery systems, with only $\approx 1\%$ of the cargo released (Gilleron et al. 2013; Rehman et al. 2013). Several theories regarding nanoparticle escape from the endosomal pathway have been postulated and refined over the years, as reviewed by Winkeljann et al. (2023). The most influential one is the proton sponge theory introduced by Behr (1997). It claims that the presence of polycationic structures in the endosomes prevents the pH from dropping due to their buffering capacity. The proton pumps counteract this buffering effect by maintaining the influx of protons into the endosomal lumen. This is followed by a passive influx of chloride ions to maintain charge equilibrium. The increased osmotic gradient leads to the uptake of water, resulting in increased osmotic pressure, which ultimately leads to the collapse of the endosomal membrane. Recent evidence suggests that in addition to this osmotically induced membrane burst, sterically induced membrane disruption and escape via (ir)reversible membrane hole formation induced by the interaction between the nanoparticles and the endosomal membrane may also play a role (Bus et al. 2018; Vermeulen et al. 2018).
- *Nuclear entry:* The use of pDNA vectors requires their transcription into messenger ribonucleic acid (mRNA) to exert their effect. Passive diffusion through nuclear pore complexes located in the nuclear envelope has an upper cut-off of 5 nm in diameter or 40 kDa in size (Knockenbauer and Schwartz 2016; Musser and Grünwald 2016), so this mechanism is not relevant for nuclear entry of pDNA molecules. Receptor-mediated transport, which allows translocation of much larger molecules, requires nuclear localization signals (Dingwall et al. 1982; Nigg 1997; Zanta et al. 1999). Haraguchi et al. (2021) demonstrated that foreign DNA is incorporated into the nucleus during nuclear envelope reassembly in the telophase of mitosis. Thus, in absence of nuclear localization signals, cell division is a prerequisite for successful transfection of pDNA (C. Wang et al. 2023).
- *Ribosomal translation of mRNA into effector protein.*

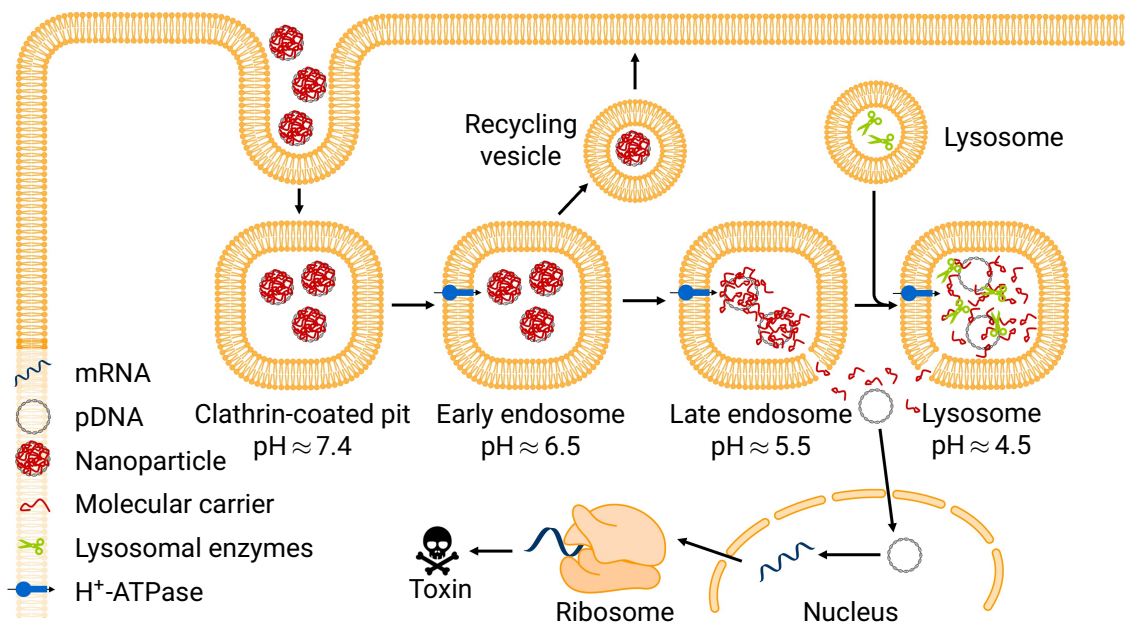


Figure 1.1: Schematic illustration of gene expression upon transfection of a pDNA vector encoding a toxin, including cellular internalization via endocytosis and subsequent trafficking via the endo-lysosomal pathway, endosomal escape, nuclear entry, transcription and translation into a cytotoxic protein.

The requirements for the pDNA vector and the molecular carrier as the two components of a non-viral gene delivery vehicle are presented below.

1.1.2.1 Plasmid DNA Vectors

As double-stranded (ds) circular DNA molecules, pDNA is a relatively stable nucleic acid compared to, for example, mRNA. Traditional pDNA vectors of bacterial origin carrying the transgene of interest can be designed, created, modified, and produced in large quantities by amplification in bacteria at low cost using molecular biology techniques. There is no theoretical limit to the size of the transgene to be integrated, although transformation efficiency decreases with increasing plasmid size (Chan et al. 2002).

Traditional pDNA vectors share canonical plasmid backbones ≥ 2.7 kb that combine the promiscuous pUC¹ origin of replication (ORI), ensuring high copy number propagation in *Escherichia coli* (*E. coli*), and antibiotic resistance-encoding genes, ensuring selection of successfully transformed bacteria for propagation. This bacterially derived pDNA backbone not only mediates the immunogenicity of pDNA vectors due to the presence of unmethyl-

¹plasmid University of California

lated CpG motifs (Hemmi et al. 2000), but also contributes to transgene silencing by heterochromatin formation on unexpressed plasmid backbones (Riu et al. 2007; Suzuki et al. 2006). Lu et al. (2012) showed that transgene silencing depends on the extragenic spacer length between the 5'- and 3'-ends of the eukaryotic transgene expression cassette. Long spacers of ≥ 1 kb in length led to silencing of transgene expression, whereas shorter spacers of ≤ 500 bp did not.

The presence of antibiotic resistance-encoding genes in conventional pDNA vectors is another disadvantage that is considered undesirable by regulatory agencies (EMA 2018; FDA 2007) due to the risk of horizontal gene transfer of antibiotic resistance-encoding genes to the endogenous microbial flora. In addition, the use of antibiotics in the pDNA production process requires extensive measures and process validation to ensure the absolute absence of residual antibiotics in the final product (Luke et al. 2010).

The described disadvantages of conventional pDNA vectors have been addressed by the development of optimized pDNA vector systems. Here, the design and production of the minimalized minicircle DNA (mcDNA) and Nanoplasmid™ (NP) vectors are particularly noteworthy. Both vectors have a significantly reduced bacterial backbone and do not contain antibiotic resistance-encoding genes, resulting in a considerably reduced size.

McDNA is produced in a specialized *E. coli* system from a precursor plasmid that allows for separation and recircularization of the bacterial backbone and the DNA fragment containing the gene of interest by recombinases at specific recognition sequences on the precursor plasmid. As a result of this recombination, the final mcDNA vector has a bacterial region of only 100 bp in size and does not encode any antibiotic resistance. However, the production process still requires the use of antibiotics and is associated with low manufacturing yields and the need to purify and isolate the produced mcDNA from the accompanying pDNA (Kay et al. 2010).

The NP technology relies on an RNA/RNA interaction to select successfully transformed bacteria, eliminating the need for antibiotics. The bacterial host strain expresses the SacB gene encoding levansucrase, an enzyme that catalyzes the formation of toxic fructose polymers from sucrose. Successfully transformed bacterial cells express an RNA-OUT sequence that inhibits levansucrase expression by annealing to the complementary sequence in the mRNA. This allows the selected bacteria to survive and propagate in the presence of sucrose. In addition, the NP vectors have the commonly used pUC ORI replaced with the much smaller R6K ORI, which is also of bacterial origin. This reduces the backbone size to ≤ 500 bp, which minimizes transgene silencing. It also provides an additional safety feature because NP vectors can only replicate within the genetically engineered, heat-inducible R6K replication protein-encoding *E. coli* host strain that is used for production. This substantially reduces the risk of horizontal gene transfer *in vivo*. By reducing the backbone size below the 500 bp threshold while maintaining the conventional pDNA amplification strategy in *E. coli*, the NP technology retains the high yield and robust manufacturing process and benefits from the reduced transgene silencing seen with mcDNA vectors (Williams and Paez 2023).

There are several advantages to using nucleic acids rather than the proteins they encode for. Even on a large scale, the production and purification of pDNA is less expensive and time-consuming and nucleic acids are significantly less immunogenic even after multiple administrations. With respect to therapeutic use in cancer, the synthesis of cytotoxic proteins by and in the target cell means that smaller amounts of protein are sufficient to induce cell death (Vago et al. 2016).

Gene therapeutic approaches for cancerous diseases include suicide gene therapy. Here, the aim is to introduce pDNA vectors into the degenerated cells, whose translation into the effector protein leads to cell death, either directly in the case of toxin-based gene therapy or by converting a non-toxic prodrug into a cytotoxic substance in the case of gene-directed enzyme product therapy (Duarte et al. 2012; Navarro et al. 2016; Vassaux and Martin-Duque 2004).

Among the large number of cytotoxic proteins suitable for toxin-based gene therapy, bacterial toxins and the group of ribosome-inactivating proteins (RIPs) are described best. Bacterial toxins such as Diphtheria toxin and Pseudomonas exotoxin A belong to the family of mono-ADP-ribosyl transferases. Their catalytic domain inactivates the eukaryotic elongation factor 2 by ADP-ribosylation. RIPs belong to the N-glycosylase family of toxins and can be divided into two classes. Type I RIPs, such as saporin from *Saponaria officinalis* L. or agrostin from *Agrostemma githago* L., are single-chain proteins consisting only of the N-glycosylase domain. Type II RIPs, such as ricin from *Ricinus communis* L., contain an additional galactose-binding lectin moiety (B-chain) that mediates the transfer of the enzymatically active A-chain across the plasma membrane. This leads to a much higher toxicity of type II RIPs. RIPs exert their cytotoxic effect by depurination of a specific adenine base in the universally conserved sarcin-ricin-loop in ribosomal RNA, which results in the ribosome losing its ability to bind the eukaryotic elongation factor 2. Through different pathways, both toxin families cause irreversible cessation of protein synthesis, resulting in cell death. These toxin-based gene therapy approaches act in a cell cycle-independent manner, making it possible to treat aggressive cancers with rapidly dividing cells as well as tumors with slower progression (Vago et al. 2016; Weise et al. 2020; Weng et al. 2012).

Gene-directed enzyme prodrug therapy involves a two-step-process. First, cancer cells are transfected with a gene that is encoding an enzyme that is itself non-toxic. Then, when a non-toxic prodrug is administered, that is converted by this enzyme to its toxic metabolite, the cells die (Portsmouth et al. 2007). Since its first description by Moolten (1986), several enzyme/prodrug combinations have been described and studied. Among the most studied is the combination of herpes simplex virus thymidine kinase with ganciclovir and the enzyme/prodrug system cytosine deaminase/5-fluorocytosine (Malekshah et al. 2016). A critical element that is considered responsible for the success of gene-directed enzyme prodrug therapy over corrective and toxin-based gene therapy is the so-called bystander effect. The local bystander effect refers to the spread of the cytotoxic effect of a drug from transduced cells to surrounding non-transduced cells in the so-called killing zone. This observation is explained either by the diffusion of small activated prodrug molecules toward

the tumor core through gap junctions or by the endocytosis of apoptotic vesicles released from dying cells by neighboring untransfected cells. In addition, a distant bystander effect is described that is immune-mediated and applies to both toxin-based gene therapy and gene-directed enzyme product therapy. Here, tumor cell death results in the release of tumor-associated antigens that activate the immune system and lead to a systemic immune response at the metastatic sites (Ardiani et al. 2012; Engelmann et al. 2002; Freeman et al. 1993; Xiao et al. 2013).

1.1.2.2 Molecular Carriers

Due to the large number of molecular carriers used for the complexation of nucleic acids, only selected examples are introduced below.

Lipid nanoparticles (LNPs), spherical particles prepared from a mixture of (ionizable) lipids incorporating nucleic acids in their core, are the most advanced non-viral gene delivery system as demonstrated by approved RNA-based therapeutics using LNPs (Yang et al. 2023). As carriers of pDNA, LNPs have demonstrated high delivery efficiencies (Cui et al. 2022; Zhu et al. 2022) and adequate nucleic acid encapsulation efficiencies ranging from 60 % to 90 % (Cui et al. 2022; Ripoll et al. 2022). Nevertheless, liver tropism due to association with apolipoprotein E after intravenous (i.v.) administration (Francia et al. 2020) limits their systemic use to hepatocyte-targeting applications.

Another widely studied approach are *polymer-based delivery systems*. Here, cationic polymers such as poly-L-lysine (PLL) and polyethylenimine (PEI) or dendrimers such as poly(amidoamine) (PAMAM) are used to complex pDNA. The electrostatic interaction between the anionic phosphate backbone of the pDNA and the cationic functional groups of the polymers results in the formation of polymeric nanoparticles, hereafter referred to as nanoplexes. The advantages of these nanoplexes include their low immunogenicity and high packing capacity. Furthermore, they are easy to manufacture, even on a large scale, and modifications for optimized biodistribution, stability, and physicochemical properties are relatively easy to implement compared to viral vectors (Sahu et al. 2023; Sayed et al. 2022).

Protonated amino nitrogen atoms present in all these polymers are essential for the electrostatic interaction with pDNA at physiological pH. Apart from this commonality, the polymers differ in their protonation state at physiological pH, the presence of ionizable groups at acidic pH values, linear or branched structure, charge density and biodegradability (Figure 1.2).

Higher gene transfection efficiencies are obtained with high molecular weight PEI (20 kDa to 30 kDa), high generation PAMAM (increasing number of protonatable amino groups with increasing generation), and modifications of PLL that introduce endosomolytic groups, such as histidine residues. These polymers have pK_a values in the physiological range, indicating the presence of ionizable groups in the acidic environment of the endo-lysosomal pathway. This results in a high buffering capacity within the endosome, so the increase in

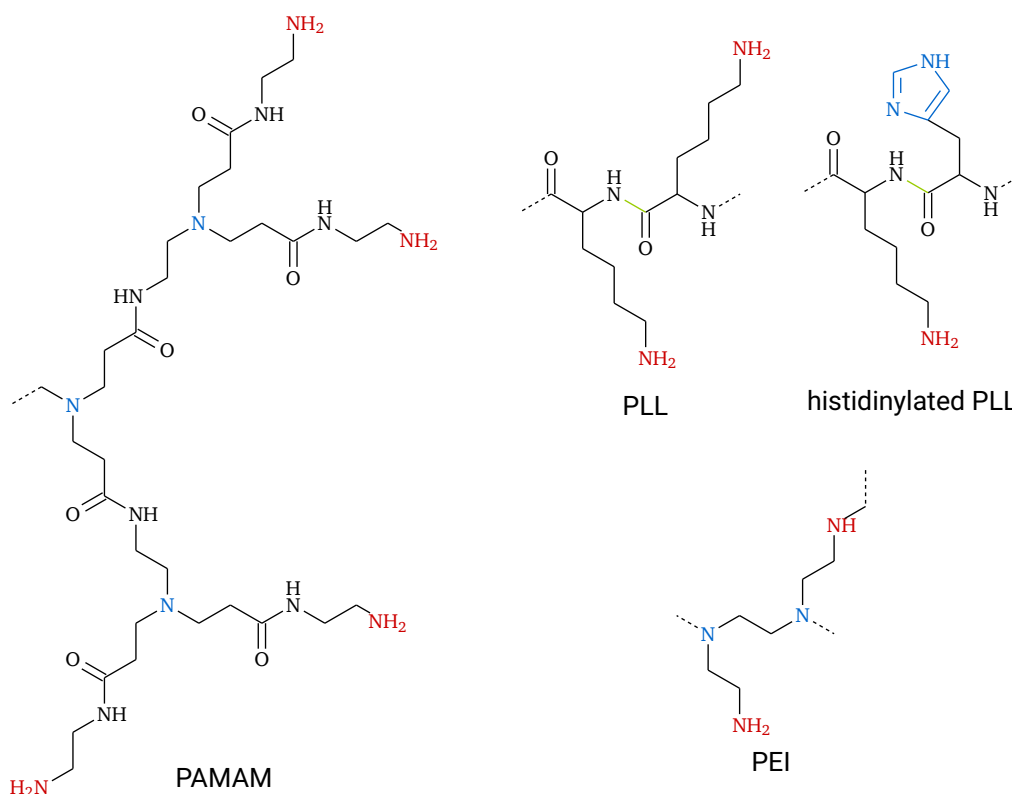


Figure 1.2: Structural formulas of polymeric molecular carriers PAMAM, PEI, unmodified and histidinylated PLL used for nanoplex formation. Functionalities responsible for electrostatic interaction at physiological pH are highlighted in red, blue denotes groups that are ionized at acidic pH and green bonds in the PLL structure indicate biodegradability.

transfection efficiency can be attributed to the described proton sponge mechanism (Section 1.1.2). Unfavorably, the endosome disruption properties are associated with increased toxicity due to cell membrane damage and apoptosis, leading to the dilemma of finding a balance between sufficient efficiency and tolerable toxicity of the polymeric molecular carrier (Horn and Obermeyer 2021; Mintzer and Simanek 2008; Pahle and Walther 2016; Yin et al. 2014; Zhou et al. 2017).

Compared to PAMAM and PEI, PLL is characterized by its inherent biocompatibility and biodegradability, low immunogenicity and high water solubility. Due to its complete protonation at physiological pH (pK_a of the side chain ≈ 9.0), native PLL has no buffering capacity in the acidic pH range of the endo-/lysosomal pathway, which results in low transfection efficiency, but also in reduced toxicity compared to PAMAM and PEI. As a polypeptide, PLL can be produced by conventional solid-phase peptide synthesis, even on a large scale, in a reproducible quality, and is easy to modify. Additional functionalities can

be implemented by introducing other amino acids or by derivatizing the primary amino groups in the lysine side chains. A common derivatization is polyethylene glycol (PEG) conjugation, i.e. PEGylation, which has been described to reduce cytotoxicity and non-specific association of serum proteins with PLL by shielding the positive charge (Schöttler et al. 2016; Zhang et al. 2014). However, recent studies have shown an increasing prevalence of anti-PEG-antibodies, which counteract the intended stealth effect of PEGylation by accelerating blood clearance (Deuker et al. 2023; Hong et al. 2020).

Summary

- Successful therapeutic application of nucleic acids requires their incorporation into gene delivery vectors. Non-viral and viral vectors can be employed.
- There are several approved gene therapeutics from the class of viral vectors, integrating viral vectors for *ex vivo* transduction of autologous cells and adeno-associated virus-based vectors for one-time therapy of monogenic diseases. Viral vectors are very effective in gene delivery, but their strong immunogenicity and complicated and expensive production are drawbacks of their use.
- Non-viral gene delivery vehicles consist of plasmid DNA (pDNA) vectors encoding the transgene and molecular carriers such as lipids or cationic polymers that package and incorporate the nucleic acid. Non-viral gene delivery is significantly less efficient than viral approaches, mainly due to endosomal entrapment and degradation of the therapeutic cargo. The advantages of non-viral gene delivery vehicles include low immunogenicity, ease of modification of both pDNA vectors and molecular carriers, and significantly lower production costs.
- Minicircle DNA and Nanoplasmid™s are optimized pDNA vectors exhibiting smaller size, no antibiotic resistance-encoding genes, and a greatly reduced bacterial backbone.
- Poly-L-lysine is a polycationic polymer used for non-viral gene delivery due to its high nucleic acid encapsulation efficiency, biocompatibility and biodegradability, low toxicity and immunogenicity, flexibility in modification, and affordable manufacturing.

1.2 Sapofection - Overcoming Endosomal Entrapment for Efficient Gene Delivery

A synergistic toxic effect of type I RIPs with triterpenoid saponins biosynthesized by the same plant was first described by Hebestreit and Melzig (2003). Triterpenoid saponins are

naturally occurring glycosides consisting of a lipophilic triterpenoid (C₃₀) aglycone and one or two hydrophilic sugar moieties. Based on the number of sugar chains, monodesmosidic and bidesmosidic saponins are distinguished.

Weng et al. (2012) showed that the mechanism behind the observed increased toxicity is an enhancement of the endosomal escape, i.e. the release of the incorporated RIPs from late endosomes/lysosomes by the saponins, hence termed endosomal escape enhancers (EEEs). With SA1641 and SA1657 from *Gypsophila paniculata* L. (Weng et al. 2012), GE1741 from *Gypsophila elegans* M. Bieb. (Sama et al. 2018a), SO1861 from *Saponaria officinalis* L. (Sama et al. 2017) and AG1856 from *Agrostemma githago* L. (Clochard et al. 2020), all plants belonging to the Caryophyllaceae family, several endosomal escape-enhancing (eee) triterpenoid saponins have been isolated, identified and characterized.

Melzig et al. (2005) identified the presence of an aldehyde group at C-4², a sugar chain at C-3, and an oligosaccharide ester chain at C-28 of the aglycone gypsogenin or quillaic acid as necessary structural features for the eee effect. Further structure-activity relationship studies revealed a branched sugar chain at C-3 (Bachran et al. 2006) including a glucuronic acid, a molecular weight ≥ 1600 g/mol, and a branched oligosaccharide (≥ 4 sugars) at C-28 including derivatives like deoxy sugars and acetyl groups (Böttger et al. 2013) to exert a beneficial effect on endosomal release. Sama et al. (2019) further specified the substitution pattern in the C-28 sugar chain to be preferably lipophilic at the C-28 fucose and hydrophilic at the C-28 xylose. The eee-promoting features mentioned above are shown in Figure 1.3 as an example for SO1861.

Using the described triterpenoid saponins to enhance gene delivery was first described by Weng et al. (2015). *In vitro*, significantly higher transfection efficiencies were observed when a solution of the eee saponin was applied together with nanoplexes made of PEI, PLL or PAMAMs, without increased levels of toxicity. The escape of the entrapped gene-loaded nanoplexes from endosomes was facilitated by the co-application of saponins, which is a prerequisite for efficient gene delivery to the nucleus. Sama et al. (2017) introduced the term sapofection for this saponin-assisted transfection. Its therapeutic potential was also demonstrated *in vivo* in an aggressively growing murine neuroblastoma model. Treatment with targeted peptide-based nanoplexes that delivered pDNA encoding saporin in combination with SO1861 resulted in a significantly higher anti-tumor effect than treatment with the described nanoplexes alone, and the therapy was shown to be well tolerated (Sama et al. 2018b). Compared to SO1861 and GE1741, we recently demonstrated increased eee activity *in vitro* with significantly reduced toxicity *in vitro*

²In the literature, this aldehyde group is sometimes referred to as the aldehyde group at C-23. In the context of this dissertation, the naming follows the IUPAC-IUB Joint Commission on Biochemical Nomenclature (1989) guidelines, according to which the carbon atom should not be specified twice (the aldehyde group contains C-23).

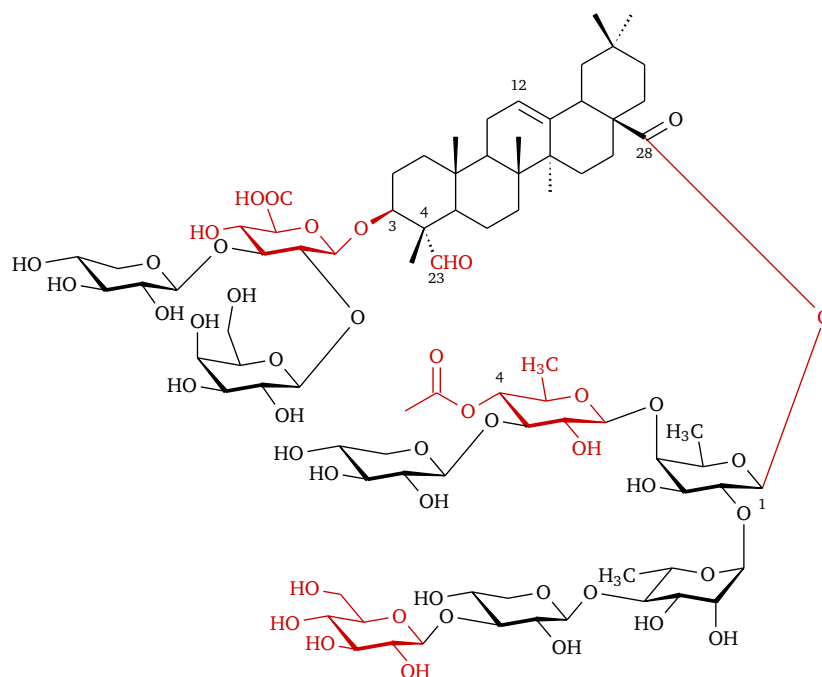


Figure 1.3: Structural formula of SO1861. Endosomal escape-enhancing structural characteristics are highlighted in red. The red color of the covalent linkage between the sugar chain and the aglycone refers to the presence of the entire sugar chain, which is beneficial for the endosomal escape enhancing performance.

(Clochard et al. 2020)³ and *in vivo* for AG1856 (Mitdank et al. 2022)⁴.

To date, gene-loaded nanoplexes and the above-mentioned eee saponins have been administered separately with the goal of achieving appropriate concentrations of both components at the target tissue simultaneously. *In vitro*, this is easily achieved by adding both components in parallel to the cell culture medium. *In vivo*, however, harmonizing the routes of administration has proven to be more challenging. I.v. injection of saponins led to massive hemolysis (Gilabert-Oriol et al. 2013), so these were applied subcutaneously (s.c.) to the nuchal fold of mice. The nanoplexes were injected i.v. into the tail vein 1 h later (Mitdank et al. 2022; Sama et al. 2018b). Detailed pharmacokinetic studies of the i.v. injected nanoplexes and the s.c. injected saponin are not available.

³Clochard, J., Jerz, G., Schmieder, P., Mitdank, H., Tröger, M., Sama, S., Weng, A. A new acetylated triterpene saponin from *Agrostemma githago* L. modulates gene delivery efficiently and shows a high cellular tolerance.

⁴Mitdank, H., Tröger, M. (Authors contributed equally), Sonntag, A., Shirazi, N. A., Woith, E., Fuchs, H., Kobelt, D., Walther, W., Weng, A. Suicide nanoplastids coding for ribosome-inactivating proteins.

Summary

- Specific triterpenoid saponins enhance endosomal release of cargo entrapped in the endo-/lysosomal pathway. As a result, they increase the toxicity of cytotoxic proteins and the transfection efficiency of non-viral gene delivery vehicles, where endosomal entrapment is an efficacy-limiting obstacle.
- To exert their endosomal escape-enhancing effect, the presence of an aldehyde group at C-4 and two branched sugar chains at C-3 and C-28 of the aglycone are necessary. Incorporation of a glucuronic acid in the C-3 sugar chain, a molecular weight ≥ 1600 g/mol and lipophilic modifications in the C-28 sugar chain are beneficial for endosomal release.
- Saponin-assisted transfection was termed sapofection. To date, it involves separate administration of the endosomal escape enhancer and the gene delivery vehicle, which requires complicated harmonization of the two components, particularly with respect to *in vivo* pharmacokinetics.

1.3 Targeted Gene Delivery

Targeted delivery of the nanoplexes' cargo is crucial for therapeutic efficacy. This is especially true for cancer suicide gene therapy which aims to kill successfully transfected cells. Ideally, therapeutic transgenes are selectively delivered to cancer cells and the cytotoxic protein is expressed exclusively in the target cells, resulting in high concentrations in the cancer tissue while minimizing the impact on healthy tissue (Karjoo et al. 2016; Malecki 2012).

The so-called enhanced permeability and retention (EPR) effect, i.e. the accumulation of macromolecules or nanoparticles in tumor tissue due to its vascular hyperpermeability and lack of lymphatic drainage, is described to be responsible for selective delivery to tumor cells (Danaei et al. 2018; Maeda et al. 2013; Subhan et al. 2023). The EPR effect is well documented in small animals, but the lack of clinical efficacy of nanomedicines suggests little, if any, EPR effect for the targeted delivery of nano-sized drugs in human cancers (Danhier 2016; Nichols and Bae 2014). Thus, in addition to passive targeting by EPR, active targeting is critical for the therapeutic success. Ligands shall interact selectively with their specific receptor or epitope expressed on the target cells leading to the uptake of the payload. Ideally, targeting ligands accumulate in pathologic tissue, exhibit a high binding affinity and specificity for their target and do not reside persistently in the bloodstream or in the organs (Vago et al. 2016). Small chemical drug-derived compounds, antibodies, carbohydrates, vitamins, and small peptides to large proteins are among the substance classes that are researched as targeting molecules (Steffens and Wagner 2022).

Natural ligands such as transferrin, epidermal growth factor (EGF) or folic acid are used

for targeting of cancerous tissue due to the overexpression of their respective receptors (Vetter and Wagner 2022). In addition to natural ligands, peptide sequences derived from these can also mediate successful targeting. One example is the targeting peptide GE11, which is specific for the epidermal growth factor receptor (EGFR). GE11 was identified by phage display and its use as a targeting ligand resulted in transfection efficiencies comparable to those achieved by targeting with the natural ligand EGF (Z. Li et al. 2005). Among tumor-targeting peptide sequences, another prominent example is the integrin-binding motif arginine-glycine-aspartic acid (RGD) identified by Arap et al. (1998). This peptide motif binds selectively to integrin $\alpha v \beta 3$ receptors, which are predominantly expressed on tumor cells and vasculature. Another example of the large group of targeting peptides is peptide Y (pepY), which has been successfully used by Mitdank et al. (2022) and Sama et al. (2018b) for targeted delivery to the murine neuroblastoma cell line Neuro-2a using the two-component sapofection approach, both *in vitro* and *in vivo*. PepY has been shown to mediate targeted delivery of nucleic acids to cells of neuronal origin (Tagalakis et al. 2011, 2013), human airway epithelium cells (Manunta et al. 2011; Tagalakis et al. 2008), primary vascular cells (Irvine et al. 2008), and rabbit aorta cells (Meng et al. 2013). Transfection was shown to occur via a receptor-mediated mechanism, although the identity of the targeted receptor remains unclear (Writer et al. 2004). PepY consists of a DNA-complexing K_{16} -tail, a GA-spacer and the targeting sequence YGLPHKF, which is cyclized by oxidation of two flanking cysteine residues (Writer et al. 2004). As another class of agents, tumor-targeting antibodies such as cetuximab, panitumumab or trastuzumab, which are approved for clinical use, are being investigated for their suitability as targeting ligands for gene delivery vehicles and toxins (Abedin et al. 2021; Dash et al. 2023; Dziawer et al. 2019; Lin et al. 2018; Patel et al. 2018).

Gene therapy approaches offer the advantage of additional transcriptional targeting. If the transgenes are under control of a target-specific promoter such as the H19 promoter, which is activated in cancer cells but silenced in normal healthy cells, the probability of off-target toxicity decreases, as erroneously delivered transgenes remain inactive. Unfavorably, the target-specific promoters identified and investigated to date have low activity compared to the optimized enhancer and promoter sequences in commonly used pDNA vectors, resulting in reduced therapeutic efficacy (Dorer and Nettelbeck 2009; Yao et al. 2011).

Summary

- Targeted delivery of the toxic therapeutic cargo is especially crucial for the treatment of cancer to minimize undesired impact on healthy tissue.
- The most studied tumor-targeted ligands include natural protein ligands, vitamins, small targeting peptides, and monoclonal antibodies.

Research Objective

The aim of the present thesis was to develop and optimize a targeted non-viral gene delivery vehicle consisting of

- a plasmid DNA vector,
- a polymeric molecular carrier,
- the endosomal escape-enhancing triterpenoid saponin SO1861, and
- a targeting ligand.

This gene delivery vehicle shall exhibit

- efficient and stable nucleic acid complexation,
- appropriate size, size distribution and surface charge,
- high transfection efficiency *in vitro* and *in vivo*,
- good tolerability *in vitro* and *in vivo*, and
- selective delivery to targeted tissues.

It shall consist of a single component-formulation that is safe and effective upon systemic administration via intravenous injection.

1.4 Chemical Strategy

The work on this thesis was carried out as part of the ENDOSCAPE⁵ project. The fundamental chemical strategy presented below was developed by Prof. Fernandez-Megia (CiQUS, Universidade de Santiago de Compostela), Ruben Postel (Sapreme Technologies) and Prof. Fuchs (Institut für Laboratoriumsmedizin, Klinische Chemie und Pathobiochemie, Charité – Universitätsmedizin Berlin) and served as a guardrail for the work on this thesis.

For the envisioned linkage of the components nucleic acid, EEE, and targeting ligand, a linear polypeptide was selected as the central element of the one-component formulation. The polypeptide, in the following referred to as peptide scaffold, was envisaged to contain a poly-L-lysine (PLL)-segment to provide efficient complexation of the pDNA vector. The installation of specific functional groups in the peptide scaffold were proposed for the conjugation of SO1861 and the ligand via click chemistry.

⁵A cross-institutional biotechnology project aiming for the development of a clinically applicable gene delivery technology using SO1861.

Click chemistry reactions as defined by Kolb et al. (2001) are characterized by their modularity, high chemical yields achieved by a high thermodynamic driving force, simple reaction conditions (ideally insensitivity towards oxygen and water), stereospecificity, readily available starting materials and reagents, use of benign solvents and generation of only benign byproducts, and simple product isolation. They are now routinely used in a variety of applications, which was rewarded with the 2022 Nobel Prize in Chemistry (Nobel Prize Outreach AB 2022). These features make click chemistry reactions the optimal choice for functionalizing the peptide scaffolds without the need for sophisticated reaction setups.

To ensure intracellular release of the EEE, its conjugation to the peptide scaffold was sought via a hydrazone linkage known for its rapid hydrolysis in the acidic endo- and lysosomal compartments of cells (Bouchard et al. 2014; Greenfield et al. 1990). The hydrazone functionality was envisaged to be introduced by the reaction of the hydrazide group of the bifunctional *N*- ϵ -maleimidocaproic acid hydrazide (EMCH)-linker with the aldehyde group at C-4 of SO1861. Subsequently, SO1861-EMCH was planned to be covalently conjugated to the peptide scaffold by means of a Michael-type addition of EMCH's maleimide group to a thiol group introduced in the peptide scaffold resulting in a stable thioether bond. The use of the acid-sensitive EMCH-linker has been described for the preparation of Doxorubicin-EMCH, either as intermediate for the preparation of immunoconjugates (Willner et al. 1993) or as i.v. injectable drug termed Aldoxorubicin (Kratz et al. 2002). In both cases, adequate stability of the hydrazone linkage at pH 7.0 and rapid cleavage at pH < 5.0 was demonstrated.

A strain-promoted azide-alkyne-cycloaddition (SPAAC) was chosen for the bioconjugation of a protein as targeting ligand to the peptide scaffold. This bioorthogonal click chemistry reaction represents an evolution of the copper(I)-catalyzed [3 + 2] cycloaddition of an azide with an alkyne forming a stable triazole bond. The alkyne is activated by ring strain, eliminating the need for toxic catalysts (Agard et al. 2004). Functionalizing the targeting ligand with a dibenzocyclooctene (DBCO) group (Debets et al. 2010) will introduce the activated alkyne to react with the azide group incorporated into the peptide scaffold.

Summary

- For the realization of the research objective, the development and optimization of a polypeptide molecular carrier consisting of a DNA-complexing poly-L-lysine-motif, a thiol group for SO1861-EMCH conjugation, and an azide functionality for bioconjugation of a targeting ligand was envisaged.
- The conjugation of SO1861-EMCH and the targeting ligand was intended to occur via a thiol-maleimide Michael-type addition and a strain-promoted azide-alkyne-cycloaddition, respectively.

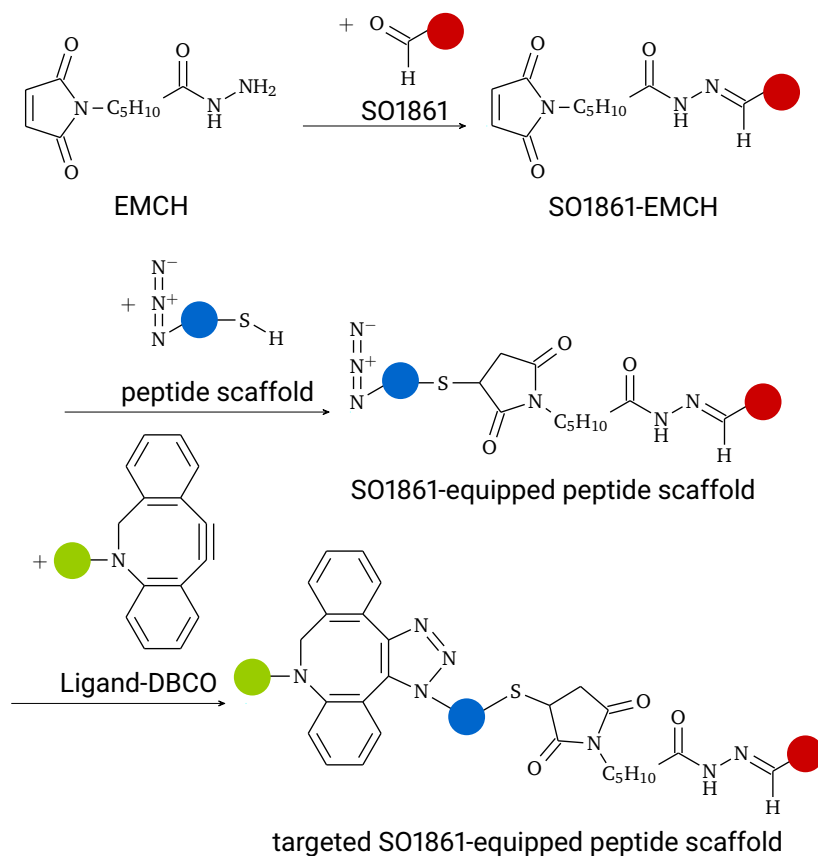


Figure 1.4: Suggested chemical strategy for the preparation of targeted, SO1861-equipped peptide scaffolds. The colored circles serve as placeholders for the parts of the respective molecules that are not crucial in this case. The aldehyde group of SO1861 reacts with the hydrazide of EMCH forming a hydrazone. A thiol group introduced in the peptide scaffolds reacts in a Michael-type addition with the maleimide of SO1861-EMCH to form the stable thioether bond of the SO1861-equipped peptide scaffold. Finally, the azide functionality of the peptide scaffold reacts in a SPAAC with the DBCO group previously introduced to the targeting ligand.

2 Materials

The following tables list all materials used for the work presented in this thesis. The manufacturers are indicated in the right-hand column, with the manufacturer applying to all subsequent entries unless otherwise stated.

2.1 Chemicals

SO1861 functionalized with an *N*- ϵ -maleimidocaproic acid hydrazide (EMCH)-linker (in the following referred to as SO1861-EMCH) was supplied within the ENDOSCAPE-Project by Sapreme Technologies (the Netherlands).

Ultrapure ($\sigma \leq 0.055 \mu\text{S}/\text{cm}$) water was constantly provided by the LaboStar™ ultrapure water system (Siemens AG, Germany) and collected as needed.

2.1.1 Molecular Biology

Water for biotechnology nuclease-free, sterile	VWR (USA)
Phusion™ High-Fidelity (HF) DNA Polymerase	Thermo Fisher Scientific (USA)
5X Phusion™ HF Buffer	
10 mM dNTPs	
Restriction Endonucleases AatII, NheI-HF, SalI-HF, SpeI-HF, & XbaI-HF	New England Biolabs (USA)
CutSmart® Buffer 10X	
T4 DNA Ligase	
T4 DNA Ligase Buffer 10X	
Gel Loading Dye, Purple 6X	New England Biolabs (USA)
Quick-Load® Purple 1 kb Plus DNA Ladder	
Agarose, DNA grade	VWR (USA)
Ethidium bromide solution 0.5 %	Carl Roth GmbH + Co. KG (Germany)
Invitrogen™ S.O.C. Medium	Thermo Fisher Scientific (USA)
LB Broth (Luria/Miller), granulated	Carl Roth GmbH + Co. KG (Germany)
Terrific-Broth modified	
LB Broth with agar (Lennox)	Sigma-Aldrich (USA)
Kanamycin sulfate, molecular biology grade	SERVA Electrophoresis GmbH (Germany)
Ampicillin sodium salt, BioScience grade	Carl Roth GmbH + Co. KG (Germany)
Glycerol from plant, Ph. Eur.	SERVA Electrophoresis GmbH (Germany)

2.1.2 Polyacrylamide Gel Electrophoresis

Acrylamide/Bis Solution 37.5:1 (30 % w/v, 2.6 % C)	SERVA Electrophoresis GmbH (Germany)
Ammonium persulfate, electrophoresis grade	
Ammonium sulfate, $\geq 99\%$, cryst.	Carl Roth GmbH + Co. KG (Germany)
Brilliant blue G 250 (C.I. 42655)	
L-Histidine CELLPURE [®] $\geq 99\%$	
<i>N,N,N',N'</i> -Tetramethyl-ethylenediamine	SERVA Electrophoresis GmbH (Germany)
Phosphoric acid 85 %	VWR (USA)

2.1.3 Cell Culture

Dulbecco's modified Eagle's medium (DMEM) with 4.5 g/L glucose without L-glutamine	Lonza Group (Switzerland)
DMEM with 1.0 g/L glucose without L-glutamine	
Dulbecco's phosphate-buffered saline, without Ca ²⁺ or Mg ²⁺ (DPBS)	
UltraGlutamine [™] I Supplement	
MEM Eagle Non-essential Amino Acid Solution (100X)	
Trypsin/EDTA (0.5 g/L trypsin 1:250, 0.2 g/L EDTA)	
Gibco [™] McCoy's Modified 5A Medium	Thermo Fisher Scientific (USA)
FBS Superior	Bio&SELL GmbH (Germany)
Dimethyl sulfoxide, BioScience grade	Carl Roth GmbH + Co. KG (Germany)
2-Propanol	Sigma-Aldrich (USA)

2.1.4 Peptides

All peptides were acquired as custom synthesis with $\geq 80\%$ purity from GeneCust (France). Table 2.1 lists the acronyms and sequences of all peptides that were used. The C-terminus of all peptides was amidated to increase the stability of the peptide and minimize its tendency to absorb moisture.

Peptides were received in lyophilized state and completely dissolved in ultrapure, sterile-filtered water to avoid weighing inaccuracies. Aliquots of peptides K₁₆C and K₁₆CPEG were snap frozen in liquid nitrogen and then subjected to lyophilization to minimize cysteine oxidation. All other peptides were stored in aliquots at $-20\text{ }^{\circ}\text{C}$.

2.1.5 Nucleid Acids

Table 2.2 lists all pDNA vectors used within this thesis.

Table 2.1: Peptide acronyms, sequences and molecular weights. All peptide sequences are given from N- to C-terminus. C-terminus was amidated. K(N₃) indicates an azidolysine, a lysine that is modified to carry an azide functionality instead of the amino group in the residue.

Acronym	Peptide Sequence	Molecular Weight
K ₁₆	K ₁₆	2 067.8
K ₁₆ C ₃	K ₁₆ CGCGCGK(N ₃)	2 703.6
K ₁₆ C ₃ PEG	K ₁₆ CGCGCG-PEG ₈ -K(N ₃)	3 126.1
K ₁₆ C	K ₁₆ G ₄ CG ₂ YK(N ₃)	2 830.6
K ₁₆ CPEG	K ₁₆ G ₄ CG ₂ Y-PEG ₈ -K(N ₃)	3 254.1
FITC-K ₁₆	FITC-K ₁₆	2 571.4
pepY	K ₁₆ GACYGLPHKFCG	3 302.2

Table 2.2: Plasmid DNA vectors, their acronyms and sources. Minicircle DNA vectors (indicated by the prefix MC in the abbreviation) were prepared from their respective parent plasmids listed in the following row.

Acronym	Vector Name	Source
pEGFP-N3	pEGFP-N3	Amplification in DH5 α - <i>E. coli</i> & kit-based preparation
NP-eGFP	NTC9385R-EGFP-BGH pA	Nature Technology Corporation (USA)
NP-Sap	NTC9385R-Sap-BGH pA	Nature Technology Corporation (USA)
NP-Luc	NTC9385R-Luc-BGH pA	Nature Technology Corporation (USA)
	MN601A1	System Biosciences (USA); amplification in ZYCY10P3S2T- <i>E. coli</i> & kit-based preparation
MC-GFP		Amplification in ZYCY10P3S2T- <i>E. coli</i> & preparation as described in section 3.1.4
	CMV/eGFP/MN501A1	Produced by molecular cloning (see Section 3.1.3); amplification in ZYCY10P3S2T- <i>E. coli</i> & kit-based preparation
MC-CMV/eGFP		Amplification in ZYCY10P3S2T- <i>E. coli</i> & preparation as described in section 3.1.4
	HLP/eGFP/MN501A1	Produced by molecular cloning (see Section 3.1.3); amplification in ZYCY10P3S2T- <i>E. coli</i> & kit-based preparation
MC-HLP/eGFP		Amplification in ZYCY10P3S2T- <i>E. coli</i> & preparation as described in section 3.1.4
	pCDNA3-HLP-5'UTR-FIX	provided by Prof. Pinotti (Università degli Studi di Ferrara)

2.1.6 Miscellaneous

Acetic acid $\geq 99\%$				Carl Roth GmbH + Co. KG (Germany)
HEPES PUFFERAN [®] CELLPURE [®] $\geq 99.5\%$				
TAPS PUFFERAN [®] $\geq 99\%$				
Tris PUFFERAN [®] $\geq 99.3\%$ D-Mannitol low endotoxin, pure, pharma grade				AppliChem GmbH (Germany)
Acetonitrile (ACN) $\geq 99.9\%$, CHROMANORM [®]		HiPerSolv		VWR (USA)
Methanol (MeOH) $\geq 99.8\%$, CHROMANORM [®]		HiPerSolv		
QuantiFluor [®] dsDNA Dye				Promega GmbH (Germany)

2.2 Biomaterials

- ZYCY10P3S2T *E. coli* Minicircle Production Strain (System Biosciences, USA)
- Library Efficiency[™] DH5 α Competent Cells (Thermo Fisher Scientific, USA)

All cell lines used for the investigations presented in this thesis are listed in the Table 2.3 with their species and organ of origin.

Table 2.3: Cell lines used within this thesis, their origin according to the Cellosaurus database (Bairoch 2018, 2023) and source. ATCC[®] = American Type Culture Collection (USA), DMSZ = German Collection of Microorganisms and Cell Cultures GmbH (Germany), Invitrogen[®] is part of Thermo Fisher Scientific (USA).

Cell line	Species of origin	Disease/Derived from	Source
A2058	Homo sapiens	Amelanotic melanoma	ATCC [®] CRL-11147 [™]
A-431	Homo sapiens	Skin squamous cell carcinoma	ATCC [®] CRL-1555 [™]
HCT 116	Homo sapiens	Colon carcinoma	ATCC [®] CCL-247 [™]
HEK293-FT	Homo sapiens	Fetal kidney	Invitrogen [®] R70007
Hepa 1-6	Mus musculus	Mouse hepatocellular carcinoma	ATCC [®] CRL-1830 [™]
Huh-7	Homo sapiens	Adult hepatocellular carcinoma	ATCC [®] PTA-4583 [™]
ECV-304	Homo sapiens	Bladder carcinoma	DMSZ ACC 310
MDA-MB-468	Homo sapiens	Breast adenocarcinoma	ATCC [®] HTB-132 [™]
Neuro-2a	Mus musculus	Mouse neuroblastoma	DMSZ ACC 148

2.3 Kits

GeneJET Gel Extraction Kit	Thermo Fisher Scientific (USA)
ROTI [®] Transform	Carl Roth GmbH + Co. KG (Germany)
ZymoPURE Plasmid Miniprep Kit	Zymo Research (USA)
ZymoPURE Plasmid Midiprep Kit	
QIAGEN Plasmid Mega Kit	Qiagen N.V. (Netherlands)
Lipofectamine [™] 3000 Transfection Reagent	Thermo Fisher Scientific (USA)
CellTiter 96 [®] AQueous One Solution Cell Proliferation Assay (MTS)	Promega GmbH (Germany)
MycosPY [®] Master Mix - PCR Mycoplasma Test Kit	Biontix Laboratories GmbH (Germany)

2.4 Consumables

2.4.1 Cell Culture

Serological pipette, with tip, plugged, 2 mL, 5 mL, 10 mL & 25 mL, PS	SARSTEDT AG & Co. KG (Germany)
Cell culture flask, 50 mL, 25 cm ² , PS, filter screw cap, Cellstar [™] , TC, sterile	Greiner-Bio-One GmbH (Germany)
Cell culture flask, 250 mL, 75 cm ² , PS, filter screw cap, Cellstar [™] , TC, sterile	
Cell culture dish, PS, 35/10 mm, glass bottom, 4 compartments	
Cell culture multiwell plate, 24 well & 48 well, PS, clear, Cellstar [™] , TC, lid with condensation rings, sterile	
Cell culture microplate, 96 well, PS, F-bottom, clear, Cellstar [™] , TC, lid with condensation rings, sterile	
Cryo.s, 2 mL, PP, round bottom, screw cap, sterile	
E-Plate L8, glass, for the iCELLigence [™]	OLS OMNI Life Science (Germany)
CytoFLEX Sheath Fluid	Beckman Coulter Life Sciences (USA)

2.4.2 Dialysis

Mini Dialysis Kit, MWCO 1 kDa, 20 µL to 250 µL samples	Cytiva (USA)
Tube-O-DIALYZER [™] medi, MWCO 1 kDa, 0.2 mL to 2.5 mL samples	VWR (USA)
ReadyLyzer 10, MWCO 1 kDa, 3 mL to 10 mL tubes	SERVA Electrophoresis GmbH (Germany)

2.4.3 Analytics

UV cuvette, 2.7 mL (working volume: 0.05 mL to 2.7 mL), special plastic, transparent	SARSTEDT AG & Co. KG (Germany)
Folded Capillary Zeta Cell, DTS1060	Malvern Panalytical (UK)
Screw Neck Vial ND8, amber, 1.5 mL	VWR/Avantor (USA)
Screw Cap for Screw Neck Vial ND8, red rubber/beige PTFE	
Micro-insert for Screw Neck Vial ND8	

2.4.4 Miscellaneous

Screw cap tube, 15 mL & 50 mL, PP, sterile	SARSTEDT AG & Co. KG (Germany)
Reaction tube, 1.5 mL & 5 mL, PP	
Reaction tube, 1.5 mL, PP, Low protein-binding, sterile	
Reaction tube, 1.5 mL, PP, Low DNA-binding, sterile	
PCR single tube, 0.2 mL, PP	
Pipette tip, 10 µL, 200 µL, 300 µL, 1 000 µL, 5 mL, PP	
Petri dish, Ø 6 cm, PS, sterile	
Microplate, 96 well, PP, black	Greiner-Bio-One GmbH (Germany)
Sterile syringe filter PES & Nylon, 0.22 µm	Membrane Solutions (USA)

2.5 Devices

In the following, all general devices used for the work presented in this thesis are listed. Specific devices for analytical purposes are given in the respective method descriptions, together with the software used for the evaluation of the obtained data.

2.5.1 Molecular Biology

PCR Thermocycler Biometra TOne	Analytik Jena (Germany)
PowerPac™ Basic Power Supply, Mini-Sub Cell GT Cell, mini-gel caster, 7×10 cm UV-transparent tray, 8-well comb	Bio-Rad Laboratories (USA)
Nano-Drop™ One Microvolume UV-Vis Spectrophotometer	Thermo Fisher Scientific (USA)
UV transilluminator USDT-20SL-8E, Dark Hood DH-10	biostep GmbH (Germany)
PHMT Thermoshaker for Microtubes	Grant Instruments (UK)
MaxQ™ 5000 Shaker	Thermo Fisher Scientific (USA)
Incubator B 5025	Heraeus Holding GmbH (Germany)
Autoclave Varioklav®	HP Labortechnik GmbH (Germany)

2.5.2 Polyacrylamide Gel Electrophoresis

Mini-PROTEAN® Tetra Handcast System	Bio-Rad Laboratories (USA)
PowerPac® 300 Power Supply	
Microplate Shaker	VWR (USA)
Epson Perfection V700 Photo	Epson (Japan)

2.5.3 Cell Culture

HERAsafe HS12 Biological Safety Cabinet	Heraeus Holding GmbH (Germany)
Water bath WB14 with shaking device SV1422 and lid	Memmert GmbH + Co. KG (Germany)
CO ₂ Incubator ICO105	
Counting chamber, improved Neubauer	BRAND GmbH + Co. KG (Germany)
Inverted Light Microscope Leica DM LS2	Leica Microsystems GmbH (Germany)
Sapphire Maxipette	Greiner-Bio-One GmbH (Germany)

2.5.4 Centrifuges and Scales

Microliter Centrifuge Mikro 20	Andreas Hettich GmbH & Co. KG (Germany)
Megafuge 1.0®	Heraeus Holding GmbH (Germany)
Centrifuge Allegra X-30R	Beckman Coulter Life Sciences (USA)
Centrifuge Avanti J-26XP	
Savant SPD111V-230 SpeedVac Concentrator	Thermo Fisher Scientific (USA)
Analytical balance MC1 AC210P	Sartorius AG (Germany)
Analytical balance XS205DU/M	Mettler Toledo (Switzerland)

2.5.5 Miscellaneous

Alpha 1-2 LDplus Lyophilizator	Christ Gefriertrocknungsanlagen GmbH (Germany)
Analytical balance MC1 AC210P	Sartorius AG (Germany)
Analytical balance XS205DU/M	Mettler Toledo (Switzerland)
Mechanical Pipettes, variable volumes	Eppendorf SE (Germany)

3 Methods

3.1 Molecular Biology

In the following, the molecular biology techniques used for the amplification and cloning of the pDNA vectors for the work described in this thesis will be presented.

3.1.1 Agarose Gel Electrophoresis

Agarose gel electrophoresis uses an electric field to separate DNA fragments according to their length. For all investigations presented in this thesis, if not stated otherwise, a 1 % agarose gel was used. For its preparation, 0.5 g agarose was dissolved in 50 mL TAE buffer (40 mM Tris (pH 7.6), 20 mM acetic acid, 1 mM EDTA) upon heating. The agarose solution was allowed to cool before adding ethidium bromide (final concentration 50 ng/mL) and casting the gel. The gel was allowed to set completely for 30 min before transferring the casting tray to the electrophoresis chamber with the sample loading wells located near the anode. The electrophoresis chamber was filled with TAE buffer until the gel was completely submerged in the buffer. Then, the comb was carefully removed and samples were mixed thoroughly with sample loading dye and were loaded in the wells ($\leq 30 \mu\text{L}$) slowly using a mechanical pipette. A DNA marker was used as standard and run in parallel for DNA fragment length determination. Electrophoresis was routinely run at 110 V for 60 min. Since ethidium bromide intercalates into DNA showing fluorescence under ultraviolet (UV) light, gels were evaluated with a UV transilluminator at $\lambda_{\text{ex}} = 254 \text{ nm}$. Exposure to UV radiation was kept to a minimum to avoid DNA damage in case the separated DNA fragments were to be used for subsequent reactions. In these cases, the portions of the gel containing the DNA fragment of interest were excised with a scalpel and the DNA was then extracted from the gel.

3.1.2 Spectrophotometric Analysis of DNA

Nucleic acids absorb UV light with a characteristic spectrum, this can be exploited for their quantification in solution. With the average extinction coefficient of dsDNA at $\lambda = 260 \text{ nm}$, the concentration of dsDNA in solution can be calculated using the Beer-Lambert law as

$$c = \frac{50 \cdot A_{260} \text{ ng} \cdot \text{cm}}{l \quad \mu\text{L}}$$

with A_{260} denoting the absorbance at $\lambda = 260$ nm and l denoting the optical path length in centimeter. Spectrophotometric analysis of a DNA solution is also used to assess the purity of the sample. The ratio of absorbance at 260 nm and 280 nm (A_{260}/A_{280}) for pure DNA samples is 1.7 to 1.9, smaller values may indicate contamination with proteins or residual phenol in the solution. Pure DNA samples have A_{260}/A_{230} , the ratio of absorbance at 260 nm and 230 nm, in the range of 2.0 to 2.2. Lower values are indicative of the presence of contaminants such as carbohydrates, glycogen, phenol, or guanidine (Monika Jansohn 2012; Thermo Fisher Scientific 2015). All DNA solutions used for the molecular biology work presented in this thesis were quantified spectrophotometrically and only used if they met the quality criteria for pure pDNA solutions. The concentration values obtained were used to calculate absolute amounts of DNA both within the cloning workflow and for nanoplex formulation.

3.1.3 Molecular Cloning of Recombinant Plasmid DNA Vectors

Molecular cloning describes a set of experimental methods in molecular biology used to assemble recombinant DNA molecules by integrating a DNA fragment of interest into a vector and directing their replication in host organisms (Watson 2007). A schematic illustration of the classical workflow of molecular cloning is shown in Figure 3.1. The creation of a recombinant DNA construct is achieved by ligation, i.e. the covalent linking of the ends of two DNA fragments by the enzyme DNA ligase. Before ligation, both the insert containing the DNA fragment of interest and the target vector are trimmed with the same restriction enzymes. The resulting cohesive ends, characterized by the overhang of unpaired nucleotides at the end of the DNA fragments, are complementary to each other and ensure unambiguous ligation. Restriction enzymes are selected based on the restriction sites present in the vector plasmid. The corresponding restriction sites are introduced in the insert DNA fragment by individually designed primer pairs for polymerase chain reaction (PCR). To propagate the recombinant DNA construct, the ligation product is transformed into *E. coli* bacteria, followed by selection of successfully transformed bacteria by incubation on lysogeny broth (LB) agar containing antibiotics. Only successfully transformed bacteria can proliferate on this substrate due to a gene encoding a specific antibiotic resistance in the vector. A colony grown on the agar plate is propagated in liquid culture, followed by isolation and purification of the pDNA from the bacterial culture. The sequence of the isolated pDNA can then be verified by Sanger sequencing to confirm cloning success. The purity of the isolated pDNA is examined using agarose gel electrophoresis and various restriction digestions.

The planning of the different molecular cloning tasks and the design of the PCR primers presented in this thesis was carried out utilizing the software PlasmaDNA v1.4.2 (Angers-Loustau et al. 2007) and SnapGene[®] Viewer v5.1.4.1 (GSL Biotech LLC, USA).

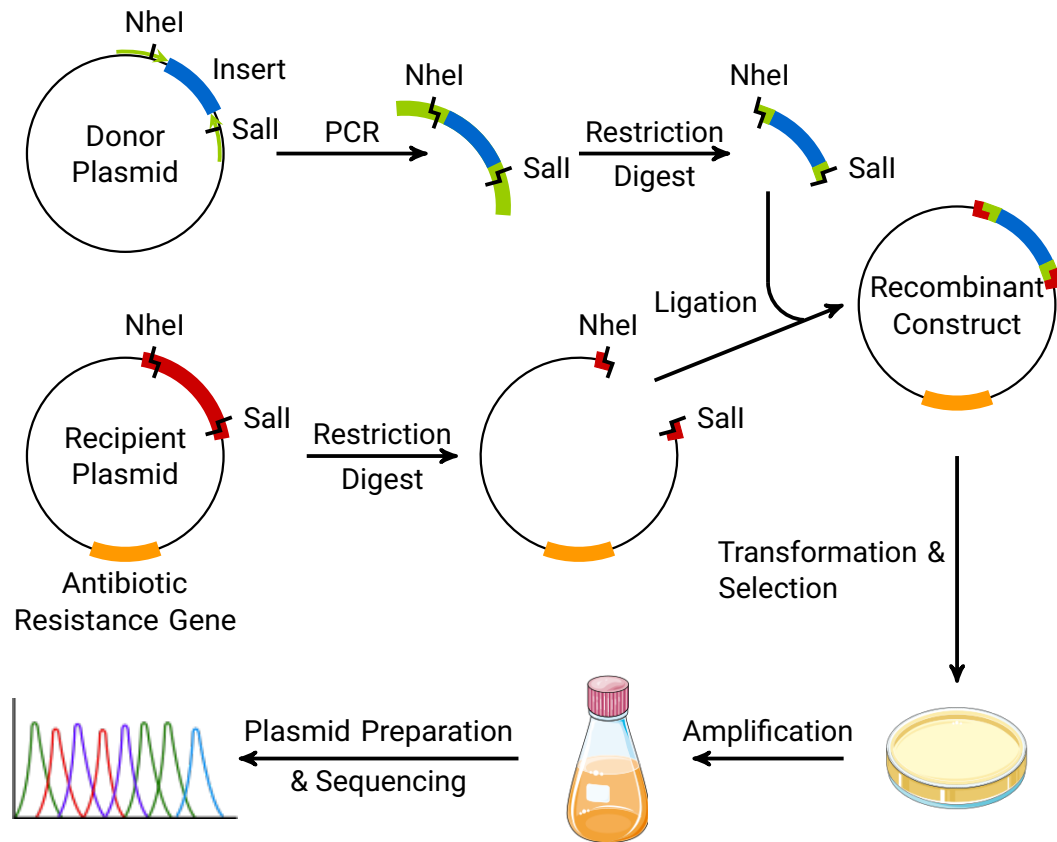


Figure 3.1: Schematic illustration of molecular cloning workflow. NheI and Sall represent the restriction enzymes to be variably selected for the respective cloning task. Width of the colored circular sections indicates whether the DNA sequence is single- or double-stranded. Green arrows indicate primers.

3.1.3.1 Polymerase Chain Reaction

PCR, a widely used method for *in vitro* amplification of genetic material, is used in a cloning task to amplify the DNA fragment of interest. This DNA sequence is inserted into the recipient plasmids backbone and is therefore also called insert. Additionally, specific primer design allows for the introduction of defined restriction sites flanking the insert, consequently enabling specific ligation into the backbone of the recipient plasmid. A classical PCR is performed with a forward and a reverse primer, which are designed to anneal at the beginning and at the end of the DNA segment to be amplified. Primer pairs were designed to exhibit the following characteristics (Monika Jansohn 2012):

-
- Restriction enzyme cut site at the beginning of the primer (5'-end), complemented with at least three preceding base pairs to ensure efficient cleavage of the restriction enzyme.
 - Overlapping sequence with insert DNA fragment.
 - Primer pairs melting temperatures difference ≤ 5 °C to allow annealing of both primers at the calculated annealing temperature.
 - Primer melting temperatures: 50 °C to 72 °C.
 - 40 % to 60 % G- and C-bases, evenly spacing of GC residues within the primer.
 - 20 to 30 nucleotides primer length.
 - Single recognition (annealing) site for each primer in the donor plasmid.
 - No hybridization of primer pairs & no formation of stable secondary structures or dimers within a primer.

PCR reactions were set up according to the manufacturer's protocol. Table 3.1 lists the specifically designed primers and the chosen PCR conditions.

3.1.3.2 Restriction Digest

Restriction enzymes, more precisely restriction endonucleases, are used as molecular scissors in molecular cloning due to their sequence-specific DNA cleavage activity. To enable a robust “cut and paste” workflow, only type II restriction enzymes that cut DNA within or in close proximity to the recognition sequence, creating cohesive ends, were used for the cloning work presented in this thesis (Figure 3.1). The use of the same restriction endonucleases for digestion of the insert DNA fragment and the receiving plasmid backbone results in complementary 5'-overhangs of the DNA fragments that ensure unambiguous ligation. When available, the high-fidelity (HF[®]) versions of the selected restriction enzymes were used. These optimized enzyme variants are characterized by a drastic reduction in their off-target cleavage activity, allowing them to be used for overnight digestion.

Restriction digests were set up according to the manufacturer's protocol using 16 h incubation and 1 μ g DNA. All of the selected combinations of restriction enzymes allowed for double digestion protocols, i.e. simultaneous digestion with both restriction enzymes.

Table 3.1: Overview of donor and recipient plasmids, insert DNA fragments, PCR primers, PCR settings, and used restriction enzymes for the molecular cloning of the constructs eGFP/MN501A1, CMV/eGFP/MN501A1, HLP/hFIX/MN501A1, and HLP/eGFP/MN501A1. Primer sequences are given from 5'- to 3'-end, restriction enzyme cut site is indicated by red letters, blue letters indicate sequence of the insert gene of interest, and the annealing part (on the donor plasmid) of the primer is denoted by underlined letters. Annealing temperatures were calculated with New England Biolabs Tm Calculator (<https://tmcalsculator.neb.com/>), extension times were chosen based on 15 s/kb to 30 s/kb as indicated in the manufacturer's product information sheet.

Construct	eGFP/MN501A1	CMV/eGFP/MN501A1
Donor Plasmid	pEGFP-N3	pEGFP-N3
Insert	eGFP	CMV Enhancer & Promoter
Recipient Plasmid	MN501A1	eGFP/MN501A1
Forward Primer	TA <u>TGT CGA CGA TCC ATC GCC ACC ATG</u>	GC <u>TAC TAG TCG CGT TAC ATA ACT TAC GGT A</u>
Reverse Primer	ATA <u>GCT AGC GCT TTA CTT GTA CAG CTC GTC</u>	ATA <u>GTC GAC AGC TCT GCT TAT ATA GAC C</u>
Annealing	60.5 °C	56.2 °C
	25 cycles	35 cycles
Extension	20 s	15 s
Final Extension	10 min	5 min
Restriction Enzymes	Sall-HF, NheI-HF	SpeI-HF, Sall-HF
Construct	HLP/hFIX/MN501A1	HLP/eGFP/MN501A1
Donor Plasmid	pCDNA3-HLP-5'UTR-FIX	pEGFP-N3
Insert	HLP/hFIX	eGFP
Recipient Plasmid	MN501A1	HLP/MN501A1
Forward Primer	GTC <u>ACT AGT TGT TTG CTG CTT GCA ATG</u>	GA <u>GGC TAG CGA TCC ATC GCC ACC ATG</u>
Reverse Primer	T <u>AAG TCG ACC CAT CTT TCA TTA AGT GAG C</u>	TAT <u>GAC GTC GCT TTA CTT GTA CAG CTC GTC</u>
Annealing	58 °C	60.5 °C
	25 cycles	35 cycles
Extension	60 s	20 s
Final Extension	10 min	5 min
Restriction Enzymes	SpeI-HF, Sall-HF	NheI-HF, AatII

3.1.3.3 Ligation

Ligation describes the ligase-catalyzed linkage of two DNA fragments at their ends by the formation of a phosphodiester bond between the 3' hydroxyl and the 5'-phosphate termini of duplex nucleic acid fragments. As part of the cloning workflow, ligation creates the recombinant construct, a pDNA vector, from the two linearized DNA fragments equipped with cohesive ends by the preceding restriction digest. Ligation reactions were set up according to the manufacturer's protocol using overnight incubation at 16 °C and 50 ng vector (recipient pDNA) for each reaction. Molar ratios of 3:1 and 5:1 (insert DNA:vector DNA) were used in parallel to increase the chances of success. The mass of insert DNA to be used was calculated by

$$m(\text{insert}) = m(\text{vector}) \cdot \frac{n(\text{insert})}{n(\text{vector})} \cdot \frac{l(\text{insert})}{l(\text{vector})}$$

with l denoting the length of the DNA fragment. To reduce the degradation of adenosine triphosphate (ATP) contained in the ligase buffer, aliquots of the buffer concentrate were thawed at room temperature, stored on ice until use and residues were subsequently discarded.

3.1.3.4 Transformation, Recovery, and Selection

In molecular biology, transformation is the non-viral uptake and incorporation of naked DNA into prokaryotic cells. The *E. coli* strains used for amplification of the recombinant DNA constructs and transformation are naturally non-competent (i.e. not capable of naked DNA uptake) and therefore require previous treatment to make them chemically competent (ROTI[®] Transform Kit, according to manufacturer's protocol). For transformation, 50 µL aliquots of competent cells were thawed on ice and mixed with 3 µL of the ligation mix. Due to the sensitivity of the competent cells, the transformation mixture was mixed only by careful movements of the pipette tip. The transformation mixtures were first incubated on ice for 30 min, followed by heat shock treatment at 42 °C for 30 s, followed by incubation on ice for 2 min. 200 µL Super optimal medium with catabolic repressor (S.O.C) medium was then added to the transformation mixtures and bacteria were incubated (90 min, 37 °C, 250 rpm orbital shaking). Outgrowth in this rich culture medium supports cell recovery and ensures expression of antibiotic resistance in successfully transformed bacterial cells. After recovery, 50 µL or 100 µL of the bacterial suspension were spread on LB agar plates containing 50 µg/mL kanamycin. The plates were then incubated at 37 °C for 16 h. Supplementation of the LB agar culture medium with antibiotic ensures that only successfully transformed cells can proliferate on the medium as the acquired recombinant DNA constructs also convey antibiotic resistance to the transformed cells.

3.1.3.5 Amplification and Preparation of Plasmid DNA

A single colony from the selection plate was picked and incubated in 2 mL LB medium containing 50 µg/mL kanamycin at 37 °C and 250 rpm orbital shaking for 16 h. Amplification of the transformed bacterial cells ensures amplification of the recombinant construct. Plasmids were extracted from the bacterial culture using commercial DNA preparation kits which use classical alkaline cell lysis, neutralization and column-based purification steps for the extraction of pure pDNA. The resulting solutions were quantified using spectrophotometry (Section 3.1.2). Various restriction digests (Section 3.1.3.2) followed by agarose gel electrophoretic analysis (Section 3.1.1) were performed to confirm the purity of the prepared pDNA, the presence of specific restriction sites, and the length of the expected DNA fragment lengths after restriction digest. Additionally, the nucleotide sequence of the recombinant construct was analyzed with Sanger sequencing, performed by LGC Genomics GmbH (Germany). The sequencing data was then aligned with the known DNA sequence using DNA Baser Assembler v5.15.0 (Heracle BioSoft, Romania) to confirm cloning success and rule out the introduction of mutations. If both techniques confirmed the successful molecular cloning of the expected recombinant pDNA vector, 500 µL bacterial suspension was mixed with 500 µL 50 % glycerol and stored in cryovials at –80 °C. These glycerol stocks of the transformed bacteria enabled the amplification and preparation of the respective pDNA vectors without the need for re-transformation.

3.1.4 Preparation of Minicircle DNA

Minicircle DNA (mcDNA) was prepared as described in a joint publication with Mitdank et al. (2021), materials are also given there. In brief, the mcDNA-producing parental plasmid including the gene of interest is propagated in *E. coli* ZYCY10P3S2T, a genetically modified strain that expresses phiC31 integrase and I-SceI homing endonuclease in an L-arabinose-induced manner. The former enzyme recognizes attachment sites in the parental plasmid and mediates their recombination resulting in mcDNA and a plasmid consisting of the bacterial backbone that is then degraded by the latter enzyme (Kay et al. 2010). McDNA was pre-purified using classic alkaline cell lysis followed by several precipitation steps and dialysis to concentrate nucleic acids while minimizing protein and RNA contamination. Final isolation of supercoiled mcDNA was done using size exclusion chromatography (SEC). The collected fraction was subjected to ultrafiltration for concentration and desalination before the final product was analyzed using agarose gel electrophoresis (Section 3.1.1) and Sanger sequencing.

3.2 Preparation of Peptide-Triterpene Conjugates

In the following, the final reaction conditions for the preparation and purification of covalent peptide-SO1861 conjugates are presented. These were the result of several optimization

steps described in Section 4.2.3.

3.2.1 Conjugation of SO1861-EMCH and Peptide Scaffolds

Peptide scaffolds (K₁₆C or K₁₆CPEG) were dissolved at 2 mg/mL and SO1861-EMCH was dissolved at 1 mg/mL in DPBS, pH 6.5 immediately before starting the reaction to minimize cysteine oxidation and hydrolysis of SO1861-EMCHs functional groups. In a 15 mL conical tube, 5 mL of the peptide solution was mixed with the appropriate amount of SO1861 EMCH solution (0.25 or 0.5 equivalents, mol/mol) and diluted with DPBS, pH 6.5 to a final peptide concentration of 1 mg/mL. The reaction mixture was incubated for 16 h under orbital shaking (800 rpm) at room temperature. After incubation, the reaction solution was transferred to dialysis tubes and dialyzed against ultrapure water for 24 h at 8 °C (molecular weight cut-off (MWCO) 1 kDa, ultrapure regenerated cellulose membrane). The dialysis buffer was exchanged twice. The dialyzate was lyophilized. To avoid weighing inaccuracies in the repetitive preparation of peptide solutions, the complete lyophilizate was dissolved in sterilized ultrapure water to 2 mg/mL. Samples of the resulting solution were taken for analytical characterization and the remainder was immediately divided into aliquots. These were lyophilized again, then sealed with laboratory film and stored at –20 °C until use. Peptide aliquots were dissolved in ultrapure, sterile-filtered water at 1 mg/mL as needed, the resulting stock solutions were stored at 8 °C.

3.2.2 Purification of Peptide Conjugates using Solid Phase Extraction

To ensure absence of any free unreacted SO1861-EMCH, batches that were produced for *in vivo* studies were subjected to solid phase extraction (SPE) after dialysis and before lyophilizing the final product. All solutions were allowed to pass the SPE column using gravity flow. A CHROMABOND HR-XAW SPE column (3 mL/60 mg) was conditioned with 5 mL methanol, followed by 5 mL ultrapure water before the dialyzate was loaded on the column. Afterwards, the column was washed twice with 2 mL ultrapure water, followed by elution with 2 mL methanol twice and a final elution step using 2 mL 1 % formic acid in methanol. The flow-through of sample loading and the following washing step were collected and pooled before lyophilization.

3.3 Nanoplex Formulation

Upon mixing with peptide scaffolds that are positively charged at physiological pH due to their K₁₆-tail, nucleic acids are complexed and form polyplex nanoparticles, so called nanoplexes.

Nanoplex composition is characterized by its N/P ratio, which is the molar ratio of charged nitrogen atoms (introduced by the protonated amino nitrogen atoms of the lysine

sidechains of the peptides) and charged oxygen atoms (introduced by the phosphate backbone of the nucleic acids). Accordingly, the mass of peptide scaffold to be used for the preparation of nanoplexes is calculated as follows:

$$m(\text{peptide}) = \frac{m(\text{DNA}) \cdot N/P \cdot M(\text{peptide})}{330 \text{ g/mol} \cdot n_+(\text{peptide})},$$

with n_+ denoting the net number of positive charges.

For nanoplex formation, equal volumes of the peptide and the DNA solution were mixed together by adding the DNA to the peptide solution followed by rapidly pipetting the resulting solution up and down 20 times. Most studies were performed with constant amount of DNA and varying peptide scaffolds or amounts of peptide. It was therefore found most effective to first add the calculated amounts of buffer and peptide scaffold into the reaction tubes for each sample. After homogenization of the peptide solutions, the DNA solution was then added to all samples while mixing. The nanoplex solutions were incubated for 30 min at room temperature to let the nanoplexes self-assemble and then optionally diluted with buffer or cell culture medium.

For the formulation of mixed nanoplexes, i.e. nanoplexes containing two different peptide components, both peptides were mixed first with the buffer before the DNA was added. The composition of the mixed nanoplexes is given in percent and refers to the proportion of the two peptide components in the complex formation of the DNA. To give an example: A nanoplex with N/P 10 is to be formulated with 70 % peptide A and 30 % peptide B. The amount of peptide A used is the same as would be required for a nanoplex with N/P 7. The amount of peptide B is based on the amount needed for N/P 3.

If not stated otherwise for the specific experiment, nanoplexes prepared for the studies presented in this thesis were prepared at N/P 10. A positive charge was contributed by each lysine as well as the N-terminal amino group, and one negative charge was considered for the conjugation of SO1861 due to the glucuronic acid it contains.

Nanoplex formulation was routinely performed in 10 mM HEPES, pH 7.1 if not stated otherwise. This buffer ensures constant pH conditions to hinder the nanoplex formation as little as possible. The latter is ensured by the choice of HEPES as buffering agent which has little effect on the ionic strength (Stellwagen et al. 2008) due to its zwitterionic structure.

For i.v. injection, isotonicity of the nanoplex solution was desirable to minimize irritations at the injection site. Based on its established use for animal studies in mice by Baumhover et al. (2015) and Fernandez et al. (2010), isotonic HEPES-buffered mannitol (HBM, 270 mM D-mannitol, 5 mM HEPES, pH 7.5) was used for all experiments with pepY-nanoplexes and the *in vivo* study. As a sugar alcohol, mannitol has no reducing carbonyl group. This eliminates the risk of Maillard reaction with the amino groups of the peptide (Hodge 1953), unlike the 5 % glucose solution routinely used as a non-ionic, isotonic solution for infusion purposes.

3.3.1 Preparation of Targeted Nanoplexes

Targeted nanoplexes, i.e. nanoplexes functionalized with a targeting ligand, were prepared by reaction of the azide functionality of the DNA-complexing peptide scaffold with the DBCO-group of the previously derivatized protein ligand by means of SPAAC. DBCO-Transferrin, DBCO-Cetuximab, DBCO-EGF, DBCO-Apolipoprotein AI (ApoAI), and DBCO-*N*-Acetylgalactosamine (GalNAc) were provided within the ENDOSCAPE project by the working group of Prof. Hendrik Fuchs (Institut für Laboratoriumsmedizin, Klinische Chemie und Pathobiochemie, Charité – Universitätsmedizin Berlin). Advised by Prof. Fernandez-Megia (CiQUS, Universidade de Santiago de Compostela), nanoplexes were formulated as described in Section 3.3 in 10 mM HEPES, pH 7.1 in reaction tubes. After the 30 min self-assembly period DBCO-functionalized ligand (stock solution in PBS, diluted in 10 mM HEPES, pH 7.1) was added and the solution was incubated for 16 h at room temperature under orbital shaking (800 rpm). Ligand loading in percent refers to the molar amount of azide groups accessible for SPAAC bioconjugation. As each peptide scaffold carries one free azide group, the molar amount of azide groups is therefore equivalent to the molar amount of peptide scaffold. To evaluate the contribution of non-covalent, electrostatic association of the ligand to the nanoplex, targeted nanoplexes were prepared in parallel as a control using the same reaction conditions, but a non-DBCO-functionalized ligand variant.

3.4 Analytical Methods

In the following, all analytical methods used for the work presented in this thesis are presented.

3.4.1 Nuclear Magnetic Resonance Spectroscopy

Nuclear magnetic resonance (NMR) spectroscopy measures the interaction between the intramolecular magnetic field of atomic nuclei of a sample, situated in a strong static magnetic field, with a high frequency alternating magnetic field. Since the intramolecular magnetic field depends on the environment of individual atoms and their interactions with neighboring atoms, functional groups in the molecule can be identified based on the chemical shift of resonance frequencies. NMR spectroscopy is therefore primarily used for structure elucidation. Since the ratio of the signal area in the NMR spectrum is proportional to the ratio of the number of resonant nuclei in the molecule, NMR spectroscopy can also be used for concentration determination.

¹H NMR was used to investigate the stability of SO1861-EMCH. 0.8 mg to 1.0 mg SO1861-EMCH was dissolved in 1.2 mL ultrapure H₂O/20 mM phosphate buffer (PB)/phosphate-buffered saline (PBS)/20 mM citrate and stirred at room temperature. Aliquots (0.40 mL) were collected at 2 h, 6 h, and 24 h, lyophilized and analyzed by ¹H NMR (500 MHz,

CD₃OD). The stability/degradation of the hydrazone and maleimide groups was determined by integrating the signal at 7.70 ppm to 7.60 ppm (hydrazone) and 6.82 ppm (maleimide) with respect to the stable multiplet signal at 5.37 ppm to 5.26 ppm, indicating three protons unaffected by hydrolysis (at C-12 of the aglycone, C-1 of fucose, and C-4 of quinovose).

Experiments were recorded on a 11.7 T Bruker DRX 500 spectrometer, acquiring 64 scans, with a pre-scan delay (d1) of 1.6 s and an acquisition time of 4 s at 300 K. MestReNova 14.2 software (Mestrelab Research, Spain) was used for spectra processing.

All ¹H NMR data presented in this thesis were generated and analyzed by Juan Correa (group of Prof. Fernandez-Megia, CiQUS, Universidade de Santiago de Compostela) within the ENDOSCAPE project.

3.4.2 Matrix-Assisted Laser Desorption/Ionization Time-of-Flight Mass Spectrometry

Matrix-assisted laser desorption/ionization time-of-flight (MALDI-TOF) is a mass spectrometry (MS) method which uses MALDI for the generation of analyte ions that are accelerated and detected according to their TOF. The analyte is mixed with a solution of an energy-absorbent matrix which co-crystallizes with the sample upon drying. For analysis, a laser beam ionizes the matrix. This triggers ablation and desorption of the co-crystallized matrix and sample material, followed by ionization of the analyte molecules in the gas phase. The extent of ionization via protonation or deprotonation is dependent on the chemical nature of the analyte. The generated singly charged analyte ions are then accelerated and separated according to their mass-to-charge ratio (m/z) before being detected in the TOF mass analyzer.

Compared to other ionization methods, MALDI is relatively gentle, resulting in little fragmentation of analytes. Other advantages include low sample input (typically 1 µg peptide per matrix used) and high sample throughput. MALDI-TOF MS analysis is inherently not suitable for absolute quantification and determination of the purity of analytes and. This is due on the one hand to the varying extent of analyte ionization and on the other hand to the manual performance of the measurement.

Analysis of the native and the equipped peptide scaffolds by MALDI-TOF MS was performed in positive mode, as the peptides are prone to protonation due to their polycationic nature. An Ultraflex-II TOF/TOF or UltrafleXtreme TOF/TOF instrument (Bruker Corporation, USA) was used. 3,5-dimethoxy-4-hydroxycinnamic acid (sinapinic acid, SA) and α-cyano-4-hydroxycinnamic acid (HCCA) were used as matrices (both as saturated solution in 33 % acetonitrile/0.1 % trifluoroacetic acid), mixed with equal volumes of the analyte solution, and the resulting analyte/matrix-solutions were deposited on the microtiter plate target using the dried droplet method. Measurements were performed in reflector or linear mode, m/z are reported either as [M+H]⁺ (mono-isotopic) or as [M+H]⁺ (average) values. The conditions applied are specified for each spectrum. Data was analyzed using FlexAnalysis 2.4 software (Bruker Corporation, USA).

All MALDI-TOF MS data presented in this thesis were generated by and analyzed together with Dr. Christoph Weise (Institute of Chemistry and Biochemistry, Freie Universität Berlin).

3.4.3 Liquid Chromatography Mass Spectrometry

Liquid chromatography (LC)-MS analysis combines the separation of the sample to be analyzed by liquid chromatography with high sensitivity mass spectrometric detection. A portion of the column eluate is continuously evaporated and ionized during the analysis by electrospray ionization (ESI). The resulting ions are accelerated and separated according to their m/z before being detected in the TOF mass analyzer. ESI can be performed with positive or negative voltage, leading to the detection of the quasi-molecular ions $[M+H]^+$ or $[M-H]^-$, respectively. Due to the described coupling, a mass spectrum is available for each point of the chromatogram. That makes LC-MS analysis particularly suitable for the detection and identification of analyte impurities.

The presence of SO1861-EMCH and SO1861 in the equipped peptide scaffold solutions was assessed with a 1290 Infinity II LC system coupled with a 6550 iFunnel Q-TOF mass spectrometer (Agilent Technologies®, USA). High pressure liquid chromatography was performed using a Kinetex, 2.6 μm C18, 100 Å, 100 \times 4.6 mm column (Phenomenex, Germany) and the following water, 0.01 % formic acid (A)/acetonitrile, 0.01 % formic acid (B) gradient: 0 min: 30 % B, 14 min: 50 % B, 24 min: 50 % B, 25 min: 30 % B, 30 min: 30 % B. Flow rate was 0.7 mL/min and sample injection volume was 5.0 μL . SO1861 tends to deprotonate due to the glucuronic acid it contains, so ESI was performed in negative mode. MestReNova 14.1 software (Mestrelab Research, Spain) was used for spectra processing.

3.4.4 Polyacrylamide Gel Electrophoresis

Sodium dodecyl sulfate polyacrylamide gel electrophoresis (SDS-PAGE) is an analytical method that is commonly used to separate proteins according to their mass. To achieve a mass-dependent migration rate in the electric field, samples are mixed with the surfactant SDS before electrophoresis. SDS binds to proteins at a constant mass ratio, masking the intrinsic charge of the proteins and giving them a similar charge-to-mass ratio.

The peptides used within the scope of this thesis were not amenable to analysis by SDS-PAGE due to their polycationic nature. Even by increasing the SDS concentration, the large number of positive charges could not be masked by SDS, consequently no migration to the anode occurred. Therefore, for the analysis of basic peptides, the electrodes were reversed. Attaching the cathode at the bottom of the gel allowed the positively charged peptides to migrate from the loading pockets into the gel. To ensure the formation of sharp bands, the buffer system was also changed. As described by Säftel et al. (2012), potassium was the leading, histidine (pK_{a2} 6.0) the trailing and *N*-tris[hydroxymethyl]methyl-3-aminopropane-sulfonic-acid (TAPS, pK_a 8.4) the common, buffering ion. A 100 mM histi-

dine, 20 mM TAPS (pH 7.6, not adjusted) running buffer was used for both electrodes. The sharpness of the bands increased with the acrylamide concentration in the gel, therefore gels with 22 % acrylamide were routinely used. These were prepared as described by Bio-Rad Laboratories (2014) using only one gel solution consisting of

TAPS 1.5 M, pH 7.5 (adjusted with KOH)	2.0 mL
Acrylamide-bisacrylamide 30 % (37.5:1)	5.92 mL
TEMED 10 %	40.0 μ L
APS 10 %	40.0 μ L

Lyophilized samples were dissolved in sample loading buffer (150 mM TAPS, 40 % glycerol, 0.02 % methylene blue), liquid samples were mixed 1:1 with this buffer. Electrophoresis was performed at 250 V for 90 min. Visualization was performed following Neuhoff et al. (1988) by overnight incubation in the staining solution (40 mL 2 % *w/v* phosphoric acid, 10 % *w/v* ammonium sulfate + 10 mL methanol + 1 mL 5 % Brilliant blue G 250) followed by destaining in 25 % methanol.

3.4.5 Fluorescence Spectroscopy

Fluorescence describes a form of luminescence in which a substance absorbs energy in the form of radiation and re-emits it as visible light. This phenomenon is exploited in fluorescence spectroscopy for characterization and quantification purposes. The utilization of fluorescent DNA-binding dyes, whose fluorescence is significantly enhanced by binding to dsDNA, enables the application of fluorescence spectroscopy for the quantification of dsDNA. This fluorescence-based method is highly selective for dsDNA and offers a greater sensitivity than concentration determination by absorption. Within the scope of this thesis, DNA quantification using fluorescent DNA-binding dyes was used to determine the DNA complexation efficiency of the peptides, i.e. their capability and extent of DNA condensation. Since the complexed DNA is no longer accessible for intercalation of the fluorescent dye after nanoplex formation, the DNA complexation efficiency was determined indirectly by quantifying the remaining free DNA. For each nanoplex, 400 ng DNA was complexed in a total volume of 20 μ L as described in Section 3.3. QuantiFluor[®] dsDNA Dye was diluted 1:400 in the nanoplex formulation buffer and 200 μ L of the resulting working solution were transferred to each well of a black 96-well plate. Following the 30 min incubation period, 5 μ L of the nanoplex solution was added per well, which equals to a total amount of 100 ng DNA per well. For the blank, the same volume of formulation buffer was used. Each sample was measured in triplicate. Fluorescence intensity was measured using an infinite F200 (Tecan Group Ltd., Switzerland) microplate reader. After mixing the solutions for 5 min at 300 rpm, the plate was incubated for another 5 min at room temperature in the dark. Fluorescence measurement was performed with $\lambda_{\text{ex}} = 485 \pm 20$ nm and $\lambda_{\text{em}} = 535 \pm 25$ nm, the gain was set to optimal. For analysis of the data, the fluorescence intensity of the blank buffer samples was subtracted from all fluorescence intensity signals. The signal for

nanoplexes formulated at N/P 0 was set to 100 % free DNA and the amount of free DNA for the other samples was calculated from its fluorescence intensity by

$$m(\text{DNA}) = \frac{\text{fluorescence intensity}}{\text{fluorescence intensity N/P 0}} \cdot 100 \%,$$

as the performed assay is linear for 0.05 ng to 200 ng of dsDNA input.

3.4.6 Dynamic and Electrophoretic Light Scattering

Dynamic light scattering (DLS) is a physical analysis method used to determine the size and size distribution of particles in dispersion or macromolecules in solution. Laser light directed at the sample is scattered in all directions by the molecules and particles in the solution (Rayleigh scattering). The light scattering emanating from the different particles interferes with each other and the intensity of the scattered light fluctuates minimally with time. This is due to the Brownian molecular motion, so that the analysis of the temporal scattering fluctuation allows a statement about the velocity of the particles in solution. From this, the hydrodynamic diameter (D_h) of a hypothetical hard sphere moving at the same speed of the nanoparticles within dispersion is calculated using the cumulant method (Berne and Pecora 2000). The advantages of DLS analytics include the rapid and parallel determination of size and size distribution, the measurement of a large number of particles thereby providing robust data, the low material input, and its non-invasiveness which allows reusing the samples after analysis. When interpreting DLS results, it shall be taken into account that the light scattering is proportional to the sixth power of the particles radii and thus the spectra are biased towards larger particles. Other limitations include the restriction of the cumulant method to monodisperse samples, the assumption of spherical particles, interference with the measurement and erroneous results when measuring colored or fluorescent samples, and low resolution (Bhattacharjee 2016).

Electrophoretic light scattering, also known as laser Doppler electrophoresis, is closely related to DLS with the difference that in the former the sample is measured in an electrophoresis cell under application of an electrical field. When a voltage is applied to the electrodes, particles migrate with a certain velocity. The measured magnitude of this velocity thus not only depends on the size of the particles but also on surface charge as well as solution viscosity and conductivity. Accordingly, with knowledge of the particle size as well as the solvent properties, the ζ -potential of the particles, defined as the electrostatic potential at the imaginary surface of hydrodynamic shear, can be calculated (Lowry et al. 2016). In relation to a reference beam, the scattered light is Doppler shifted, which allows the determination of the particles migration direction. ζ -Potential measurements are highly sensitive to changes in pH and ionic strength of the analyte solution. Furthermore, the electrophoresis of the sample may lead to degradation, so samples cannot be reused.

The D_h and ζ -potential of all nanoplexes investigated within the scope of this thesis were determined with a Zetasizer Nano ZS (Malvern Instruments, UK) instrument, equipped with

a 4 mV HeNe laser, $\lambda = 633 \text{ nm}$, at a fixed scattering angle of 173° . For each nanoplex, $2.5 \mu\text{g}$ DNA was complexed in a total volume of $50 \mu\text{L}$ as described in Section 3.3. The nanoplex solution was incubated at room temperature for 30 min and transferred into a disposable UV-transparent micro cuvette for size measurements. Each measurement was performed three times. Cumulants analysis, as defined in ISO 13321:1996 and ISO 22412:2008, was used for the analysis of the autocorrelation functions by the Zetasizer software, producing a mean value for the D_h (Z-Average) and a width parameter of the monomodal curve known as polydispersity index (Pdi) (Malvern Instruments Ltd. 2013). The Pdi can range from 0.0 (for a perfectly uniform distribution in terms of particle size) to 1.0 (for highly polydisperse samples). For ζ -potential measurements, the nanoplex solution was diluted with the buffer that was used for nanoplex formulation to a final volume of $800 \mu\text{L}$ before transferring the complete solution to a folded capillary cell. Each measurement was performed three times with a minimum number of 10 sub-runs per measurement. ζ -Potential values were calculated by the Zetasizer software from the measured electrophoretic mobility using the Henry equation and the Smoluchowski approximation (Malvern Instruments Ltd. 2013).

3.4.7 Electron Microscopy

Electron microscopes use a beam of accelerated electrons instead of light for illumination. Since the de Broglie wavelength that can be assigned to fast electrons is much shorter than the wavelengths of visible light, a higher resolution can be achieved with an electron microscope than with a light microscope.

In scanning electron microscopy (SEM), a focused beam of electrons scans the surface of the specimen in a raster pattern. The interaction of the electrons in the focused beam with the specimen is recorded by detectors that convert the relative number of backscattered or emitted electrons into brightness. SEM measurement requires dry samples under high vacuum. Visualizing non-conductive objects like biological samples with low electron density requires conductive coating prior to the measurement.

Cryogenic transmission electron microscopy (Cryo-TEM) measures the interaction of the electrons with the sample as the beam is transmitted through an ultra-thin section of the specimen at cryogenic temperatures ($\leq -150^\circ\text{C}$). For the examination of biological materials, Cryo-TEM offers the advantage of eliminating the use of fixatives and contrast agents and allowing examination close to the native state. This is achieved by ultra-fast shock-freezing of the samples, which embeds the analyte in an environment of vitreous ice.

Within the work described in this thesis, both SEM and Cryo-TEM were used for the characterization and size determination of nanoplexes. All electron micrographs were acquired at the Core Facility BioSupraMol supported by the Deutsche Forschungsgemeinschaft (DFG).

For SEM, $10 \mu\text{L}$ nanoplex solution ($0.1 \mu\text{g}/\mu\text{L}$ DNA, prepared in ultrapure water as described in Section 3.3) were transferred to silicon wafers and dried overnight in a desiccator at room temperature. Samples were sputtered with gold before analyzing their

size using a Hitachi SU8000 scanning electron microscope (Hitachi, Japan) operated at 10 kV.

For Cryo-TEM, perforated carbon film-coated microscopic 200-mesh grids (either R1/4 or R1.2/1.3 batches of QUANTIFOIL[®], MicroTools GmbH, Germany) were cleaned with chloroform and hydrophilized by glow discharge before 4 μ L aliquots of the nanoplex solutions (0.3 μ g/ μ L complexed DNA) were applied to the grids. Samples were vitrified by automatic blotting and plunge freezing with a FEI Vitrobot Mark IV (Thermo Fisher Scientific[™], USA) using liquid ethane as cryogen. The vitrified specimens were transferred to the autoloader of a Talos Arctica[™] transmission electron microscope (Thermo Fisher Scientific[™], USA), which is equipped with a X-FEG field emission gun and operated at 200 kV acceleration voltage. Micrographs were acquired on a Falcon 3 direct electron detector (Thermo Fisher Scientific[™], USA) using the 100 μ m condenser aperture at a nominal magnification of 28000 \times corresponding to a calibrated pixel size of 3.75 \AA per pixel. Nanoplex sizes were measured using ImageJ v1.53k (<https://imagej.net/>, (Schneider et al. 2012)).

3.4.8 Flow Cytometry

Flow cytometry can be used to count and analyze cells or particles present in suspension. By hydrodynamic focusing, each cell/particle is passed individually through a flow cell. Here, irradiation with laser light of suitable wavelength and detection of the scattered and emitted light takes place. The use of several lasers and filters of different wavelengths for the detection enables the simultaneous analysis of different object properties. Forward and side scatter are recorded and evaluated to characterize the size and granularity of the cells. In addition, fluorescence intensity due to expression of fluorescent proteins, uptake of fluorescent or fluorescently labeled molecules, or surface-labeling with fluorescently labeled antibodies can also be measured using appropriate laser light for excitation and band-pass filters for emission detection. Due to the analysis of single objects, high flow rates and the parallel determination of numerous characteristics, flow cytometry allows a fast and detailed investigation of cell suspensions.

For the investigations presented in this thesis, flow cytometry was used to determine the transfection efficiency of enhanced green fluorescent protein (eGFP)-encoding plasmids and the internalization of cyanine5 (Cy5)-labeled EGF based on the fluorescence signals of the cells. To ensure a reproducible evaluation and quantitative statement, only single, intact cells were included in the analysis. These were gated based on their forward scatter. The gate was established manually using blank (untreated) cell suspensions. As shown in Figure 3.2A, the peak width was plotted against the peak height of the forward scatter signal in a dot plot and the population of singlets was selected manually. Cell debris exhibits both lower signal heights and widths, a broadening of the signal with no change in height occurs with groups of cells (i.e., more than one). A minimum number of 5000 singlets were included in the analysis of each condition. Cell suspensions were prepared

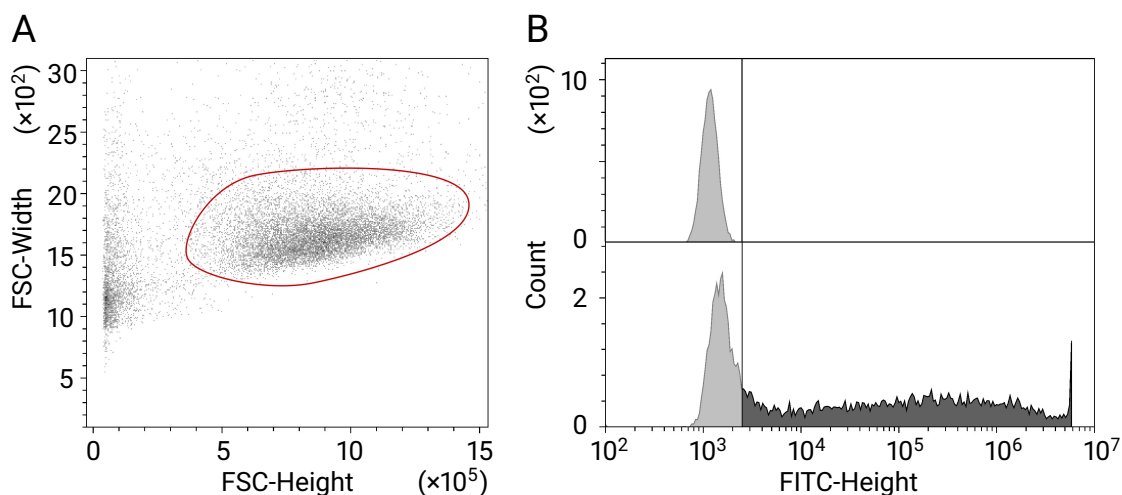


Figure 3.2: Evaluation of flow cytometry experiments. (A) Gating of singlets (single, intact cells), indicated by red circle in the dot plot. FSC = forward scatter. (B) Evaluation of eGFP expression. The autofluorescence of a blank (untreated) cell population (upper panel) is used to establish the threshold for eGFP-expression. All cells exhibiting higher eGFP-related fluorescence intensities (FITC-height values above the threshold), were considered transfected as depicted by the dark grey color in the lower panel.

by detaching the cells from the well plate using trypsin/ethylenediaminetetraacetic acid (EDTA). After detachment, cell suspensions were homogenized by pipetting to ensure a single-cell-suspension, transferred in a reaction tube and kept on ice until analysis. All flow cytometry analysis were recorded on a CytoFLEX S Flow Cytometer (Beckman Coulter, USA) using CytoFLEX Sheath Fluid and a flow rate of 30 $\mu\text{L}/\text{min}$. Data was analyzed using CytExpert v2.5 (Beckman Coulter, USA).

For the evaluation of eGFP-expression, peak height of the fluorescence signal in the fluorescein isothiocyanate (FITC)-channel (excitation with blue laser $\lambda = 488 \text{ nm}$; excitation band-pass filter $\lambda = 525 \pm 40 \text{ nm}$) was determined. As depicted in Figure 3.2B, all cells exhibiting eGFP-related fluorescence signals in the FITC-channel above the threshold set by the blank cell population were considered transfected. The transfection efficiency in percent indicates the proportion of transfected singlets of all singlets measured.

For the evaluation of the internalization of Cy5-labeled EGF, fluorescence intensity in the allophycocyanin (APC)-channel (excitation with red laser $\lambda = 638 \text{ nm}$; excitation bandpass filter $\lambda = 660 \pm 10 \text{ nm}$) was recorded.

Table 3.2: Cell culture media and seeding densities of all cell lines used within this thesis. Numbers indicate number of cells per well, 96-well plates were used for both transfection and EGF internalization assays. E-Plate L8 were used for impedance-based measurement of cell viability.

Cell line	Culture medium	E-Plate L8	Transfection	Internalization
A2058	DMEM, 4.5 g/L glucose	10000	5000	20000
A-431	DMEM, 4.5 g/L glucose			20000
HCT 116	McCoy's Modified 5A Medium		5000	20000
HEK293-FT	DMEM, 4.5 g/L glucose	10000	7500	
Hepa 1-6	DMEM, 4.5 g/L glucose	20000	10000	
Huh-7	DMEM, 4.5 g/L glucose	20000	10000	
ECV-304	DMEM, 4.5 g/L glucose		5000	
MDA-MB-468	DMEM, 4.5 g/L glucose	20000	10000	20000
Neuro-2a	DMEM, 1.0 g/L glucose	10000	5000	

3.5 *In Vitro* Investigations

3.5.1 Culture Conditions

Cell lines were cultivated at 37 °C in a humidified 5% CO₂ atmosphere. Depending on their growth rate, cells were subcultured every two to four days using trypsin/EDTA to detach the cells. Cells with passage numbers ≤ 30 were used for *in vitro* experiments. Table 3.2 lists the culture media for each cell line, all culture media were supplemented with 10% fetal bovine serum (FBS) and contained 2 mM alanyl-L-glutamine, either directly formulated in the medium or supplemented with UltraGlutamine™ I Supplement.

3.5.2 Transfection

To examine transfection efficiency *in vitro*, cell suspensions obtained during routine passaging were counted using a Neubauer counting chamber and cells were seeded into clear 96-well plates using a culture volume of 100 µL per well. Seeding densities are listed in the “Transfection” column of Table 3.2. Cells were incubated under normal culture conditions for 24 h prior to transfection. The complete cell culture medium was then removed using a vacuum pump aspiration system and immediately replaced with 80 µL of fresh complete cell culture medium. Afterwards, 20 µL nanoplex solution (100 ng complexed DNA in 10 mM HEPES, pH 7.1, formulated as described in Section 3.3) was added per well. For external SO1861-EMCH supplementation, 70 µL medium, 20 µL nanoplex solution, and 10 µL SO1861-EMCH solution (20 µg/mL in cell culture medium) were added. Cells were incubated with the nanoplex-containing media for 48 h (pEGFP-N3- and NP-eGFP transfections) or 72 h (NP-Sap transfections) under regular culture conditions. A control

cell population was incubated in parallel and was provided with 100 μL fresh cell culture medium at the time of transfection.

Lipofectamine transfection was performed according to the manufacturer's instructions, but adapted to the nanoplex transfection process to ensure maximum comparability. In deviation from the usual protocol, the Lipofectamine particles were formulated in 10 mM HEPES, pH 7.1, and the transfection was carried out with complete culture medium, i.e. containing FBS, which was not exchanged during the 48 h or 72 h incubation.

For transfection in E-Plates L8 as described in Section 3.5.4, 40 μL nanoplex solution (5 ng/ μL complexed DNA) and optionally in addition 10 μL SO1861-EMCH (120 $\mu\text{g}/\text{mL}$) were added after the initial 24 h incubation period.

For kinetic studies of the endosomal release of the nanoplexes, fluorescently labeled nanoplexes were prepared using a FITC-labeled peptide. NP-Luc, which encodes luciferase and thus is neither cytotoxic nor causes fluorescence of the cells, was used as pDNA. The preparation of the nanoplexes is described in Section 3.3 ("mixed nanoplexes"). CELLview cell culture dishes were used for cultivation of the cells. Twice the number of cells as indicated in column "Transfection" of Table 3.2 were seeded into one compartment (1.9 cm^2) using a total culture volume of 200 μL . For transfection, 200 ng complexed DNA was used per compartment. The transfection process was continuously monitored using the brightfield and green fluorescence ($\lambda_{\text{ex}} = 452 \pm 45 \text{ nm}$, $\lambda_{\text{em}} = 512 \pm 23 \text{ nm}$) channel of the Lux3 FL (CytoSMART[®], the Netherlands) live-cell imaging fluorescence microscope.

3.5.3 Transfection Efficiency

For the majority of *in vitro* studies, eGFP-encoding plasmids were used. Upon successful transfection, eGFP is expressed, which allows for the detection and quantification of transfected cells. This evaluation can be done in the living cell, thus does not require termination of the experiment and can therefore be done continuously. As illustrated in Figure 3.2B, a disadvantage of the evaluation via the green fluorescence intensity is the difficulty in distinguishing the autofluorescence of the cells from weak eGFP expression.

During the 48 h incubation period, eGFP-expression was monitored using the small fluorescence live-cell imaging microscope CytoSMART[®] Lux3 FL (CytoSMART[®], the Netherlands). This microscope was placed inside the CO₂ incubator, allowing continuous evaluation of both eGFP expression and cell growth during cultivation. Cell coverage, also called confluency, in the brightfield and green fluorescence ($\lambda_{\text{ex}} = 452 \pm 45 \text{ nm}$, $\lambda_{\text{em}} = 512 \pm 23 \text{ nm}$) channel was determined by the CytoSMART[®] Cloud Service by means of image analysis. Transfection efficiency defined as the share of eGFP-expressing cells was calculated from these values by

$$\text{Fluorescence Coverage} = \frac{\text{Confluency Green Fluorescence}}{\text{Confluency Brightfield}} \cdot 100\%.$$

Fluorescence microscopic live cell imaging with the Lux3 FL only allows the observation of one well and has low sensitivity. Routine evaluation of parallel transfections was therefore performed by flow cytometry as described in Section 3.4.8. Flow cytometric analysis allows conclusions to be drawn regarding both fluorescence intensity and the proportion of transfected cells. This is not the case with the frequently used spectrophotometric analysis of fluorescence expression with a microplate reader, since the fluorescence intensity of the entire well is measured here.

For transfections of NP-Sap, which is encoding the cytotoxic protein saporin, transfection efficiency was determined by assessing cell viability 72 h after transfection using MTS (3-(4,5-dimethylthiazol-2-yl)-5-(3-carboxymethoxyphenyl)-2-(4-sulfophenyl)-2H-tetrazolium, inner salt) assay. CellTiter 96[®] AQueous One Solution Cell Proliferation Assay (Promega GmbH, Germany) was used according to the manufacturer's protocol with an incubation time of 2 h. Absorbance values were recorded on an infinite F200 (Tecan Group Ltd., Switzerland) microplate reader. The reagent solution, which is added to the cells for evaluation of cell viability, contains the tetrazolium compound MTS and the electron coupling reagent phenazine ethosulfate (PES). The MTS tetrazolium compound is bio-reduced by cells into a colored formazan product, whereby the amount of formazan product is proportional to the number of living cells (Cory et al. 1991) and thus provides information about cell viability. PES is required as intermediate electron acceptor to enable formazan formation. In contrast to the commonly used 3-(4,5-dimethylthiazol-2-yl)-2,5-diphenyl tetrazolium bromide (MTT) assay, which uses a closely related tetrazolium compound, the MTS assay allows absorbance measurement immediately after incubation (Bartrop et al. 1991). This is due to the water solubility of the MTS formazan product, which eliminates the need for the error-prone solubilization of the formazan granule by DMSO.

Each *in vitro* transfection experiment was performed independently three times.

3.5.4 Cellular Impedance

Cellular impedance measurement is a highly sensitive method to investigate cell viability. Cells are cultivated in special microtiter plates, the well bottom of which is covered with gold microelectrodes. When a voltage is applied, a flow of electrons occurs across the conductive cell culture medium. The presence of adherent cells at the well bottom, and thus at the electrode-medium interface, impedes electron flow. This electric resistance caused by the adhesion of cells on the well surface is referred to as cellular impedance.

The cellular impedance is reported using the unitless parameter Cell Index, which is calculated as follows:

$$\text{Cell Index} = \frac{\text{impedance at time point } t - \text{impedance in the absence of cells}}{\text{nominal impedance value}}$$

The measurement of cellular impedance can be performed in real time during the run time of the experiment, works without labeling agents, and is non-invasive.

The data recording over the entire experimental period as well as a possible combination with other evaluation techniques at the endpoint of the experiment represent advantages over the established and routinely used formazan-generating assays for cell viability assessment. Compared to optical evaluation of confluence by image analysis, which only takes into account the well area covered by cells and is prone to errors in the recording and evaluation of the images, the magnitude of cellular impedance is not only dependent on the well area covered but also on the cell-substrate attachment quality.

Within this thesis, impedance-based measurements were performed to determine cell viability during incubation with varying saponin concentrations and nanoplex transfections. For this, two E-Plates L8 were filled with 150 μ L cell culture medium per well to measure the blank impedance. Afterwards, cells were added in 400 μ L cell culture medium, resulting in a culture volume of 550 μ L per well. Seeding densities are listed in the column “E-Plate L8” of Table 3.2. The procedure for transfection experiments is described in Section 3.5.2. For the investigation of the tolerability of SO1861-EMCH *in vitro*, 50 μ L SO1861-EMCH in cell culture medium was added to each well after an initial 24 h incubation period. The concentration of these added stock solutions was twelve times the specified final SO1861-EMCH concentration. Cells were incubated using the regular cultivation conditions while the cellular impedance was measured every 10 min with the RTCA iCelligence™ system (ACEA Biosciences, USA). Data was analyzed by the RCTA data analysis software (ACEA Biosciences, USA). Normalized cell indices are reported, which is the measured cell index normalized to the cell index measured at the time point of intervention.

3.5.5 Internalization of Epidermal Growth Factor

To investigate and characterize internalization of Cy5-EGF, cells were incubated with the fluorescently labeled EGF-mutant (provided by Melanie Krass, working group of Prof. Hendrik Fuchs, Institut für Laboratoriumsmedizin, Klinische Chemie und Pathobiochemie, Charité – Universitätsmedizin Berlin) in varying concentrations and for different time periods. The evaluation was carried out using flow cytometry as described in Section 3.4.8.

Cells were seeded in 96-well plates using a culture volume of 100 μ L, seeding densities are listed in the column “Internalization” of Table 3.2. After a 24 h cultivation period, the culture medium was exchanged against Cy5-EGF-containing culture medium.

For evaluation of concentration-dependent internalization, Cy5-EGF was used in concentrations ranging from 0.1 nM to 1 000 nM. The free labeling dye Sulfo-Cy5-NHS was tested in parallel as control. Cells were incubated with Cy5-EGF for 24 h.

To investigate time-dependent uptake, a constant Cy5-EGF concentration of 100 nM was used. The Cy5-EGF-containing cell culture medium was added to the cells at different time points and the experiment was terminated simultaneously in all wells.

For evaluation of competitive inhibition of Cy5-EGF uptake by an excess of unlabeled

EGF, cells were incubated with 100 nM Cy5-EGF and varying concentrations of unlabeled EGF for 4 h.

Fluorescence micrographs of Cy5-EGF uptake by A-431 cells were recorded using the brightfield and red fluorescence ($\lambda_{\text{ex}} = 561 \pm 14 \text{ nm}$, $\lambda_{\text{em}} = 630 \pm 90 \text{ nm}$) channel of the Lux3 FL (CytoSMART[®], the Netherlands) live-cell imaging fluorescence microscope during incubation with 1 000 nM Cy5-EGF in one compartment (1.9 cm²) of a CELLview cell culture dish with glass bottom using 100 μL culture volume.

3.6 *In Vivo* Investigations

The *in vivo* tolerability and efficacy studies were performed in close accordance with the settings of the described *in vivo* investigation on sapofection using SO1861 and PLL-based nanoplexes in the two-component setting by Sama et al. (2018b). All animal experiments were performed by Britta Büttner under supervision of Prof. Walther at Experimental Pharmacology & Oncology Berlin-Buch GmbH, Germany in accordance with the United Kingdom Coordinated Committee on Cancer Research (UKCCR) guidelines and were approved by the responsible local authorities (State Office of Health and Social Affairs, Berlin, Germany; approval No. G03333/18 and Reg0010/19).

In the Neuro-2a neuroblastoma allograft model, the anti-tumor-efficacy of treatment nanoplexes (NP-Sap complexed with 70 % pepY and 30 % K₁₆CPEGeq0.5, hereinafter referred to as pepY-SO1861-nanoplex) were compared to non-equipped nanoplexes (NP-Sap complexed with 70 % pepY and 30 % K₁₆CPEG, hereinafter referred to as pepY-nanoplex) and vehicle control as placebo.

Nanoplexes for the *in vivo* investigations were formulated as described in Section 3.3 using sterile-filtered HBM as buffer. To allow for the exact injection of 100 μL nanoplex solution, 110 % of the required quantity was prepared. To enable the preparation of the highly concentrated nanoplex solutions for injection, the two peptide components were lyophilized in the calculated quantities as combined aliquots before the start of the study. The evening before the injection, the peptide aliquots were solubilized in 55 μL HBM per aliquot and the resulting solution was stored overnight at 8 °C. The next day, nanoplexes were formed by adding the DNA solution (33 μg NP-Sap in 55 μL). The resulting nanoplex solutions were stored at room temperature and used for injection within 24 h.

3.6.1 Tolerability Studies

The tolerability of the treatment nanoplexes (pepY-SO1861-nanoplex) was assessed in three six- to eight-week-old NMRI nu/nu female mice without tumor induction. Mice were injected i.v. with treatment nanoplexes (30 μg complexed NP-Sap in 100 μL) every two days with a total number of five injections. Mice were monitored for condition and

potential side effects, including skin reactions (flush) at the injection site. Furthermore, body weight was measured every two days for two weeks.

3.6.2 Anti-Tumor Efficacy

1×10^6 Neuro-2a-cells in DPBS were injected subcutaneously (s.c.) in the left flank of 30 six- to eight-week-old NMRI nu/nu female mice to induce neuroblastoma tumors. The animals were then randomly allocated to three treatment groups ($n = 10$ mice/group). Injection schedule was the same for all groups: a total of five injections was administered i.v. on day 1, 3, 5, 7, and 9 after tumor induction. The control group received 100 μ L HBM as vehicle control, the pepY-nanoplex group received 100 μ L pepY-nanoplex in HBM (30 μ g NP-Sap per injection), and the pepY-SO1861-nanoplex group received 100 μ L pepY-SO1861-nanoplex in HBM (30 μ g NP-Sap per injection). Tumor size and body weight was determined twice a week during the study period. The treatment efficacy was determined by measurement of tumor volumes (TVs). TV measurement was performed with a digital caliper and TVs were calculated using the formula

$$TV = 0.5 \cdot \text{length} \cdot \text{width}^2.$$

When animals reached a TV $> 1.5 \text{ cm}^3$, studies were terminated for ethical reasons.

3.7 Statistical Analysis

Statistical analysis was performed using R: A Language and Environment for Statistical Computing (R Core Team 2022; Xu et al. 2021). Normality was assessed with Shapiro-Wilk test assuming a 95 % confidence level. If normal distribution was confirmed, statistical significant differences between groups were determined with unpaired, two-sided Student's *t*-test. If data was not normally distributed, Wilcoxon signed-rank tests were performed to investigate differences. Grubbs's test was used to test for outliers assuming a 95 % confidence level.

4 Results and Discussion

4.1 Stability of SO1861-EMCH

As discussed in Section 1.4, the hydrazone linkage of SO1861 and the DNA-complexing peptide scaffold via the *N*- ϵ -maleimidocaproic acid hydrazide (EMCH)-linker was chosen based on its hydrolysis at pH < 7.0. This shall ensure release of the saponin in the acidic endosomal compartments. To confirm this hypothesis and gain information on the specific kinetics of SO1861 release from its EMCH-derivative, the stability of SO1861-EMCH was investigated in different buffers and pH values over time using NMR. These studies were carried out by the group of Prof. Fernandez-Megia (CIQUS, Universidade de Santiago de Compostela) within the ENDOSCAPE project. The data generated is presented in the following as it influenced the optimization efforts described in Section 4.2.3.

The observed hydrolysis rates (Table 4.1) indicated complete stability of both the maleimide and the hydrazone group in phosphate-buffered saline (PBS) at pH 7.4, while incubation in 20 mM phosphate buffer at pH 7.4 or 7.0 and water led to increasing hydrolysis of the maleimide group over time. Hydrolysis of the hydrazone group at acidic pH occurred to a much lesser extent than expected for SO1861-EMCH. In 20 mM citrate buffer, both the maleimide and hydrazone groups were completely stable at pH 6.0. Incubation at pH 4.5 resulted in appreciable hydrolysis rates of the hydrazone group. However, it is questionable whether the actual release rate is sufficient for the hoped-for endosomal escape-enhancing (eee) activity of SO1861 *in vitro* and *in vivo*, as only 29 % SO1861 was released after 24 h incubation at pH 4.5 and 37 °C. The problematic low release rate is likely exacerbated by nanoplexing SO1861-EMCH, which further hinders the accessibility of the hydrazone group compared to the free diffusion of SO1861-EMCH in the buffer.

As hydrolysis of the hydrazones' carbon-nitrogen double bond at acidic pH values is generally described to be initiated by protonation of the imine nitrogen, followed by nucleophilic attack of a water molecule at the imine carbon (Christie et al. 2010; West and Otto 2005), substituents adjacent to the hydrazone massively influence its hydrolysis rate. In comparison of SO1861-EMCH with Aldoxorubicin (Doxorubicin-EMCH) (Figure 4.1), one must denote the presence of a hydroxyl group at C-9 of Aldoxorubicin instead of the methyl group at C-4 of SO1861-EMCH and a hydroxymethyl group at C-13 of Aldoxorubicin. Both additional groups are electron-withdrawing and decrease the electron density of the imine carbon, thus making it more susceptible to nucleophilic attack by water. This could contribute to the markedly different hydrolysis rate of both components' hydrazone

Table 4.1: Hydrolysis rates in % of hydrazone and maleimide group in SO1861-EMCH in different buffers (first line of header), pH values (second line of header) and for different incubation times. Values were determined by ^1H NMR as described in Section 3.4.1. Non-filled boxes indicate that no hydrolysis was observed under these conditions.

		PBS 7.4	PB 7.4	PB 7.0	H ₂ O	Citrate 6.0	Citrate 5.5	Citrate 5.0	Citrate 4.5	Citrate 4.5 37 °C
Hydrazone	2 h									4
	6 h									5
	24 h						2	4	12	29
Maleimide	2 h		37							
	6 h		40	11	6					
	24 h		42	54	47					11

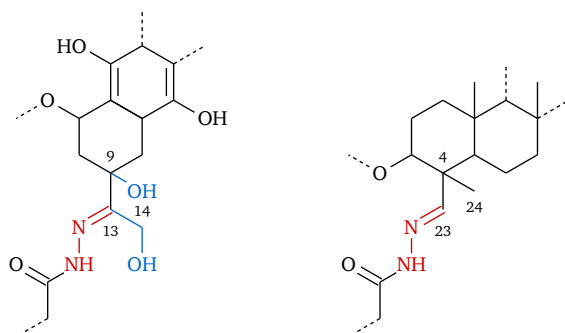


Figure 4.1: Hydrazone groups (indicated in red) with adjacent molecular structures of Aldoxorubicin (left) and SO1861-EMCH (right). Additional electron-withdrawing substituents in Aldoxorubicin are denoted in blue.

groups at acidic pH (Aldoxorubicin covalently conjugated to human serum albumin: 50 % hydrolysis after ≈ 25 min at 37 °C and pH 5.0 (Kratz et al. 2002), Aldoxorubicin covalently conjugated to albumin-binding domain: ≈ 25 % hydrolysis after 2 h at 37 °C and pH 5.0 (Yousefpour et al. 2019), SO1861-EMCH: 4 % hydrolysis after 2 h at 37 °C and pH 4.5).

Summary

- The maleimide and the hydrazone group of SO1861-EMCH were completely stable for 24 h in PBS, pH 7.4 and 20 mM citrate buffer, pH 6.0.
- Hydrolysis of the hydrazone group at acidic pH occurred to a lesser extent than expected, with only 5 % released SO1861 after 6 h incubation at 37 °C and pH 4.5.

4.2 Peptide Scaffolds

The sequence of the peptide scaffold and its functionalization are closely linked. Therefore the initial conditions as well as the optimization steps of both are outlined in the following. This section is completed by the characterization of the functionalized peptide scaffolds.

4.2.1 Initial Peptide Design

As introduced in Section 1.4, the peptide scaffold is central in linking all elements of the one-component gene delivery vehicle. Accordingly, the design of the peptide sequence was guided by the different functions that were required.

A polylysine domain (K_{16}) was installed for the complexation of DNA via electrostatic interactions of the cationic amino acid side chains and the anionic phosphate backbone of the nucleic acid at physiological pH. A chain length of 16 lysines has been shown to be optimal in terms of stable particle formation and transfection efficiency (Kwok et al. 2016) and has been used in previous studies on the sapofection of plasmid DNA (pDNA).

As described in Section 1.4, the covalent conjugation of SO1861-EMCH by means of a Michael-type thiol-maleimide addition requires the presence of a thiol group on the peptide scaffold. This functionality can either be installed directly by incorporating cysteines or by converting amino to thiol groups with 2-iminothiolane. The first option was selected to avoid the thiolation and purification step prior to the Michael-addition. Furthermore, based on previous investigations using the unmodified K_{16} domain for nucleic acid complexation, it seemed advisable not to heterogenize the K_{16} part by modification of the side chains and conjugation of SO1861-EMCH molecules. In addition, the functionalization with 2-iminothiolane would result in a stoichiometric mixture of peptides exhibiting a distribution of functionalization, both with regard to number and localization of the thiol groups.

For the conjugation of a dibenzocyclooctene(DBCO)-functionalized ligand via strain-promoted azide-alkyne-cycloaddition (SPAAC) reaction, an azide functionality was introduced by incorporating an azidolysine, denoted by $K(N_3)$. The azidolysine, a lysine that is modified to carry an azide functionality instead of the amino group in the residue, was installed C-terminally, at the opposite end to the K_{16} -tail, to ensure accessibility of the azide group for SPAAC reaction. Figure 4.2 depicts a schematic illustration of the initially designed peptide scaffolds $K_{16}C_3$ and $K_{16}C_3PEG$, which were used for first conjugation reactions. The PEG₈-spacer introduced in one of the scaffolds should be tested for its influence on the stability and solubility of the scaffold and the nanoplexes formed with it.



Figure 4.2: Schematic illustration of initially designed peptide scaffolds $K_{16}C_3$ and $K_{16}C_3PEG$.

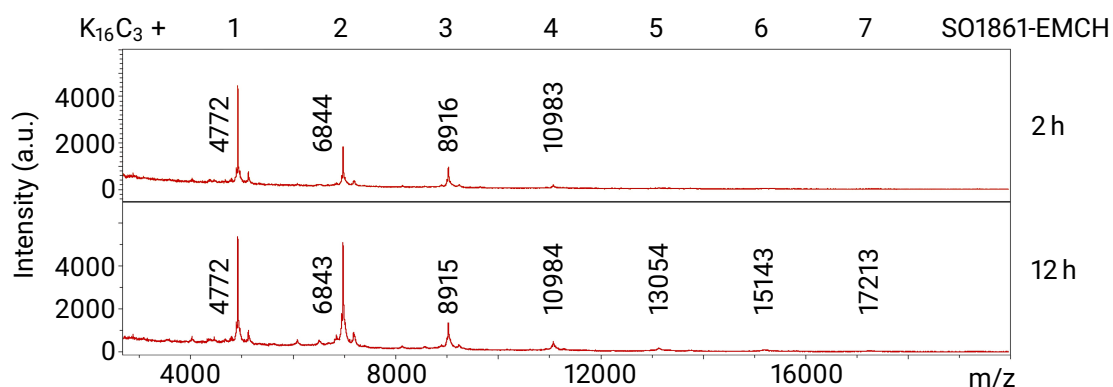


Figure 4.3: MALDI-TOF MS spectra of peptide scaffold $K_{16}C_3$ functionalization with SO1861-EMCH using different incubation times (indicated to the right of the spectra). Measurements were performed as described in Section 3.4.2 using SA as matrix. Peaks are labeled with average m/z of $[M+H]^+$. Numbers on top of the spectra indicate the number of conjugated SO1861-EMCH molecules per peptide scaffold.

4.2.2 Initial Functionalization Conditions

Maleimide ligation through Michael-addition is described to be highly specific for sulfhydryl groups at pH 6.5 to 7.5 (Kratz 2007). First conjugation reactions were therefore conducted at room temperature in DPBS at pH 7.0 using different incubation times (Figure 4.3) and molar ratios (amount of SO1861-EMCH relative to one cysteine) (Figure 4.4) for the conjugation reaction.

Matrix-assisted laser desorption/ionization time-of-flight mass spectrometry (MALDI-TOF MS) analysis of the resulting product confirmed the conjugation of SO1861-EMCH to the three thiol groups of the peptide scaffold. Regardless of the conditions, a heterogeneous mixture of different conjugates with varying numbers of bound SO1861 molecules was detected for all reaction conditions. Although MALDI-TOF MS spectra do not enable a quantitative evaluation, the intensity of the different peaks within a spectrum allowed a semi-quantitative assessment. As expected, longer incubation times and a larger excess of SO1861-EMCH yielded larger amounts of higher substituted peptide scaffolds. Surprisingly, the coupling of more than three SO1861-EMCH molecules per peptide scaffold was observed, especially when an excess of SO1861-EMCH was used or the reaction mixture was incubated overnight. A probable explanation for this observation is a side reaction of the maleimide group of SO1861-EMCH with the amino groups in the lysine side chains. At the pH value of 7.0 that was used, the reaction of the maleimide with the thiol groups is described to proceed 1000 times faster than the reaction with the amino groups (Hermanson 2013). Therefore, the extent of this side reaction was unexpected. It is noteworthy that conjugates with

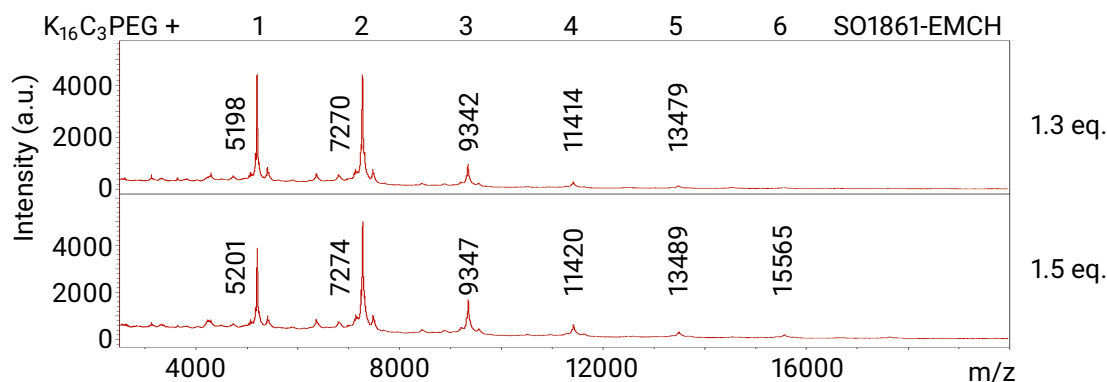


Figure 4.4: MALDI-TOF MS-spectra of peptide scaffold $K_{16}C_3$ PEG functionalization with SO1861-EMCH using different molar ratios. Used molar equivalents of SO1861-EMCH relative to one cysteine are indicated to the right of the spectra. Measurement and labeling as given in Figure 4.3 description.

one or two bound SO1861-EMCH molecules are dominant in the heterogeneous reaction mixture. Despite a large excess of SO1861-EMCH, the amount of triple conjugate did not significantly increase, so it is reasonable to assume that steric effects were responsible for the hindered attachment of the third SO1861-EMCH molecule. A hindrance to the reaction of the maleimide with the sulfhydryl group could also have contributed to the conjugation to the easily accessible lysine residues.

The obtained heterogeneous product mixture required a following purification step. Here, the main goal was the removal of unreacted SO1861-EMCH and all conjugates carrying more than three SO1861 molecules, since these are most likely bound to the lysine residues and may therefore influence the complexation efficiency of the K_{16} -tail. Optimally, the purification procedure would result in the isolation of a single species, meaning a peptide scaffold carrying a precise number of SO1861 molecules.

Several chromatographic methods were tested for this purpose. By using size exclusion chromatography (SEC), separation of unreacted SO1861-EMCH from the conjugates was possible, but separation of the heterogeneous mixture of conjugates was not achieved due to the small differences in size. Multiple attempts using Reverse Phase (RP) C-8 or RP C-18 liquid chromatography (LC) as well as hydrophilic interaction liquid chromatography (HILIC) also did not yield the envisaged separations. Treating the product mixture with Tris(2-carboxyethyl)phosphine (TCEP), thereby reducing disulfide bonds in the peptides, resulted in significant changes in the HILIC chromatograms. This indicated formation of disulfide bridges between the SO1861-equipped peptide scaffolds. The presence of the conjugates as a covalently linked structure is problematic with respect to their solubility as well as complexing properties. This observation also explained the inability to separate the

conjugates based on their size. While reductive treatment with TCEP was very valuable as a diagnostic tool, unfortunately this was not an option for the conjugation reaction itself or the subsequent purification, as treatment with TCEP would equally lead to a reduction of the free azide functionality in the peptide scaffold.

4.2.3 Optimization of Peptide Sequence and Functionalization Conditions

Based on the observed problems with the initial peptide scaffold design, the following modifications were included for the synthesis of the optimized peptide scaffolds K₁₆C and K₁₆CPEG (schematically shown in Figure 4.5):

- In order to minimize the potential of aggregate formation due to disulfide bond formation, the number of cysteines was reduced to one. In addition, calculation of the SO1861 amounts used in the established two-component sapofection system indicated SO1861 loadings ≤ 1 equivalent per peptide scaffold to be appropriate. Furthermore, due to the amphiphilic character of SO1861, the introduction of several SO1861 molecules per peptide scaffold was concerning with regard to its influence on complexation efficiency.
- To avoid steric hindrance in SO1861-EMCH conjugation, the number of glycines surrounding the single cysteine was increased. The four glycines between the K₁₆-tail and the cysteine shall additionally ensure that the complexation capability of the K₁₆-motif is not influenced by conjugated SO1861-EMCH.
- A single tyrosine was introduced in the peptide sequence to facilitate detection and quantification of the peptide scaffolds using UV/Vis- spectrophotometry. Additionally, the free hydroxyl group of the tyrosine may be valuable for another functionalization reaction.

The reaction conditions of the thiol-maleimide addition were optimized in parallel by implementing the following modifications:

- To favor thiol-over-amine chemoselectivity, the conjugation reaction was performed in 20 mM citrate at pH 6.0. This slightly acidic pH value ensures complete protonation of the amino groups of the lysine residues, thus making them less susceptible for reaction with the maleimide group of SO1861-EMCH. Complete stability of both the

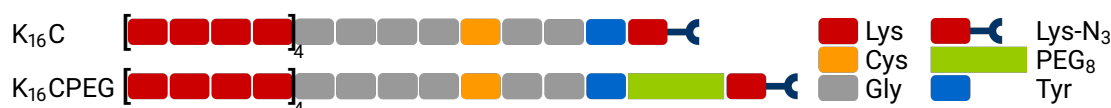


Figure 4.5: Schematic illustration of optimized peptide scaffolds K₁₆C and K₁₆CPEG.

hydrazone and the maleimide group of SO1861-EMCH were confirmed for these conditions beforehand (Table 4.1).

- The amount of SO1861-EMCH molecules was drastically reduced to 0.25 and 0.5 equivalents SO1861-EMCH per cysteine to ensure complete reaction of the SO1861-EMCH even in the case of minimal interpeptide disulfide formation, thus avoiding the subsequent purification step for the removal of unreacted SO1861-EMCH. Using ≤ 1 equivalent SO1861-EMCH should also minimize the risk of lysine-functionalization.
- In order to ensure complete reaction of SO1861-EMCH, the conjugation reaction was incubated at room temperature for 16 h.
- After incubation in 20 mM citrate buffer, the resulting product was first dialyzed against 150 mM NaCl before the final dialysis against ultrapure water. This additional step should ensure exchange of the citrate against chloride anions to secure presence of the final, lyophilized product as hydrochloride salt.

The sequence-optimized peptides K₁₆C and K₁₆CPEG were each functionalized with 0.25 and 0.5 equivalents of SO1861-EMCH using the described optimized reaction conditions. The produced peptide-SO1861-conjugates are in the following referred to as equipped peptide scaffolds

- K₁₆Ceq0.25: S-SO1861_{0.25}-(K₁₆G₄CG₂YK(N₃)),
- K₁₆Ceq0.5: S-SO1861_{0.5}-(K₁₆G₄CG₂YK(N₃)),
- K₁₆CPEGeq0.25: S-SO1861_{0.25}-(K₁₆G₄CG₂Y-(PEG₈)-K(N₃)), and
- K₁₆CPEGeq0.5: S-SO1861_{0.5}-(K₁₆G₄CG₂Y-(PEG₈)-K(N₃)).

MALDI-TOF MS analysis of this set of equipped peptide scaffolds confirmed conjugation of SO1861-EMCH under the described conditions. Conjugates with more than one SO1861-EMCH molecule bound to the scaffold were not observed, making cross-reactivity with the lysines highly unlikely. Additional peaks were observed in the MALDI-TOF MS chromatograms of both the native peptide scaffolds, that were also incubated in 20 mM citrate buffer, pH 6.0, and the equipped peptide scaffolds. Some of the observed peaks were attributable to the formation of citrate-peptide adducts, as described for oxytocin degradation products in citrate-buffered solutions (Hawe et al. 2009; R. A. Poole et al. 2011; Wiśniewski et al. 2013). In addition, analysis of the nanoplexes (described in the following Section 4.3) that were formed with the equipped peptide scaffolds indicated problems with DNA complexation (Figure 4.10) and nanoplex stability (Table 4.2). This was ascribed to interfering effects of residual citrate anions.

Based on these observations, the reaction conditions for the thiol-maleimide addition were further optimized to incubation in DPBS at pH 6.5. Incubation in DPBS ensures a hydrochloride salt as final product, pH 6.5 is the lower limit of DPBSs buffering capacity.

MALDI-TOF MS analysis of the equipped peptides produced using these further optimized reaction conditions confirmed conjugation of SO1861-EMCH to the scaffolds. The MALDI chromatograms of all batches that were produced with these final reaction conditions over the course of this thesis are shown in the appendix (Section 7.2).

4.2.4 Purification of Equipped Peptide Scaffolds

MALDI-TOF MS analysis of the equipped peptide scaffolds showed no free SO1861-EMCH or SO1861 in the final product, bearing in mind the low sensitivity for the negatively charged saponins in the positive ion detection mode of MALDI-TOF MS. Especially with regard to envisaged *in vivo* studies, the absence of free saponin is crucial. Therefore, further analysis was performed using LC-MS as described in Section 3.4.3. Detection by electrospray ionization (ESI)-MS in negative ion mode is highly sensitive for saponins and the preceding chromatographic separation allows the clear distinction between free and conjugated SO1861. Trace amounts of both SO1861-EMCH and SO1861 were found in the equipped peptide scaffolds by LC-MS analysis, demonstrating the need for a purification step to remove the contamination with free saponin.

The peptides with their numerous primary amino groups can be classified as poly-cationic substances, while both SO1861 and SO1861-EMCH carry a negative charge at physiological pH due to their glucuronic acid. Thus, trying a separation of both species by ion-exchange chromatography was obvious. Classically, a cation-exchange column would be used in the present case, which would initially hold the peptides as the target product, while the saponin impurities would be removed by washing steps. In the subsequent elution, the peptides would then be eluted from the stationary phase by changing the pH or increasing the ion concentration of the mobile phase. Unfortunately, due to the polycationic nature of the peptides and the strong interaction with the stationary phase associated with this, elution of the peptides was not possible by increasing the ion concentration only, and elution occurred only at $\text{pH} \geq 12$. Due to the instability of the conjugate in the alkaline, this method was thus not applicable for preparative purification.

One way of circumventing the problem of excessive interaction with the column material was to use an anion exchange column. Here, the column material is positively charged, so the peptides should not be retained and elute with the flow-through of the column loading, while the saponin species are retained on the column. Experiments with different solid phase extraction (SPE) columns with anion-exchange capacities confirmed this hypothesis. The best separation was achieved with an HR-XAW stationary phase consisting of a hydrophobic spherical polystyrene-divinylbenzene copolymer with secondary and tertiary ammonium modification that exhibits weak anion exchange and RP properties. Peptide species eluted with the sample loading and first wash fraction as demonstrated by TAPS-PAGE (Figure 4.6). LC-MS analysis confirmed retention of SO1861 and SO1861-EMCH on the column. Elution of the saponin species occurred with the final acidic elution step using 1 % formic acid in MeOH.

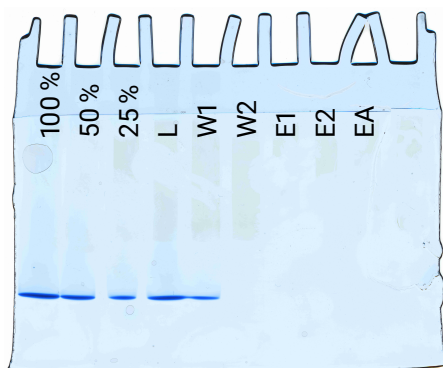


Figure 4.6: Purification of equipped peptide scaffold $K_{16}Ceq0.25$ using SPE as described in Section 3.2.2. Fractions were collected and concentrated using a vacuum centrifuge concentrator and subsequent lyophilization. The lyophilizate was dissolved in sample loading buffer and analyzed using Histidine-TAPS-PAGE as described in Section 3.4.4. Lanes 1-3: $K_{16}Ceq0.25$, percentages indicate amount relative to total amount loaded onto the SPE column, following lanes: sample loading (L), washing 1 (W1), washing 2 (W2), elution 1 (E1), elution 2 (E2), and acidic elution (EA).

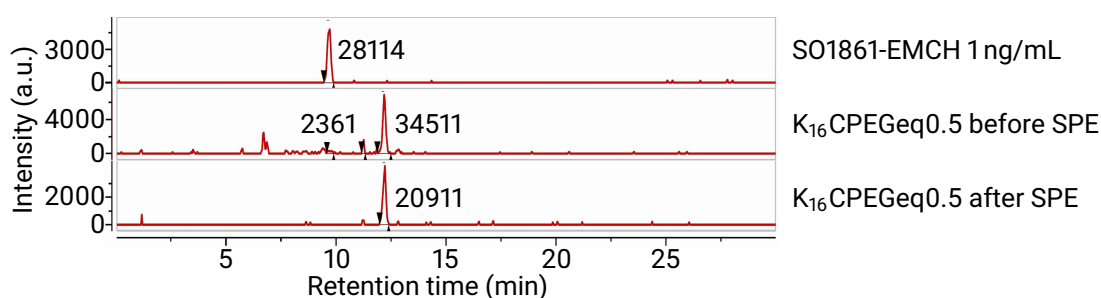


Figure 4.7: Chromatograms of $m/z 2069.8 \pm 0.25$ representing SO1861-EMCH in LC-MS analysis performed as given in Section 3.4.3. Chromatograms are derived from MS detection data, showing the appearance of ions with $m/z 2069.8 \pm 0.25$ over the course of the HPLC run. Peaks are labeled with peak area. Analyzed samples are given to the right of each chromatogram. Peaks at 12.2 min represent SO1861-EMCH which is released from the equipped peptide scaffold during MS-detection.

The SPE purification step was included in the conjugation protocol after incubation and before desalting by dialysis as described in Section 3.2.1. LC-MS-analysis of $K_{16}CPEGeq0.5$ produced with the optimized conjugation reaction including the SPE purification step revealed complete removal of unreacted SO1861-EMCH by SPE (Figure 4.7). The amount of free SO1861 was reduced by including the SPE purification step, but trace amounts were still detectable in the final product. Since free SO1861 was not available as reference material, absolute quantification could not be performed. It is unlikely that purification by ion-exchange chromatography is of different effectiveness for SO1861-EMCH and SO1861. Based on the absence of SO1861-EMCH, the traces of SO1861 detected owing to the high sensitivity of ESI-MS detection were therefore in all likelihood due to the release of minimal amounts of SO1861 from the final product.

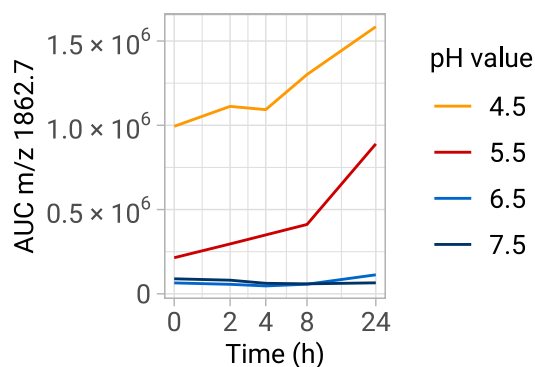


Figure 4.8: Release of SO1861 from the equipped peptide scaffold K₁₆CPEGeq0.5 depending on pH value. K₁₆CPEGeq0.5 was dissolved at 1 µg/µL in HBM, pH 7.5; 100 mM MES, pH 6.5; and 100 mM NH₄CH₃COO, pH 5.5 or 4.5 and incubated at 37 °C under orbital shaking. 20 µL aliquots were taken at the beginning of the incubation and after 2 h, 4 h, 8 h, and 24 h and kept at -20 °C until analysis by LC-MS as described in Section 3.4.3. AUC of the SO1861 peak with m/z 1862.7 ± 0.25 was used as semi-quantitative indicator of the SO1861 amount.

4.2.5 Release of SO1861

To investigate the release of SO1861 from the equipped peptide scaffolds, the equipped peptide scaffold K₁₆CPEGeq0.5 was incubated at varying pH values for a period of 24 h at 37 °C. Samples collected during this incubation time were analyzed for the presence and amount of SO1861 and SO1861-EMCH by LC-MS analysis. The sensitive detection by ESI-MS allowed the use of relatively low amounts of conjugate for this assay and the preceding chromatographic separation allowed the clear distinction and parallel determination of SO1861 and SO1861-EMCH. Unfortunately, quantification of SO1861 and SO1861-EMCH was not possible due to lack of available reference material. Therefore, the AUC of the SO1861 peak in the chromatogram derived from the MS detection data using the m/z of the saponin ion was used as a semi-quantitative indicator of the amount of saponin released (Figure 4.8). No release of SO1861-EMCH was detected for any pH or incubation period, confirming the stability of the thiosuccinimide linkage reported in literature. As expected, the release of SO1861 occurred as a function of pH and incubation period. While incubation at pH 7.5 and pH 6.5 did not result in any significant release even after 24 h incubation, at pH 5.5 and pH 4.5 a significant increase in the amount of free SO1861 was detected over the time period studied. Interestingly, the amounts of SO1861 already varied considerably at the start of incubation, i.e., in the samples taken and frozen immediately after dissolution of the peptide lyophilizate in the corresponding buffers. For lower pH values, larger amounts of SO1861 were detected, indicating a very rapid initial hydrolysis as a function of pH. Note that the mobile phase used for LC has a slightly acidic pH due to the addition of 0.01 % formic acid. A release during the chromatographic separation would therefore be conceivable in principle. However, since the chromatographic conditions were constant for all samples, this scenario does not explain the significantly different amounts of SO1861 released. Without providing a quantitative conclusion, the present study broadly confirmed the stability data found for non-conjugated SO1861-EMCH (Table 4.1) for SO1861-EMCH covalently bound to the peptide scaffolds.

4.2.6 Batch-to-Batch Reproducibility

During the course of the doctoral project presented in this thesis, several batches of the same functionalized peptides were prepared using the optimized reaction conditions. To assess reproducibility, the different batches were evaluated with respect to their most relevant property, their *in vitro* transfection efficiency. Aliquots of the different batches were stored as lyophilizate at -20°C for up to 30 months before *in vitro* testing.

No significant differences were observed between three batches each of the unmodified peptide K_{16}C and the equipped peptide scaffold $\text{K}_{16}\text{Ceq0.25}$ (Figure 4.9), each stored for different periods of time. This underlines the reproducibility of the optimized conjugation protocol and the stability of the peptide scaffolds under the described conditions.

Summary

- Unexpectedly, performing the Michael-type thiol-maleimide addition at pH 7.0 led not only to functionalization of the sulfhydryl groups of the cysteines but likewise to reaction with the amino groups of the lysines.
- The peptide scaffold sequence was optimized to consist of a K_{16} -domain for DNA complexation, one cysteine for conjugation of SO1861-EMCH, several glycines to avoid steric hindrance, a tyrosine for analytical purposes, an optional PEG₈-spacer and an azidolysine for bioconjugation of a targeting ligand.
- The functionalization of the peptide scaffold by means of thiol-maleimide addition was optimized to be performed in DPBS, pH 6.5 at room temperature for 16 h using submolar amounts of SO1861-EMCH (0.25 to 0.5 equivalents SO1861-EMCH per peptide scaffold).
- Trace amounts of unreacted SO1861-EMCH were separated from the peptide species after the conjugation reaction by anion exchange chromatography.
- The comparative evaluation of the *in vitro* transfection efficiency of several peptide batches confirmed batch-to-batch reproducibility and robustness of the optimized conjugation reaction conditions.
- The thiosuccinimide group formed by thiol-maleimide addition is stable at pH 4.5 to pH 7.0 and 37°C for up to 24 h.
- No significant release of SO1861 from the equipped peptide scaffolds was observed at pH 7.0 and pH 6.5 after incubation at 37°C for up to 24 h. At lower pH values, SO1861 was released from the equipped peptide scaffolds. The amount of SO1861 released correlated with acidity and incubation time.

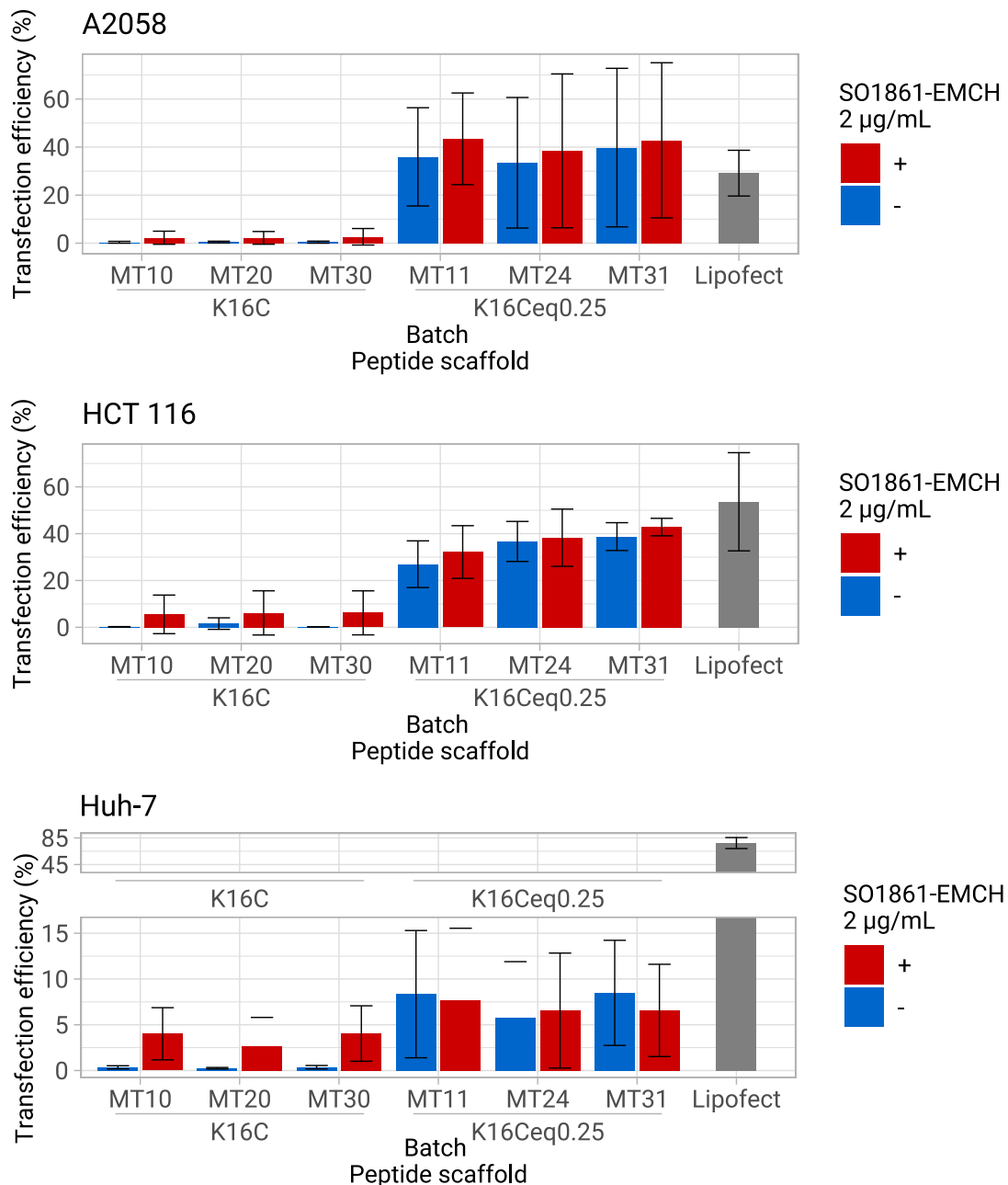


Figure 4.9: Transfection efficiency *in vitro* indicating reproducibility of the peptide functionalization reaction. Nanoplexes were prepared as described in Section 3.3 using batches of the unmodified peptide scaffold K₁₆C or equipped peptide scaffold K₁₆Ceq0.25 for complexation of pEGFP-N3, *in vitro* evaluation is described in Section 3.5.3. Bar height indicates mean of three independent experiments, error bars show standard deviation. No statistically significant differences between the different batches of the same peptide were found with Wilcoxon signed-rank tests.

4.3 Nanoplex Characterization

Mixing of the peptide scaffolds with nucleic acids as described in Section 3.3 results in the formation of nanoplexes due to the electrostatic interaction of both components. The physicochemical properties and the efficiency of nucleic acid complexation of these polymeric nanoparticles are critical for their cellular uptake and biodistribution and thus for their transfection efficiency *in vitro* as well as *in vivo*. Accordingly, characterization and optimization of the nanoplexes preceded *in vitro* testing of the most promising prototypes.

4.3.1 DNA Complexation Efficiency

As described in Section 3.4.5, the amount of free plasmid DNA (pDNA) was quantified after nanoplex formulation to determine the efficiency of DNA complexation of the peptide scaffolds. A highly selective, double-stranded DNA-binding fluorescent dye was used due to its high sensitivity, specificity and linearity over a broad concentration range.

The set of SO1861-equipped peptide scaffolds prepared in 20 mM citrate buffer varying in the incorporation of the PEG₈-spacer and the SO1861 loading was tested for its capability to complex pEGFP-N3 as model plasmid. As expected, all tested peptide scaffolds complexed DNA to a higher extent with rising N/P values. At N/P 10 \geq 89 % of the DNA was complexed by the peptides, except for the nanoplexes formulated with K₁₆Ceq0.5, which exhibited a DNA complexation efficiency of 59 % at N/P 10. Covalent conjugation of SO1861-EMCH reduced the complexation efficiency, this effect was particularly noteworthy for the conjugation of 0.5 equivalents of SO1861-EMCH per peptide scaffold. The incorporation of a PEG₈-spacer increased the complexation efficiency compared to the non-PEGylated analogs (Figure 4.10, left panel).

The same investigation using the optimized SO1861-equipped peptide scaffolds prepared in DPBS at pH 6.5 showed significantly higher DNA complexation efficiencies¹ (Figure 4.10, right panel). Increasing N/P ratios also led to higher complexation rates here. In deviation from the previous observations, using the set of optimized peptide scaffolds, a slight impairment of complexation efficiency was observed due to the incorporation of the PEG₈-spacer, while the functionalization with SO1861-EMCH had no clear effect on DNA complexation. All investigated optimized peptide scaffolds complexed \geq 97.8 % of DNA at N/P 10.

4.3.2 Size, Size Distribution and ζ -Potential

Particle size is a critical factor in determining the route and efficiency of cellular uptake and subsequent intracellular trafficking of nanoparticles used for gene delivery purposes, as described in detail in Section 1.1.2. The size of the nanoplexes formulated for the work on this thesis was therefore routinely checked using dynamic light scattering (DLS).

¹Note that in both cases the nanoplex formulation was carried out in 10 mM HEPES, pH 7.1.

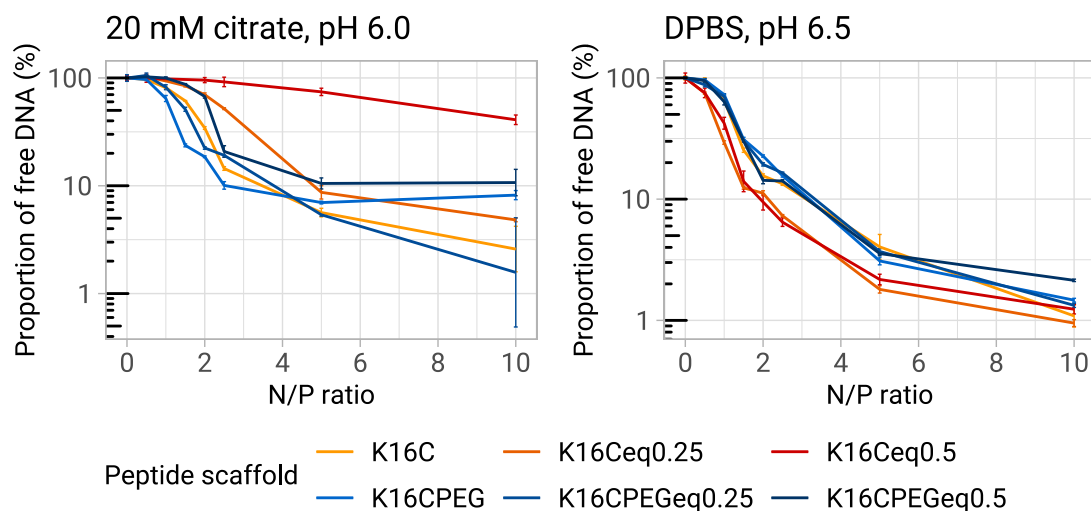


Figure 4.10: DNA complexation efficiency of peptide scaffolds as a function of N/P ratio used for nanoplex formation and buffer used for SO1861-EMCH conjugation (indicated above the graphs). Nanoplexes were formulated in 10 mM HEPES, pH 7.1 and evaluated as described in Section 3.4.5. Data is given as mean of triplicates, error bars indicate standard deviation.

DLS analysis of nanoplexes, produced by complexing pEGFP-N3 with the set of peptide scaffolds produced in 20 mM citrate buffer, revealed Z-Averages, the intensity weighted mean D_h s, of 450 nm to 1 120 nm and $P_{dis} > 0.49$, indicating particle size distributions heterogeneity. This pointed to a polydisperse particle size distribution and nanoplex aggregation (Table 4.2). This aggregation tendency can be related to the measured ζ -potentials, describing the value of electrostatic potential at the surface of hydrodynamic shear (Lowry et al. 2016), which fluctuated around zero and clearly indicated a non-stable suspension. In addition, the presence of citrate anions, which might not have been completely removed by dialysis, could have contributed to the aggregation of both peptide strands and nanoplexes because of their multivalency. Solely the nanoplexes formulated with $K_{16}Ceq0.5$, with $D_h \approx 150$ nm and $PDI \approx 0.3$, exhibited an acceptable size for *in vitro* application, but the ζ -potential of -31.7 mV made successful *in vitro* utilization seem unlikely. The negative ζ -potential indicated stabilization of this nanoplex solution by electrostatic repulsion and was in accordance with the detection of 41 % free DNA in the complexation assay (Figure 4.10).

The hypothesized interfering effect of citrate anions on nanoplex formation and stability was addressed by optimizing the peptide-saponin conjugation reaction (see Section 4.2.3).

Nanoplexes formulated with the resulting set of (equipped) peptide scaffolds prepared in DPBS, pH 6.5 exhibited D_h s of 80 nm to 160 nm and P_{dis} of 0.1 to 0.4 30 min after nanoplex

Table 4.2: Hydrodynamic diameter (D_h), polydispersity index (Pdi), and ζ -potential of nanoplexes formulated with pEGFP-N3 and (equipped) peptide scaffolds produced in 20 mM citrate, pH 6.0 as described in Section 3.4.6. Data is expressed as mean of triplicates \pm standard deviation.

Peptide scaffold	D_h (nm)	Pdi	ζ -Potential (mV)
K ₁₆ C	663.3 \pm 49.4	0.577 \pm 0.087	-2.11 \pm 0.18
K ₁₆ Ceq0.25	453.6 \pm 46.7	0.497 \pm 0.051	-2.71 \pm 0.63
K ₁₆ Ceq0.5	150.9 \pm 6.7	0.313 \pm 0.008	-31.70 \pm 1.87
K ₁₆ CPEG	794.6 \pm 226.3	0.694 \pm 0.231	-0.598 \pm 0.046
K ₁₆ CPEGeq0.25	1 118 \pm 370	0.798 \pm 0.192	3.20 \pm 0.40
K ₁₆ CPEGeq0.5	597.4 \pm 273.3	0.710 \pm 0.214	-0.366 \pm 0.789

Table 4.3: Hydrodynamic diameter (D_h), polydispersity index (Pdi), and ζ -potential of nanoplexes formulated with pEGFP-N3 and (equipped) peptide scaffolds produced in DPBS, pH 6.5 as described in Section 3.4.6. Data is expressed as mean of triplicates \pm standard deviation.

Peptide scaffold	Incubation time	D_h (nm)	Pdi	ζ -Potential (mV)
K ₁₆ C	30 min	86.24 \pm 5.19	0.276 \pm 0.030	32.8 \pm 3.8
	48 h	79.66 \pm 3.36	0.321 \pm 0.034	
K ₁₆ Ceq0.25	30 min	96.64 \pm 0.29	0.159 \pm 0.004	35.6 \pm 2.0
	48 h	123.7 \pm 1.2	0.239 \pm 0.016	
K ₁₆ Ceq0.5	30 min	117.1 \pm 22.9	0.277 \pm 0.016	32.1 \pm 1.2
	48 h	185.6 \pm 10.7	0.306 \pm 0.038	
K ₁₆ CPEG	30 min	137.80 \pm 4.97	0.366 \pm 0.013	28.8 \pm 3.5
	48 h	118.60 \pm 6.03	0.349 \pm 0.016	
K ₁₆ CPEGeq0.25	30 min	153.30 \pm 4.03	0.343 \pm 0.020	29.6 \pm 1.5
	48 h	280.5 \pm 0.7	0.287 \pm 0.007	
K ₁₆ CPEGeq0.5	30 min	90.30 \pm 1.09	0.100 \pm 0.007	30.8 \pm 1.0
	48 h	100.7 \pm 0.6	0.137 \pm 0.020	

formulation (Table 4.3). Hence, all investigated nanoplexes considerably undercut the upper size limit for clathrin-mediated endocytosis of 200 nm as discussed in Section 1.1.2.

As shown in Figure 4.11, the intensity-weighted size distributions of all investigated nanoplexes displayed a dominant peak at D_h s around 100 nm. A minor share of aggregates with $D_h > 1\ 000$ nm was detected for all nanoplexes except for the ones formulated with K₁₆Ceq0.25 and K₁₆CPEGeq0.5. It must be kept in mind that larger particles are over-represented in DLS size determination. The extent of aggregate formation was therefore lower than the depicted size distributions suggest. Saponin conjugation was shown to reduce the mean size and heterogeneity of the nanoplexes, with 0.5 equivalents showing superior results for K₁₆CPEG and 0.25 equivalents performing best for K₁₆C. D_h s and Pdis

of the nanoplexes formulated with equipped peptide scaffolds were increased after a 48 h incubation period, indicating a swelling of the nanoplexes and increased aggregate formation over time. $K_{16}Ceq0.25$ - and $K_{16}CPEGeq0.5$ -nanoplexes exhibited the best stability, with $D_{hs} < 125$ nm and $PdI < 0.25$ after incubation for 48 h.

All investigated nanoplexes showed ζ -potentials around 30 mV, with slightly smaller values for the $K_{16}CPEG$ -derived peptide scaffolds. A significant effect of SO1861 conjugation on surface charge, which might be expected given the saponins glucuronic acids negative charge at pH 7.1, was not observed (Table 4.3).

Summary

- Nanoplexes prepared with the peptide scaffolds incubated in 20 mM citrate buffer exhibited a strong aggregation tendency, which was attributed to the presence of residual citrate anions.
- Nanoplexes prepared with the peptide scaffolds prepared in DPBS, pH 6.5 exhibited mean hydrodynamic diameters < 160 nm, polydispersity indices < 0.4 , ζ -potentials ≈ 30 mV and DNA complexation efficiency $\approx 98\%$ 30 min after nanoplex formulation. These properties suggested a successful *in vitro* application.
- $K_{16}Ceq0.25$ - and $K_{16}CPEGeq0.5$ -nanoplexes exhibited the narrowest size distributions and highest stability at 48 h incubation.

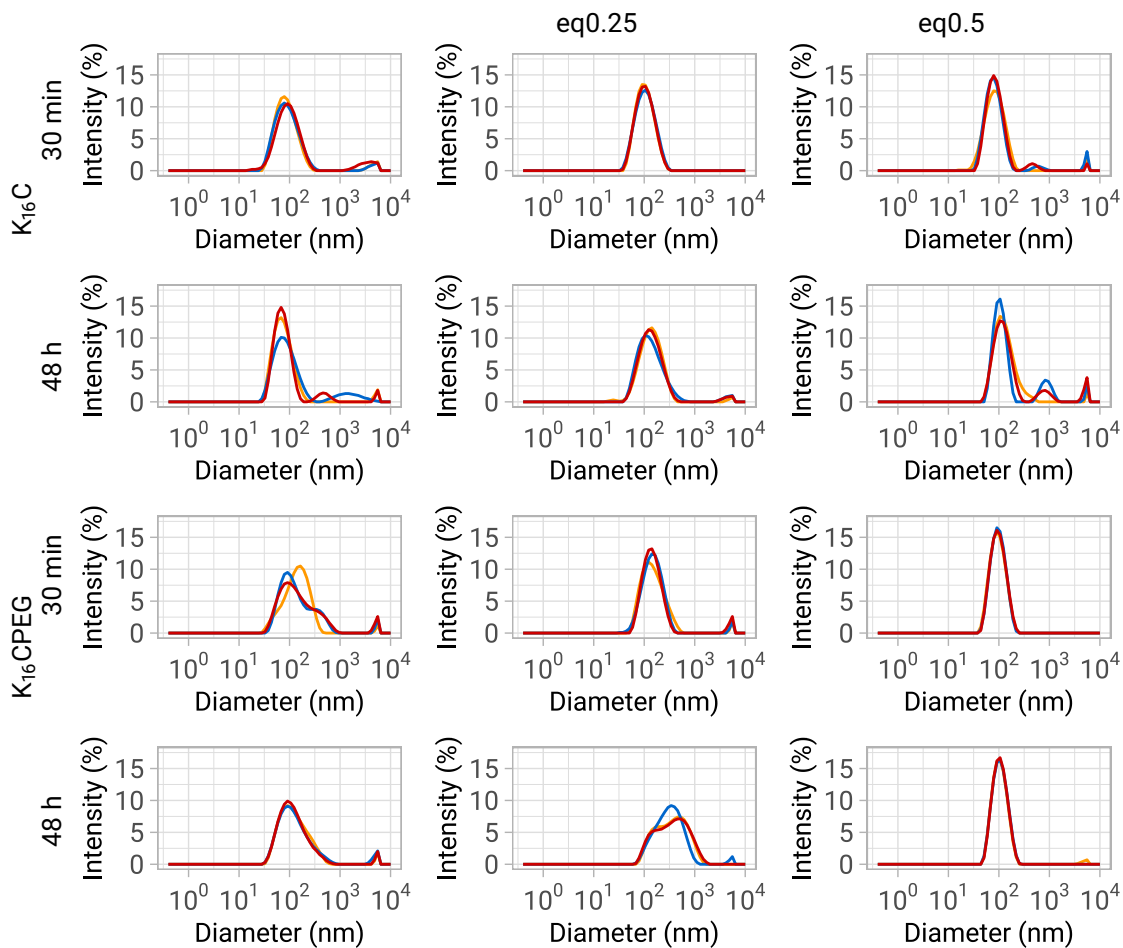


Figure 4.11: Size distribution by intensity of nanoplexes formulated with peptide scaffolds produced in DPBS, pH 6.5 at N/P 10 as described in section 3.4.6. Size distribution was measured after a 30 min incubation period and 48 h later. Size distributions of three measurements (different colors) are shown. First line shows (from left to right) size distributions of K₁₆C-, K₁₆Ceq0.25-, and K₁₆Ceq0.5-nanoplexes 30 min after nanoplex formulation. The row below shows the same nanoplexes 48 h later. The bottom rows show size distributions of K₁₆CPEG-, K₁₆CPEGeq0.25-, and K₁₆CPEGeq0.5-nanoplexes 30 min (third row) and 48 h (fourth row) after nanoplex formulation.

4.4 In Vitro Investigations of Nanoplexes

The equipped peptide scaffolds optimized based on their physicochemical properties and the nanoplexes formulated from them were extensively studied *in vitro*. The aim was not only to determine their transfection efficiency in a variety of cell lines, but also to characterize their tolerability and to compare the SO1861-integrated nanoplexes as a single-component system with the established two-component sapofection approach.

4.4.1 Preliminary Investigations with SO1861-EMCH

The transfection efficiency of SO1861-integrated nanoplexes was to be compared with the previous sapofection method, which involved the separate application of nanoplex and saponin. Since SO1861 was not available in sufficient quantities as the saponin to be supplemented, it was therefore first investigated whether external supplementation with SO1861-EMCH could be considered equivalent to free saponin SO1861. For this purpose, non-equipped nanoplexes either without saponin supplementation, with SO1861, or SO1861-EMCH supplementation were used for transfection. The molar concentration of saponin supplementation was kept constant. The measured transfection efficiencies, shown in Figure 4.12, did not demonstrate a significant difference between supplementation with SO1861 or SO1861-EMCH. Therefore, supplementation with SO1861-EMCH was chosen for the following transfection experiments.

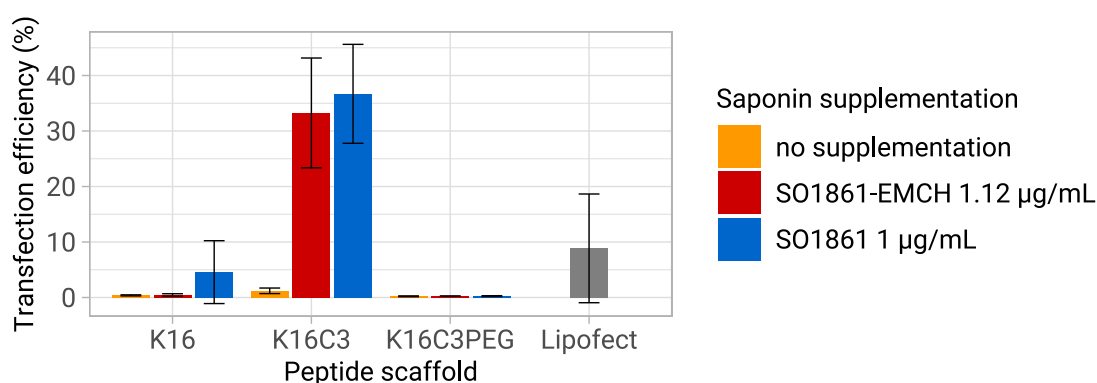


Figure 4.12: Comparison of transfection-enhancing capability of SO1861 and SO1861-EMCH in Huh-7 cell line. Nanoplexes were formed as indicated in Section 3.3 using the peptide scaffolds K₁₆, K₁₆C₃ and K₁₆C₃PEG and pEGFP-N3. Transfection was performed and evaluated as given in sections 3.5.2 and 3.5.3. Bar height indicates mean value, error bars indicate standard deviation of three independent experiments. SO1861 or SO1861-EMCH were supplemented at the same molar concentration. No significant differences between SO1861 and SO1861-EMCH supplementation were detected with unpaired, two-sided Student's *t*-test.

As discussed in Section 1.2, the presence of the aldehyde group at C-4 of the aglycone was identified in previous studies as a necessary characteristic for the eee effect of specific triterpenoid saponins (Hebestreit and Melzig 2003). Since functionalization with the EMCH-linker modifies this free aldehyde group in SO1861 to a hydrazone functionality, the comparable activity of SO1861 and SO1861-EMCH *in vitro* was surprising. Kovaříková et al. (2008) and Buss and Ponka (2003) have shown significantly accelerated decomposition of various aroylhydrazones in plasma that was attributable to low molecular weight compounds (<30 kDa) and, to a lesser extent, plasma proteins (e.g., albumin). Accordingly, a possible explanation for the observed activity of SO1861-EMCH could be the much stronger than expected hydrolysis of the hydrazone bond in the serum-supplemented transfection medium, in contrast to complete stability in PBS as confirmed by SO1861-EMCH stability studies (Table 4.1).

The next step was to determine the concentration of SO1861-EMCH to be supplemented. The aim was to determine the highest possible SO1861-EMCH concentration that does not impair cell growth, on the one hand to exclude toxic effects caused by the saponin alone and, on the other hand, to achieve the maximum possible transfection efficiency. For this purpose, Huh-7 cells, which have been shown to be relatively sensitive to saponin supplementation in daily handling, were incubated with increasing concentrations of SO1861-EMCH. Cell viability was assessed during cultivation by measuring the impedance as described in Section 3.5.4. Cell growth curves depicted in Figure 4.13 show slightly promoted cell growth for SO1861-EMCH concentrations $\leq 1.5 \mu\text{g/mL}$, this could be due to the cleavage of individual sugars from the glycoside chains. SO1861-EMCH concentrations $\geq 2.5 \mu\text{g/mL}$ impaired cell growth, so supplementation with $2 \mu\text{g/mL}$ SO1861-EMCH was determined to be the best option for all following *in vitro* transfection experiments.

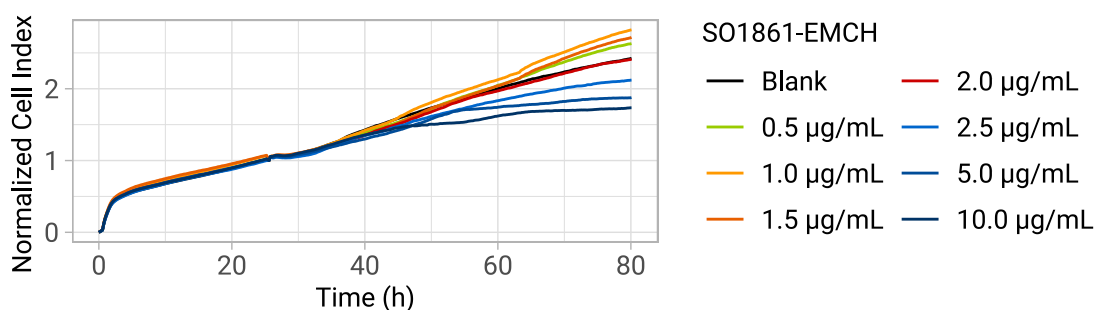


Figure 4.13: Tolerability of SO1861-EMCH *in vitro* in Huh-7 cell line. Cell viability was investigated using impedance measurement during incubation as described in Section 3.5.4 and is indicated by cell indices normalized to the time point of SO1861-EMCH addition (≈ 24 h after cell seeding). The experiment was performed twice. For each experiment and condition, two separate wells were used in parallel. Both experiments revealed no impairment of cell growth for SO1861-EMCH concentrations $\leq 2 \mu\text{g/mL}$. For the sake of clarity, the mean values from one experiment are shown in this figure.

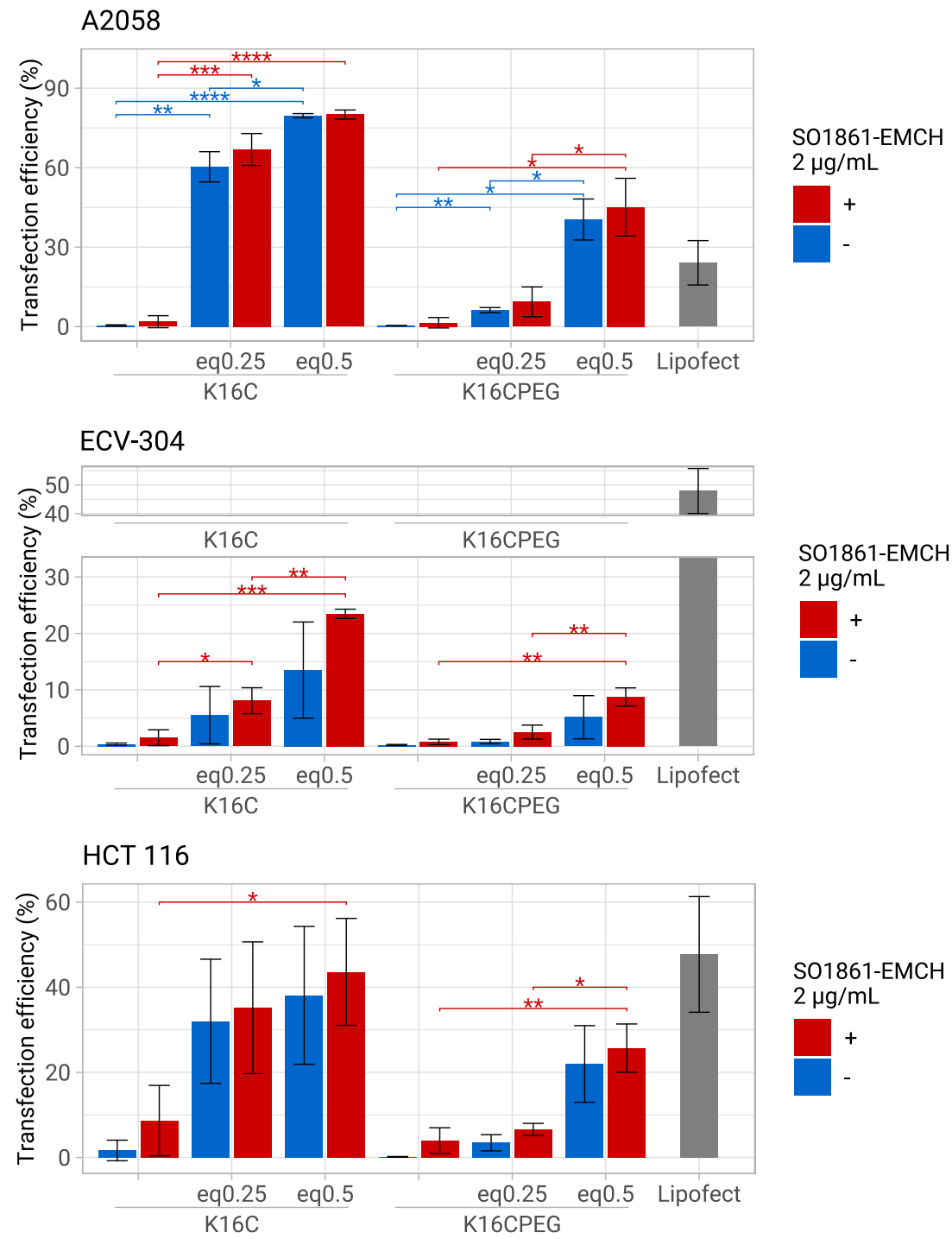
4.4.2 Transfection Efficiency of Equipped Peptide Scaffolds

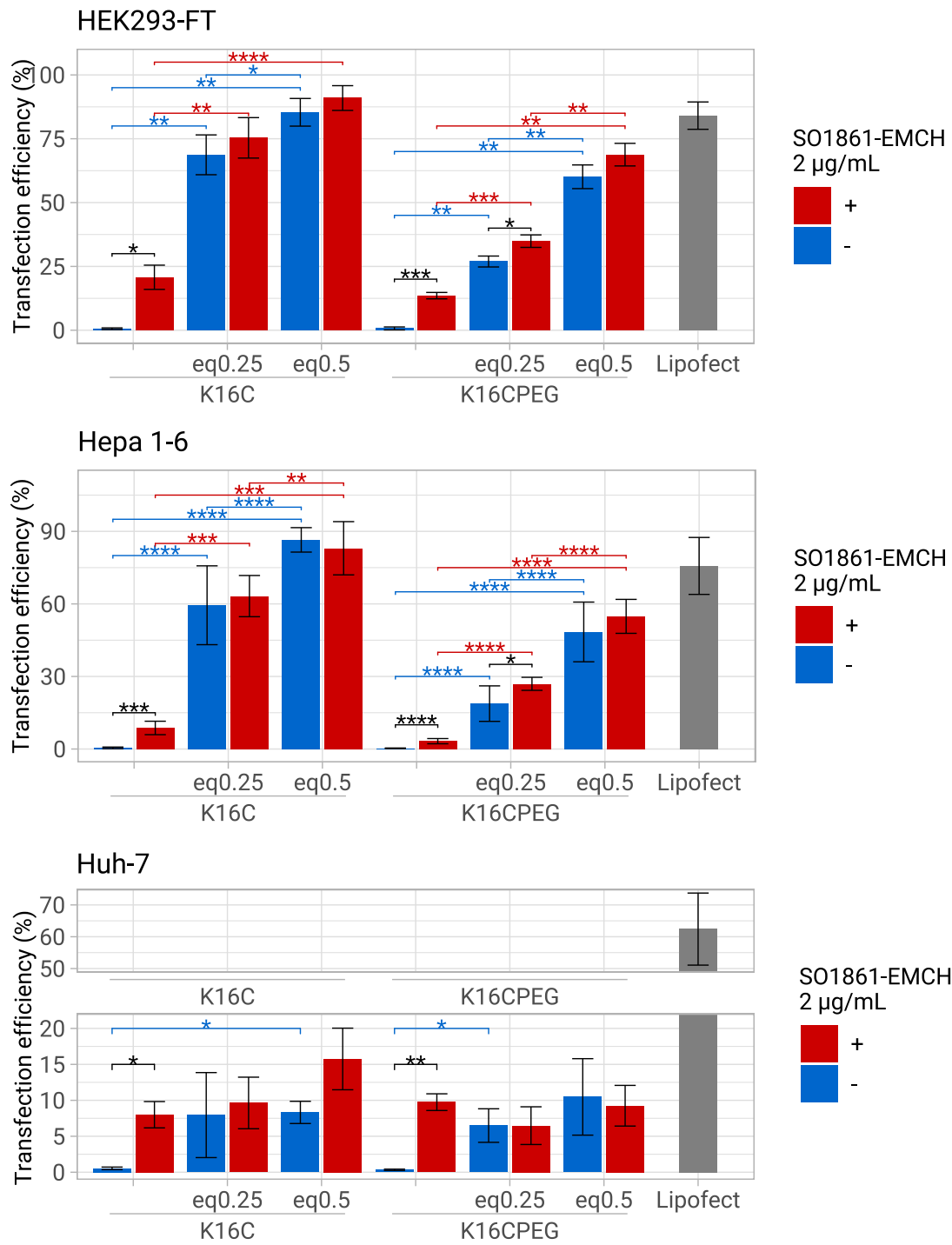
Transfection efficiency of nanoplexes formulated with pEGFP-N3 and the equipped and non-equipped peptide scaffolds was determined in cell lines A2058 (human melanoma), ECV-304 (human urinary bladder carcinoma), HCT 116 (human colon carcinoma), HEK293-FT (human embryonic kidney cells), Hepa 1-6 (murine hepatoma), Huh-7 (human hepatoma), MDA-MB-468 (human adenocarcinoma), and Neuro-2a (murine neuroblastoma) representing a variety of tissues, origin organisms and susceptibility to transfection. For all cell lines, Figure 4.14 shows that significant higher transfection efficiencies were achieved by nanoplexes formulated with equipped peptide scaffolds compared to their non-equipped analogs. This confirms the hypothesized transfection-enhancing capability of nanoplex-integrated SO1861.

The optimum amount of SO1861 seems to vary with the cell lines. In A2058, ECV-304, HCT 116, HEK293-FT, Hepa 1-6, and MDA-MB-468 cells the nanoplexes formulated with 0.5 equivalents SO1861-equipped peptides transfected more efficiently than their counterparts formulated with 0.25 equivalents-equipped peptides, while no significant differences between the SO1861-loading of the peptide scaffolds was found for cell lines Huh-7 and Neuro-2a.

The addition of further external SO1861-EMCH to the transfection medium (final concentration: 2 µg/mL), which was included to achieve maximum transfection efficiency, did not further increase transfection efficiency in the case of nanoplexes with internal SO1861, except for transfection of K₁₆CPEGeq0.25-nanoplexes in HEK293-FT and Hepa 1-6 cells. In Neuro-2a cells, transfection efficiency was significantly decreased by the addition of external SO1861-EMCH to K₁₆CPEGeq0.25- and K₁₆CPEGeq0.5-nanoplexes. The combination of SO1861-equipped peptide scaffolds with external supplementation of SO1861-EMCH leads to a higher total amount of SO1861-EMCH than previously considered tolerable in the tolerability studies (Section 4.4.1). Toxic effects that negatively influence cell division and thus transfection efficiency (see Section 1.1.2) are therefore conceivable as an explanation for the reduced transfection efficiency. This hypothesis was investigated in several cell lines and the results are presented and discussed in the following Section 4.4.3.

In all cell lines tested except Huh-7, the transfection efficiencies of the K₁₆PEG-derived peptide scaffolds were lower than for their non-PEGylated K₁₆C-derived analogs. This is in line with the slightly smaller cationic surface charge of the PEGylated nanoplexes (see Section 4.3.2), which reduces the electrostatic interaction between the positively charged nanoplexes and the negatively charged cell membrane (Asati et al. 2010).





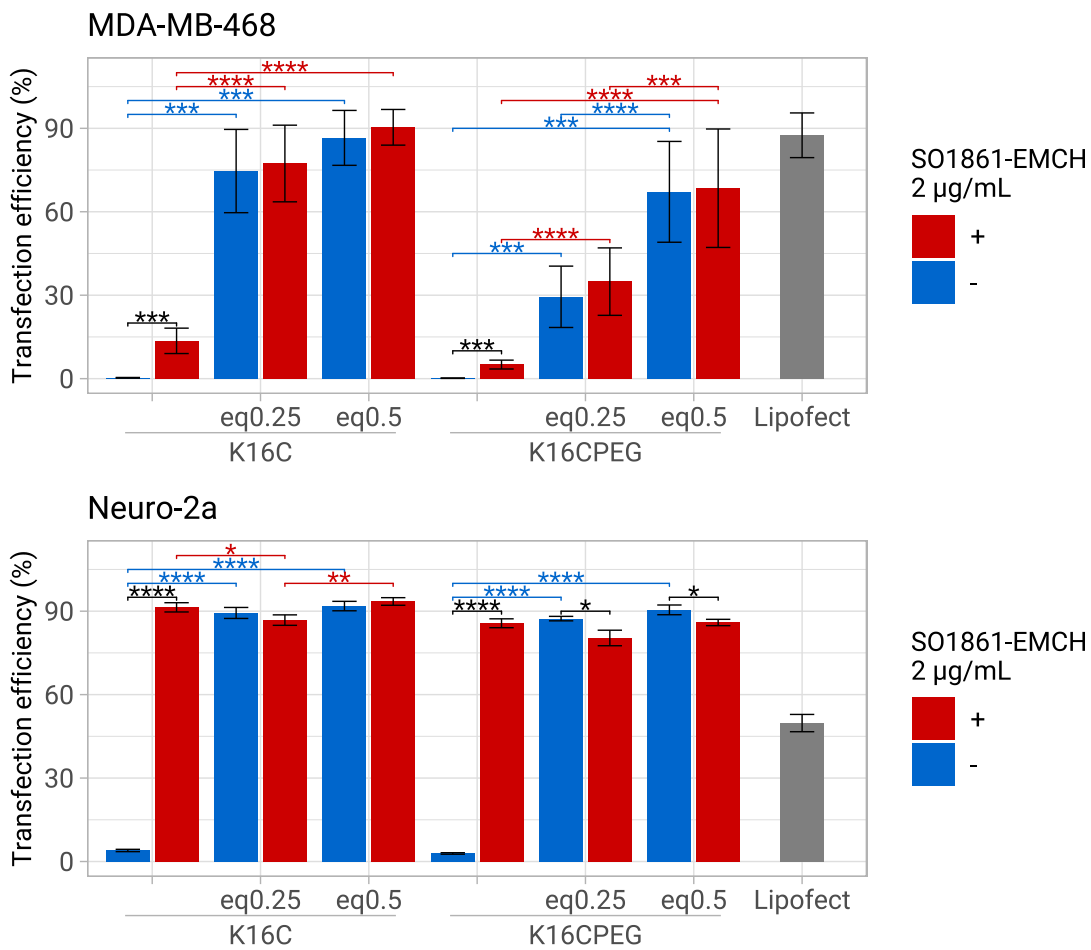


Figure 4.14: Transfection efficiency of pEGFP-N3/peptide scaffold nanoplexes in various cell lines. Transfection was performed and evaluated as described in Sections 3.5.2 and 3.5.3. Nanoplexes were formed in 10 mM HEPES, pH 7.1 at N /P 10. Cells were incubated with nanoplexes and external SO1861-EMCH optionally for 48 h before transfection efficiency was determined using flow cytometry. Lipofectamine transfections were performed accordingly. Bar height indicates mean of three independent experiments (each of them in triplicate for MDA-MB-468 and Hepa 1-6 resulting in n = 9), error bars show standard deviation. Significant differences were calculated with unpaired, two-sided Student's *t*-test for cell lines A2058, Neuro-2a, HEK293-FT, ECV-304, HCT 116, and Huh-7 and Wilcoxon signed-rank test for cell lines MDA-MB-468 and Hepa 1-6. * $p < 0.05$, ** $p < 0.01$, *** $p < 0.001$, **** $p < 0.0001$.

The transfection efficiency of SO1861-functionalized peptide scaffolds was comparable to that of Lipofectamine in cell lines HCT 116, HEK293-FT, Hepa 1-6, and MDA-MB-468. In A2058 and Neuro-2a cells, transfection efficiency of the investigated equipped peptide scaffolds was higher than that of Lipofectamine, while it was lower in ECV-304 and Huh-7 cells. Given the large variability of cell lines with regard to transfectability and the fundamentally different nanoparticles (peptide-based nanoplexes vs. lipid nanoparticle technology of Lipofectamine™ 3000 Reagent (Thermo Fisher Scientific 2023)), it is not surprising that the transfection capacity of the tested nanoplexes and Lipofectamine particles did not show the same relationship in all cell lines.

The supplementation of 2 µg/mL SO1861-EMCH in the transfection medium corresponds to the amount of SO1861-EMCH in the K₁₆Ceq0.5- and K₁₆CPEGeq0.5-nanoplexes. The comparison between external and conjugated SO1861-EMCH (i.e., K₁₆C + external SO1861-EMCH vs. K₁₆Ceq0.5 as well as K₁₆CPEG + external SO1861-EMCH vs. K₁₆CPEGeq0.5) showed distinctly higher transfection efficiencies for the nanoplexes with conjugated SO1861-EMCH in cell lines A2058, ECV-304, HCT 116, HEK293-FT, Hepa 1-6, and MDA-MB-468. The improved performance of conjugated SO1861-EMCH is also evident in the fluorescence micrographs of the transfected cells shown in Figure 4.15.

The superiority of SO1861-EMCH bound in the nanoplex was expected and is plausible given the hypothesized higher concentration of SO1861-EMCH achieved locally in the endosome. The incorporation of SO1861-EMCH into the cationic nanoplexes increases the total amount of saponin taken up by enhancing internalization due to the negative charge of the cell surface (Asati et al. 2010). In addition, the use of both components required for successful transfection (SO1861 + pDNA) in the same nanoplex leads to an accumulation of SO1861-EMCH in nanoplex-containing endosomes. Furthermore, the incorporation of EEE and effector DNA in the same nanoparticle results in SO1861-EMCH being present only in the endosomes, where its eee effect leads to a measurable result.

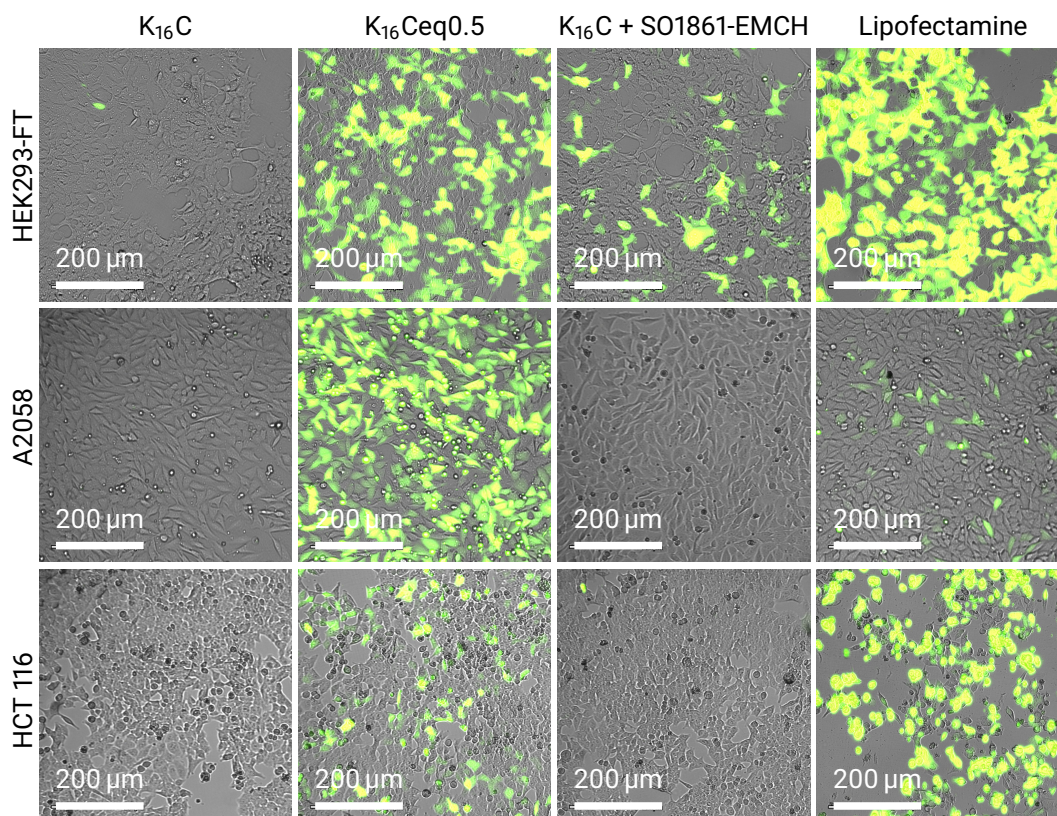


Figure 4.15: Fluorescence micrographs of cell lines HEK293-FT, A2058, and HCT 116 48 h after transfection with pEGFP-N3-nanoplexes illustrating the transfection-enhancing performance of covalently conjugated and externally supplemented SO1861-EMCH. Peptide scaffolds that were used for nanoplex formulation are noted on the top of each column, cell line is given left of each row. For $K_{16}C + SO1861-EMCH$, $2 \mu\text{g}/\text{mL}$ SO1861-EMCH was supplemented in the nanoplex-containing transfection medium, the absolute amount of free SO1861-EMCH for this condition equals the amount of SO1861-EMCH that is conjugated to the peptide scaffold in case of the $K_{16}Ceq0.5$ -nanoplexes. The micrographs for each cell line (presented in one row) were taken with constant exposure time, gain, and intensity to ensure comparability of the conditions. Scale bar equals $200 \mu\text{m}$. $n=1$.

4.4.3 Tolerability of Equipped Peptide Scaffolds

Impedance-based measurement of cell viability was used to investigate effects of the nanoplexes on cell growth during the 48 h transfection period in five different cell lines (Figure 4.16). Nanoplexes were formed with pEGFP-N3. Clear toxic effects were not observed, but a slightly slower cell growth was detected for Lipofectamine, K₁₆Ceq0.5-, and K₁₆CPEGeq0.5-nanoplex transfections in some cell lines. In the case of the latter transfections, roughly 400 ng of covalently conjugated SO1861-EMCH per well were included in the nanoplexes.² The observed slightly impaired cell viability does not seem to be primarily due to the amount of saponin, but rather to the covalent binding of it, since 1 200 ng of free SO1861-EMCH supplemented in the cell culture medium without nanoplexes (Blank with external SO1861-EMCH supplementation, indicated by dotted green line in Figure 4.16) did not show a comparable effect. Given the higher efficiency of SO1861 bound in the nanoplex (see Section 4.4.2), which can be explained by the higher concentration present locally in the endosome, the slightly increased toxicity observed seems conclusive. Since no clear toxic effect was observed for the use of 0.5 equivalents of conjugated saponin, the concentration range presented in this study appears to provide a good guide, but further increasing the amount of bound saponin seems inadvisable in view of the results.

4.4.4 Kinetics of Endosomal Release

Comparison of transfection efficiencies 48 h after addition of the nanoplexes revealed a clear superiority of nanoplex-integrated SO1861-EMCH compared with supplementation of the same amount of free SO1861-EMCH in the transfection medium (see Section 4.4.2). To elaborate on this observation, kinetic studies were performed to investigate the timing of endosomal release in these two transfection settings. For this purpose, fluorescently labeled nanoplexes were produced by including FITC-K₁₆ in the nanoplexes as described in Section 3.3. The fluorescent nanoplexes were used for transfection and the cells were observed after addition of the nanoplexes using a fluorescence microscope located in the incubator. The sensitivity, exposure time, and gain of the fluorescence microscope was chosen such that neither the autofluorescence of the cells nor the fluorescence of the FITC-labeled nanoplexes present in the transfection medium was detected at the beginning of the transfection period. During incubation, detectable fluorescence intensities in the cytosol of the cells were interpreted as release of the FITC-labeled peptides from the endosomes. Interestingly, the release from the endosomes appears to happen concerted for the majority of transfected cells. By comparing fluorescence microscopy images taken every 10 min, it was very clear when several cells abruptly exhibited fluorescence. In the further course of

²As described in sections 3.5.2 and 3.5.4, tolerability studies were conducted using E-Plate L8 for cell cultivation with a total cell culture volume of 600 μ L per well, 200 ng complexed DNA was used for transfection per well.

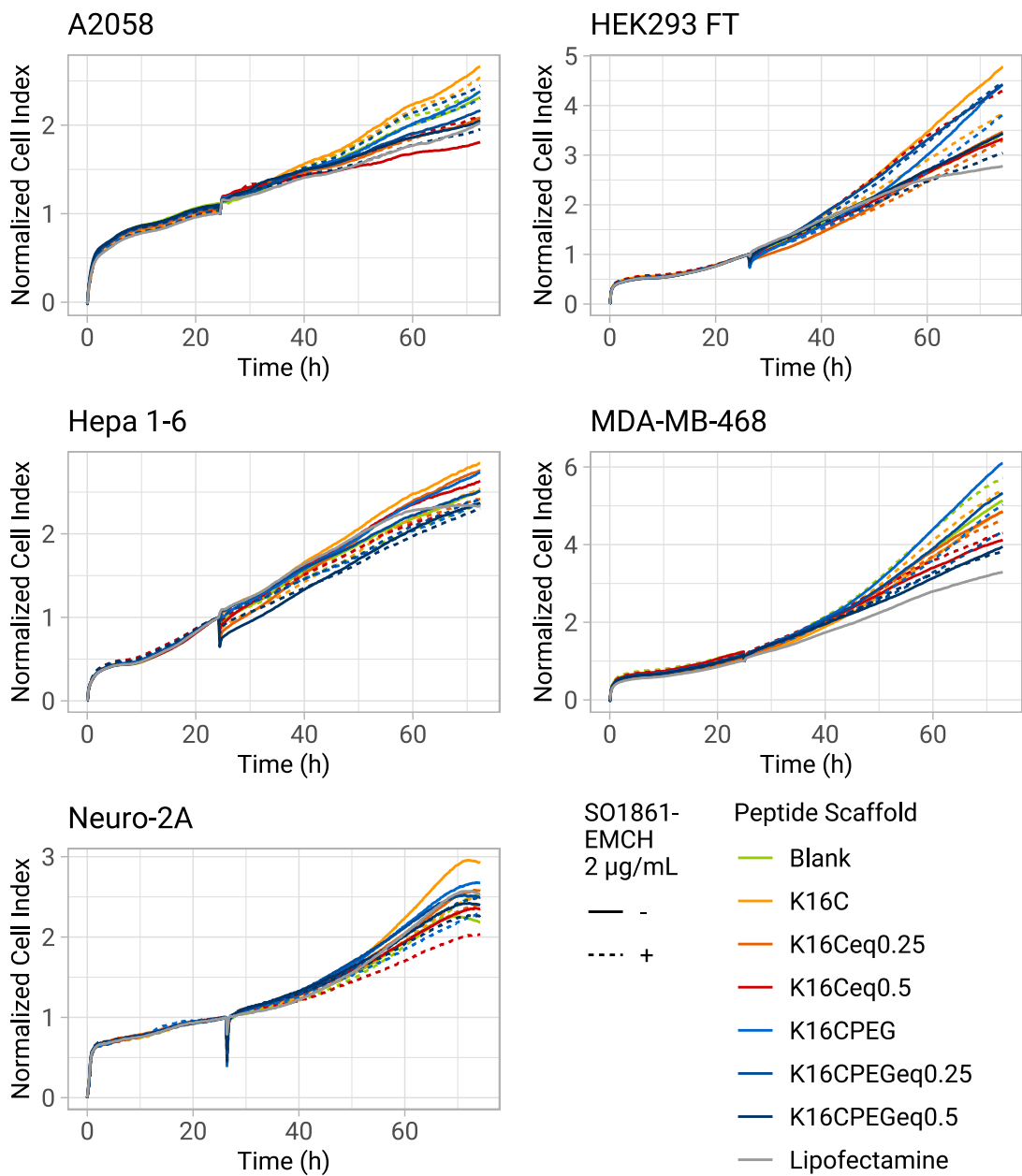


Figure 4.16: Cell viability during transfection with SO1861-EMCH-equipped and non-equipped nanoplexes indicated by normalized cell index during transfection in various cell lines. Nanoplexes were added 24 h after seeding the cells (evident by the vertical spike in the curves) and cell growth and viability was monitored by measuring impedance as described in Section 3.5.4 for the following 48 h. Cell indices were normalized to the cell index at the time of transfection. n=1.

incubation, the proportion of fluorescent cells increased only slightly (Figure 4.17).

In the three cell lines studied, A2058, Huh-7, and MDA-MB-468, endosomal release in the case of nanoplex-integrated SO1861-EMCH occurred at least 90 min before release in the case of externally supplemented SO1861-EMCH. The chosen methodology does not allow a quantitative statement on the amount of nanoplex released, but the comparable results in three different cell lines provide strong evidence that integration of SO1861-EMCH into the nanoplexes leads to earlier endosomal release compared to external supplementation.

The exact mechanism of endosomal escape by SO1861 and related triterpenoid saponins is not known, so the explanation of the temporal shift is subject to speculation. In principle, this temporal shift can occur either during internalization, endosomal maturation, or release from endosomal vesicles, with combinations also conceivable. In view of the positive surface charge of the nanoplexes, an increased and faster uptake of the SO1861-EMCH integrated in nanoplexes compared to the free SO1861-EMCH in solution is likely. However, since an altered release of the nanoplexes was observed, only the comparison of the nanoplex internalization is relevant here. The ζ -potential of the equipped nanoplexes was not significantly different from that of the non-equipped nanoplexes (see Section 4.3.2), so altered internalization of the nanoplexes due to surface charge is unlikely. However, a direct effect of the integrated SO1861 on endosomal uptake would be possible. For the glucuronic acid contained in SO1861, a pK_a value of 3.21 is given by Peter et al. (2012) for the unconjugated molecule, an influence of the saponin on acidification from pH 7.4 to pH 4.5 during endosome maturation is therefore unlikely. However, the pK_a value of free glucuronic acid is not necessarily comparable to that present in SO1861. Biedermann et al. (2019) indicate a pK_a of $\approx 4.6^3$ for the glucuronic acid present in the saponin, making an influence on acidification conceivable. Considering all aspects, earlier release due to higher endosomal SO1861 concentration seems most likely. The reduced time spent in the endo-lysosomal compartments, with its degradative nature, would be conclusive with the demonstrated increased transfection efficiency of nanoplexes with integrated SO1861-EMCH (Section 4.4.2). As discussed in Section 4.4.2, a higher SO1861-EMCH concentration in endosomes compared to supplementation of free saponin is likely in the case of SO1861-containing nanoplexes due to concentrating SO1861-EMCH in nanoplexes and the enhanced uptake by the positive surface charge of the nanoplexes.

³No further references, conference contribution without peer review.

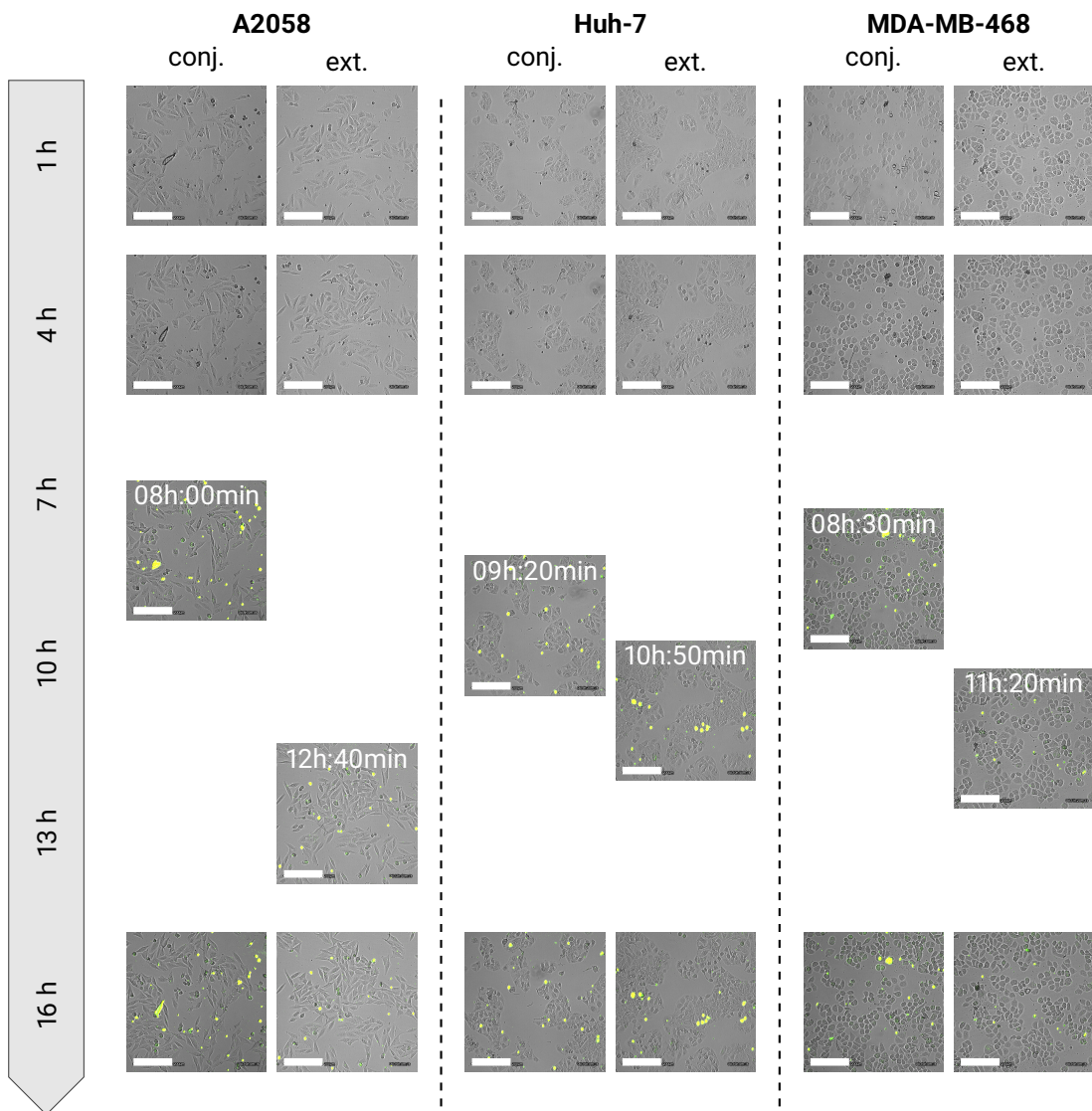


Figure 4.17: Kinetics of endosomal release of nanoplexes as a function of mode of SO1861-EMCH supplementation in A2058, Huh-7 and MDA-MB-468 cell lines. FITC-labeled nanoplexes were produced by incorporating 50 % FITC-K₁₆ in the nanoplexes. For SO1861-equipped nanoplexes (conj.), 50 % K₁₆Ceq0.5 were used additionally for the complexation of NP-Luc. For external supplementation (ext.), nanoplexes were formulated with 50 % K₁₆C and the transfection medium was supplemented with 200 ng SO1861-EMCH, which equals the amount of SO1861-EMCH covalently conjugated in case of the equipped nanoplexes. Transfection was observed with a live-cell imaging fluorescence microscope located in the incubator. Exposure time, gain and intensity were selected so that no fluorescence was detected at the beginning of the incubation. The first image with detected fluorescence is highlighted by the incubation period elapsed at this time printed in white at the top of the image. Scale bar equals 200 μ m. n=1.

Summary

- Supplementing transfection medium with SO1861-EMCH in the two-component sapofection approach is as efficient as supplementation with equal molar amounts of SO1861. Supplementation with 2 µg/mL SO1861-EMCH is not impairing cell growth and was therefore chosen as concentration for all *in vitro* transfection investigations.
- Integration of SO1861-EMCH in the nanoplexes by using SO1861-EMCH-equipped peptide scaffolds for nanoplex formulation significantly increases transfection efficiency *in vitro* in a wide variety of cell lines.
- The optimum amount of conjugated SO1861-EMCH in the nanoplexes depends on the cell line.
- Transfection efficiency of the nanoplexes with integrated SO1861-EMCH could not be increased by adding additional SO1861-EMCH in the cell culture medium, with isolated exceptions.
- Nanoplexes formulated with non-PEGylated peptide scaffolds exhibited significantly higher transfection efficiencies than their PEGylated analogs.
- Comparison of equal amounts of nanoplex-integrated and free SO1861-EMCH showed clear superiority of the one-component system with conjugated SO1861-EMCH. Kinetic studies indicated earlier endosomal release in the case of nanoplex-integrated SO1861-EMCH.
- Transfection of nanoplexes formulated with equipped peptide scaffolds carrying 0.25 or 0.5 equivalents of SO1861-EMCH was well tolerated.

4.5 Targeted Nanoplexes

As introduced in Section 1.3, targeted delivery of the nanoplexes' therapeutic cargo is crucial for therapeutic efficacy, especially *in vivo*. The azidolysine incorporated in the peptide scaffolds provided a free azide group for covalent conjugation of a targeting ligand using SPAAC (Section 1.4). Within the ENDOSCAPE project, numerous DBCO-functionalized ligands were conjugated via this interface to nanoplexes formulated with SO1861-equipped peptides that were then tested for their *in vitro* transfection efficiency in target- and non-target cell lines. In the following, the studies on epidermal growth factor (EGF) for targeted delivery to carcinogenic tissue are presented as an example.

4.5.1 Epidermal Growth Factor as Targeting Ligand

Functionalization of the nanoplexes with EGF aims to target the epidermal growth factor receptor (EGFR). As introduced in Section 1.3, this receptor has been shown to be overexpressed and/or hyperactivated in many types of cancer and is crucial for promoting cell proliferation and preventing apoptosis. As such, EGFR is a prime candidate for targeted cancer therapy and diagnosis using ligand-directed therapeutics (Rowinsky 2004; Wee and Z. Wang 2017). The successful application of EGF-functionalization for targeted delivery of anticancer agents following the uptake via EGFR has been demonstrated in various studies for liposomes (Skóra and Szychowski 2022; Zalba et al. 2016), lipid nanoparticles (Nan 2019), poly(lactic-co-glycolic acid)-nanoparticles (Wu et al. 2020), and carbon nanotubes (Bhirde et al. 2009). EGFR-targeted delivery of pDNA has been described for PAMAM/DNA/EGF-nanocomplexes by J. Li et al. (2015) and Zhang et al. (2012) and EGF-modified liposomes by Buñuales et al. (2011).

Epidermal growth factor receptor signaling is regulated via ligand-mediated endocytosis. The EGFR/EGF complex is internalized mainly by clathrin-mediated endocytosis, but recent studies suggest that clathrin-independent pathway(s) also contribute to internalization (Henriksen et al. 2013; Sigismund et al. 2008). From the early endosome, the EGFR:EGF-complex is predominantly delivered to the late endosome/multivesicular body, which then fuses with the lysosome, ultimately leading to degradation of both the ligand and receptor (P. 2011). In parallel, a share of EGFR is recycled back to the cell surface (Henriksen et al. 2013; Masui et al. 1993; Roepstorff et al. 2009). However, the degradation pathway is critical for the intended efficacy of EGF-functionalized nanoplexes equipped with SO1861. The rationale here is an improved and selective uptake by EGFR and a saponin-mediated release from the endo-/lysosome.

To achieve site-specific functionalization of the ligand with the DBCO-group required for the SPAAC conjugation reaction, an EGF mutant was designed and produced by recombinant protein expression by Melanie Krass (working group of Prof. Hendrik Fuchs, Institut für Laboratoriumsmedizin, Klinische Chemie und Pathobiochemie, Charité – Universitätsmedizin Berlin) within the ENDOSCAPE project. This EGF variant carried a polyhistidine-tag for purification purposes and was generously provided for all studies presented in the following.

4.5.1.1 Characterization of Cellular Internalization

To confirm the uptake of the recombinantly produced EGF mutant via its target receptor EGFR, its interaction with cells was tested *in vitro*. For this purpose, four different cell lines were chosen, exhibiting significantly differing EGFR expression levels. RNA sequencing data, which quantifies EGFR mRNA transcripts and thus indicates EGFR expression levels, provided in the *The Human Protein Atlas* (2023) (Marti-Solano et al. 2020) allowed the classification of the cell lines

- A2058 (0.1 nTPM) as non-target cell line (EGFR-),
- HCT 116 (22.6 nTPM) as low-expression cell line (EGFR+),
- MDA-MB-468 (702.8 nTPM) as medium-expression cell line (EGFR++), and
- A-431 (2 978.0 nTPM) as high-expression cell line (EGFR+++).

To allow sensitive detection and quantification of internalized EGF, a cyanine5 (Cy5)-labeled EGF variant was used for *in vitro* investigations. Cy5 was chosen as labeling dye as its far-red-fluorescence ($\lambda_{\text{ex}} = 647 \text{ nm}$, $\lambda_{\text{em}} = 665 \text{ nm}$) allows clear distinction from the autofluorescence of cells that is very low in this region of the spectrum. In addition, detection in flow cytometry was possible using the APC-channel as described in Section 3.4.8.

As shown in Figure 4.18, a concentration-dependent uptake of Cy5-EGF was demonstrated in all cell lines studied. Within the concentration range studied, 0.1 nM to 1 000 nM, no saturation of the Cy5-EGF-internalization was detected. As expected, the uptake of Cy5-EGF increased with rising EGFR expression levels, suggesting EGFR-dependent internalization. This hypothesis was further supported by the finding that Cy5-EGF was internalized to a higher extent than equimolar concentrations of the free dye Sulfo-Cy5-NHS (comparison of 1 000 nM Cy5-EGF (dark red) with 250 nM Sulfo-Cy5-NHS (dark blue) in Figure 4.18). However, both observations are also true for the non-target cell line A2058, which suggests an alternative, most presumably additional, and EGF-dependent, but non-EGFR-dependent internalization mechanism. EGF-internalization is known to occur not only through EGFR, but also through the other members of the ErbB family of receptor tyrosine kinases (Hynes and MacDonald 2009). In fact, the expression of ErbB2 (31.2 nTPM) and ErbB3 (31.2 nTPM) in the A2058 cell line (Marti-Solano et al. 2020; *The Human Protein Atlas* 2023) is probably the reason for the observed uptake of Cy5-EGF in absence of EGFR. The expression levels of ErbB2 and ErbB3 are in the same order of magnitude for the other cell lines examined and thus contribute little to the overall uptake of EGF in view of the much higher EGFR expression, especially in the MDA-MB-468 and A-431 cell lines. ^{4 5 6}

Further investigations revealed a time-dependent uptake of Cy5-EGF in all cell lines studied (Figure 4.19, left panel). Cy5-related fluorescence intensity increased steadily over the first 8 h of incubation with 100 nM Cy5-EGF. For 24 h incubation, the Cy5-related fluorescence intensity decreased in the cell lines A2058 and MDA-MB-468 in comparison to the signal at 8 h incubation, while it was minimally increased in cell lines HCT 116 and A-431. The observed decreasing internalization rates are in line with reported partial recycling of internalized EGFR to the cell membrane and degradation of EGF-activated EGFR

⁴HCT 116: ErbB2 31.3 nTPM, ErbB3 11.1 nTPM (*The Human Protein Atlas* 2023)

⁵MDA-MB-468: ErbB2 17.6 nTPM, ErbB3 23.0 nTPM (*The Human Protein Atlas* 2023)

⁶A-431: ErbB2 58.3 nTPM, ErbB3 42.1 nTPM (*The Human Protein Atlas* 2023)

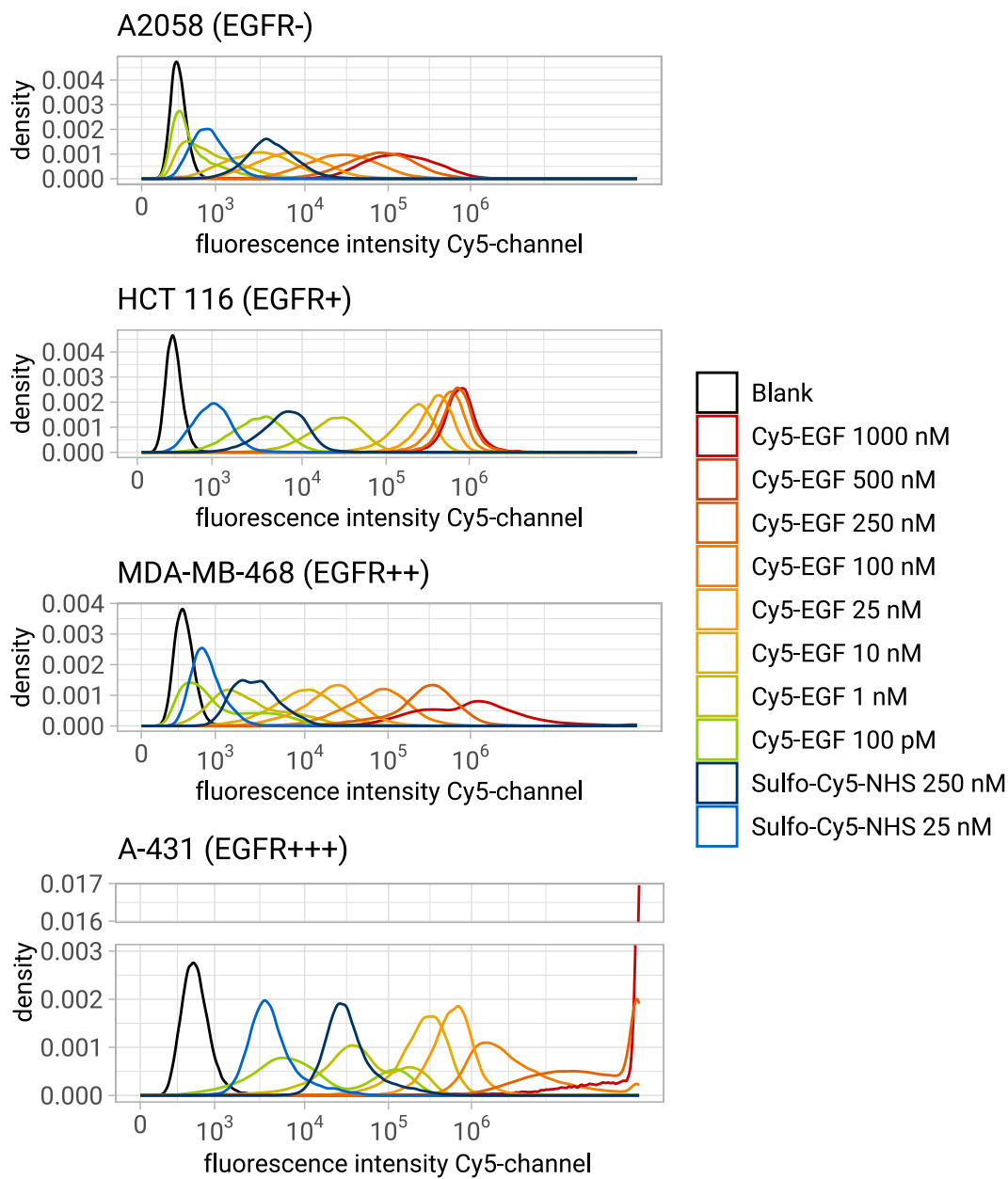


Figure 4.18: Cy5-EGF-internalization in target- and non-target cell lines determined by flow cytometry as described in Section 3.4.8. Density plots show aggregated data from three independent experiments. The position of each peak on the x-axis (fluorescence intensity in Cy5-channel = peak height in APC-channel) indicates extent of Cy5-EGF internalization. Peak shape indicates width of the distribution. Cell lines and EGFR expression levels are given above each plot. Cy5-EGF carried 0.25 equivalents Cy5 per EGF molecule. Sulfo-Cy5-NHS as free dye was tested in parallel as non-targeted control, 250 nM free dye equals 1000 nM targeted dye.

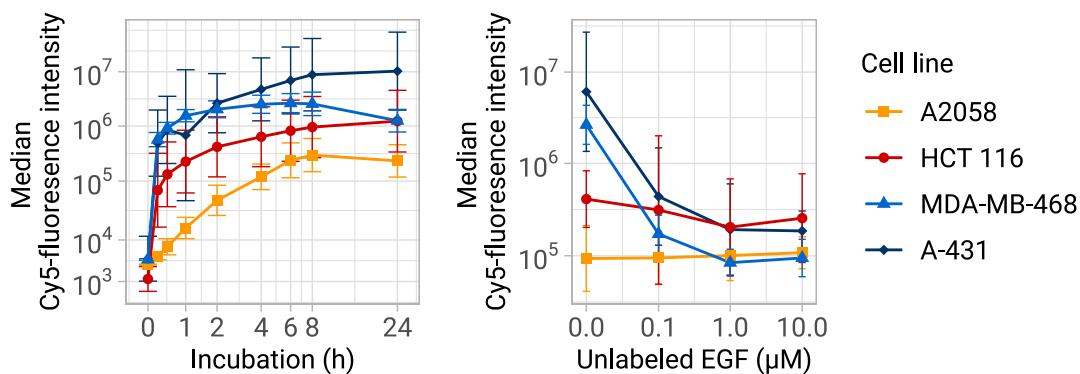


Figure 4.19: Time dependency (left) and competitive inhibition (right) of Cy5-EGF-internalization. Cells were incubated with 100 nM Cy5-EGF in both assays. Incubation time in the competitive inhibition assay was 4 h. Mean and standard deviation of three independent experiments are shown. Fluorescence intensity in Cy5-channel = peak height in APC-channel.

in the lysosomes (Roepstorff et al. 2009), which in total results in EGFR down-regulation upon stimulation with EGF.

The hypothesis of EGFR-dependent internalization of the Cy5-labeled EGF mutant was further investigated by an assay examining the competitive inhibition of Cy5-EGF internalization by an excess of unlabeled EGF. As expected and shown in Figure 4.19, right panel, reduced Cy5-EGF internalization in presence of EGF excess was observed for the EGFR-expressing target cell lines. The amount of Cy5-EGF that was taken up decreased with increasing EGF excess.⁷ This observed EGFR expression-dependent competitive inhibition provided further evidence for the assumed EGFR-mediated uptake of fluorescently labeled EGF. Interestingly, in the non-target cell line A2058, an up to 100-fold molar excess of unlabeled EGF did not influence the uptake of Cy5-EGF. This observation contradicts the hypothesized uptake of Cy5-EGF in A2058 cells via ErbB2 and ErbB3 and rather suggests the internalization of Cy5-EGF through receptor-independent endocytosis.

It must be stated, that analysis by flow cytometry in principle does not allow any statement about the localization of the fluorescence-labeled EGF, so in principle the discussed observations could be due to both internalization and extracellular binding to the receptors. Thorough washing of the cells with DPBS twice after incubation and before flow cytometric evaluation should have removed extracellularly associated EGF, but this assumption was not experimentally validated.

To confirm the internalization of Cy5-EGF in its EGFR-expressing target cell lines, incu-

⁷It should be noted that there is no saturation of the uptake capacity at the EGF concentration of 100 nM used. Therefore, a reduction in the amount of Cy5-EGF incorporated by the factor corresponding to the excess of unlabeled EGF is not expected.

bation of A-431 cells with Cy5-EGF was observed with fluorescence microscopy. Due to the detection limit of the used live cell imaging fluorescence microscope, A-431 cells were chosen based on their abnormally high EGFR-expression. In addition, a high EGF-concentration of 1 000 nM was used. As shown in Figure 4.20, a Cy5-related red fluorescence associated with cells was detected. The proportion of fluorescent cells (calculated by the fluorescence coverage as described in Section 3.5.3) increased steadily, reaching 12% after 60 h. The detected Cy5-related fluorescence was clearly located in the cytosol of the cells, thereby confirming the internalization of the fluorescently labeled EGF-mutant.

A further indication that internalization has taken place is the observed toxic effect of EGF on the A-431 cells evident by the change of cell morphology that is clearly recognizable in Figure 4.20. EGF-mediated apoptosis has been described by several researchers for cell lines that overexpress the EGFR such as A-431 and MDA-MB-468 cells (Armstrong et al. 1994; Gill and Lazar 1981; Kottke et al. 1999; Tikhomirov and Carpenter 2004). Hyatt and Ceresa (2008) demonstrated that only internalized, activated EGFRs induce cell death, so the observed apoptotic effect indicates internalization of the Cy5-labeled EGF mutant.

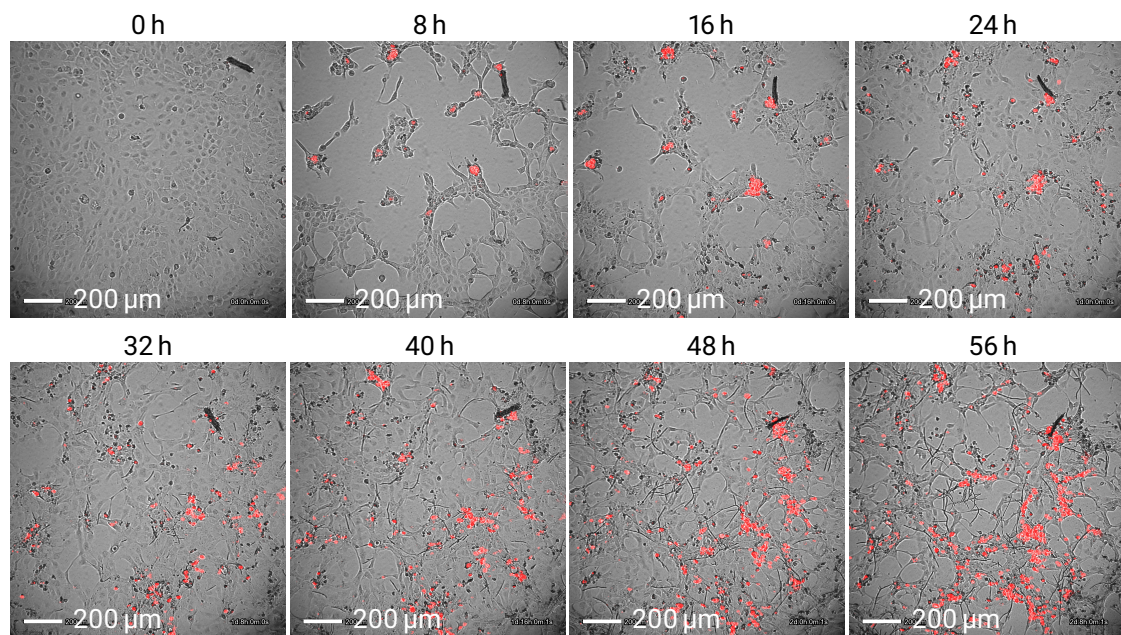


Figure 4.20: Fluorescence micrographs of Cy5-EGF-internalization in A-431 cell line. Cells were incubated with Cy5-EGF and evaluated as described in Section 3.5.5, incubation time is given on top of the micrographs. All presented micrographs were taken with constant exposure time, gain, and intensity. n=1.

4.5.1.2 Transfection Efficiency of Epidermal Growth Factor Receptor-Targeted Nanoplexes

For the preparation of EGFR-targeted nanoplexes, a DBCO-functionalized variant of the previously described EGF mutant was covalently conjugated to the nanoplexes via SPAAC as introduced in Section 1.4 and described in Section 3.3.1. The loading of EGF in percent refers to the molar amount of azide groups accessible for SPAAC bioconjugation. As each peptide scaffold carries one free azide group, EGF loading in percent therefore indicates the proportion of peptide scaffolds that are bioconjugated to EGF.

The EGF mutant used has an isoelectric point of 5.87 (determined with Isoelectric Point Calculator by Kozłowski (2016)). In the buffer used for nanoplex formulation, 10 mM HEPES, pH 7.1, EGF is accordingly negatively charged. Attachment to the K₁₆Ceq0.25-nanoplexes with their positive ζ -potential (see Table 4.3) due to electrostatic attraction is therefore also possible without the covalent linkage. In order to investigate the influence of these parallel attachment mechanisms, nanoplexes with the same molar amounts of the non-functionalized EGF mutant (i.e. without the DBCO functionality) were prepared and examined for their transfection efficiency in parallel. For the formulation of the non-covalent EGF/nanoplex complexes, different incubation times of 30 min and 16 h (equivalent to the incubation for SPAAC bioconjugation) were tested.

Figure 4.21 shows the transfection efficiencies of the prepared targeted nanoplexes in the non-target cell line A2058 and the target cell lines HCT 116 and MDA-MB-468. As hypothesized, targeted nanoplexes carrying 1 % to 10 % covalently conjugated EGF yielded higher transfection efficiencies than the non-functionalized (0 % EGF loading) nanoplexes in the target cell lines. In the non-target cell line A2058, targeted (≤ 10 % EGF loading) and non-targeted K₁₆Ceq0.25-nanoplexes transfected with comparable efficiency. In view of the low EGF loading, unaltered uptake of the nanoplexes by non-receptor-mediated endocytosis was probably responsible for this. In this low loading range, the nanoplexes with covalently bound EGF tended to transfect best, further indicating the observed slight transfection-enhancing effect of EGF in the target cell lines. This observation may be attributed not only to increased EGFR-mediated uptake but also to the endosomolytic effect of the introduced histidine residues of the EGF mutant functionalized with a polyhistidine-tag.

Transfection efficiency was noticeably reduced in all investigated cell lines for EGF-loadings ≥ 25 %. Given the higher EGF loading, which shields the positive surface charge of the nanoplexes, this reduced transfection efficiency is likely due to reduced uptake by receptor-independent endocytosis. This hypothesis is supported by the observation that the decrease in transfection efficiency was lowest for the EGF/nanoplex complexes incubated for only 30 min, which most presumably had the least effective EGF loading. Reduced transfection efficiencies were observed in all cell lines which suggests that the decrease in non-specific uptake in the target cell lines was not compensated by specific, EGFR-mediated transfection.

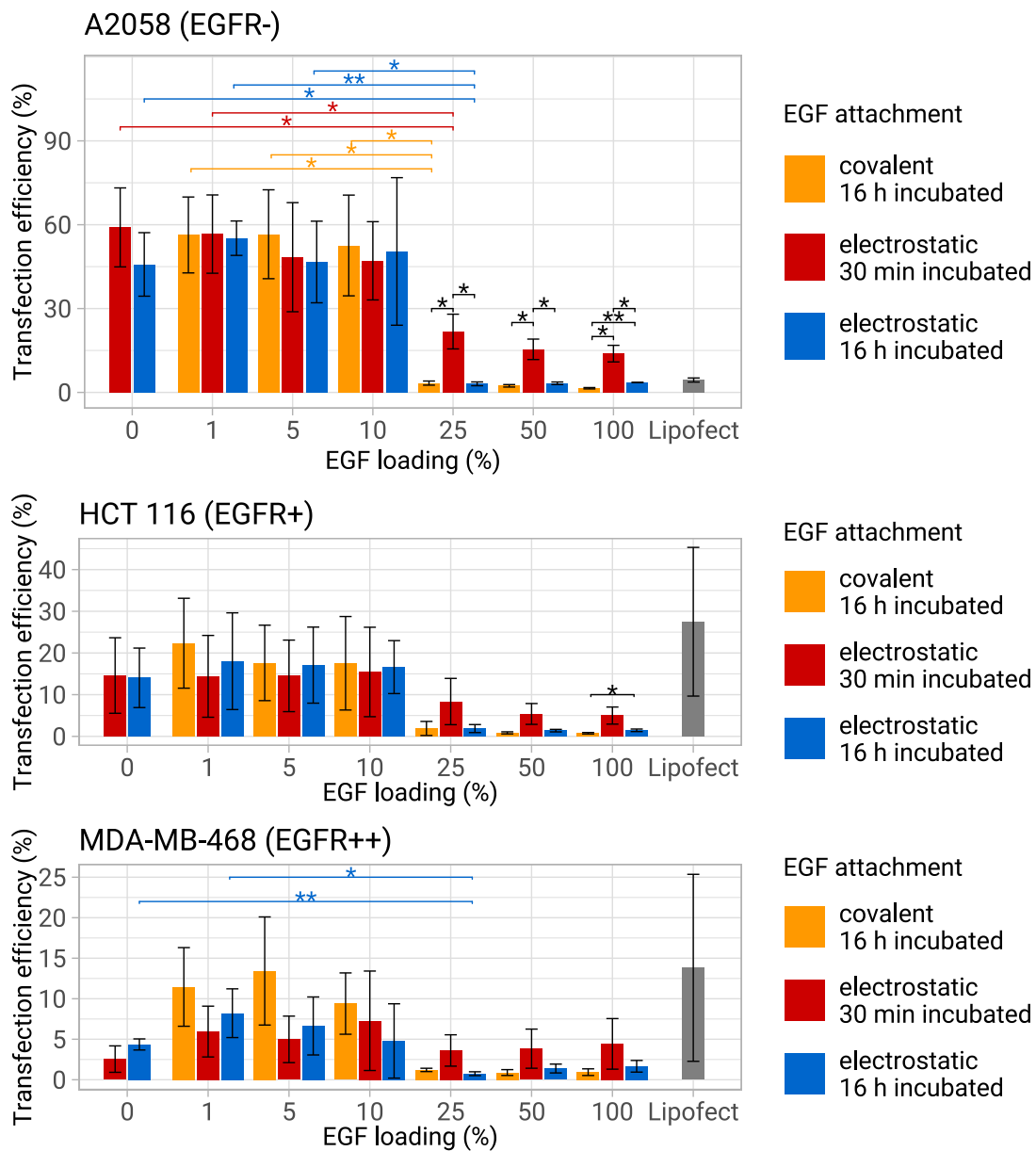


Figure 4.21: Transfection efficiency of EGF-functionalized nanoplexes in non-target and target cell lines. Cell line and EGFR-expression level are given on top of each graph, color of the bars indicates mode of EGF attachment. Bar height indicates mean of three independent experiments, error bars show standard deviation. Unpaired, two-sided Student's *t*-test was used to test for significant differences between attachment modes within the same EGF loading and between EGF loadings for constant attachment mode, **p* < 0.05. No significant differences were found for 0 % to 10 % and 25 % to 100 % EGF loading. Significant differences between EGF loadings are only depicted for 0 % to 25 % to avoid overloading of the graph.

Various explanations are conceivable for the observed lack of a distinct transfection-enhancing effect of EGF conjugation. The physicochemical characterization of the prepared EGF-functionalized nanoplexes indicated a strong aggregation tendency and thus massively increased D_h s. Unfortunately, no accurate data could not be obtained by DLS due to the presence of large sedimenting particles. However, it is safe to say that the D_h s of the EGF-decorated nanoplexes exceeded 200 nm, the established upper size limit for clathrin-mediated endocytosis (Rejman et al. 2004). It therefore seems likely that the targeted nanoplexes are not internalized via EGFR uptake due to their size. As ζ -potentials of ≈ 30 mV determined for the non-functionalized nanoplexes (see Table 4.3) indicated stabilization of their suspension by electrostatic repulsion, a reduction of the suspension stability in the case of the targeted nanoplexes due to reduced ζ -potential appears likely. Such a reduction of the surface charge is conclusive in view of the functionalization with ligands on the nanoplex surface. Unfortunately, this hypothesis could not be confirmed analytically because accurate measurement of the ζ -potential by electrophoretic light scattering is not possible for aggregated particles. Another reason for the observed aggregate formation could be the increased ion concentration in the buffer due to the addition of the EGF stock solution prepared in PBS. In support of this theory, J. Li et al. (2015) and Zhang et al. (2012) reported the preparation of EGF/dendriplexes of ≈ 300 nm in diameter using PBS for the nanoparticle formulation. This would not have been possible with the PLL-based nanoplexes investigated in this thesis, as these rapidly aggregated in the presence of high ion concentrations.⁸

Furthermore, fluorescence microscopy images of the transfection of EGF-functionalized nanoplexes in MDA-MB-468 cells indicated a toxic effect of EGF exposure (Figure 4.22). As discussed in Section 1.1.2, transcription of the plasmid DNA vector required for successful transfection inevitably requires cell division, so the apoptotic effect of EGF exposure inhibits transfection. The difference in cell morphology after 48 h incubation with the nanoplexes was obvious between 10 % and 25 % EGF loading and was in good agreement with the sudden drop in transfection efficiency at exactly the same EGF loading. As discussed in the previous section, the observed toxic effect is consistent with published data from other researchers and suggests internalization of EGF-activated EGFR.

At first sight, this seems to be in contradiction with the hypothesis of a blockade of the uptake of the EGF-functionalized nanoplexes due to their size. However, both hypotheses can be combined by assuming an incomplete aggregation and/or stabilization of the particles in the serum-containing transfection medium by the formation of a protein corona (Aggarwal et al. 2009). Studies on the trafficking of the functionalized nanoplexes in a large number of cells would be necessary to elucidate the mechanisms responsible for the reduced transfection efficiency at EGF loadings ≥ 25 %.

⁸As the aggregated samples contained large sedimenting particles, determination of the D_h s by DLS was not possible.

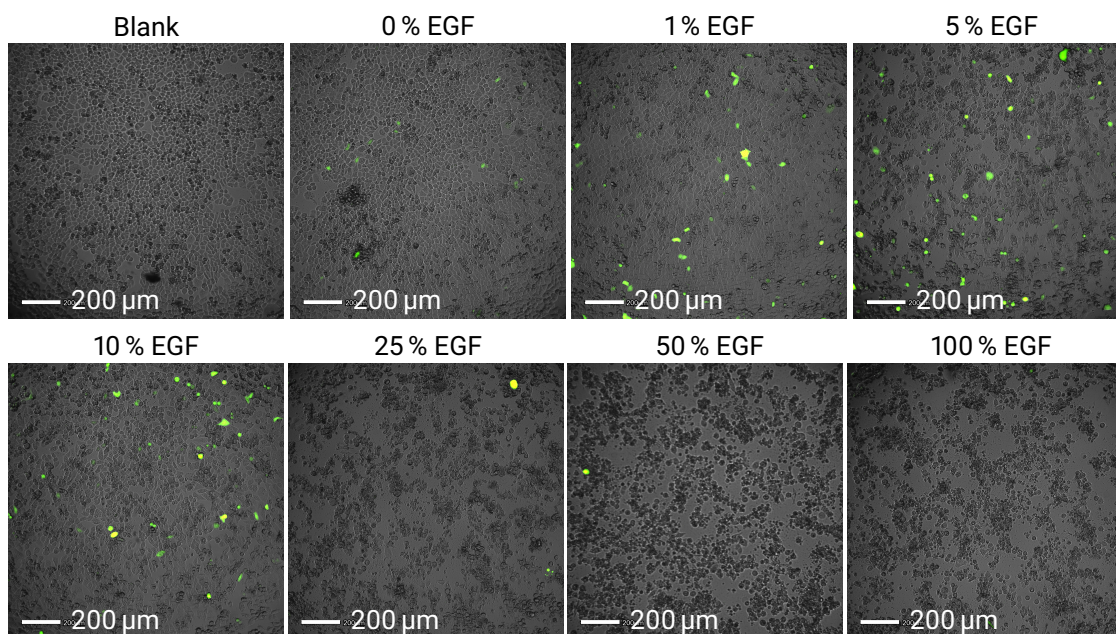


Figure 4.22: Fluorescence micrographs of transfections with EGF-functionalized nanoplexes in MDA-MB-468 cell line. Nanoplexes were formulated as described in Section 3.3, fluorescence microscopy is described in Section 3.5.3. EGF loading is indicated above the micrographs. $n=1$.

4.5.2 Targeting with Peptide Y

Within ENDOSCAPE, various targeting ligands (EGF, Cetuximab, Transferrin, ApoAI, GalNAc) were bioconjugated to the SO1861-equipped peptide scaffolds and evaluated *in vitro* for their transfection efficiency. The latter was partially performed by the ENDOSCAPE consortium partners. The analysis of the EGF-loaded nanoplexes was performed in the scope of this thesis, but the results presented in the previous Section 4.5.1.2, in particular the significantly reduced transfection efficiencies upon bioconjugation of targeting ligands, serve as an example of the *in vitro* transfection-enhancing capabilities of all prepared targeted SO1861-equipped nanoplexes.

Aggregation of the targeted nanoplexes was macroscopically evident by the formation of colored particles during incubation for SPAAC-functionalization of the nanoplexes with the fluorescently labeled targeting ligands. As discussed for EGF-functionalized nanoplexes, this aggregation is most probably due to the reduced ζ -potential and/or the lack of nanoplex stability in ionic solutions.

In view of these observations, short peptide sequences were identified as alternative, less bulky targeting motif. For nanoplex formulation, the peptides can be used dissolved in water, which prevents the introduction of destabilizing salt concentrations by PBS addition.

In addition, the smaller size of the peptide ligands should shield the surface charge of the nanoplexes to a lesser extent, which enables the stabilization of the nanoplex suspension via the ζ -potential.

As introduced in Section 1.3, pepY has been exploited for targeted delivery to the murine neuroblastoma cell line Neuro-2a using the two-component saponin approach *in vitro* and *in vivo*. Based on these reports, pepY was selected as the first prototype for peptide motif targeting of SO1861-equipped nanoplexes.

4.5.2.1 Transfection Efficiency *In Vitro*

To integrate both SO1861 as endosomal escape enhancer and the targeting motif of pepY into the nanoplex, the equipped peptide scaffold K₁₆CPEGeq0.5 and pepY were used in parallel for nanoplex formulation. K₁₆CPEGeq0.5 was chosen based on the size, homogeneity and stability of the nanoplexes formulated with it (Table 4.3 and Figure 4.11). As described in Section 3.3, the peptides were mixed prior to addition of pDNA. The resulting mixed nanoplexes are in the following referred to as PepMix-nanoplexes.

For the optimization of the ratio of K₁₆CPEGeq0.5 and pepY, PepMix-nanoplexes varying in their peptide components proportions were tested for their transfection efficiency *in vitro*. As control, nanoplexes with equivalent peptide composition, but lacking the covalently conjugated saponin were assessed in parallel, both with and without the supplementation of SO1861-EMCH in the transfection medium (“SO1861 supplementation”).

For transfections without SO1861 supplementation (yellow bars in Figure 4.23), decreasing transfection efficiencies were observed with decreasing pepY content in the nanoplex, from 4.9 % for a nanoplex formulated exclusively with pepY to 2.4 % for a nanoplex formulated exclusively with K₁₆PEG, although not statistically significant. When SO1861-EMCH was supplemented in the cell culture medium in amounts equivalent to the conjugated amount of SO1861 in the respective equipped nanoplex (red bars), increasing transfection efficiencies from 10 % for 20 ng SO1861-EMCH to 81 % for 200 ng SO1861-EMCH in 100 μ L well volume were observed, which is in line with previous observations of dose-dependent transfection-enhancing properties for the group of eee triterpenoid saponins (Clochard et al. 2020). Strikingly, when the same amount of SO1861 was covalently conjugated to the peptide scaffold (blue bars), transfection was significantly more efficient, with transfection efficiencies of 82 % to 91 % for saponin amounts of 20 ng to 200 ng. The absence of a significant dose-dependency effect of conjugated saponin in the investigated quantity range showed a clear superiority of conjugated over externally supplemented saponin and already comparatively low amounts of conjugated saponin were proven to be sufficient for the investigated cell line to achieve maximum transfection efficiency. This observation is consistent with the classification of Neuro-2a cells as readily transfectable based on previous experience (Clochard et al. 2020; Sama et al. 2017).

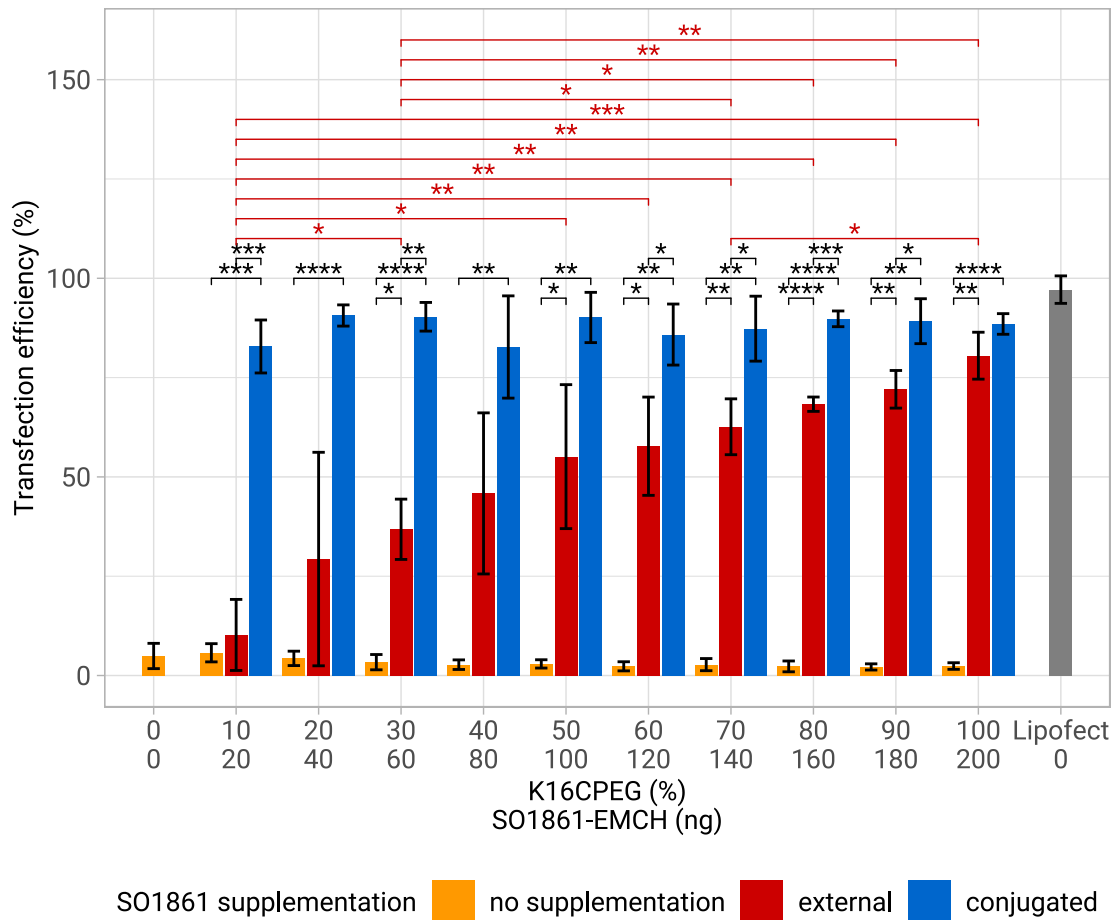


Figure 4.23: *In vitro* transfection efficiency of PepMix-nanoplexes in Neuro-2a cell line. Nanoplexes were formed and evaluated as described in sections 3.3 and 3.5.3. Upper panel of the x axis labeling gives the proportion of peptides $K_{16}CPEG$ (for the yellow and red bars) or $K_{16}CPEGeq0.5$ (for the blue bars), the proportion of pepY is calculated by subtracting the given values from 100 %. The lower panel of the x axis labeling states the absolute amount of SO1861-EMCH per well, which is the same for externally supplemented (red bars) and conjugated (blue bars) SO1861-EMCH. Bar height indicates mean of three independent experiments, error bars show standard deviation. Significant differences were calculated with unpaired, two-sided Student's *t*-test. * $p < 0.05$, ** $p < 0.01$, *** $p < 0.001$, **** $p < 0.0001$.

Based on *in vitro* transfection efficiencies, a nanoplex formulated with 70 % pepY and 30 % $K_{16}CPEGeq0.5$ incorporating NP-Sap, in the following referred to as pepY-SO1861-nanoplex, was selected as the most promising candidate for an *in vivo* anti-tumor efficacy

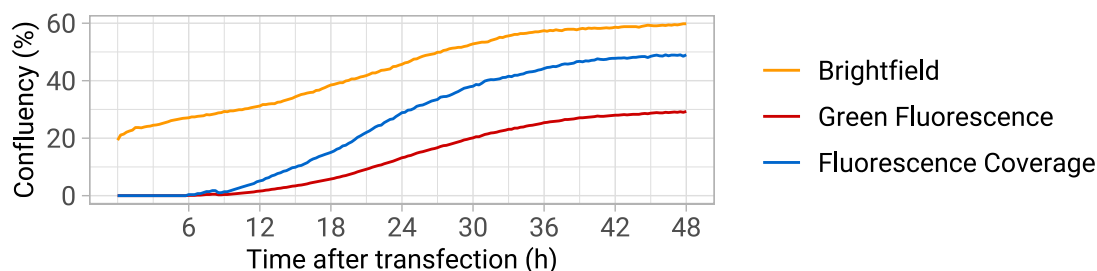


Figure 4.24: Kinetic profile of eGFP expression in Neuro-2a cell line during transfection with pepY-SO1861-nanoplexes (NP-eGFP complexed with 70 % pepY and 30 % K₁₆CPEGeq0.5). Transfection was performed as described in Section 3.5.2, evaluation is given in Section 3.5.3. Fluorescence Coverage is indicating the share of eGFP-expressing cells. n=1.

study.

To evaluate the kinetics of the transfection with this pepY-SO1861-nanoplex, NP-eGFP was used for complexation and the cells were constantly observed with a fluorescence microscope during transfection. The first eGFP-expressing cells were detected as early as 5.5 h after transfection and the percentage of transfected cells increased continuously until 48 h after transfection (Figure 4.24 and video in the Appendix 7.3).

To evaluate the effect of the different nanoplex components, dose-response curves of the pepY-SO1861-nanoplex and corresponding controls, in each of which one element was changed, were generated and are shown in Figure 4.25. As saporin is a ribosome-inactivating protein leading to cell death, transfection efficiency was determined by measuring cell viability 72 h after transfection using MTS assay in comparison to an untreated control cell population. In comparison of the pepY-SO1861-nanoplex (with conjugated saponin, dark blue line) with a targeted non-equipped nanoplex (pepY-nanoplex, green line), the transfection-enhancing effect of the conjugated SO1861-EMCH was confirmed. Interestingly, in the case of NP-Sap transfections, supplementation with equivalent amounts of free SO1861-EMCH in the transfection medium led to comparable effects as transfection with the SO1861-nanoplexes, which had the same amounts of saponin conjugated to the complexing peptide. The incorporation of targeting pepY instead of a non-targeted K₁₆ peptide (red line) reduced cell viability by approximately 25 % at all nanoplex concentrations examined, confirming the hypothesized enhancement of the internalization of the nanoplexes by pepY. Transfection with the pepY-SO1861-nanoplex formulated with the nontoxic eGFP-encoding plasmid pEGFP-N3 (light blue line) did not significantly reduce cell viability, except for the highest nanoplex concentration of 834 ng complexed DNA per well. At this high nanoplex concentration, a total of ≈500 ng of conjugated SO1861-EMCH is available per well, which is readily internalized due to its integration into the pepY-nanoplex. The observed reduced cell viability is therefore probably due to the toxic effect of high concentrations of nanoplex-conjugated SO1861-EMCH (Section 4.4.3).

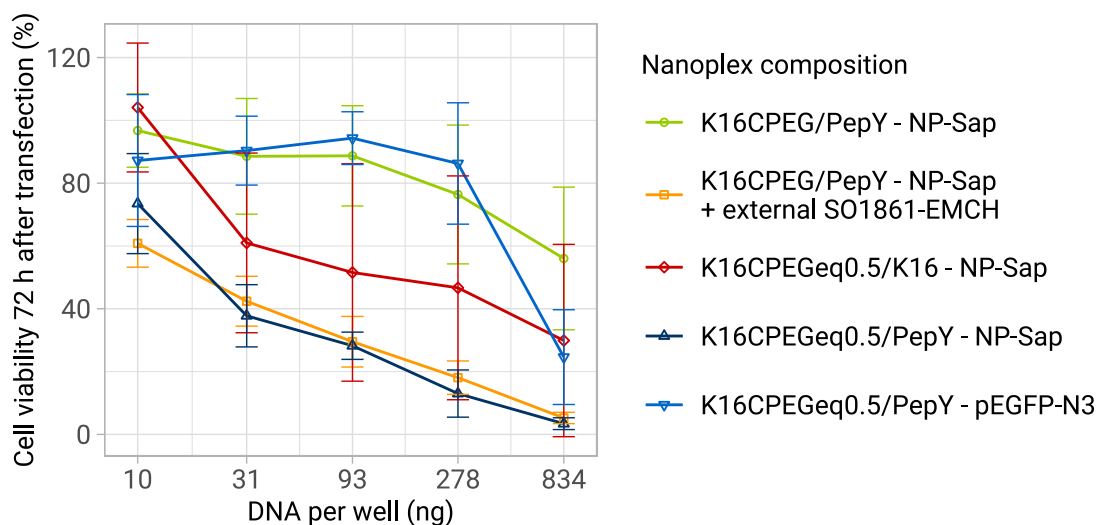


Figure 4.25: Dose-response curves of PepMix-nanoplexes in Neuro-2a cell line. Nanoplexes were formed in HBM at N/P 10 as described in Section 3.3. Cells were incubated with nanoplexes and external SO1861-EMCH optionally for 72 h before cell viability was determined using MTS assay, details are given in sections 3.5.2 and 3.5.3. Amounts of externally supplemented SO1861-EMCH (yellow line) were equivalent to the amounts of conjugated saponin in the equipped nanoplexes. All nanoplexes were prepared with 70 % of the first-named peptide and 30 % of the second-named peptide (see Nanoplex composition). Symbols indicate mean, error bars indicate standard deviation of three independent experiments with each of them performed in triplicate, resulting in $n = 9$.

4.5.2.2 Characterization of PepY-Nanoplexes

Physicochemical characterization of the pepY-SO1861-nanoplex and a pepY-nanoplex lacking the SO1861-EMCH-conjugation (NP-Sap complexed with 70 % pepY and 30 % K₁₆CPEG) preceded *in vivo* tolerability and efficacy testing. The preparation of the PepMix-nanoplexes for their characterization was carried out in HEPES-buffered mannitol (HBM), as this buffer was intended for i.v. injection in the *in vivo* study.

DNA complexation efficiency was determined to be $96.71 \pm 0.04\%$ and $96.95 \pm 0.07\%$ for pepY-SO1861-nanoplexes and pepY-nanoplexes, respectively. DLS analysis of the PepMix-nanoplexes revealed D_h s well below 90 nm. $P_{dis} < 0.3$ and the particle size distributions indicated a minimal extent of aggregate formation (Figure 4.26 and Table 4.4). The pepY-SO1861-nanoplexes, prepared with the functionalized peptide K₁₆CPEGeq0.5, were slightly larger. After 72 h incubation at room temperature, both nanoplexes studied were enlarged marginally, but the hydrodynamic diameters were clearly maintained below 100 nm, indicating stability of the nanoplex suspension.

Table 4.4: Hydrodynamic diameter (D_h), polydispersity index (Pdi), and ζ -potential of pepY-nanoplexes and pepY-SO1861-nanoplexes formulated at N/P 10 in HBM and evaluated as described in Section 3.4.6. Mean of triplicates \pm standard deviation is reported.

Nanoplex	Incubation time	D_h (nm)	Pdi	ζ -Potential (mV)
pepY-nanoplex	30 min	68.20 ± 1.11	0.232 ± 0.015	25.8 ± 1.0
	72 h	75.77 ± 0.32	0.248 ± 0.003	
PepY-SO1861-nanoplex	30 min	80.93 ± 1.26	0.260 ± 0.016	26.9 ± 1.4
	72 h	90.60 ± 1.75	0.268 ± 0.014	

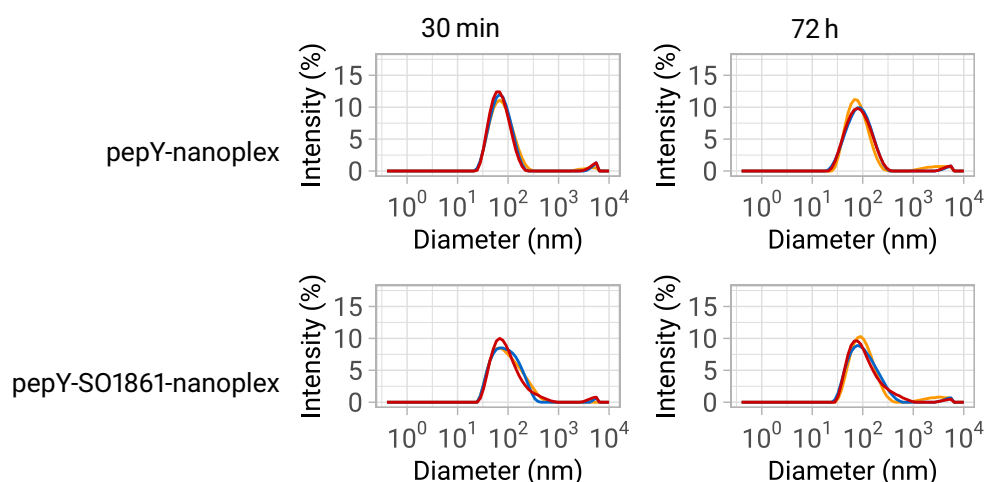


Figure 4.26: Size distribution by intensity of pepY-nanoplexes and pepY-SO1861-nanoplexes. Nanoplexes were formulated at N/P 10 in HBM and evaluated as described in Section 3.4.6. First row shows the size distribution of pepY-nanoplexes 30 min (left) and 72 h (right) after nanoplex formulation. Lower panel shows size distribution of pepY-SO1861-nanoplexes 30 min (left) and 72 h (right) after nanoplex formulation. Size distributions of three measurements (different colors) are shown.

The determination of particle size by DLS is performed under certain assumptions that reduce the accuracy of the results (see Section 3.4.6). The size of the nanoplexes was therefore additionally determined using electron microscopy.

First, the nanoplexes were examined with a scanning electron microscope (Figure 4.27). Unfortunately, upon drying of the samples, the nanoplexes aggregated. In addition, the samples had to be sputtered with gold to improve secondary electron emission for detection. Because of these difficulties, the nanoplexes were additionally examined by Cryo-TEM (Figure 4.28). Here, the analysis of the sample in vitrified ice made it possible to visualize the nanoplexes virtually in their solution state.

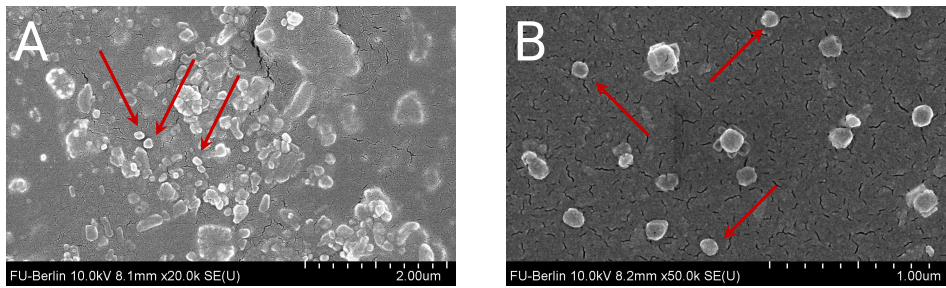


Figure 4.27: Scanning electron micrographs of pepY-nanoplexes (A) and pepY-SO1861-nanoplexes (B) acquired as described in Section 3.4.7. Single particles are highlighted with the red arrows.

The measurement of individual nanoparticles revealed nanoplex diameters of 30 nm to 100 nm, which confirmed the sizes determined by DLS. Nanoplexes were shown to exhibit spherical shape. PepY-nanoplexes (without SO1861-EMCH conjugation) showed slightly smaller sizes on average.

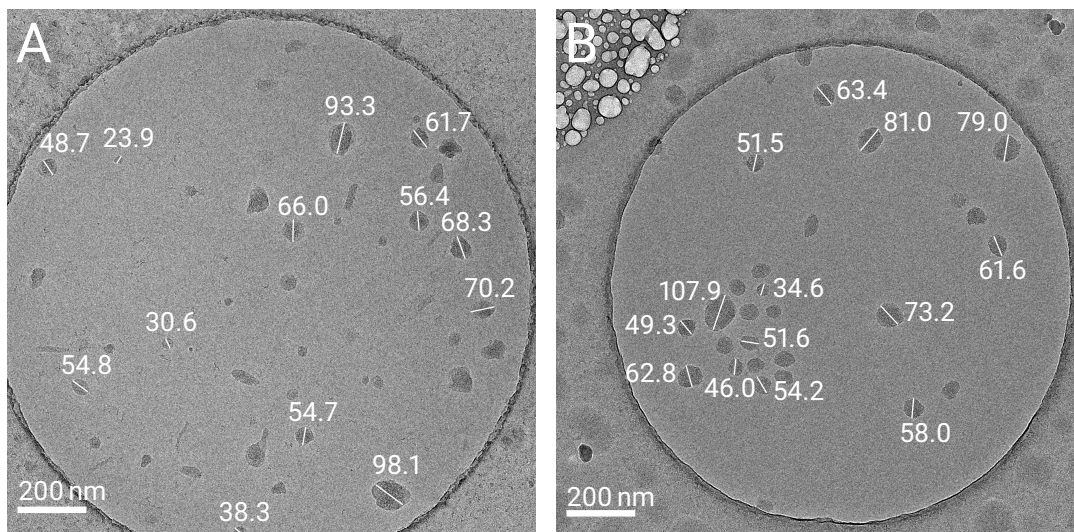


Figure 4.28: Cryogenic transmission electron micrographs of pepY-nanoplexes (A) and pepY-SO1861-nanoplexes (B) acquired and evaluated as described in Section 3.4.7. White lines indicate the diameters used for the calculation of nanoplex sizes (white letters, in nm) based on the calibrated pixel size.

As described in Section 1.1.2, a D_h of ≈ 50 nm is optimal for uptake of nanoparticles via clathrin-mediated endocytosis. The presented size distribution of the nanoplexes with D_h s of 30 nm to 100 nm lied slightly above this optimum, but still ensured uptake of the nanoplexes via clathrin-mediated endocytosis.

Both nanoplexes exhibited moderately strong positive surface charge with ζ -potential values around 26 mV (Table 4.4). This cationic surface charge contributes to efficient internalization of the nanoplexes, due to the negatively charged character of the cell plasma membrane (Rivolta et al. 2012).

4.5.2.3 Tolerability *In Vivo*

Before the start of the therapy study to test the anti-tumor efficacy, the tolerability of the pepY-SO1861-nanoplexes was first examined in three non-tumor-bearing mice. As described in Section 3.6.1, the mice received a total of five injections of the pepY-SO1861-nanoplex (NP-Sap complexed with 70 % pepY and 30 % K_{16} CPEGeq0.5, analogous to the planned efficacy study.

All three mice in the tolerance study did not show any sign of therapy related side effects over the two-week study. Their body weight was stable with minimal fluctuations. All mice gained approximately 2 g of body weight over the two weeks (Figure 4.29); no loss of body weight $> 10\%$ was observed. As massive hemolysis at the injection site was expected for i.v. injection of free SO1861 (Gilbert-Oriol et al. 2013), the injection site was closely monitored during the study. Here, only minimal short term flush was noticed at the injection sites and no other severe alterations were observed. This indicated that the i.v. administered pepY-SO1861-nanoplexes were well tolerated in mice, thus allowing the initiation of the therapeutic study.

4.5.2.4 Efficacy *In Vivo*

Anti-tumor efficacy of pepY-SO1861-nanoplexes (pepY-SO1861-nanoplex) was investigated *in vivo* in an aggressively growing Neuro-2a neuroblastoma allograft model in mice, with non-equipped pepY-nanoplexes (NP-Sap complexed with 70 % pepY and 30 % K_{16} CPEG)

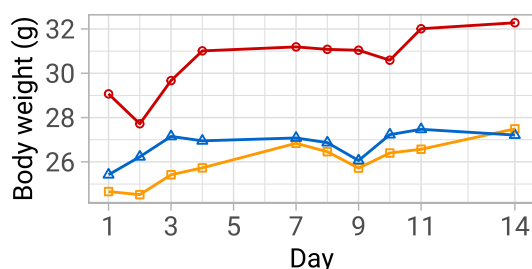


Figure 4.29: Body weight of three mice during tolerability study. Each color represents a single mouse.

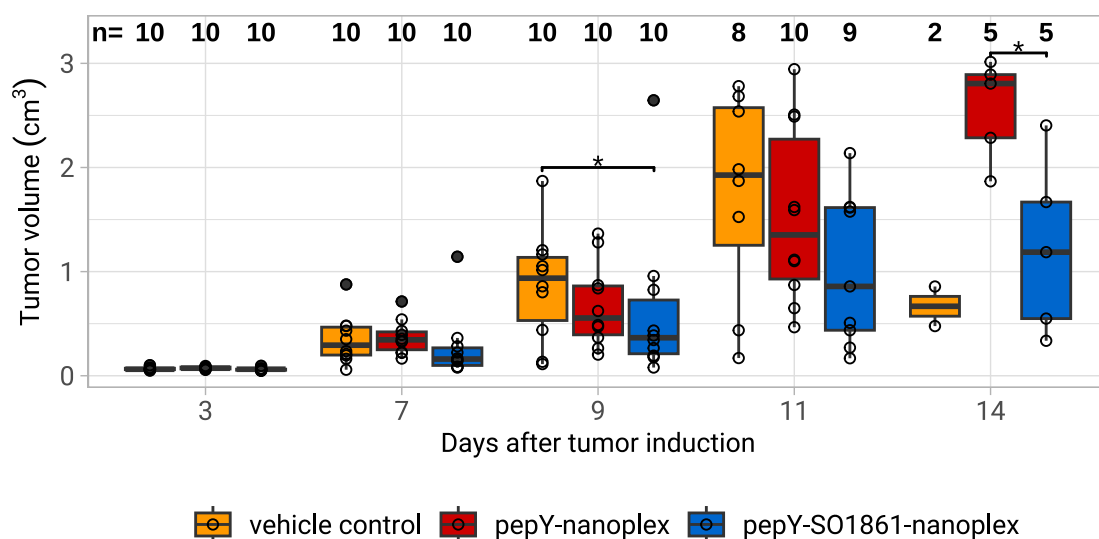


Figure 4.30: Anti-tumor efficacy of pepY-SO1861-nanoplexes and pepY-nanoplexes *in vivo* indicated by TVs and survival rates during the study period. Boxes of the box plots represent the middle 50 % of the data, the interquartile range (IQR). The horizontal line inside the box is the median. Whiskers represent minimum and maximum values. Any values lying outside $1.5 \times \text{IQR}$ are plotted separately as filled dot. All data points were plotted as dots and above each box plot the number of observations per group is given in bold, indicating survival rates. Decreasing group sizes over the course of the study were due to the termination of animals with tumor volumes $>1.5 \text{ cm}^3$. Significant differences were calculated with unpaired, two-sided Student's *t*-test, the highest value in the pepY-SO1861-nanoplex group was confirmed to be an outlier using Grubbs's test and was not taken into account for statistical testing. * $p < 0.05$.

and buffer (HBM) as control. As described in Section 3.6.2, ten mice per group received five i.v. injections (100 μL with 30 μg complexed NP-Sap in the tail vein) each on days 1, 3, 5, 7, and 9 after s.c. tumor induction. Tumor volumes (TVs) were measured to determine treatment efficacy.

TV changes during the treatment clearly showed slowed tumor growth by treatment with pepY-nanoplexes (red boxes) or pepY-SO1861-nanoplexes (blue boxes) compared to placebo (vehicle control, yellow boxes) as depicted in Figure 4.30. Nine days after tumor induction, tumors in the vehicle group had a mean volume of 0.87 cm^3 . Treatment with pepY-nanoplexes resulted in a reduced mean TV of 0.68 cm^3 . Conjugation of SO1861 in the pepY-SO1861-nanoplexes further reduced mean TV to 0.41 cm^3 (excluding 1 confirmed outlier, mean TV including the outlier: 0.63 cm^3). At day 14, tumors in the pepY-SO1861-nanoplex group were significantly smaller than those in the pepY-nanoplex control group (mean TV 1.23 cm^3 vs. mean TV 2.57 cm^3 , respectively), with both groups consisting of

five animals at that time.

Treatment efficiency was also illustrated by improved survival rates in the treatment groups. Since the Neuro-2a allograft tumor model is an aggressively growing tumor model, untreated, tumors reach the limiting size of $>1.5 \text{ cm}^3$ already 14 days after tumor inoculation; 80 % of the animals from the placebo group had to be sacrificed for ethical reasons. The remaining animals showed slow tumor growth throughout the study. This suggests problems with tumor cell inoculation. With a survival rate of 50 % after 14 days for both the pepY-nanoplex and the pepY-SO1861-nanoplex group, treatment was shown to prolong survival (Figure 4.30).

Compared to the promising efficacy of the pepY-SO1861-nanoplexes *in vitro*, the observed effect in the *in vivo* model seems to be smaller. This is not surprising, assuming a potentially complex biodistribution *in vivo*. After i.v. injection, the nanoplexes encounter several barriers that compete with or influence their delivery to the tumor tissue. These include, but are not limited to, particle aggregation, protein adsorption, uptake by cells of the mononuclear phagocyte system (MPS), and renal clearance (Wilhelm et al. 2016; Zhu et al. 2022). The significantly enlarged livers of three mice in the pepY-SO1861-nanoplex-treatment group compared to three mice in the vehicle control group ($600.4 \pm 35.4 \text{ mg}$ vs. $326.1 \pm 21.2 \text{ mg}$, raw data in Appendix 7.1) suggest an interaction of the nanoplexes with Kupffer cells. These liver-resident macrophages are part of the MPS and the accumulation of the injected nanoplexes may have led to Kupffer cell hyperplasia and inflammatory cell infiltration as observed for silver nanoparticle exposure by Al-Doaiss et al. (2020). The analysis of 117 manuscripts from 2005 to 2015 on the administration of nanoparticles by Wilhelm et al. (2016) showed that on average (median) only 0.7 % of the injected nanoparticle dose reached the tumor. The tested pepY-nanoplexes give no reason to assume that their delivery efficiency is significantly higher than 1 %, so this is a key element for optimization.

The enormously high growth rate of the tumor is another factor that could contribute to the observed lower efficacy. Even with high transfection efficiencies, non-transfected cells remain unaffected and continue to divide leading to progressive tumor growth. This effect is more pronounced in the *in vivo* evaluation after several days than in the *in vitro* evaluation after 48 h to 72 h. In addition, the complex three-dimensional structure of the tumor *in vivo* has to be taken into account, which makes a comparison with *in vitro* cell culture data somewhat difficult and of limited value.

Although the pepY-SO1861-nanoplexes were more effective than the non-equipped pepY-nanoplexes in the therapy study, the effect of SO1861 incorporation into the pepY-nanoplexes was smaller *in vivo* than suggested by preliminary *in vitro* experiments. This may be due to the slightly larger particle size of the pepY-SO1861-nanoplexes (see Table 4.4 and Figure 4.26), which reduces the internalization efficiency compared to the smaller pepY-nanoplexes. It is also conceivable that optimization of SO1861 loading *in vivo* would lead to different results. Therefore, different saponin loadings should be considered for future *in vivo* optimization studies.

Summary

- Dibenzocyclooctene-functionalized protein ligands were covalently conjugated to SO1861-EMCH-equipped nanoplexes using strain-promoted azide-alkyne-cycloaddition (SPAAC). The resulting targeted, equipped nanoplexes exhibited significantly increased hydrodynamic diameters and a strong tendency to aggregate. This observation was attributed to the introduction of PBS as an ionic solution and the shielding of the suspension-stabilizing surface charge of the nanoplexes, associated with ligand conjugation via SPAAC.
- As demonstrated for EGF-functionalized nanoplexes, ligand loadings $\geq 25\%$ led to a drastic reduction of transfection efficiency in both target and non-target cells. Thus, the hypothesized reduction of non-specific uptake of the nanoplexes by targeting ligand functionalization could not be compensated by the receptor-mediated uptake of the functionalized nanoplexes.
- Short peptide sequences were identified as less bulky targeting motifs that can be introduced to the nanoplexes by linking of the targeting sequence to a DNA-complexing K_{16} -segment. Peptide Y (pepY), which was successfully used for the targeted delivery of nanoplexes to Neuro-2a cells for two-component sapofection, was tested as a first prototype for peptide motif targeting.
- Complexation of the DNA with pepY and K_{16} CPEGeq0.5 in parallel resulted in the formation of pepY-SO1861-nanoplexes. *In vitro* transfection studies of these nanoplexes confirmed the superiority of conjugated over externally supplemented SO1861-EMCH, and pepY was shown to further enhance transfection efficiency, presumably due to enhanced uptake.
- A pepY-SO1861-nanoplex, prepared by complexing NP-Sap, encoding the cytotoxic protein saporin, with 70 % pepY and 30 % K_{16} CPEGeq0.5 and a control nanoplex lacking the the conjugated SO1861-EMCH were tested *in vivo* in mice. The nanoplexes were shown to encapsulate $\approx 97\%$ of the DNA. Electron microscopy revealed diameters of 30 nm to 100 nm and the nanoplexes were shown to exhibit spherical shape. PepY-SO1861-nanoplexes were shown to be well tolerated *in vivo*. In the aggressively growing Neuro-2a allograft model, treatment with the pepY-SO1861-nanoplex and the pepY-nanoplex without conjugated SO1861-EMCH resulted in slower tumor growth, with the pepY-SO1861-nanoplex being more effective. The anti-tumor efficacy was further confirmed by improved survival rates in the treatment groups compared to the vehicle control.

4.6 Molecular Biology

The aim of the molecular biology work in this thesis was to compare and optimize different pDNA vectors as component of the envisaged optimized, non-viral gene delivery tool. Based on the established *in vitro* evaluation of transfection efficiency, eGFP-encoding pDNA vectors were used. A transfer of the obtained findings to other genes of interest is plausible, the investigations can therefore be regarded as universal.

4.6.1 Molecular Cloning of Minicircle DNA Vectors

The established and widely used vector pEGFP-N3 was to be compared with a pDNA vector having the same promoter and gene sequence but smaller overall size to assess the influence of plasmid size on transfection efficiency. As described in Section 3.1.4, the reduced backbone of mcDNA was used for this purpose. Thus, the goal of molecular cloning was to introduce the promoter and gene sequence of pEGFP-N3 into the mcDNA-generating plasmid MN501A1. Unfortunately, the introduction of the complete insert, i.e. promoter and gene sequence, in one cloning step was not successful, so a two-step molecular cloning process was applied. A vector with the eGFP gene sequence was generated first (construct eGFP/MN501A1), whose promoter sequence was then replaced by the CMV enhancer + promoter sequence of pEGFP-N3 in the subsequent cloning process.

To evaluate target-specific expression of plasmid vectors containing the hybrid liver promoter (HL promoter, HLP), a mcDNA-vector containing eGFP as gene of interest under control of the HL promoter was created. For this purpose, an insert consisting of the HL promoter and hFIX gene (generously provided by Prof. Pinotti, Università degli studi di Ferrara) was first inserted into the mcDNA-generating vector creating the construct HLP/hFIX/MN501A1. From this vector, the hFIX gene sequence was excised by restriction digestion with NheI-HF and the plasmid was recircularized by subsequent ligation yielding the construct HLP/MN501A. This vector was then used for the final molecular cloning process as the receiving backbone plasmid for the eGFP-encoding gene sequence.

The steps of the molecular cloning processes were performed as described in Section 3.1.3. Quality control of the prepared pDNA vectors is shown in Figure 4.31 for eGFP/MN501A1 and CMV/eGFP/MN501A1 and in Figure 4.32 for HLP/hFIX/MN501A1 and HLP/eGFP/MN501A1. Restriction digests confirmed the expected total size of the constructs and the integration of the insert flanked by the introduced restriction sites. Multiple bands in the pDNA preparation are due to different conformations, acceptable purity of all preparations was confirmed by linearization. The sequences of all described constructs were additionally confirmed by Sanger sequencing.

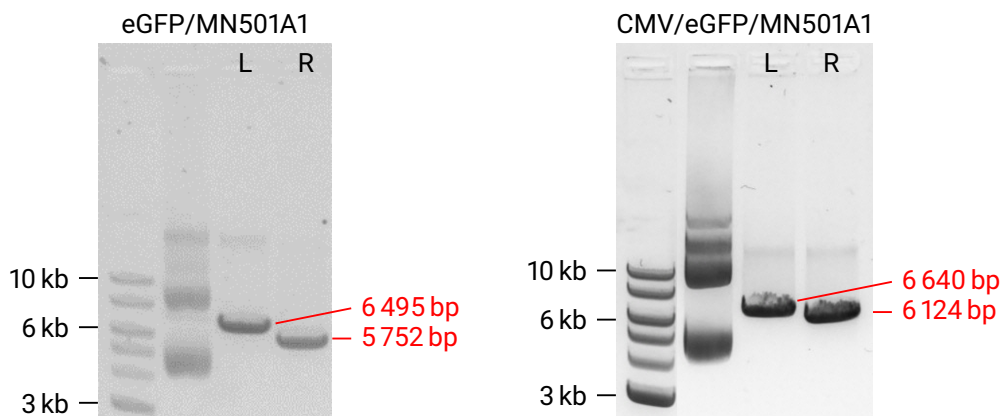


Figure 4.31: Quality control of constructs eGFP/MN501A1 and CMV/eGFP/MN501A1. Plasmid DNA was prepared as described in Section 3.1.3.5 and analyzed using agarose gel electrophoresis as described in Section 3.1.1. Name of constructs is given on top of each panel. Leftmost lane: 1 kb Plus DNA ladder, on the right of it: plasmid DNA preparation undigested, linearized (L) and double-digested (R). Restriction digests were performed as described in Section 3.1.3.2 using the following restriction enzymes: eGFP/MN501A1 L: NheI-HF and R: NheI-HF + Sall-HF & CMV/eGFP/MN501A1 L: Sall-HF and R: Sall-HF + SpeI-HF.

4.6.2 Preparation of Minicircle DNA

McDNA was prepared as described in Section 3.1.4 and analyzed using restriction digest (Section 3.1.3.2) and agarose gel electrophoresis (Section 3.1.1, 2% agarose gel) (Figure 4.33).

McDNA preparations were shown to contain almost exclusively mcDNA in the supercoiled together with minimal amounts of mcDNA in the open-circular conformation, which is desirable as the supercoiled pDNA conformation has been shown to be most efficient for transfection purposes due to its ability to reach the perinuclear region (Cherng et al. 1999; Remaut et al. 2006; Weintraub et al. 1986). The FDA recommends >80% supercoiled plasmid content for industrially produced therapeutic pDNA (FDA 2007), both mcDNA preparations clearly meet these requirements. Comparing the feeding solution (FS) added to the SEC column and the collected fraction (F), it is clear that both genomic DNA and parental plasmid contamination (above the mcDNA bands) and RNA (large, smeared band in the lower part of the gel) were successfully removed by SEC. Linearization confirmed the total size of the mcDNA vectors, the integration of both the promoter and the eGFP sequence flanked by the introduced restriction sites was confirmed by parallel digestion using three restriction enzymes (Figure 4.33)

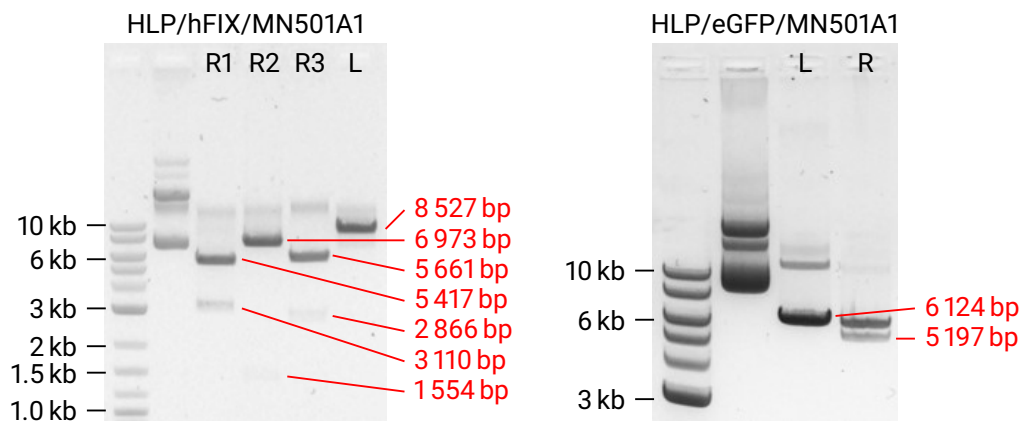


Figure 4.32: Quality control of constructs HLP/hFIX/MN501A1 and HLP/eGFP/MN501A1. Preparation and labeling as given in Section 4.31 description. The following restriction enzymes were used: HLP/hFIX/MN501A1 R1: Sall-HF + SpeI-HF, R2: XbaI-HF, R3: NheI-HF, and L: XbaI-HF & HLP/eGFP/MN501A1 L: NheI-HF and R: NheI-HF + AatII.

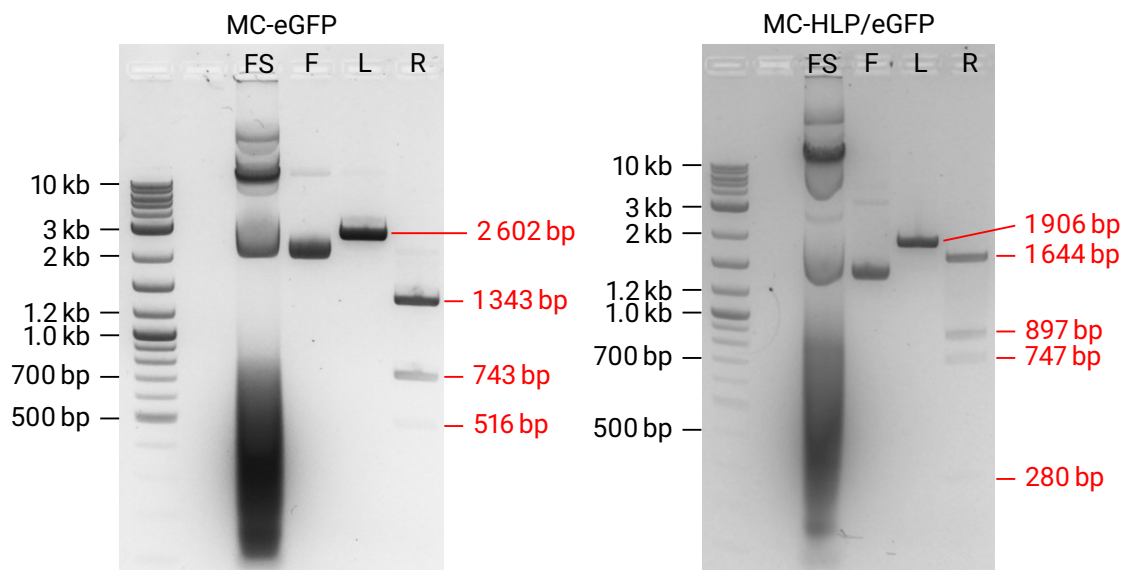


Figure 4.33: Quality control of produced mcDNA MC-eGFP and MC-HLP/eGFP. Name of constructs are given on top of each panel. Leftmost lane: 1 kb Plus DNA ladder; FS: feeding solution for SEC; F: collected fraction containing mcDNA, concentrated and desalted; L: linearized mcDNA; R: triple-digested mcDNA. Restriction digests were performed using the following restriction enzymes: MC-eGFP L: NheI-HF & R: NheI-HF + SpeI-HF + Sall-HF; MC-HLP/eGFP L: NheI-HF & R: NheI-HF + SpeI-HF + AatII.

4.6.3 Optimization of DNA Vector

Table 4.5: Overview of GFP-encoding pDNA vectors tested *in vitro*.

Name	Size (bp)	Promoter	GFP variant	Antibiotic resistance
pEGFP-N3	4729	CMV enhancer + promoter	eGFP	Kanamycin
NP-eGFP	2487	CMV enhancer + promoter + HTLV-I R	eGFP	<i>none</i>
MN601A1	5562	CMV promoter	copGFP	Kanamycin
MC-GFP	1523	CMV promoter	copGFP	<i>none</i>
CMV/eGFP/ MN501A1	6640	CMV enhancer + promoter	eGFP	Kanamycin
MC-CMV/GFP	2602	CMV enhancer + promoter	eGFP	<i>none</i>
HLP/eGFP/ MN501A1	5944	HL promoter	eGFP	Kanamycin
MC-HLP/eGFP	1906	HL promoter	eGFP	<i>none</i>

A set of GFP-encoding pDNA vectors varying in size, promoters, GFP variants and the presence of antibiotic resistance genes in the pDNA (Table 4.5) were investigated for their influence on transfection efficiency *in vitro* in cell lines A2058 and Huh-7 (Figure 4.34).

Higher transfection efficiencies were achieved by mcDNA vectors in comparison with their parental plasmids (MC-GFP vs. MN601A1, MC-CMV/eGFP vs. CMV/eGFP/MN501A1, and MC-HLP/eGFP vs. HLP/eGFP/MN501A1), although not statistically significant in all cases. This confirms the results of various authors (Chen et al. 2003; Florian et al. 2021; Munye et al. 2016). It should be noted that the study design allows further explanations for these observations besides the pure vector length. On the one hand, the varying quality of the pDNA preparations with a higher proportion of the preferred supercoiled conformation in the mcDNA preparations, and on the other hand, the correspondingly higher amount of complexing peptide scaffold in the larger parental plasmids and possibly associated toxicity (see Section 4.4.3) could have contributed to the superiority of the smaller vectors. However, the larger amount of peptide scaffold per plasmid molecule also results in a larger amount of complexed SO1861, which should contribute to increased transfection efficiency of the larger vectors due to its eee properties.

Liver-specific expression by incorporation of the HL promoter was evident to some extent but cannot be confirmed in the absoluteness described by McIntosh et al. (2013). Whereas transfection efficiency in the non-target cell line was significantly reduced by replacement of CMV enhancer + promoter with HL promoter, the reduced transfection efficiency similarly observed in the target cell line Huh-7 was not significant. Furthermore, for the interpretation of the achieved transfection efficiency of 31 % for MC-HLP/eGFP in the non-target cell line A2058, the generally easy transfectability of this cell line has to be taken into account.

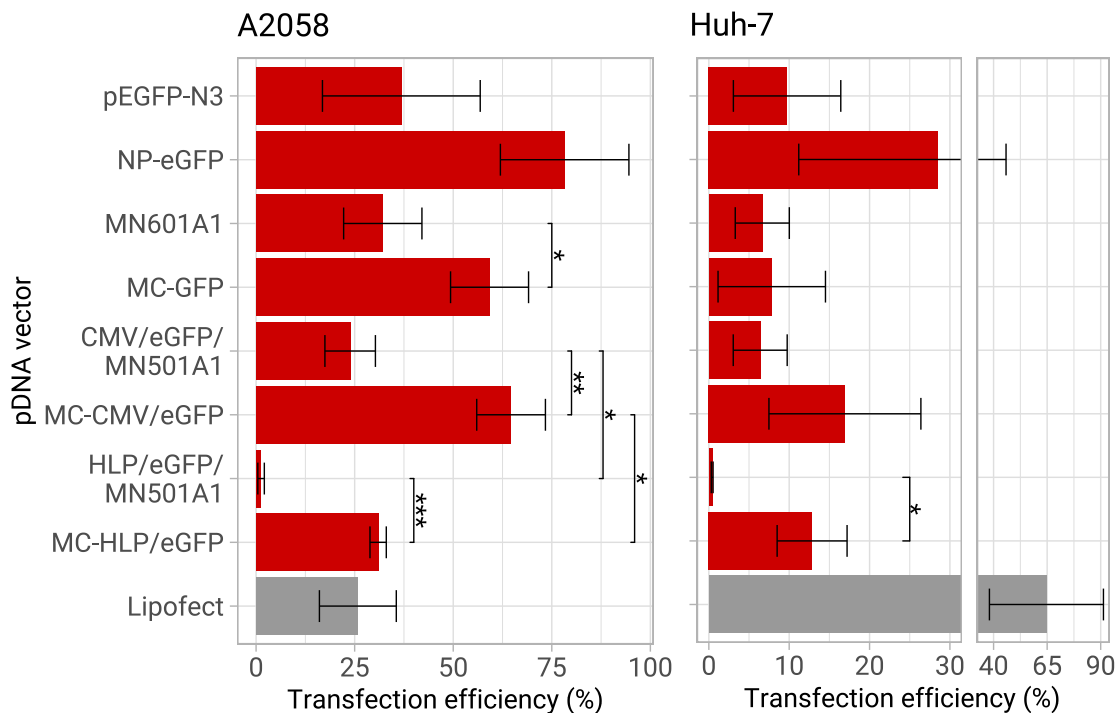


Figure 4.34: *In vitro* transfection efficiency of nanoplexes formulated with different GFP-encoding pDNA vectors in cell lines A2058 and Huh-7. To minimize other factors influencing transfection efficiency, all nanoplexes were formulated with K_{16} Ceq0.25 at N/P 10, and the molar amount of transfected pDNA per well was kept constant at 65 fmol (= 100 ng NP-eGFP). Transfection was performed and evaluated as given in sections 3.5.2 and 3.5.3. Bar width indicates mean of three independent experiments, error bars show standard deviation. Significant differences were calculated with unpaired, two-sided Student's *t*-test. * $p < 0.05$, ** $p < 0.01$, *** $p < 0.001$.

The nanoplasmid™ vector NP-eGFP achieved highest transfection efficiencies in both cell lines. The comparison with MC-CMV/eGFP, which is of approximately the same size but lacks the incorporation of the human T-lymphotropic virus type I region (HTLV-I R), confirms the increased transgene expression of the combined CMV-HTLV-I R promoter (incorporation of HTLV-I R as part of exon 1 and intron 1 downstream of the CMV promoter) in NP-eGFP described by Luke et al. (2010).

Examination of expression kinetics after transfection with NP-eGFP or pEGFP-N3 revealed no clear differences with respect to the detection of first eGFP-positive cells. However, for NP-eGFP, an increase in eGFP-expressing cells was shown up to 72 h after transfection, whereas for pEGFP-N3 transfection, no further increase of transfection efficiency was observed from 48 h after transfection (Figure 4.35). One possible explanation for this observation is the increased mRNA translation efficiency described for the incorporation of

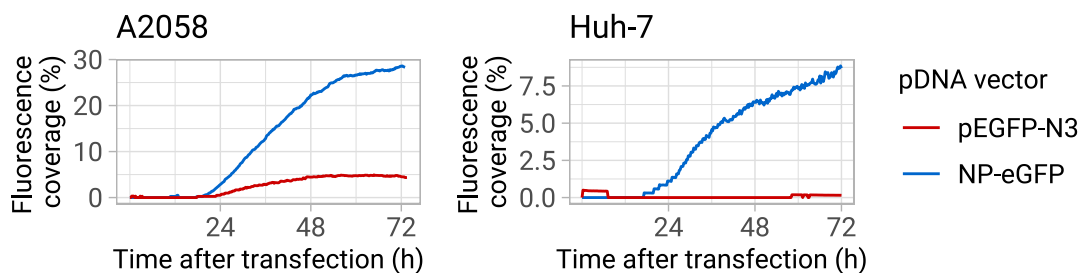


Figure 4.35: Kinetic profile of eGFP expression after transfection with pEGFP-N3 and NP-eGFP in cell lines A2058 and Huh-7. Fluorescence coverage is indicating the share of eGFP-expressing cells and was calculated as described in Section 3.5.3. Data acquisition and image analysis was done with constant settings within each cell line to ensure comparability of the results. n=1.

the combined CMV-HTLV-I R promoter by Luke et al. (2010). In addition, due to the longer extragenic spacer length, transgene silencing as discussed in Section 1.1.2 is expected to be much more pronounced in the case of pEGFP-N3. The absolute fluorescence coverage values shown in Figure 4.35 are lower than the transfection efficiencies determined by flow cytometry analysis due to the much less sensitive evaluation in the fluorescence microscope.

As described in detail in Section 1.1.2.1, the minimized bacterial backbone, the resulting reduced immunogenicity, and the absence of antibiotic resistance-conferring gene sequences are further advantages of the minimized nanoplasmid™ and mcDNA vectors, especially for *in vivo* applications, in addition to their reduced size. As evident from the previous sections, commercially available nanoplasmid™ vectors were ultimately used for the *in vivo* studies within this thesis. In addition to their superior transfection performance, the time-consuming nature and low yields of mcDNA production led to this decision. All basic physicochemical and *in vitro* studies, on the other hand, were performed with pEGFP-N3, as this could be produced inexpensively in sufficient quantities in-house (see Section 3.1.3.5).

Summary

- McDNA vectors encoding eGFP under control of CMV enhancer + promoter and HL promoter were produced in high purity with >80 % supercoiled conformation.
- Reducing the size of the pDNA while maintaining the sequences of the promoter and transgene significantly increased the transfection efficiency (constant molar amount of pDNA).
- Nanoplasmid™ vectors achieved highest transfection efficiency due to the incorporation of the combined CMV-HTLV-I R promoter.

5 Conclusion and Outlook

The objective of the scientific work presented in this thesis was to develop an optimized targeted non-viral gene delivery vehicle incorporating a pDNA vector, a polymeric molecular carrier, the endosomal escape-enhancing (eee) triterpenoid saponin SO1861, and a targeting ligand as an i.v. injectable one-component formulation. The goal was for the gene delivery vehicle to exhibit efficient and stable nucleic acid complexation, appropriate size, size distribution and surface charge, high transfection efficiency *in vitro* and *in vivo*, good tolerability *in vitro* and *in vivo* as well as selective delivery to target tissues.

To achieve this goal, a PLL-derived peptide scaffold was designed to contain not only a K₁₆-motif for nucleic acid complexation, but also one cysteine for covalent conjugation of SO1861-EMCH via Michael-type thiol-maleimide addition, and an azidolysine, whose azide group is accessible for conjugation of a DBCO-functionalized ligand using SPAAC.

Using the optimized reaction conditions for thiol-maleimide addition, SO1861-equipped peptide scaffolds carrying either 0.25 or 0.5 equivalents of covalently conjugated SO1861-EMCH molecules per peptide molecule were obtained. After purification by anion-exchange chromatography, the peptide-triterpene conjugates were found free of unreacted SO1861-EMCH. The SO1861-equipped peptide scaffolds were able to efficiently condensate pDNA ($\geq 98\%$ at N/P 10) and the resulting nanoplexes exhibited appropriate sizes ($D_{hs} \leq 160$ nm), low-to-moderate Pdis of 0.1 to 0.4, moderately high ζ -potentials of ≈ 30 mV, and adequate stability for 48 h incubation at room temperature.

The conjugation of SO1861-EMCH to the peptide scaffolds forming the nanoplexes significantly increased the *in vitro* transfection efficiency of the nanoplexes, while exposure to the SO1861-equipped nanoplexes was well tolerated. The comparison of equal amounts of nanoplex-conjugated and externally supplemented SO1861-EMCH revealed a clear superiority of the single-component formulation over the previously practiced combinatorial sapofection approach of parallel application of the nanoplexes and the saponin. These effects were demonstrated in numerous cell lines, highlighting the universal applicability of the developed saponin-containing nanoplexes for transfection of cells of different origin. The higher activity of nanoplex-conjugated SO1861-EMCH was hypothesized to be due to higher concentrations of SO1861-EMCH in the endosomes. This hypothesis was supported by earlier endosomal release of the SO1861-containing nanoplexes and slightly increased toxicity of nanoplex-integrated SO1861-EMCH.

As shown exemplary for EGF, conjugation of a DBCO-functionalized targeting ligand via SPAAC resulted in targeted, SO1861-equipped nanoplexes. These ligand-decorated

nanoplexes exhibited a strong aggregation tendency. Their transfection efficiency in non-target and target cells was significantly reduced at ligand loadings high enough to suppress unspecific, non-receptor-mediated internalization in non-target cell lines.

Short peptide sequences were identified as alternative, less bulky targeting motifs. Their incorporation into the nanoplexes was achieved by linking the targeting sequence to a DNA-complexing K₁₆-motif. The parallel use of the targeting peptide and the SO1861-equipped peptide scaffold for DNA complexation enabled the preparation of peptide-targeted nanoplexes including conjugated SO1861-EMCH as endosomal escape enhancer (EEE). The introduction of the targeting peptide pepY further enhanced the transfection efficiency *in vitro*.

A pepY-SO1861-nanoplex (NP-Sap complexed with 70 % pepY and 30 % K₁₆CPEGeq0.5) and a control nanoplex lacking the conjugated SO1861-EMCH (pepY-nanoplex), both carrying pDNA encoding the cytotoxic protein saporin were tested for their anti-tumor efficacy *in vivo* in a mouse neuroblastoma model. The integration of SO1861 into the nanoplex eliminated the need to harmonize different biodistribution and application routes for two components, as required by the previously used combinatorial sapofection process. The pepY-nanoplexes were shown to encapsulate ≈97 % of the DNA. Diameters of 30 nm to 100 nm and spherical shape were observed by electron microscopy. The pepY-SO1861-nanoplexes proved to be i.v. injectable and well-tolerated *in vivo* in mice. In the allograft model with an aggressively growing neuroblastoma (Neuro-2a) tumor, treatment with the pepY-SO1861-nanoplexes and the pepY-nanoplexes resulted in slower tumor growth, with the SO1861-containing nanoplexes being more effective. Improved survival rates in the treatment groups compared to the vehicle control further confirmed the anti-tumor efficacy.

Returning to the goal of this work, the intended development of an optimized non-viral gene delivery system was successful with minor deviations from the original plan. The conjugation of a protein as a targeting ligand proved to be difficult. Nevertheless, i.v. injectable and effective SO1861-containing targeted nanoplexes were prepared by integrating a targeting peptide sequence.

The present work is the first report of successful gene delivery using a covalently conjugated triterpenoid saponin as EEE and provides evidence for the safety and efficacy of the prepared SO1861-peptide conjugates for improved gene delivery. Since the exchange of the therapeutic DNA vector is easy to implement, this is of interest not only for the treatment of cancer, but also for other indications that can be treated by gene therapeutic approaches. The conjugates presented here are the first representatives of a new class of compounds that offer numerous opportunities for optimization.

Manipulation of the nanoplex surface, e.g. by extensive PEGylation could lead to increased stability of the nanoplex suspension in ionic solutions. In addition, PEGylation is described to prolong blood circulation, which could consequently improve the efficacy of delivery. The efficacy of targeted delivery could also be improved by using alternative peptide ligands such as GE11 to target the EGFR.

The use of other triterpenoid saponins with better properties and better activity-to-toxicity ratio, such as AG1856, as well as optimization of the linker chemistry (e.g., degradation by lysosomal enzymes or reductive environment, improvement of pH-triggered release in acidic environment) between saponin and peptide is conceivable.

In addition, the use of the presented saponin-peptide conjugates for the delivery of other nucleic acids such as mRNA is a plausible option. This would eliminate the need for nuclear delivery, thereby extending the applicability of the described gene delivery vehicle to non-dividing cells.

Finally, the optimized reaction conditions for the thiol-maleimide addition, together with the developed protocol for the removal of unreacted SO1861-EMCH, allow the use of an excess of SO1861-EMCH for the peptide functionalization reaction in future studies. In addition, since conjugation of a targeting ligand via SPAAC has not proven to be successful, the azidolysine in the peptide sequence could be omitted, allowing the use of TCEP for disulfide reduction prior to the conjugation of SO1861-EMCH. Implementation of these changes could allow the production of a simple K₁₆-derived peptide with exactly one saponin molecule per peptide. The use of this peptide for the production of mixed nanoplexes would allow for a higher proportion of the targeting peptide and consequently a potentially better targeting effect. The production of this stoichiometrically precisely characterizable peptide would also permit the formulation of nanoplexes with higher saponin concentrations and therefore the optimization of the amount of saponin over a wider mass range.

6 Bibliography

- Abedin, M. R., Powers, K., Aiardo, R., Barua, D., and Barua, S. (Apr. 2021). “Antibody–drug nanoparticle induces synergistic treatment efficacies in HER2 positive breast cancer cells”. In: *Scientific Reports* 11.1. ISSN: 2045-2322. DOI: 10.1038/s41598-021-86762-6.
- Agard, N. J., Prescher, J. A., and Bertozzi, C. R. (Nov. 2004). “A Strain-Promoted [3 + 2] Azide–Alkyne Cycloaddition for Covalent Modification of Biomolecules in Living Systems”. In: *Journal of the American Chemical Society* 126.46, pp. 15046–15047. ISSN: 1520-5126. DOI: 10.1021/ja044996f.
- Aggarwal, P., Hall, J. B., McLeland, C. B., Dobrovolskaia, M. A., and McNeil, S. E. (June 2009). “Nanoparticle interaction with plasma proteins as it relates to particle biodistribution, biocompatibility and therapeutic efficacy”. In: *Advanced Drug Delivery Reviews* 61.6, pp. 428–437. ISSN: 0169-409X. DOI: 10.1016/j.addr.2009.03.009.
- Ahi, Y. S., Bangari, D. S., and Mittal, S. K. (Aug. 2011). “Adenoviral Vector Immunity: Its Implications and Circumvention Strategies”. In: *Current Gene Therapy* 11.4, pp. 307–320. DOI: 10.2174/156652311796150372.
- Angers-Loustau, A., Rainy, J., and Wartiovaara, K. (2007). “PlasmaDNA: a free, cross-platform plasmid manipulation program for molecular biology laboratories”. In: *BMC Molecular Biology* 8.1, p. 77. ISSN: 1471-2199. DOI: 10.1186/1471-2199-8-77.
- Arap, W., Pasqualini, R., and Ruoslahti, E. (Jan. 1998). “Cancer Treatment by Targeted Drug Delivery to Tumor Vasculature in a Mouse Model”. In: *Science* 279.5349, pp. 377–380. DOI: 10.1126/science.279.5349.377.
- Ardiani, A., Johnson, A. J., Ruan, H., Sanchez-Bonilla, M., Serve, K., and Black, M. E. (Mar. 2012). “Enzymes To Die For: Exploiting Nucleotide Metabolizing Enzymes for Cancer Gene Therapy”. In: *Current Gene Therapy* 12.2, pp. 77–91. DOI: 10.2174/156652312800099571.
- Armstrong, D. K., Kaufmann, S. H., Ottaviano, Y. L., Furuya, Y., Buckley, J. A., Isaacs, J. T., and Davidson, N. E. (Oct. 1994). “Epidermal growth factor-mediated apoptosis of MDA-MB-468 human breast cancer cells.” In: *Cancer research* 54 (20), pp. 5280–5283. ISSN: 0008-5472. ppublish.

-
- Asati, A., Santra, S., Kaittanis, C., and Perez, J. M. (Aug. 2010). "Surface-Charge-Dependent Cell Localization and Cytotoxicity of Cerium Oxide Nanoparticles". In: *ACS Nano* 4.9, pp. 5321–5331. DOI: 10.1021/nn100816s.
- Bachran, C., Sutherland, M., Heisler, I., Hebestreit, P., Melzig, M. F., and Fuchs, H. (Apr. 2006). "The Saponin-Mediated Enhanced Uptake of Targeted Saporin-Based Drugs is Strongly Dependent on the Saponin Structure". In: *Experimental Biology and Medicine* 231.4, pp. 412–420. DOI: 10.1177/153537020623100407.
- Bairoch, A. (July 2018). "The Cellosaurus, a Cell-Line Knowledge Resource". In: *Journal of Biomolecular Techniques*: *JBT* 29.2, pp. 25–38. ISSN: 1943-4731. DOI: 10.7171/jbt.18-2902-002.
- Bairoch, A. (Nov. 23, 2023). *Cellosaurus - a knowledge resource on cell lines*. Version 47. SIB - Swiss Institute of Bioinformatics. URL: <https://www.cellosaurus.org/> (visited on 11/23/2023).
- Bartrop, J. A., Owen, T. C., Cory, A. H., and Cory, J. G. (Jan. 1991). "5-(3-carboxymethoxyphenyl)-2-(4,5-dimethylthiazolyl)-3-(4-sulfophenyl)tetrazolium, inner salt (MTS) and related analogs of 3-(4,5-dimethylthiazolyl)-2,5-diphenyltetrazolium bromide (MTT) reducing to purple water-soluble formazans As cell-viability indicators". In: *Bioorganic & Medicinal Chemistry Letters* 1.11, pp. 611–614. DOI: 10.1016/S0960-894X(01)81162-8.
- Baumhover, N. J., Duskey, J. T., Khargharia, S., White, C. W., Crowley, S. T., Allen, R. J., and Rice, K. G. (Nov. 2015). "Structure-Activity Relationship of PEGylated Polylysine Peptides as Scavenger Receptor Inhibitors for Non-Viral Gene Delivery". In: 12.12, pp. 4321–4328. DOI: 10.1021/acs.molpharmaceut.5b00513.
- Behr, J.-P. (Feb. 1997). "The Proton Sponge: a Trick to Enter Cells the Viruses Did Not Exploit". In: *CHIMIA* 51.1-2, p. 34. DOI: 10.2533/chimia.1997.34.
- Berne, B. and Pecora, R. (2000). *Dynamic Light Scattering: With Applications to Chemistry, Biology, and Physics*. Dover Books on Physics Series. Dover Publications. ISBN: 9780486411552. URL: <https://books.google.de/books?id=vBB54ABhmuEC>.
- Bhattacharjee, S. (Aug. 2016). "DLS and zeta potential – What they are and what they are not?" In: *Journal of Controlled Release* 235, pp. 337–351. DOI: 10.1016/j.jconrel.2016.06.017.
- Bhirde, A. A., Patel, V., Gavard, J., Zhang, G., Sousa, A. A., Masedunskas, A., Leapman, R. D., Weigert, R., Gutkind, J. S., and Rusling, J. F. (Jan. 2009). "Targeted Killing of Cancer Cells in Vivo and in Vitro with EGF-Directed Carbon Nanotube-Based Drug Delivery". In: *ACS Nano* 3.2, pp. 307–316. ISSN: 1936-086X. DOI: 10.1021/nn800551s.

-
- Biedermann, N., Nuccio, S., Vaumas, R. de, and Faure, K. (June 2019). *Comprehensive two-dimensional analysis of saponins from Quillaja Saponaria: comparison of RPLC x RPLC and HILIC x RPLC modes*. 48th International Symposium on High Performance Liquid Phase Separations and Related Techniques (HPLC 2019). Poster. URL: <https://hal.science/hal-03749136>.
- Bio-Rad Laboratories, I. (2014). *Handcasting Polyacrylamide Gels. Bulletin 6201*. URL: https://www.bio-rad.com/webroot/web/pdf/lsr/literature/Bulletin_6201.pdf (visited on 10/07/2023).
- Boorjian, S. A., Alemozaffar, M., Konety, B. R., Shore, N. D., Gomella, L. G., Kamat, A. M., Bivalacqua, T. J., Montgomery, J. S., Lerner, S. P., Busby, J. E., Poch, M., Crispen, P. L., Steinberg, G. D., Schuckman, A. K., Downs, T. M., Svatek, R. S., Mashni, J., Lane, B. R., Guzzo, T. J., Bratslavsky, G., Karsh, L. I., Woods, M. E., Brown, G., Canter, D., Luchey, A., Lotan, Y., Krupski, T., Inman, B. A., Williams, M. B., Cookson, M. S., Keegan, K. A., Andriole, G. L., Sankin, A. I., Boyd, A., O'Donnell, M. A., Sawutz, D., Philipson, R., Coll, R., Narayan, V. M., Treasure, F. P., Yla-Herttuala, S., Parker, N. R., and Dinney, C. P. N. (Jan. 2021). "Intravesical nadofaragene firadenovec gene therapy for BCG-unresponsive non-muscle-invasive bladder cancer: a single-arm, open-label, repeat-dose clinical trial". In: *The Lancet Oncology* 22.1, pp. 107–117. DOI: 10.1016/s1470-2045(20)30540-4.
- Böttger, S., Westhof, E., Siems, K., and Melzig, M. F. (Oct. 2013). "Structure–activity relationships of saponins enhancing the cytotoxicity of ribosome-inactivating proteins type I (RIP-I)". In: *Toxicicon* 73, pp. 144–150. DOI: 10.1016/j.toxicicon.2013.07.011.
- Bouchard, H., Viskov, C., and Garcia-Echeverria, C. (Dec. 2014). "Antibody–drug conjugates—A new wave of cancer drugs". In: *Bioorganic & Medicinal Chemistry Letters* 24.23, pp. 5357–5363. DOI: 10.1016/j.bmcl.2014.10.021.
- Bulcha, J. T., Wang, Y., Ma, H., Tai, P. W. L., and Gao, G. (Feb. 2021). "Viral vector platforms within the gene therapy landscape". In: *Signal Transduction and Targeted Therapy* 6.1. DOI: 10.1038/s41392-021-00487-6.
- Buñuales, M., Düzgüneş, N., Zalba, S., Garrido, M. J., and Tros de Ilarduya, C. (Jan. 2011). "Efficient gene delivery by EGF-lipoplexes in vitro and in vivo". In: *Nanomedicine* 6.1, pp. 89–98. ISSN: 1748-6963. DOI: 10.2217/nnm.10.100.
- Burdett, T. and Nuseibeh, S. (Sept. 2022). "Changing trends in the development of AAV-based gene therapies: a meta-analysis of past and present therapies". In: *Gene Therapy* 30.3-4, pp. 323–335. DOI: 10.1038/s41434-022-00363-0.
- Bus, T., Traeger, A., and Schubert, U. S. (2018). "The great escape: how cationic polyplexes overcome the endosomal barrier". In: *Journal of Materials Chemistry B* 6.43, pp. 6904–6918. DOI: 10.1039/c8tb00967h.

-
- Buss, J. L. and Ponka, P. (Jan. 2003). "Hydrolysis of pyridoxal isonicotinoyl hydrazone and its analogs". In: *Biochimica et Biophysica Acta (BBA) - General Subjects* 1619.2, pp. 177–186. DOI: 10.1016/s0304-4165(02)00478-6.
- Chan, V., Dreolini, L., Flintoff, K., Lloyd, S., and Mattenley, A. (Jan. 2002). "The Effect of Increasing Plasmid Size on Transformation Efficiency in *Escherichia coli*". In: *J Exp Microbiol Immunol* 2.
- Check, E. (Oct. 2002). "Regulators split on gene therapy as patient shows signs of cancer". In: *Nature* 419.6907, pp. 545–546. DOI: 10.1038/419545a.
- Chen, Z.-Y., He, C.-Y., Ehrhardt, A., and Kay, M. A. (Sept. 2003). "Minicircle DNA vectors devoid of bacterial DNA result in persistent and high-level transgene expression in vivo". In: *Molecular Therapy* 8.3, pp. 495–500. ISSN: 1525-0016. DOI: 10.1016/s1525-0016(03)00168-0.
- Cherng, J.-Y., Schuurmans-Nieuwenbroek, N., Jiskoot, W., Talsma, H., Zuidam, N., Hennink, W., and Crommelin, D. (Aug. 1999). "Effect of DNA topology on the transfection efficiency of poly((2-dimethylamino)ethyl methacrylate)–plasmid complexes". In: *Journal of Controlled Release* 60.2-3, pp. 343–353. DOI: 10.1016/s0168-3659(99)00089-9.
- Christie, R. J., Anderson, D. J., and Grainger, D. W. (Aug. 2010). "Comparison of Hydrazone Heterobifunctional Cross-Linking Agents for Reversible Conjugation of Thiol-Containing Chemistry". In: *Bioconjugate Chemistry* 21.10, pp. 1779–1787. DOI: 10.1021/bc100049c.
- Clochard, J., Jerz, G., Schmieder, P., Mitdank, H., Tröger, M., Sama, S., and Weng, A. (Nov. 2020). "A new acetylated triterpene saponin from *Agrostemma githago* L. modulates gene delivery efficiently and shows a high cellular tolerance". In: *International Journal of Pharmaceutics* 589, p. 119822. DOI: 10.1016/j.ijpharm.2020.119822.
- Cory, A. H., Owen, T. C., Barltrop, J. A., and Cory, J. G. (July 1991). "Use of an Aqueous Soluble Tetrazolium/Formazan Assay for Cell Growth Assays in Culture". In: *Cancer Communications* 3.7, pp. 207–212. DOI: 10.3727/095535491820873191.
- Cui, L., Renzi, S., Quagliarini, E., Digiaco, L., Amenitsch, H., Masuelli, L., Bei, R., Ferri, G., Cardarelli, F., Wang, J., Amici, A., Pozzi, D., Marchini, C., and Caracciolo, G. (Aug. 2022). "Efficient Delivery of DNA Using Lipid Nanoparticles". In: *Pharmaceutics* 14.8, p. 1698. DOI: 10.3390/pharmaceutics14081698.
- Danaei, M., Dehghankhold, M., Ataei, S., Davarani, F. H., Javanmard, R., Dokhani, A., Khorasani, S., and Mozafari, M. (May 2018). "Impact of Particle Size and Polydispersity Index on the Clinical Applications of Lipidic Nanocarrier Systems". In: *Pharmaceutics* 10.2, p. 57. DOI: 10.3390/pharmaceutics10020057.

-
- Danhier, F. (Dec. 2016). “To exploit the tumor microenvironment: Since the EPR effect fails in the clinic, what is the future of nanomedicine?” In: *Journal of Controlled Release* 244, pp. 108–121. ISSN: 0168-3659. DOI: 10.1016/j.jconrel.2016.11.015.
- Dash, B. S., Lu, Y.-J., Luo, S.-H., and Chen, J.-P. (Aug. 2023). “Cetuximab-Conjugated Magnetic Poly(Lactic-co-Glycolic Acid) Nanoparticles for Dual-Targeted Delivery of Irinotecan in Glioma Treatment”. In: *Materials* 16.16, p. 5526. ISSN: 1996-1944. DOI: 10.3390/ma16165526.
- Debets, M. F., Berkel, S. S. van, Schoffelen, S., Rutjes, F. P. J. T., Hest, J. C. M. van, and Delft, F. L. van (2010). “Aza-dibenzocyclooctynes for fast and efficient enzyme PEGylation via copper-free (3+2) cycloaddition”. In: *Chem. Commun.* 46.1, pp. 97–99. ISSN: 1364-548X. DOI: 10.1039/b917797c.
- Deuker, M. F. S., Mailänder, V., Morsbach, S., and Landfester, K. (2023). “Anti-PEG antibodies enriched in the protein corona of PEGylated nanocarriers impact the cell uptake”. In: *Nanoscale Horizons* 8.10, pp. 1377–1385. ISSN: 2055-6764. DOI: 10.1039/d3nh00198a.
- Dingwall, C., Sharnick, S. V., and Laskey, R. A. (Sept. 1982). “A polypeptide domain that specifies migration of nucleoplasmin into the nucleus”. In: *Cell* 30.2, pp. 449–458. ISSN: 0092-8674. DOI: 10.1016/0092-8674(82)90242-2.
- Al-Doaiss, A., Jarrar, Q., and Moshawih, S. (June 2020). “Hepatic histopathological and ultrastructural alterations induced by 10 nm silver nanoparticles”. In: *IET Nanobiotechnology* 14.5, pp. 405–411. ISSN: 1751-875X. DOI: 10.1049/iet-nbt.2020.0039.
- Donsante, A., Miller, D. G., Li, Y., Vogler, C., Brunt, E. M., Russell, D. W., and Sands, M. S. (July 2007). “AAV Vector Integration Sites in Mouse Hepatocellular Carcinoma”. In: *Science* 317.5837, pp. 477–477. DOI: 10.1126/science.1142658.
- Dorer, D. E. and Nettelbeck, D. M. (July 2009). “Targeting cancer by transcriptional control in cancer gene therapy and viral oncolysis”. In: *Advanced Drug Delivery Reviews* 61.7-8, pp. 554–571. DOI: 10.1016/j.addr.2009.03.013.
- Duarte, S., Carle, G., Faneca, H., Lima, M. C. P. de, and Pierrefite-Carle, V. (Nov. 2012). “Suicide gene therapy in cancer: Where do we stand now?” In: 324.2, pp. 160–170. DOI: 10.1016/j.canlet.2012.05.023.
- Dziawer, Ł., Majkowska-Pilip, A., Gaweł, D., Godlewska, M., Pruszyński, M., Jastrzębski, J., Wąs, B., and Bilewicz, A. (Apr. 2019). “Trastuzumab-Modified Gold Nanoparticles Labeled with 211At as a Prospective Tool for Local Treatment of HER2-Positive Breast Cancer”. In: *Nanomaterials* 9.4, p. 632. ISSN: 2079-4991. DOI: 10.3390/nano9040632.
- Ehrlich, M., Boll, W., Oijen, A. van, Hariharan, R., Chandran, K., Nibert, M. L., and Kirchhausen, T. (Sept. 2004). “Endocytosis by Random Initiation and Stabilization of Clathrin-

-
- Coated Pits”. In: *Cell* 118.5, pp. 591–605. ISSN: 0092-8674. DOI: 10.1016/j.cell.2004.08.017.
- EMA (Mar. 22, 2018). *Guideline on the quality, non-clinical and clinical aspects of gene therapy medicinal products*. CPMP/BWP/3088/99. URL: https://www.ema.europa.eu/en/documents/scientific-guideline/guideline-quality-non-clinical-clinical-aspects-gene-therapy-medicinal-products_en.pdf (visited on 07/21/2023).
- Engelmann, C., Heslan, J.-M., Fabre, M., Lagarde, J.-P., Klatzmann, D., and Panis, Y. (May 2002). “Importance, mechanisms and limitations of the distant bystander effect in cancer gene therapy of experimental liver tumors”. In: *Cancer Letters* 179.1, pp. 59–69. DOI: 10.1016/S0304-3835(01)00854-0.
- FDA (Nov. 2007). *Guidance for Industry: Considerations for Plasmid DNA Vaccines for Infectious Disease Indications*. URL: <https://www.fda.gov/media/73667/download> (visited on 07/07/2023).
- FDA (Jan. 13, 2023). *Adstiladrin*. URL: <https://www.fda.gov/vaccines-blood-biologics/cellular-%20gene-therapy-products/adstiladrin> (visited on 04/20/2023).
- FDA (Feb. 21, 2024). *Approved Cellular and Gene Therapy Products*. URL: <https://www.fda.gov/vaccines-blood-biologics/cellular-gene-therapy-products/approved-cellular-and-gene-therapy-products> (visited on 02/23/2024).
- Fernandez, C. A., Baumhover, N. J., Duskey, J. T., Khargharia, S., Kizzire, K., Ericson, M. D., and Rice, K. G. (Aug. 2010). “Metabolically stabilized long-circulating PEGylated polyacridine peptide polyplexes mediate hydrodynamically stimulated gene expression in liver”. In: 18.1, pp. 23–37. DOI: 10.1038/gt.2010.117.
- Florian, M., Wang, J.-P., Deng, Y., Souza-Moreira, L., Stewart, D. J., and Mei, S. H. J. (Mar. 2021). “Gene engineered mesenchymal stem cells: greater transgene expression and efficacy with minicircle vs. plasmid DNA vectors in a mouse model of acute lung injury”. In: *Stem Cell Research & Therapy* 12.1. ISSN: 1757-6512. DOI: 10.1186/s13287-021-02245-5.
- Foroozandeh, P. and Aziz, A. A. (Oct. 2018). “Insight into Cellular Uptake and Intracellular Trafficking of Nanoparticles”. In: *Nanoscale Research Letters* 13.1. DOI: 10.1186/s11671-018-2728-6.
- Francia, V., Schifflers, R. M., Cullis, P. R., and Witzigmann, D. (Aug. 2020). “The Biomolecular Corona of Lipid Nanoparticles for Gene Therapy”. In: *Bioconjugate Chemistry* 31.9, pp. 2046–2059. DOI: 10.1021/acs.bioconjchem.0c00366.

-
- Freeman, S. M., Abboud, C. N., Whartenby, K. A., Packman, C. H., Koeplin, D. S., Moolten, F. L., and Abraham, G. N. (Nov. 1993). "The "bystander effect": tumor regression when a fraction of the tumor mass is genetically modified." In: *Cancer research* 53 (21), pp. 5274–5283. ISSN: 0008-5472.
- Garnett, C. T., Erdman, D., Xu, W., and Gooding, L. R. (Nov. 2002). "Prevalence and Quantitation of Species C Adenovirus DNA in Human Mucosal Lymphocytes". In: *Journal of Virology* 76.21, pp. 10608–10616. DOI: 10.1128/jvi.76.21.10608-10616.2002.
- Gilabert-Oriol, R., Mergel, K., Thakur, M., Mallinckrodt, B. von, Melzig, M. F., Fuchs, H., and Weng, A. (Apr. 2013). "Real-time analysis of membrane permeabilizing effects of oleanane saponins". In: *Bioorganic & Medicinal Chemistry* 21.8, pp. 2387–2395. DOI: 10.1016/j.bmc.2013.01.061.
- Gill, G. N. and Lazar, C. S. (Sept. 1981). "Increased phosphotyrosine content and inhibition of proliferation in EGF-treated A431 cells". In: *Nature* 293.5830, pp. 305–307. ISSN: 1476-4687. DOI: 10.1038/293305a0.
- Gilleron, J., Querbes, W., Zeigerer, A., Borodovsky, A., Marsico, G., Schubert, U., Manygoats, K., Seifert, S., Andree, C., Stöter, M., Epstein-Barash, H., Zhang, L., Kotliansky, V., Fitzgerald, K., Fava, E., Bickle, M., Kalaidzidis, Y., Akinc, A., Maier, M., and Zerial, M. (June 2013). "Image-based analysis of lipid nanoparticle-mediated siRNA delivery, intracellular trafficking and endosomal escape". In: *Nature Biotechnology* 31.7, pp. 638–646. DOI: 10.1038/nbt.2612.
- Greenfield, R. S., Kaneko, T., Daves, A., Edson, M. A., Fitzgerald, K. A., Olech, L. J., Grattan, J. A., Spitalny, G. L., and Braslawsky, G. R. (Oct. 1990). "Evaluation in vitro of adriamycin immunoconjugates synthesized using an acid-sensitive hydrazone linker." In: *Cancer research* 50 (20), pp. 6600–6607. ISSN: 0008-5472. ppublish.
- Haraguchi, T., Koujin, T., Shindo, T., Bilir, Ş., Osakada, H., Nishimura, K., Hirano, Y., Asakawa, H., Mori, C., Kobayashi, S., Okada, Y., Chikashige, Y., Fukagawa, T., Shibata, S., and Hiraoka, Y. (July 2021). "Transfected plasmid DNA is incorporated into the nucleus via nuclear envelope reformation at telophase". In: DOI: 10.21203/rs.3.rs-478612/v1.
- Hardee, C., Arévalo-Soliz, L., Hornstein, B., and Zechiedrich, L. (Feb. 2017). "Advances in Non-Viral DNA Vectors for Gene Therapy". In: *Genes* 8.2, p. 65. ISSN: 2073-4425. DOI: 10.3390/genes8020065.
- Hawe, A., Poole, R., Romeijn, S., Kasper, P., Heijden, R. van der, and Jiskoot, W. (Apr. 2009). "Towards Heat-stable Oxytocin Formulations: Analysis of Degradation Kinetics and Identification of Degradation Products". In: *Pharmaceutical Research* 26.7, pp. 1679–1688. DOI: 10.1007/s11095-009-9878-2.

-
- Hebestreit, P. and Melzig, M. (Oct. 2003). "Cytotoxic Activity of the Seeds from *Agrostemma githago* var. *githago*". In: *Planta Medica* 69.10, pp. 921–925. DOI: 10.1055/s-2003-45101.
- Hemmi, H., Takeuchi, O., Kawai, T., Kaisho, T., Sato, S., Sanjo, H., Matsumoto, M., Hoshino, K., Wagner, H., Takeda, K., and Akira, S. (Dec. 2000). "A Toll-like receptor recognizes bacterial DNA". In: *Nature* 408.6813, pp. 740–745. DOI: 10.1038/35047123.
- Henriksen, L., Grandal, M. V., Knudsen, S. L. J., Deurs, B. van, and Grøvdal, L. M. (Mar. 2013). "Internalization Mechanisms of the Epidermal Growth Factor Receptor after Activation with Different Ligands". In: *PLoS ONE* 8.3. Ed. by C. Lamaze, e58148. DOI: 10.1371/journal.pone.0058148.
- Hermanson, G. T. (2013). "The Reactions of Bioconjugation". In: *Bioconjugate Techniques*. Elsevier, pp. 229–258. DOI: 10.1016/b978-0-12-382239-0.00003-0.
- Hodge, J. E. (Oct. 1953). "Dehydrated Foods, Chemistry of Browning Reactions in Model Systems". In: *Journal of Agricultural and Food Chemistry* 1.15, pp. 928–943. ISSN: 1520-5118. DOI: 10.1021/jf60015a004.
- Hong, L., Wang, Z., Wei, X., Shi, J., and Li, C. (Mar. 2020). "Antibodies against polyethylene glycol in human blood: A literature review". In: *Journal of Pharmacological and Toxicological Methods* 102, p. 106678. ISSN: 1056-8719. DOI: 10.1016/j.vascn.2020.106678.
- Horn, J. M. and Obermeyer, A. C. (Dec. 2021). "Genetic and Covalent Protein Modification Strategies to Facilitate Intracellular Delivery". In: *Biomacromolecules* 22.12, pp. 4883–4904. DOI: 10.1021/acs.biomac.1c00745.
- Hyatt, D. C. and Ceresa, B. P. (Nov. 2008). "Cellular localization of the activated EGFR determines its effect on cell growth in MDA-MB-468 cells". In: *Experimental Cell Research* 314.18, pp. 3415–3425. ISSN: 0014-4827. DOI: 10.1016/j.yexcr.2008.08.020.
- Hynes, N. E. and MacDonald, G. (Apr. 2009). "ErbB receptors and signaling pathways in cancer". In: *Current Opinion in Cell Biology* 21.2, pp. 177–184. ISSN: 0955-0674. DOI: 10.1016/j.ceb.2008.12.010.
- Irvine, S. A., Meng, Q.-H., Afzal, F., Ho, J., Wong, J. B., Hailes, H. C., Tabor, A. B., McEwan, J. R., and Hart, S. L. (Mar. 2008). "Receptor-targeted Nanocomplexes optimized for Gene Transfer to Primary Vascular Cells and Explant Cultures of Rabbit Aorta". In: *Molecular Therapy* 16.3, pp. 508–515. DOI: 10.1038/sj.mt.6300381.
- IUPAC-IUB Joint Commission on Biochemical Nomenclature (Dec. 1989). "The nomenclature of steroids. Recommendations 1989." In: *European Journal of Biochemistry* 186.3, pp. 429–458. ISSN: 1432-1033. DOI: 10.1111/j.1432-1033.1989.tb15228.x.

-
- Jeune, V. L., Joergensen, J. A., Hajjar, R. J., and Weber, T. (Apr. 2013). "Pre-existing Anti-Adeno-Associated Virus Antibodies as a Challenge in AAV Gene Therapy". In: *Human Gene Therapy Methods* 24.2, pp. 59–67. doi: 10.1089/hgtb.2012.243.
- Jooss, K. and Chirmule, N. (May 2003). "Immunity to adenovirus and adeno-associated viral vectors: implications for gene therapy". In: *Gene Therapy* 10.11, pp. 955–963. doi: 10.1038/sj.gt.3302037.
- Karjoo, Z., Chen, X., and Hatefi, A. (Apr. 2016). "Progress and problems with the use of suicide genes for targeted cancer therapy". In: *Advanced Drug Delivery Reviews* 99, pp. 113–128. doi: 10.1016/j.addr.2015.05.009.
- Kay, M., Glorioso, J., and Naldini, L. (Jan. 2001). "Viral vectors for gene therapy: the art of turning infectious agents into vehicles of therapeutics". In: *Nature Medicine* 7.1, pp. 33–40. doi: 10.1038/83324.
- Kay, M., He, C.-Y., and Chen, Z.-Y. (Nov. 2010). "A robust system for production of minicircle DNA vectors". In: *Nature Biotechnology* 28.12, pp. 1287–1289. doi: 10.1038/nbt.1708.
- Knockenbauer, K. E. and Schwartz, T. U. (Mar. 2016). "The Nuclear Pore Complex as a Flexible and Dynamic Gate". In: *Cell* 164.6, pp. 1162–1171. ISSN: 0092-8674. doi: 10.1016/j.cell.2016.01.034.
- Kolb, H. C., Finn, M. G., and Sharpless, K. B. (June 2001). "Click Chemistry: Diverse Chemical Function from a Few Good Reactions". In: *Angewandte Chemie International Edition* 40.11, pp. 2004–2021. doi: 10.1002/1521-3773(20010601)40:11<2004::aid-anie2004>3.0.co;2-5.
- Kottke, T. J., Blajeski, A. L., Martins, L. M., Mesner, P. W., Davidson, N. E., Earnshaw, W. C., Armstrong, D. K., and Kaufmann, S. H. (May 1999). "Comparison of Paclitaxel-, 5-Fluoro-2'-deoxyuridine-, and Epidermal Growth Factor (EGF)-induced Apoptosis". In: *Journal of Biological Chemistry* 274.22, pp. 15927–15936. ISSN: 0021-9258. doi: 10.1074/jbc.274.22.15927.
- Kovaříková, P., Mrkvičková, Z., and Klimeš, J. (June 2008). "Investigation of the stability of aromatic hydrazones in plasma and related biological material". In: *Journal of Pharmaceutical and Biomedical Analysis* 47.2, pp. 360–370. doi: 10.1016/j.jpba.2008.01.011.
- Kozłowski, L. P. (Oct. 2016). "IPC – Isoelectric Point Calculator". In: *Biology Direct* 11.1. ISSN: 1745-6150. doi: 10.1186/s13062-016-0159-9.
- Kratz, F. (May 2007). "DOXO-EMCH (INNO-206): the first albumin-binding prodrug of doxorubicin to enter clinical trials". In: *Expert Opinion on Investigational Drugs* 16.6, pp. 855–866. doi: 10.1517/13543784.16.6.855.

-
- Kratz, F., Warnecke, A., Scheuermann, K., Stockmar, C., Schwab, J., Lazar, P., Drückes, P., Esser, N., Dreves, J., Rognan, D., Bissantz, C., Hinderling, C., Folkers, G., Fichtner, I., and Unger, C. (Nov. 2002). "Probing the Cysteine-34 Position of Endogenous Serum Albumin with Thiol-Binding Doxorubicin Derivatives. Improved Efficacy of an Acid-Sensitive Doxorubicin Derivative with Specific Albumin-Binding Properties Compared to That of the Parent Compound". In: *Journal of Medicinal Chemistry* 45.25, pp. 5523–5533. DOI: 10.1021/jm020276c.
- Kulkarni, J. A., Witzigmann, D., Thomson, S. B., Chen, S., Leavitt, B. R., Cullis, P. R., and Meel, R. van der (May 2021). "The current landscape of nucleic acid therapeutics". In: *Nature Nanotechnology* 16.6, pp. 630–643. DOI: 10.1038/s41565-021-00898-0.
- Kwok, A., McCarthy, D., Hart, S. L., and Tagalakis, A. D. (Feb. 2016). "Systematic Comparisons of Formulations of Linear Oligolysine Peptides with siRNA and Plasmid DNA". In: *Chemical Biology & Drug Design* 87.5, pp. 747–763. DOI: 10.1111/cbdd.12709.
- Li, J., Chen, L., Liu, N., Li, S., Hao, Y., and Zhang, X. (Feb. 2015). "EGF-coated nano-dendriplexes for tumor-targeted nucleic acid delivery in vivo". In: *Drug Delivery*, pp. 1–8. ISSN: 1521-0464. DOI: 10.3109/10717544.2015.1004381.
- Li, Z., Zhao, R., Wu, X., Sun, Y., Yao, M., Li, J., Xu, Y., and Gu, J. (Dec. 2005). "Identification and characterization of a novel peptide ligand of epidermal growth factor receptor for targeted delivery of therapeutics". In: *The FASEB Journal* 19.14, pp. 1978–1985. DOI: 10.1096/fj.05-4058com.
- Lin, C.-Y., Yang, S.-J., Peng, C.-L., and Shieh, M.-J. (Feb. 2018). "Panitumumab-Conjugated and Platinum-Cored pH-Sensitive Apoferritin Nanocages for Colorectal Cancer-Targeted Therapy". In: *ACS Applied Materials & Interfaces* 10.7, pp. 6096–6106. ISSN: 1944-8252. DOI: 10.1021/acsami.7b13431.
- Lopez-Gordo, E., Podgorski, I. I., Downes, N., and Alemany, R. (Apr. 2014). "Circumventing Antivector Immunity: Potential Use of Nonhuman Adenoviral Vectors". In: *Human Gene Therapy* 25.4, pp. 285–300. DOI: 10.1089/hum.2013.228.
- Lowry, G. V., Hill, R. J., Harper, S., Rawle, A. F., Hendren, C. O., Klaessig, F., Nobbmann, U., Sayre, P., and Rumble, J. (2016). "Guidance to improve the scientific value of zeta-potential measurements in nanoEHS". In: *Environmental Science: Nano* 3.5, pp. 953–965. DOI: 10.1039/c6en00136j.
- Lu, J., Zhang, F., Xu, S., Fire, A. Z., and Kay, M. A. (Nov. 2012). "The Extragenic Spacer Length Between the 5' and 3' Ends of the Transgene Expression Cassette Affects Transgene Silencing From Plasmid-based Vectors". In: *Molecular Therapy* 20.11, pp. 2111–2119. DOI: 10.1038/mt.2012.65.

-
- Luke, J. M., Vincent, J. M., Du, S. X., Gerdemann, U., Leen, A. M., Whalen, R. G., Hodgson, C. P., and Williams, J. A. (Nov. 2010). “Improved antibiotic-free plasmid vector design by incorporation of transient expression enhancers”. In: *Gene Therapy* 18.4, pp. 334–343. DOI: 10.1038/gt.2010.149.
- Maeda, H., Nakamura, H., and Fang, J. (Jan. 2013). “The EPR effect for macromolecular drug delivery to solid tumors: Improvement of tumor uptake, lowering of systemic toxicity, and distinct tumor imaging in vivo”. In: *Advanced Drug Delivery Reviews* 65.1, pp. 71–79. ISSN: 0169-409X. DOI: 10.1016/j.addr.2012.10.002.
- Malecki, M. (2012). “Frontiers in Suicide Gene Therapy of Cancer”. In: *Journal of Genetic Syndromes & Gene Therapy* 03.04. DOI: 10.4172/2157-7412.1000119.
- Malekshah, O. M., Chen, X., Nomani, A., Sarkar, S., and Hatefi, A. (Oct. 2016). “Enzyme/Pro-drug Systems for Cancer Gene Therapy”. In: *Current Pharmacology Reports* 2.6, pp. 299–308. DOI: 10.1007/s40495-016-0073-y.
- Mali, S. (2013). “Delivery systems for gene therapy”. In: *Indian Journal of Human Genetics* 19.1, p. 3. DOI: 10.4103/0971-6866.112870.
- Malvern Instruments Ltd. (2013). *Zetasizer Nano User Manual*.
- Manunta, M. D. I., McAnulty, R. J., Tagalakakis, A. D., Bottoms, S. E., Campbell, F., Hailes, H. C., Tabor, A. B., Laurent, G. J., O’Callaghan, C., and Hart, S. L. (Oct. 2011). “Nebulisation of Receptor-Targeted Nanocomplexes for Gene Delivery to the Airway Epithelium”. In: *PLoS ONE* 6.10. Ed. by M. Antopolsky, e26768. DOI: 10.1371/journal.pone.0026768.
- Marti-Solano, M., Crilly, S. E., Malinverni, D., Munk, C., Harris, M., Pearce, A., Quon, T., Mackenzie, A. E., Wang, X., Peng, J., Tobin, A. B., Ladds, G., Milligan, G., Gloriam, D. E., Puthenvedu, M. A., and Babu, M. M. (Nov. 2020). “Combinatorial expression of GPCR isoforms affects signalling and drug responses”. In: *Nature* 587.7835, pp. 650–656. DOI: 10.1038/s41586-020-2888-2.
- Masui, H., Castro, L., and Mendelsohn, J. (Jan. 1993). “Consumption of EGF by A431 cells: evidence for receptor recycling.” In: *The Journal of cell biology* 120.1, pp. 85–93. ISSN: 1540-8140. DOI: 10.1083/jcb.120.1.85.
- McIntosh, J., Lenting, P. J., Rosales, C., Lee, D., Rabbanian, S., Raj, D., Patel, N., Tuddenham, E. G. D., Christophe, O. D., McVey, J. H., Waddington, S., Nienhuis, A. W., Gray, J. T., Fagone, P., Mingozzi, F., Zhou, S.-Z., High, K. A., Cancio, M., Ng, C. Y. C., Zhou, J., Morton, C. L., Davidoff, A. M., and Nathwani, A. C. (Apr. 2013). “Therapeutic levels of FVIII following a single peripheral vein administration of rAAV vector encoding a novel human factor VIII variant”. In: *Blood* 121.17, pp. 3335–3344. DOI: 10.1182/blood-2012-10-462200.

-
- Melzig, M., Hebestreit, P., Gaidi, G., and Lacaille-Dubois, M. (Oct. 2005). "Structure-Activity-Relationship of Saponins to Enhance Toxic Effects of Agrostin". In: *Planta Medica* 71.11, pp. 1088–1090. DOI: 10.1055/s-2005-873112.
- Meng, Q.-H., Irvine, S., Tagalakis, A. D., McAnulty, R. J., McEwan, J. R., and Hart, S. L. (May 2013). "Inhibition of neointimal hyperplasia in a rabbit vein graft model following non-viral transfection with human iNOS cDNA". In: *Gene Therapy* 20.10, pp. 979–986. DOI: 10.1038/gt.2013.20.
- Mintzer, M. A. and Simanek, E. E. (Dec. 2008). "Nonviral Vectors for Gene Delivery". In: *Chemical Reviews* 109.2, pp. 259–302. DOI: 10.1021/cr800409e.
- Mitdank, H., Sama, S., Tröger, M., Testa, M. F., Ferrarese, M., Balestra, D., Pinotti, M., and Weng, A. (Aug. 2021). "An advanced method for the small-scale production of high-quality minicircle DNA". In: *International Journal of Pharmaceutics* 605, p. 120830. DOI: 10.1016/j.ijpharm.2021.120830.
- Mitdank, H., Tröger, M., Sonntag, A., Shirazi, N. A., Woith, E., Fuchs, H., Kobelt, D., Walther, W., and Weng, A. (Mar. 2022). "Suicide nanoplastids coding for ribosome-inactivating proteins". In: *European Journal of Pharmaceutical Sciences* 170, p. 106107. DOI: 10.1016/j.ejps.2021.106107.
- Monika Jansohn, S. R., ed. (2012). *Gentechnische Methoden. Eine Sammlung von Arbeitsanleitungen für das molekularbiologische Labor*. Spektrum-Akademischer Verlag. ISBN: 978-3-8274-2429-7.
- Moolten, F. L. (Oct. 1986). "Tumor chemosensitivity conferred by inserted herpes thymidine kinase genes: paradigm for a prospective cancer control strategy." In: *Cancer research* 46 (10), pp. 5276–5281. ISSN: 0008-5472. ppublish.
- Munye, M. M., Tagalakis, A. D., Barnes, J. L., Brown, R. E., McAnulty, R. J., Howe, S. J., and Hart, S. L. (Mar. 2016). "Minicircle DNA Provides Enhanced and Prolonged Transgene Expression Following Airway Gene Transfer". In: *Scientific Reports* 6.1. ISSN: 2045-2322. DOI: 10.1038/srep23125.
- Musser, S. M. and Grünwald, D. (May 2016). "Deciphering the Structure and Function of Nuclear Pores Using Single-Molecule Fluorescence Approaches". In: *Journal of Molecular Biology* 428.10, pp. 2091–2119. ISSN: 0022-2836. DOI: 10.1016/j.jmb.2016.02.023.
- Nan, Y. (Sept. 2019). "Lung carcinoma therapy using epidermal growth factor receptor-targeted lipid polymeric nanoparticles co-loaded with cisplatin and doxorubicin". In: *Oncology Reports*. ISSN: 1791-2431. DOI: 10.3892/or.2019.7323.

-
- Navarro, S. A., Carrillo, E., Griñán-Lisón, C., Martín, A., Perán, M., Marchal, J. A., and Boulaiz, H. (July 2016). “Cancer suicide gene therapy: a patent review”. In: 26.9, pp. 1095–1104. DOI: 10.1080/13543776.2016.1211640.
- Neuhoff, V., Arold, N., Taube, D., and Ehrhardt, W. (1988). “Improved staining of proteins in polyacrylamide gels including isoelectric focusing gels with clear background at nanogram sensitivity using Coomassie Brilliant Blue G-250 and R-250”. In: *Electrophoresis* 9.6, pp. 255–262. DOI: 10.1002/elps.1150090603.
- Nichols, J. W. and Bae, Y. H. (Sept. 2014). “EPR: Evidence and fallacy”. In: *Journal of Controlled Release* 190, pp. 451–464. ISSN: 0168-3659. DOI: 10.1016/j.jconrel.2014.03.057.
- Nigg, E. A. (Apr. 1997). “Nucleocytoplasmic transport: signals, mechanisms and regulation”. In: *Nature* 386.6627, pp. 779–787. ISSN: 1476-4687. DOI: 10.1038/386779a0.
- Nobel Prize Outreach AB (Oct. 5, 2022). *Press Release*. The Royal Swedish Academy of Sciences. URL: <https://www.nobelprize.org/prizes/chemistry/2022/press-release/> (visited on 01/21/2024).
- Ohkuma, S. and Poole, B. (July 1978). “Fluorescence probe measurement of the intralysosomal pH in living cells and the perturbation of pH by various agents.” In: *Proceedings of the National Academy of Sciences of the United States of America* 75 (7), pp. 3327–3331. ISSN: 0027-8424. DOI: 10.1073/pnas.75.7.3327. ppublish.
- P., B. (Nov. 2011). “Endocytic Trafficking of the Epidermal Growth Factor Receptor in Transformed Cells”. In: *Breast Cancer - Carcinogenesis, Cell Growth and Signalling Pathways*. InTech. DOI: 10.5772/22541.
- Pahle, J. and Walther, W. (Jan. 2016). “Vectors and strategies for nonviral cancer gene therapy”. In: *Expert Opinion on Biological Therapy* 16.4, pp. 443–461. DOI: 10.1517/14712598.2016.1134480.
- Patel, J., Amrutiya, J., Bhatt, P., Javia, A., Jain, M., and Misra, A. (Feb. 2018). “Targeted delivery of monoclonal antibody conjugated docetaxel loaded PLGA nanoparticles into EGFR overexpressed lung tumour cells”. In: *Journal of Microencapsulation* 35.2, pp. 204–217. ISSN: 1464-5246. DOI: 10.1080/02652048.2018.1453560.
- PEI (Jan. 25, 2024). *Gene Therapy Medicinal Products*. URL: <https://www.pei.de/EN/medicinal-products/atmp/gene-therapy-medicinal-products/gene-therapy-node.html> (visited on 02/23/2024).
- Pei, D. and Buyanova, M. (Dec. 2018). “Overcoming Endosomal Entrapment in Drug Delivery”. In: *Bioconjugate Chemistry* 30.2, pp. 273–283. DOI: 10.1021/acs.bioconjchem.8b00778.

-
- Peter, M. G., Lützen, A., and Seibel, J. (2012). *d-Glucuronsäure*. de. Ed. by F. Böckler, B. Dill, G. Eisenbrand, F. Faupel, B. Fugmann, T. Gamse, R. Matissek, G. Pohnert, A. Rühling, S. Schmidt, and G. Sprenger. Stuttgart. URL: <https://roempp.thieme.de/lexicon/RD-07-01401>.
- Poole, R. A., Kasper, P. T., and Jiskoot, W. (July 2011). “NOTES: Formation of Amide- and Imide-Linked Degradation Products Between the Peptide Drug Oxytocin and Citrate in Citrate-Buffered Formulations”. In: *Journal of Pharmaceutical Sciences* 100.7, pp. 3018–3022. DOI: 10.1002/jps.22495.
- Portsmouth, D., Hlavaty, J., and Renner, M. (Feb. 2007). “Suicide genes for cancer therapy”. In: *Molecular Aspects of Medicine* 28.1, pp. 4–41. DOI: 10.1016/j.mam.2006.12.001.
- R Core Team (2022). *R: A Language and Environment for Statistical Computing*. R Foundation for Statistical Computing. URL: <https://www.R-project.org/>.
- Raper, S. E., Chirmule, N., Lee, F. S., Wivel, N. A., Bagg, A., Gao, G.-p., Wilson, J. M., and Batshaw, M. L. (Sept. 2003). “Fatal systemic inflammatory response syndrome in a ornithine transcarbamylase deficient patient following adenoviral gene transfer”. In: *Molecular Genetics and Metabolism* 80.1-2, pp. 148–158. DOI: 10.1016/j.ymgme.2003.08.016.
- Rehman, Z. ur, Hoekstra, D., and Zuhorn, I. S. (Nov. 2011). “Protein kinase A inhibition modulates the intracellular routing of gene delivery vehicles in HeLa cells, leading to productive transfection”. In: *Journal of Controlled Release* 156.1, pp. 76–84. DOI: 10.1016/j.jconrel.2011.07.015.
- Rehman, Z. ur, Hoekstra, D., and Zuhorn, I. S. (Apr. 2013). “Mechanism of Polyplex- and Lipoplex-Mediated Delivery of Nucleic Acids: Real-Time Visualization of Transient Membrane Destabilization without Endosomal Lysis”. In: *ACS Nano* 7.5, pp. 3767–3777. DOI: 10.1021/nn3049494.
- Rejman, J., Oberle, V., Zuhorn, I. S., and Hoekstra, D. (Jan. 2004). “Size-dependent internalization of particles via the pathways of clathrin- and caveolae-mediated endocytosis”. In: *Biochemical Journal* 377.1, pp. 159–169. DOI: 10.1042/bj20031253.
- Remaut, K., Sanders, N. N., Fayazpour, F., Demeester, J., and Smedt, S. C. D. (Oct. 2006). “Influence of plasmid DNA topology on the transfection properties of DOTAP/DOPE lipoplexes”. In: *Journal of Controlled Release* 115.3, pp. 335–343. DOI: 10.1016/j.jconrel.2006.08.009.
- Ripoll, M., Martin, E., Enot, M., Robbe, O., Rapisarda, C., Nicolai, M.-C., Deliot, A., Tabelaing, P., Authelin, J.-R., Nakach, M., and Wils, P. (June 2022). “Optimal self-assembly of lipid nanoparticles (LNP) in a ring micromixer”. In: *Scientific Reports* 12.1. DOI: 10.1038/s41598-022-13112-5.

-
- Riu, E., Chen, Z.-Y., Xu, H., He, C.-Y., and Kay, M. A. (July 2007). “Histone Modifications are Associated with the Persistence or Silencing of Vector-mediated Transgene Expression In Vivo”. In: *Molecular Therapy* 15.7, pp. 1348–1355. DOI: 10.1038/sj.mt.6300177.
- Rivolta, I., Panariti, and Miserocchi (Sept. 2012). “The effect of nanoparticle uptake on cellular behavior: disrupting or enabling functions?” In: *Nanotechnology, Science and Applications*, p. 87. DOI: 10.2147/nsa.s25515.
- Roepstorff, K., Grandal, M. V., Henriksen, L., Knudsen, S. L. J., Lerdrup, M., Grøvdal, L., Willumsen, B. M., and Van Deurs, B. (July 2009). “Differential Effects of EGFR Ligands on Endocytic Sorting of the Receptor”. In: *Traffic* 10.8, pp. 1115–1127. ISSN: 1600-0854. DOI: 10.1111/j.1600-0854.2009.00943.x.
- Rowinsky, E. K. (Feb. 2004). “The erbB Family: Targets for Therapeutic Development Against Cancer and Therapeutic Strategies Using Monoclonal Antibodies and Tyrosine Kinase Inhibitors”. In: *Annual Review of Medicine* 55.1, pp. 433–457. ISSN: 1545-326X. DOI: 10.1146/annurev.med.55.091902.104433.
- Säftel, W., Winkler, U., and Stabenau, H. (2012). *Separation of Native Basic Proteins by Cathodic, Discontinuous Polyacrylamide Gel Electrophoresis*. Tech. rep. Carl von Ossietzky Universität Oldenburg.
- Sahu, K. K., Pradhan, M., Singh, D., Singh, M. R., and Yadav, K. (Feb. 2023). “Non-viral nucleic acid delivery approach: A boon for state-of-the-art gene delivery”. In: *Journal of Drug Delivery Science and Technology* 80, p. 104152. DOI: 10.1016/j.jddst.2023.104152.
- Sama, S., Jerz, G., Schmieder, P., Joseph, J. F., Melzig, M. F., and Weng, A. (Oct. 2018a). “Plant derived triterpenes from *Gypsophila elegans* M.Bieb. enable non-toxic delivery of gene loaded nanoplexes”. In: 284, pp. 131–139. DOI: 10.1016/j.jbiotec.2018.07.037.
- Sama, S., Jerz, G., Schmieder, P., Woith, E., Melzig, M. F., and Weng, A. (Dec. 2017). “Sapofectosid - Ensuring non-toxic and effective DNA and RNA delivery”. In: *International Journal of Pharmaceutics* 534.1-2, pp. 195–205. DOI: 10.1016/j.ijpharm.2017.10.016.
- Sama, S., Jerz, G., Thakur, M., Melzig, M., and Weng, A. (Mar. 2019). “Structure-Activity Relationship of Transfection-Modulating Saponins - A Pursuit for the Optimal Gene Trafficker”. In: *Planta Medica* 85.06, pp. 513–518. DOI: 10.1055/a-0863-4795.
- Sama, S., Woith, E., Walther, W., Jerz, G., Chen, W., Hart, S., Melzig, M. F., and Weng, A. (Apr. 2018b). “Targeted suicide gene transfections reveal promising results in nu/nu mice with aggressive neuroblastoma”. In: *Journal of Controlled Release* 275, pp. 208–216. DOI: 10.1016/j.jconrel.2018.02.031.

-
- Sayed, N., Allawadhi, P., Khurana, A., Singh, V., Navik, U., Pasumarthi, S. K., Khurana, I., Banothu, A. K., Weiskirchen, R., and Bharani, K. K. (Apr. 2022). “Gene therapy: Comprehensive overview and therapeutic applications”. In: *Life Sciences* 294, p. 120375. DOI: 10.1016/j.lfs.2022.120375.
- Schneider, C. A., Rasband, W. S., and Eliceiri, K. W. (June 2012). “NIH Image to ImageJ: 25 years of image analysis”. In: *Nature Methods* 9.7, pp. 671–675. DOI: 10.1038/nmeth.2089.
- Schöttler, S., Becker, G., Winzen, S., Steinbach, T., Mohr, K., Landfester, K., Mailänder, V., and Wurm, F. R. (Feb. 2016). “Protein adsorption is required for stealth effect of poly(ethylene glycol)- and poly(phosphoester)-coated nanocarriers”. In: *Nature Nanotechnology* 11.4, pp. 372–377. ISSN: 1748-3395. DOI: 10.1038/nnano.2015.330.
- Shirley, J. L., Jong, Y. P. de, Terhorst, C., and Herzog, R. W. (Mar. 2020). “Immune Responses to Viral Gene Therapy Vectors”. In: *Molecular Therapy* 28.3, pp. 709–722. DOI: 10.1016/j.ymthe.2020.01.001.
- Sigismund, S., Argenzio, E., Tosoni, D., Cavallaro, E., Polo, S., and Fiore, P. P. D. (Aug. 2008). “Clathrin-Mediated Internalization Is Essential for Sustained EGFR Signaling but Dispensable for Degradation”. In: *Developmental Cell* 15.2, pp. 209–219. DOI: 10.1016/j.devcel.2008.06.012.
- Singh, V., Khan, N., and Jayandharan, G. R. (Apr. 2021). “Vector engineering, strategies and targets in cancer gene therapy”. In: *Cancer Gene Therapy* 29.5, pp. 402–417. DOI: 10.1038/s41417-021-00331-7.
- Skóra, B. and Szychowski, K. A. (June 2022). “Molecular mechanism of the uptake and toxicity of EGF-LipoAgNPs in EGFR-overexpressing cancer cells”. In: *Biomedicine & Pharmacotherapy* 150, p. 113085. ISSN: 0753-3322. DOI: 10.1016/j.biopha.2022.113085.
- Steffens, R. C. and Wagner, E. (Sept. 2022). “Directing the Way-Receptor and Chemical Targeting Strategies for Nucleic Acid Delivery”. In: *Pharmaceutical Research* 40.1, pp. 47–76. DOI: 10.1007/s11095-022-03385-w.
- Stellwagen, E., Prantner, J. D., and Stellwagen, N. C. (Feb. 2008). “Do zwitterions contribute to the ionic strength of a solution?” In: *Analytical Biochemistry* 373.2, pp. 407–409. DOI: 10.1016/j.ab.2007.10.038.
- Subhan, M. A., Parveen, F., Filipczak, N., Yalamarty, S. S. K., and Torchilin, V. P. (2023). “Approaches to Improve EPR-Based Drug Delivery for Cancer Therapy and Diagnosis”. In: *Journal of Personalized Medicine* 13.3. ISSN: 2075-4426. DOI: 10.3390/jpm13030389. URL: <https://www.mdpi.com/2075-4426/13/3/389>.

-
- Sung, H., Ferlay, J., Siegel, R. L., Laversanne, M., Soerjomataram, I., Jemal, A., and Bray, F. (Feb. 2021). “Global Cancer Statistics 2020: GLOBOCAN Estimates of Incidence and Mortality Worldwide for 36 Cancers in 185 Countries”. In: *CA: A Cancer Journal for Clinicians* 71.3, pp. 209–249. DOI: 10.3322/caac.21660.
- Suzuki, M., Kasai, K., and Saeki, Y. (Apr. 2006). “Plasmid DNA Sequences Present in Conventional Herpes Simplex Virus Amplicon Vectors Cause Rapid Transgene Silencing by Forming Inactive Chromatin”. In: *Journal of Virology* 80.7, pp. 3293–3300. DOI: 10.1128/jvi.80.7.3293-3300.2006.
- Tagalakis, A. D., He, L., Saraiva, L., Gustafsson, K. T., and Hart, S. L. (Sept. 2011). “Receptor-targeted liposome-peptide nanocomplexes for siRNA delivery”. In: *Biomaterials* 32.26, pp. 6302–6315. DOI: 10.1016/j.biomaterials.2011.05.022.
- Tagalakis, A. D., McAnulty, R. J., Devaney, J., Bottoms, S. E., Wong, J. B., Elbs, M., Writer, M. J., Hailes, H. C., Tabor, A. B., O’Callaghan, C., Jaffe, A., and Hart, S. L. (May 2008). “A Receptor-targeted Nanocomplex Vector System Optimized for Respiratory Gene Transfer”. In: *Molecular Therapy* 16.5, pp. 907–915. DOI: 10.1038/mt.2008.38.
- Tagalakis, A. D., Saraiva, L., McCarthy, D., Gustafsson, K. T., and Hart, S. L. (Feb. 2013). “Comparison of Nanocomplexes with Branched and Linear Peptides for siRNA Delivery”. In: *Biomacromolecules* 14.3, pp. 761–770. DOI: 10.1021/bm301842j.
- The Human Protein Atlas* (Oct. 3, 2023). URL: [v23 . proteinatlas . org / ENSG00000146648-EGFR/cell%20line](https://v23.proteinatlas.org/ENSG00000146648-EGFR/cell%20line).
- The Journal of Gene Medicine (2023). *Gene Therapy Clinical Trials Worldwide*. URL: <https://a873679.fmphost.com/fmi/webd/GTCT> (visited on 04/11/2024).
- Thermo Fisher Scientific (2015). *Assessment of Nucleic Acid Purity. Technical Note 52646*. URL: <https://tools.thermofisher.com/content/sfs/brochures/TN52646-E-0215M-NucleicAcid.pdf> (visited on 06/08/2023).
- Thermo Fisher Scientific (Dec. 22, 2023). *Lipofectamine™ 3000 Transfection Reagent*. URL: <https://www.thermofisher.com/order/catalog/product/L3000001>.
- Tikhomirov, O. and Carpenter, G. (Mar. 2004). “Ligand-induced, p38-dependent Apoptosis in Cells Expressing High Levels of Epidermal Growth Factor Receptor and ErbB-2”. In: *Journal of Biological Chemistry* 279.13, pp. 12988–12996. ISSN: 0021-9258. DOI: 10.1074/jbc.m311655200.
- Vago, R., Collico, V., Zuppone, S., Prospero, D., and Colombo, M. (Sept. 2016). “Nanoparticle-mediated delivery of suicide genes in cancer therapy”. In: *Pharmacological Research* 111, pp. 619–641. DOI: 10.1016/j.phrs.2016.07.007.

-
- Vargas, J. E., Chicaybam, L., Stein, R. T., Tanuri, A., Delgado-Cañedo, A., and Bonamino, M. H. (Oct. 2016). “Retroviral vectors and transposons for stable gene therapy: advances, current challenges and perspectives”. In: *Journal of Translational Medicine* 14.1. DOI: 10.1186/s12967-016-1047-x.
- Vassaux, G. and Martin-Duque, P. (Apr. 2004). “Use of suicide genes for cancer gene therapy: study of the different approaches”. In: *Expert Opinion on Biological Therapy* 4.4, pp. 519–530. DOI: 10.1517/14712598.4.4.519.
- Vermeulen, L. M. P., Brans, T., Samal, S. K., Dubruel, P., Demeester, J., Smedt, S. C. D., Remaut, K., and Braeckmans, K. (Mar. 2018). “Endosomal Size and Membrane Leakiness Influence Proton Sponge-Based Rupture of Endosomal Vesicles”. In: *ACS Nano* 12.3, pp. 2332–2345. DOI: 10.1021/acsnano.7b07583.
- Vetter, V. C. and Wagner, E. (June 2022). “Targeting nucleic acid-based therapeutics to tumors: Challenges and strategies for polyplexes”. In: *Journal of Controlled Release* 346, pp. 110–135. DOI: 10.1016/j.jconrel.2022.04.013.
- Wang, C., Pan, C., Yong, H., Wang, F., Bo, T., Zhao, Y., Ma, B., He, W., and Li, M. (Aug. 2023). “Emerging non-viral vectors for gene delivery”. In: *Journal of Nanobiotechnology* 21.1. ISSN: 1477-3155. DOI: 10.1186/s12951-023-02044-5.
- Wang, S.-H., Lee, C.-W., Chiou, A., and Wei, P.-K. (Dec. 2010). “Size-dependent endocytosis of gold nanoparticles studied by three-dimensional mapping of plasmonic scattering images”. In: *Journal of Nanobiotechnology* 8.1. DOI: 10.1186/1477-3155-8-33.
- Watson, J. D. (2007). *Recombinant DNA : genes and genomes - a short course*. eng. 3. ed., 1. print. New York: Freeman [u.a.] ISBN: 0-7167-2866-4.
- Wee, P. and Wang, Z. (May 2017). “Epidermal Growth Factor Receptor Cell Proliferation Signaling Pathways”. In: *Cancers* 9.5, p. 52. ISSN: 2072-6694. DOI: 10.3390/cancers9050052.
- Weintraub, H., Cheng, P. F., and Conrad, K. (July 1986). “Expression of transfected DNA depends on DNA topology”. In: *Cell* 46.1, pp. 115–122. DOI: 10.1016/0092-8674(86)90865-2.
- Weise, C., Schrot, A., Wuerger, L. T. D., Adolf, J., Gilibert-Oriol, R., Sama, S., Melzig, M. F., and Weng, A. (Sept. 2020). “An unusual type I ribosome-inactivating protein from *Agrostemma githago* L.” In: *Scientific Reports* 10.1. DOI: 10.1038/s41598-020-72282-2.
- Weng, A., Manunta, M. D., Thakur, M., Gilibert-Oriol, R., Tagalakakis, A. D., Eddaoudi, A., Munye, M. M., Vink, C. A., Wiesner, B., Eichhorst, J., Melzig, M. F., and Hart, S. L. (May 2015). “Improved intracellular delivery of peptide- and lipid-nanoplexes by natural

-
- glycosides". In: *Journal of Controlled Release* 206, pp. 75–90. DOI: 10.1016/j.jconrel.2015.03.007.
- Weng, A., Thakur, M., Mallinckrodt, B. von, Beceren-Braun, F., Gilabert-Oriol, R., Wiesner, B., Eichhorst, J., Böttger, S., Melzig, M. F., and Fuchs, H. (Nov. 2012). "Saponins modulate the intracellular trafficking of protein toxins". In: *Journal of Controlled Release* 164.1, pp. 74–86. DOI: 10.1016/j.jconrel.2012.10.002.
- West, K. and Otto, S. (Sept. 2005). "Reversible Covalent Chemistry in Drug Delivery". In: *Current Drug Discovery Technologies* 2.3, pp. 123–160. DOI: 10.2174/1570163054866882.
- Wilhelm, S., Tavares, A. J., Dai, Q., Ohta, S., Audet, J., Dvorak, H. F., and Chan, W. C. W. (Apr. 2016). "Analysis of nanoparticle delivery to tumours". In: *Nature Reviews Materials* 1.5. ISSN: 2058-8437. DOI: 10.1038/natrevmats.2016.14.
- Williams, J. A. and Paez, P. A. (June 2023). "Improving cell and gene therapy safety and performance using next-generation Nanoplasmid vectors". In: *Molecular Therapy - Nucleic Acids* 32, pp. 494–503. DOI: 10.1016/j.omtn.2023.04.003.
- Willner, D., Trail, P. A., Hofstead, S. J., King, H. D., Lasch, S. J., Braslawsky, G. R., Greenfield, R. S., Kaneko, T., and Firestone, R. A. (Nov. 1993). "(6-Maleimidocaproyl)hydrazide of doxorubicin. A new derivative for the preparation of immunoconjugates of doxorubicin". In: *Bioconjugate Chemistry* 4.6, pp. 521–527. DOI: 10.1021/bc00024a015.
- Winkeljann, B., Keul, D. C., and Merkel, O. M. (Jan. 2023). "Engineering poly- and micelle-plexes for nucleic acid delivery – A reflection on their endosomal escape". In: *Journal of Controlled Release* 353, pp. 518–534. DOI: 10.1016/j.jconrel.2022.12.008.
- Wiśniewski, K., Finnman, J., Flipo, M., Galyean, R., and Schteingart, C. D. (July 2013). "On the mechanism of degradation of oxytocin and its analogues in aqueous solution". In: *Biopolymers* 100.4, pp. 408–421. DOI: 10.1002/bip.22260.
- Writer, M. J., Marshall, B., Pilkington-Miksa, M. A., Barker, S. E., Jacobsen, M., Kritz, A., Bell, P. C., Lester, D. H., Tabor, A. B., Hailes, H. C., Klein, N., and Hart, S. L. (May 2004). "Targeted Gene Delivery to Human Airway Epithelial Cells with Synthetic Vectors Incorporating Novel Targeting Peptides Selected by Phage Display". In: *Journal of Drug Targeting* 12.4, pp. 185–193. DOI: 10.1080/10611860410001724459.
- Wu, P., Zhou, Q., Zhu, H., Zhuang, Y., and Bao, J. (Apr. 2020). "Enhanced antitumor efficacy in colon cancer using EGF functionalized PLGA nanoparticles loaded with 5-Fluorouracil and perfluorocarbon". In: *BMC Cancer* 20.1. ISSN: 1471-2407. DOI: 10.1186/s12885-020-06803-7.
- Xiao, J., Zhang, G., Qiu, P., Liu, X., Wu, Y., Du, B., Li, J., Zhou, J., Li, J., and Tan, Y. (July 2013). "Tanshinone IIA Increases the Bystander Effect of Herpes Simplex Virus

-
- Thymidine Kinase/Ganciclovir Gene Therapy via Enhanced Gap Junctional Intercellular Communication”. In: *PLoS ONE* 8.7. Ed. by E. Scemes, e67662. DOI: 10.1371/journal.pone.0067662.
- Xu, S., Chen, M., Feng, T., Zhan, L., Zhou, L., and Yu, G. (Nov. 2021). “Use ggbreak to Effectively Utilize Plotting Space to Deal With Large Datasets and Outliers”. In: *Frontiers in Genetics* 12. DOI: 10.3389/fgene.2021.774846.
- Yang, W., Mixich, L., Boonstra, E., and Cabral, H. (Feb. 2023). “Polymer-Based mRNA Delivery Strategies for Advanced Therapies”. In: *Advanced Healthcare Materials* 12.15. DOI: 10.1002/adhm.202202688.
- Yao, X.-L., Nakagawa, S., and Gao, J.-Q. (Sept. 2011). “Current Targeting Strategies for Adenovirus Vectors in Cancer Gene Therapy”. In: *Current Cancer Drug Targets* 11.7, pp. 810–825. DOI: 10.2174/156800911796798896.
- Yin, H., Kanasty, R. L., Eltoukhy, A. A., Vegas, A. J., Dorkin, J. R., and Anderson, D. G. (July 2014). “Non-viral vectors for gene-based therapy”. In: *Nature Reviews Genetics* 15.8, pp. 541–555. DOI: 10.1038/nrg3763.
- Yousefpour, P., Ahn, L., Tewksbury, J., Saha, S., Costa, S. A., Bellucci, J. J., Li, X., and Chilkoti, A. (Feb. 2019). “Conjugate of Doxorubicin to Albumin-Binding Peptide Outperforms Aldoxorubicin”. In: *Small* 15.12, p. 1804452. DOI: 10.1002/smll.201804452.
- Zalba, S., Contreras, A. M., Merino, M., Navarro, I., Ilarduya, C. T. de, Trocóniz, I. F., Koning, G., and Garrido, M. J. (Mar. 2016). “EGF-liposomes promote efficient EGFR targeting in xenograft colocal carcinoma model”. In: *Nanomedicine* 11.5, pp. 465–477. ISSN: 1748-6963. DOI: 10.2217/nnm.15.208.
- Zanta, M. A., Belguise-Valladier, P., and Behr, J.-P. (Jan. 1999). “Gene delivery: A single nuclear localization signal peptide is sufficient to carry DNA to the cell nucleus”. In: *Proceedings of the National Academy of Sciences* 96.1, pp. 91–96. ISSN: 1091-6490. DOI: 10.1073/pnas.96.1.91.
- Zhang, X., Yin, Liu, Ma, Wang, and Hao (Aug. 2012). “A novel EGFR-targeted gene delivery system based on complexes self-assembled by EGF, DNA, and activated PAMAM dendrimers”. In: *International Journal of Nanomedicine*, p. 4625. ISSN: 1178-2013. DOI: 10.2147/ij.n.s30671.
- Zhang, X., Wang, H., Ma, Z., and Wu, B. (Sept. 2014). “Effects of pharmaceutical PEGylation on drug metabolism and its clinical concerns”. In: *Expert Opinion on Drug Metabolism & Toxicology* 10.12, pp. 1691–1702. ISSN: 1744-7607. DOI: 10.1517/17425255.2014.967679.
- Zhou, Z., Liu, X., Zhu, D., Wang, Y., Zhang, Z., Zhou, X., Qiu, N., Chen, X., and Shen, Y. (June 2017). “Nonviral cancer gene therapy: Delivery cascade and vector nanoproperty

integration”. In: *Advanced Drug Delivery Reviews* 115, pp. 115–154. DOI: 10.1016/j.addr.2017.07.021.

Zhu, Y., Shen, R., Vuong, I., Reynolds, R. A., Shears, M. J., Yao, Z.-C., Hu, Y., Cho, W. J., Kong, J., Reddy, S. K., Murphy, S. C., and Mao, H.-Q. (July 2022). “Multi-step screening of DNA/lipid nanoparticles and co-delivery with siRNA to enhance and prolong gene expression”. In: *Nature Communications* 13.1. DOI: 10.1038/s41467-022-31993-y.

7 Appendix

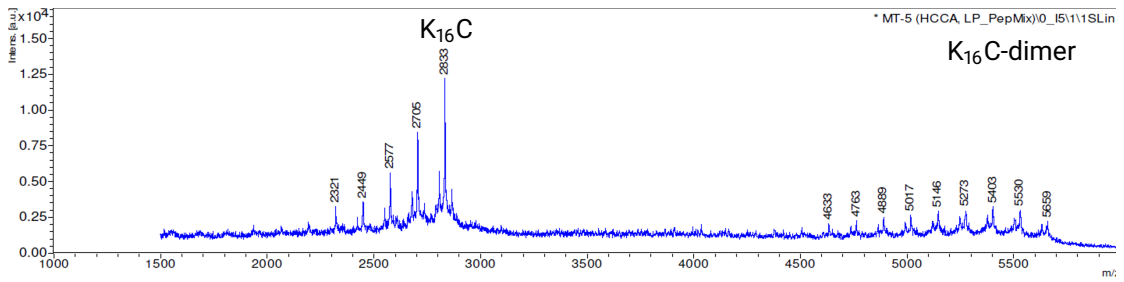
7.1 Organ Weights of Mice

Table 7.1: Organ weights of mice included in the *in vivo* efficacy study. Liver, spleen, and kidney of three mice from each the vehicle control group (indicated by C in the column header) and the pepY-SO1861-nanoplex-receiving treatment group (indicated by T in the column header) were removed and immediately frozen in liquid nitrogen. After thawing, the organs were carefully dissected and weighed. Organ weights are given in mg.

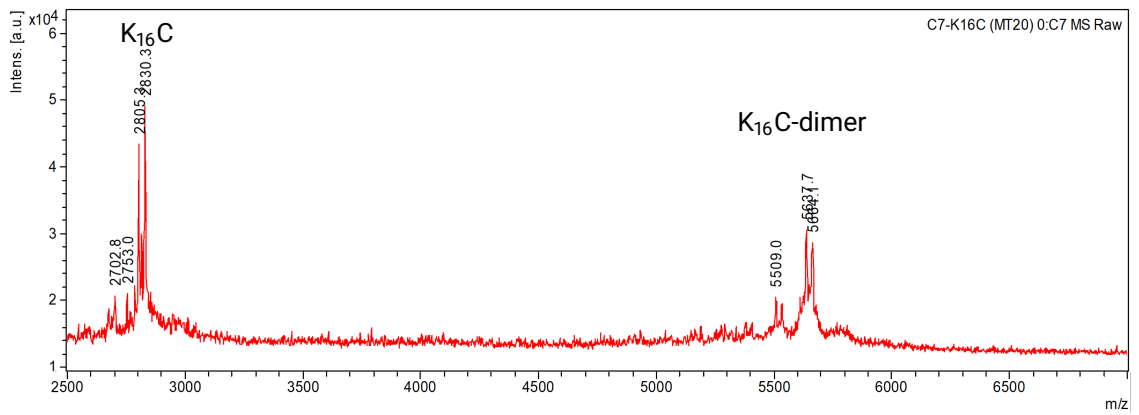
Organ	C1	C2	C3	T1	T2	T3
liver	311.1	313.4	341.0	636.1	565.3	599.8
spleen	220.8	254.7	198.3	249.4	186.8	221.1
kidney	228.0	197.1	203.3	244.9	208.1	198.1

7.2 MALDI-Spectra of Peptide Batches

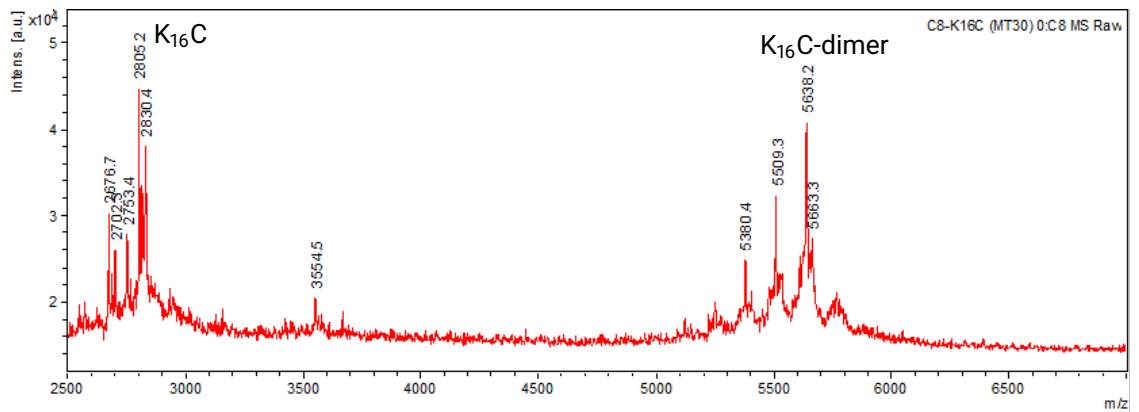
For all batches of SO1861-equipped peptide scaffolds, successful conjugation of SO1861-EMCH to the peptide was confirmed using MALDI-TOF-MS as the following spectra indicate. The peptide, batch, matrix and mode of MALDI-measurement are given below each spectrum. Peaks with $\Delta m/z = -129$ relative to the peptide peaks represent peptides which lost one lysine. Peaks with $\Delta m/z = \approx +208$ relative to the peptide peak represent the addition of the matrix substance SA. Peaks with $\Delta m/z = \approx -909$ relative to the conjugate peaks represent peptide-SO1861-conjugates which lost the sugar chain at C-28.



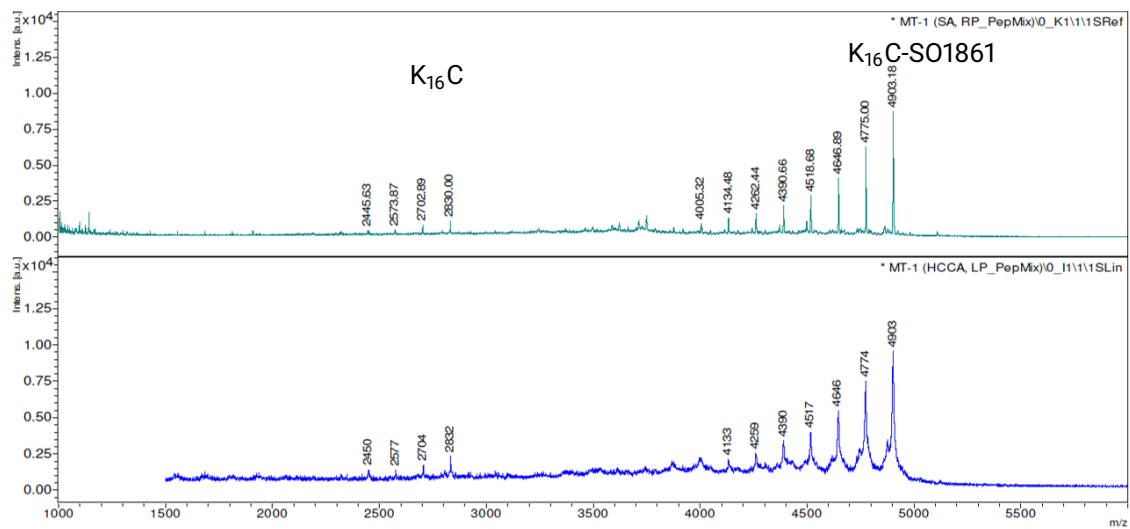
K₁₆C batch MT10, matrix HCCA, linear mode, m/z reported as [M+H]⁺ (average)



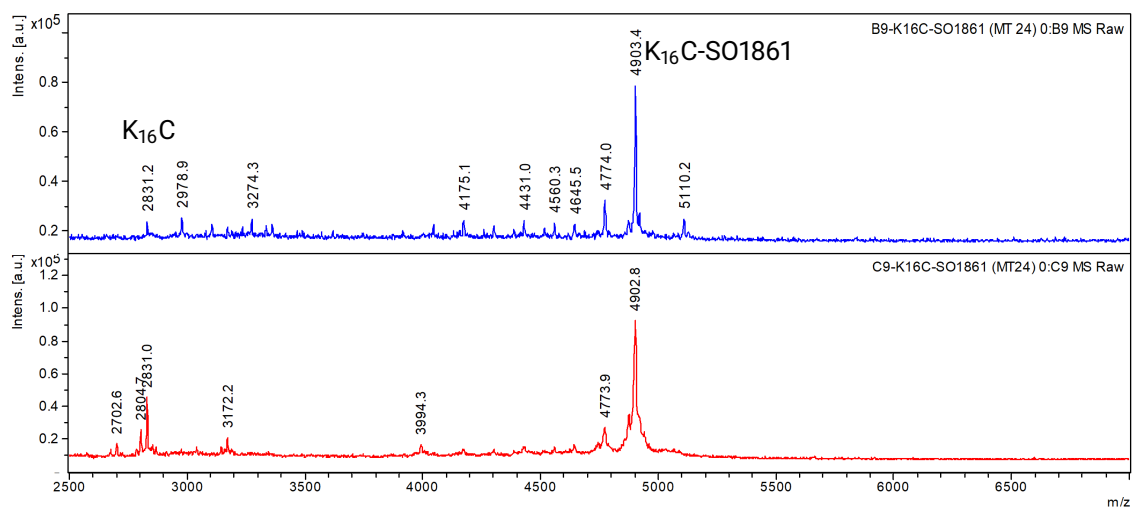
K₁₆C batch MT20, matrix HCCA, linear mode, m/z reported as [M+H]⁺ (average)



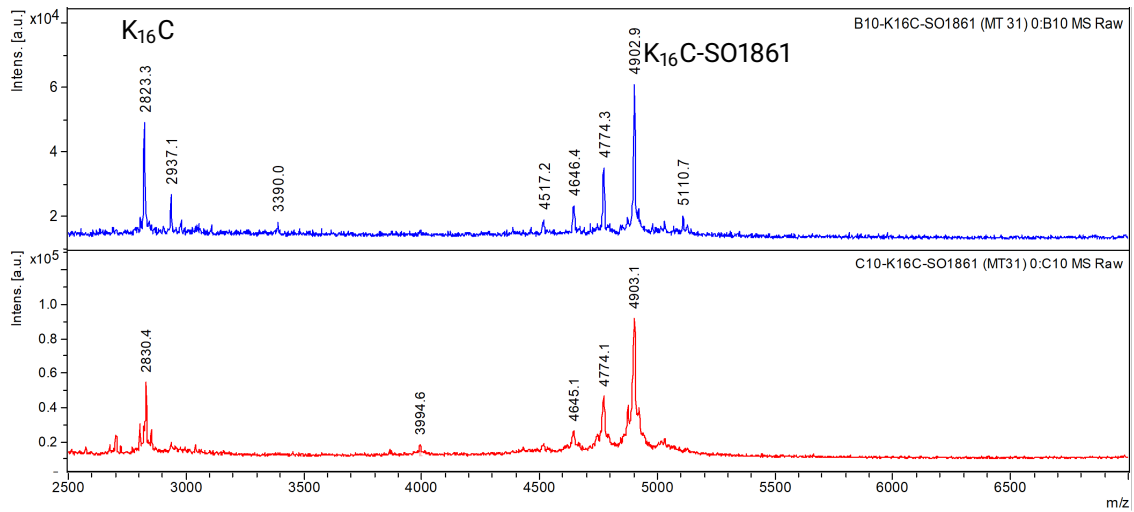
K₁₆C batch MT30, matrix HCCA, linear mode, m/z reported as [M+H]⁺ (average)



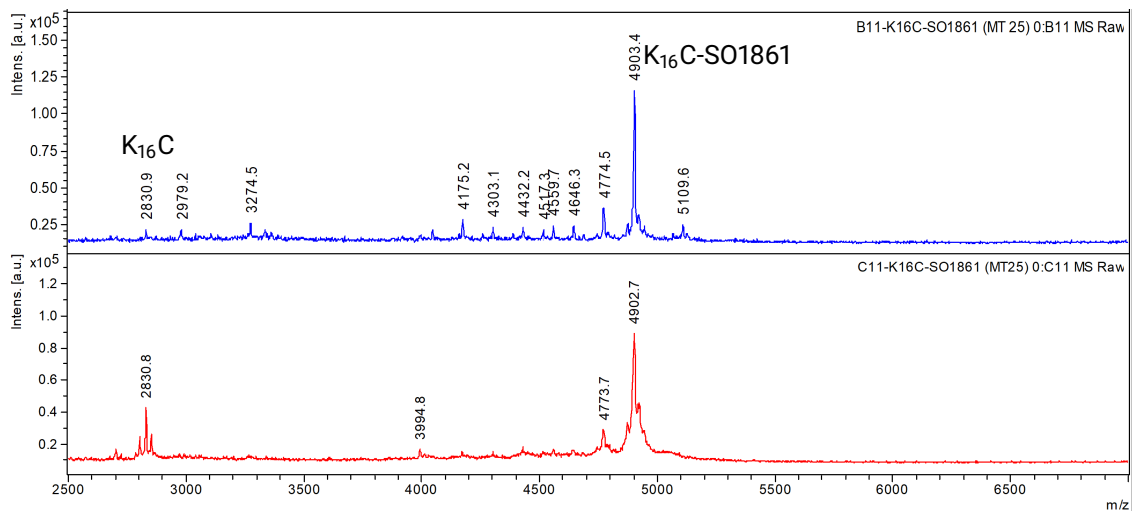
K₁₆Ceq0.25 batch MT11, upper panel: matrix SA, reflector mode, m/z reported as [M+H]⁺ (mono-isotopic), lower panel: matrix HCCA, linear mode, m/z reported as [M+H]⁺ (average)



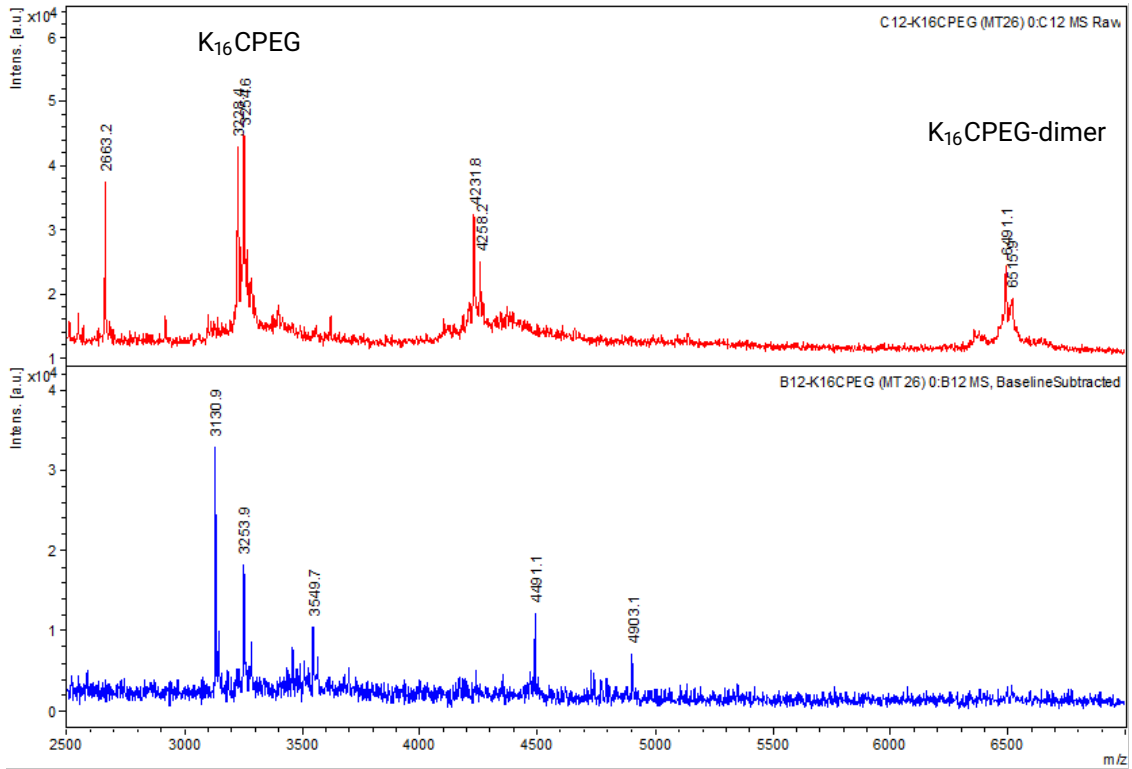
K₁₆Ceq0.25 batch MT24, upper panel: matrix SA, linear mode, m/z reported as [M+H]⁺ (average), lower panel: matrix HCCA, linear mode, m/z reported as [M+H]⁺ (average)



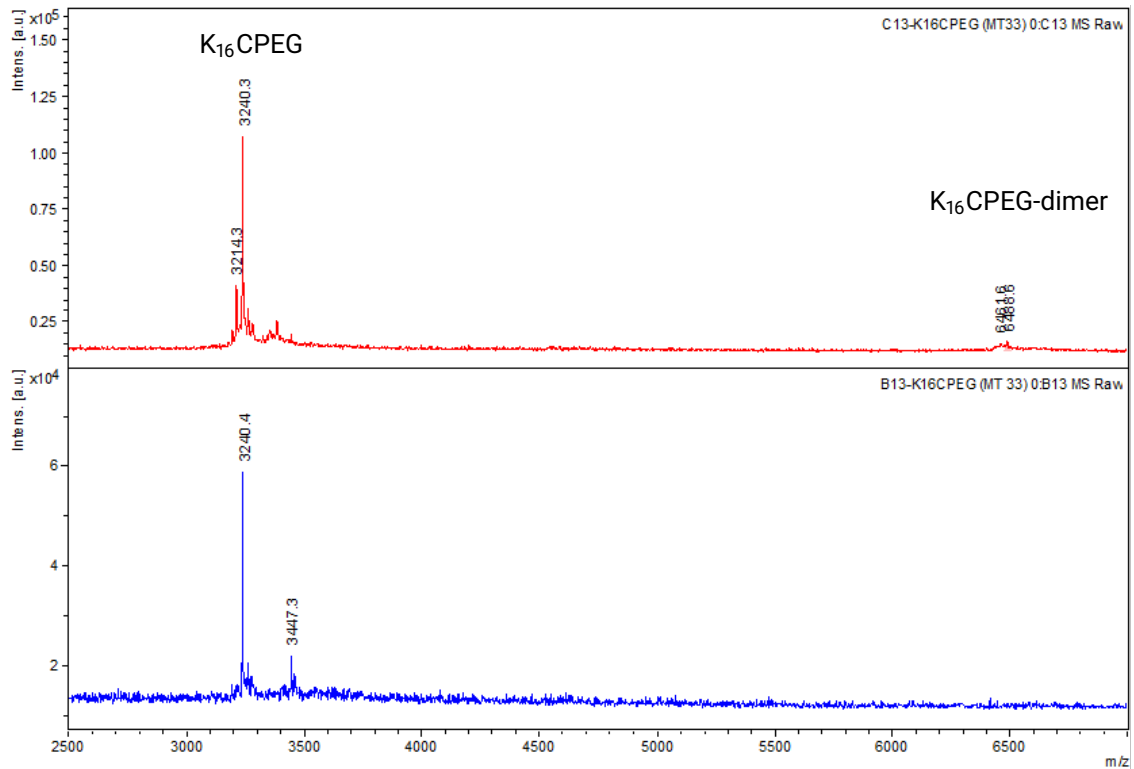
$K_{16}C_{eq0.25}$ batch MT31, upper panel: matrix SA, linear mode, m/z reported as $[M+H]^+$ (average), lower panel: matrix HCCA, linear mode, m/z reported as $[M+H]^+$ (average)



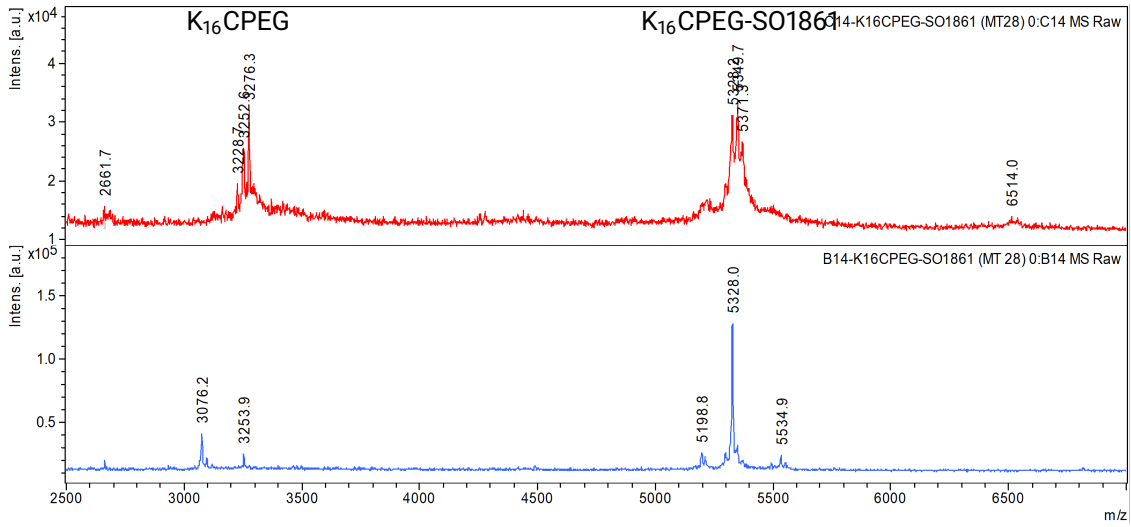
$K_{16}C_{eq0.5}$ batch MT25, upper panel: matrix SA, linear mode, m/z reported as $[M+H]^+$ (average), lower panel: matrix HCCA, linear mode, m/z reported as $[M+H]^+$ (average)



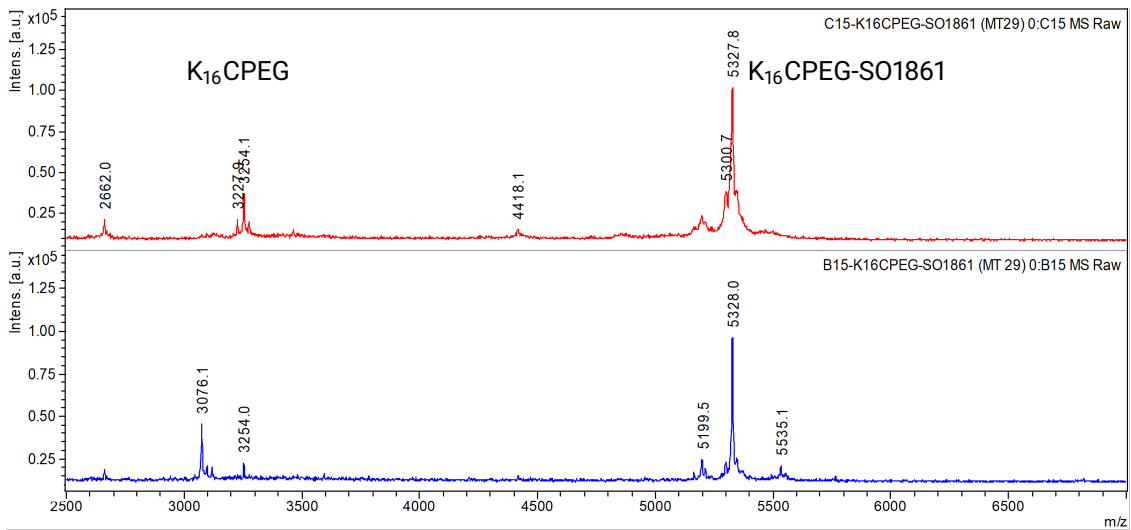
K₁₆CPEG batch MT26, upper panel: matrix HCCA, linear mode, m/z reported as [M+H]⁺ (average), lower panel: matrix SA, linear mode, m/z reported as [M+H]⁺ (average)



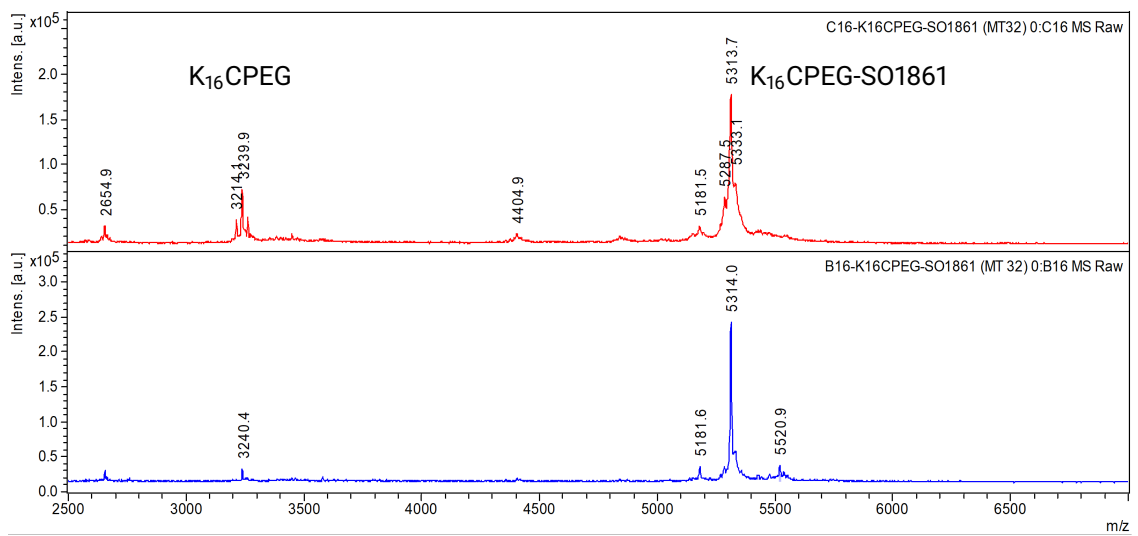
K₁₆CPEG batch MT33, upper panel: matrix HCCA, linear mode, m/z reported as [M+H]⁺ (average), lower panel: matrix SA, linear mode, m/z reported as [M+H]⁺ (average)



$K_{16}CPEGq0.25$ batch MT28, upper panel: matrix HCCA, linear mode, m/z reported as $[M+H]^+$ (average), lower panel: matrix SA, linear mode, m/z reported as $[M+H]^+$ (average)



$K_{16}CPEGq0.5$ batch MT29, upper panel: matrix HCCA, linear mode, m/z reported as $[M+H]^+$ (average), lower panel: matrix SA, linear mode, m/z reported as $[M+H]^+$ (average)



K₁₆CPEG_{q0.5} batch MT32, upper panel: matrix HCCA, linear mode, m/z reported as [M+H]⁺ (average), lower panel: matrix SA, linear mode, m/z reported as [M+H]⁺ (average)

7.3 Kinetics of Transfection with PepY-SO1861-Nanoplex

A time-lapse video of fluorescence micrographs recorded during transfection of Neuro-2a cells with pepY-SO1861-nanoplexes (NP-eGFP complexed with 70 % pepY and 30 % K₁₆CPEGeq0.5) was uploaded associated with this document.

Acknowledgments

First of all, I would like to thank PD Alexander Weng, the supervisor of my dissertation, for giving me the opportunity to work on this exciting question. Thank you for the freedom you gave me and the constant encouragement to believe in myself, my judgment and my gut feeling. I would like to thank Prof. Melzig, the former head of the working group, for his sympathetic ear and for his willingness to share his, not only scientific, expertise. I thank Prof. Niedermeyer for taking on the role as second assessor of this thesis.

It has been a pleasure to work on this thesis as part of the ENDOSCAPE project. I would like to thank the entire consortium, especially Prof. Hendrik Fuchs for the organizational, personal, and scientific excellent project coordination. I also thank Dr. Gregor Nagel, who despite his obligations as a postdoc in his “own” group, was always available to me and was of great help with his experience, and to Melanie Krass for many phone calls, “our” report D3.3, sample handovers and transport in the morning, and the uncomplicated and enriching collaboration. I would also like to thank Prof. Eduardo Fernandez-Megia and his working group for their willingness to share their experience, for good advice, and for their collaboration on the publication.

I want to thank the “Pharmaceutical Biology” working group for the relaxed working atmosphere and the shared coffee breaks. I would especially like to thank Conny and Louisa for the many conversations and lunch breaks, Eric and Alex for sharing the lab, and Simko for the introduction to cell culture and sapofection. My special thanks go to Hardy, who introduced me to the practical work in molecular biology, made the production of minicircle DNA possible with his basic work, showed me some practical “lab assistant” tricks, and was available for discussions. Our business trips together were a great pleasure! I would also like to thank Stefan for his hospitality and great support. Thank you for making me feel welcome in your realm over the last few months. I thank Jan, Louisa, Hardy and Alex for their extensive, precise and critical proofreading of this thesis. Your comments have improved it in many places and hopefully made it easier to understand, thank you!

I would like to thank Dr. Chris Weise for performing the MALDI-MS measurements. It was great to benefit from your extensive knowledge and experience. I would also like to thank Ellen Christmann for the uncomplicated and flexible LC-MS measurements and some hallway chats, Anke Schindler and Dr. Boris Schade for the electron microscopy measurements, Prof. Kleuser and his working group for the opportunity to use the flow cytometer, and Prof. Bodmeier, Dr. Staufenbiel and his group for the uncomplicated access to the Zetasizer. I would also like to thank Marie, Vanessa and Abby for their assistance in

preparing the minicircle DNA during their internship. Birgit Zeidler and Petra Heine were a great help in the administrative jungle of the university, thank you.

I would like to thank Marei Peischl for publicly sharing the LaTeX template used for this thesis.

Finally, I would like to thank my friends and family for their constant support, especially Marit for her time. My special thanks go to Till, for his patience and understanding and for his extensive help with all LaTeX-specific formatting issues.